Climate Monitoring and Diagnostics Laboratory

No. 20

Summary Report 1991

U.S. DEPARTMENT OF COMMERCE

NATIONAL OCEANIC AND ATMOSPHERIC ADMINISTRATION

ENVIRONMENTAL RESEARCH LABORATORIES

Climate Monitoring and Diagnostics Laboratory No. 20

Summary Report 1991

Eldon E. Ferguson, Editor
Rita M. Rosson, Assistant Editor

Boulder, Colorado

December 1992

U.S. DEPARTMENT OF COMMERCE
Barbara Hackman Franklin, Secretary

National Oceanic and Atmospheric Administration
John A. Knauss, Under Secretary for Oceans and Atmosphere/Administrator

Environmental Research Laboratories
Joseph O. Fletcher, Director

NOTICE

Mention of a commercial company or product does not constitute an endorsement by NOAA Environmental Research Laboratories. Use for publicity or advertising purposes of information from this publication concerning proprietary products or the tests of such products is not authorized.

For sale by the National Technical Information Service, 5285 Port Royal Road
Springfield, VA 22161

Contents

CMDL Staff, 1991

Director's Office

Eldon Ferguson, Director
James Peterson, Deputy Director
Donna Leise, Administrative Officer
Sandra Howe, Administrative Assistant
Ellen Hardman, Secretary
Rita Rosson, Editorial Assistant
Denise Theede, Program Clerk

Special Projects

Russell Schnell, CIRES
Kellie Crowder, CIRES
S.J.S. Khalsa, CIRES
Martin Miles, CIRES
Craig Quincy, CIRES
Mark Serreze, CIRES
Patrick Sheridan, CIRES
Spencer Shiotani, Physical Science Aid

Atmospheric Radiation Monitoring Division

Gary Herbert, Chief
Sheri Cox, Secretary
Mark Bieniulis, CIRES
Thomas Mefford, CIRES
Kenneth Thaut, Electronic Technician

Carbon Cycle Division

Pieter Tans, Chief
Lee Prendergast, Secretary
Carol Brandes, Secretary
Peter Bakwin, CIRES
Thinh Minh Cao CIRES
Thomas Conway, Research Chemist
Wyatt Coy, CIRES
Edward Dlugokencky, CIRES
Douglas Guenther, CIRES
Duane Kitzis, CIRES
Patricia Lang, Physical Scientist
Terry Lesoing, CIRES
Martin Manning, Visiting Scientist
Kenneth Masarie, CIRES
Paul Novelli, CIRES
Aaron Patton, CO-OP
Michael Stavish, CO-OP
Kirk Thoning, Physicist
Michael Trolier, CIRES
Anthony Vaughn, Physical Science Aid
Lee Waterman, Research Chemist
Conglong Zhao, CIRES
Ni Zhang, CIRES

Aerosols, Radiation, Ozone & Water Vapor Division

David Hofmann, Chief
Lee Prendergast, Secretary
Gail Widger, Secretary
Jennifer Barnett, Physical Science Aid
Catherine Baxter, Physical Science Aid
Barry Bodhaine, Meteorologist
Theodore Chen, Physical Science Aid
Paul Chilson, Physical Science Aid
John DeLuisi, Meteorologist
Ellsworth Dutton, Meteorologist
Robert Evans, CIRES
Juan Martin Gonzales, Visiting Scientist
Robert Grass, Physicist
Rudy Haas, Mathematician
Bradley Halter, CIRES
Joyce Harris, Physical Scientist
Gloria Koenig, Computer Programmer
Walter Komhyr, Physicist
Fred Kreiner, CIRES
Jeffrey Lathrop, CO-OP
Javier de La Cruz Leiva, Visiting Scientist
David Longenecker, CIRES
Donald Nelson, Meteorologist
John Ogren, Physical Scientist
Samuel Oltmans, Physicist
Greg Orleans, Physical Science Aid
Frank Polacek, III, Meteorological Technician
Gayland Pounder, Physical Science Aid
Dorothy Quincy, CIRES
Gretchen Roth, CIRES
Scott Sio, Physical Science Aid
Robert Stone, CIRES
Holger Vömel, CIRES
James Wendell, Electronic Technician

Nitrous Oxide and Halocarbons Division

James Elkins, Chief
Marilyn Van Asche, Secretary
Carol Brandes, Secretary
Dave Alexander, CIRES
Thomas Baring, Physical Science Aid
James Butler, Research Chemist
Scott Cummings, CIRES
Jeannie Dolan, CIRES
Andrew Duang, CIRES
Geoffrey Dutton, CIRES
Timothy Gilpin, NRC
Brad Hall, CIRES
Arnold Hayden, CIRES
Garry Holcomb, Electronic Engineer
Patrick Judge, Physical Science Aid
Kristen Kauffman, C.U. Work Study
Richard Myers, Physical Science Technician
Steve Montzka, Research Chemist
Jae W. Nam, C.U. Work Study
Matthew Nowick, C.U. Work Study
William Sturges, CIRES
Thomas Swanson, CIRES
Thayne Thompson, Physicist

Observatory Operations Division

Bernard Mendonca, Chief
Sheri Cox, Secretary

Daniel Endres, Station Chief, **Barrow**
Christopher Churylo, Electronic Engineer

Elmer Robinson, Director, **Mauna Loa**
Judith Pereira, Program Support Technician
John Chin, Physicist
Thomas DeFoor, Electronic Engineer
Lynne Hanzawa, Physical Science Aid
Barbara Kerecman, Data Clerk
Darryl Kuniyuki, NOAA Jr. Fellow
Steven Ryan, Physical Scientist
Mamoru Shibata, Electronic Technician
Robert Uchida, Electronic Technician
Terrie Yokoi, Physical Science Aid
Alan Yoshinaga, Chemist

Carl Farmer, Station Chief, **Samoa**
Mark Winey, Electronic Engineer

John Lowell, NOAA Corps, **South Pole**
Michael O'Neill, Electronic Engineer
Carl Groeneveld, NOAA Corps
Dale Tysor, NOAA Corps
David Gaines, Electronic Engineer

CMDL Station Information

	Barrow (BRW)	**Mauna Loa (MLO)**
Name:		
Latitude:	71.323	19.539
Longitude:	156.609	155.578
Elevation:	8 m	3397 m
Time Zone:	GMT -9	GMT -10
Office Hours:	8:00 am-5:00 pm	8:00 am-5:00 pm
Telephone		
Office hours:	(907) 852-6500	(808) 961-3788
Fax:	(907) 852-4622	(808) 961-3789
Postal Address:	Officer in Charge NOAA/ERL/CMDL Pouch 8888 Barrow, AK 99723	U.S. Dept. of Commerce NOAA - Mauna Loa Observatory P.O. Box 275 Hilo, HI 96720
Freight Address:	Same as above	U.S. Dept. of Commerce NOAA - Mauna Loa Observatory 154 Waianuenue Ave. Hilo, HI 96720

	Samoa (SMO)	**South Pole (SPO)**
Name:		
Latitude:	-14.232	-89.997
Longitude:	170.563	-102.0
Elevation:	77 m	2841 m
Time Zone:	GMT -11	GMT +12
Office Hours:	8:00 am-5:00 pm	8:00 am - 5:00 pm
Telephone:		
Office hours:	011 (684) 622-7455	Relayed through CMDL Boulder
After hours:	011 (684) 699-9953	
Fax:	011 (684) 699-4440	
Postal Address:	U.S. Dept. of Commerce NOAA - GMCC Samoa Observatory Pago Pago, American Samoa 96799	Officer in Charge NOAA/CMDL Clean Air Facility S-257 South Pole, Antarctica PSC 468 Box 402 FPO AP 96598-5402
Freight Address:	Same as above	Same as above

1. Observatory Operations Division

1.1. Mauna Loa Observatory

R. C. Schnell

1.1.1. Operations

The normal climate monitoring routine at MLO experienced and recorded one anthropogenically induced and two geophysical events in 1991, namely, the Kuwait oil fires beginning in February, the Mt. Pinatubo volcanic eruption June 15-17, and the total solar eclipse on July 11.

Kilauea volcano on the southwest flank of Mauna Loa continued to flow and occasionally created heavy "vog" events in the marine boundary layer over the southern parts of the island. Impacts on MLO measurements from Kilauea effluents are minimal to nonexistent, depending on whether moist boundary air is temporarily advected to the observatory in the afternoon upslope flow.

The MLO director, Elmer Robinson, retired in December. Dr. Robinson arrived shortly after the 1984 eruption of Mauna Loa. Among many other things, he was instrumental in bringing to completion the construction of a lava barrier above the observatory to protect it from any new volcanic activity. He came to MLO from the University of Washington at Pullman and has now taken a position at the University of Hawaii at Hilo on a part-time basis teaching introductory meteorology.

Russell Schnell, formerly of the University of Colorado, Boulder, was appointed the new director of MLO. Dr. Schnell has had a decade-long association with NOAA/CMDL through CIRES and is most recently recognized as the director of the ongoing Arctic Gas and Aerosol Sampling Program (AGASP), which he founded in 1982.

1.1.2. Programs

The Kuwait oil fires initiated a number of research projects by both NOAA and cooperative program scientists to measure the onset, concentration, and chemical composition of the smoke reaching MLO. In a paper by *Bodhaine et al.* [1992], it was argued that Kuwait oil-fire smoke was first detected by the aethalometer at MLO on February 7, 1991.

The effects of the Pinatubo aerosols on solar radiation, lidar backscatter and stratospheric ozone concentrations are discussed in the following subsection of this MLO report. The measurements at MLO showed stratospheric aerosol loadings from Pinatubo, and the resulting perturbations on solar radiation are comparable with those produced by the 1982 El Chichon eruption. The measurable effects of Pinatubo aerosol in the stratosphere over MLO are expected to last for another 5 years if the recovery dynamics of the Pinatubo cloud are similar to those of the El Chichon stratospheric aerosol record.

The total solar eclipse on July 11 attracted a large number of solar scientists to MLO from around the world. Some of the institutions represented with instrumentation and their projects were as follows: the Max-Planck Institute, Lindau, solar coronograph; New Zealand CSIRO, N_2O profiles from zenith scattering; Tokyo Science University, fine structure corona measurements; Walt Disney Studios, Anaheim, California, solar photography; University of Denver, Colorado, solar IR spectra; University of California, Berkeley, coronal morphology; Rhodes College, Memphis, coronal telescope studies; and NASA Ames, sunphotometry.

Table 1.1 summarizes the principal ongoing programs conducted at MLO during 1991. Details of some of the programs are as follows:

Carbon Dioxide

The CMDL Siemens Ultramat-3 IR CO_2 analyzer and the SIO Applied Physics IR CO_2 analyzer were operated in parallel without major problems throughout the year. Routine maintenance and calibrations were done on both instruments on schedule. The SIO analyzer developed an excessively noisy output signal problem during the latter part of the year when the thermal controller was no longer able to keep the detector in a stable operating temperature environment. Strip chart recorder traces showed drifting from one side when the instrument room warmed up and drifting to the opposite side when the room cooled down. Replacement parts will be installed in early 1992 as soon as they are received from SIO.

The preliminary CO_2 data showed an average concentration of 355.4 ppm for 1991. The CO_2 annual growth rate between 1990 and 1991 was approximately 1.3 ppm. Outgassing from the volcanic vents at the Mauna Loa caldera and along the northeast rift zone at Mauna Loa continued to cause periodic and detectable scatter in some of the CO_2 data record. As in prior years, these venting events occurred mostly between midnight and 0800 LST of the following day, during the downslope wind regime. The erratic concentration data resulting from venting events were easily identified by visually scanning the chart records or by setting up a computerized data screening procedure, and thus they have been separated from the clean-air record without difficulty. Such venting episodes were detected mainly on the basis of criteria for CO_2 concentration, CO_2 variability, and wind sector. The criterion for the CO_2 standard deviation screening was 1.0 ppm, which is the value suggested by *Thoning et al.* [1989]. The monthly occurrences of observable outgassing from volcanic vents on Mauna Loa for 1991 are listed in Table 1.2. Annual occurrences totaled 26 (hours) in 1991, compared with 48 in 1990, 84 in 1989, and 200 in 1988.

The weekly CO_2, as well as CH_4 and other gas sampling programs using flasks at MLO and at Cape Kumukahi were carried out according to schedule throughout the year without problems.

TABLE 1.1. Summary of Measurement Programs at MLO in 1991

Program	Instrument	Sampling Frequency
Gases		
CO_2	Siemens Ultramat-3 IR analyzer	Continuous
	3-L glass flasks†	1 pair wk^{-1}
	0.5-L glass flasks, through analyzer	1 pair wk^{-1}
CO_2, CH_4, CO, ^{13}C, ^{18}O of CO_2	2.5-L glass flasks, MAKS pump unit†	1 pair wk^{-1}
CH_4	Carle automated GC	1 sample $(24\ min)^{-1}$
Surface O_3	Dasibi ozone meter	Continuous
Total O_3	Dobson spectrophotometer no. 76	3 day^{-1}, weekdays
O_3 profiles	Dobson spectrophotometer no. 76 (automated Umkehr method)	2 day^{-1}
	Balloonborne ECC sonde	1 wk^{-1}
CFC-11, CFC-12, N_2O	300-mL stainless steel flasks	1 pair wk^{-1}
CFC-11, CFC-12, N_2O, CCl_4, CH_3CCl_3, CFC-113	HP5890 automated GC	1 sample $(h)^{-1}$
CH_3Br, HCFC-22, CFC-113 CCl_4, CH_3CCl_3, CFC-113 Halon-1211, Halon-1301	0.8-L stainless-steel flasks	monthly
N_2O	Shimadzu automated GC	1 sample $(h)^{-1}$
Radon	Two-filter system	Continuous integrated 30-min samples
Aerosols		
Condensation nuclei	Pollak CNC	1 day^{-1}
	TSI CNC*	Continuous
Optical properties	Four-wavelength nephelometer*: 450, 500, 700, 850 nm	Continuous
Stratospheric and upper tropospheric aerosols	Lidar, 694.3 nm	1-3 profiles wk^{-1}
Black carbon	Aethalometer	Continuous
Total suspended particles	High-volume sampler	2 samples $(mo)^{-1}$
Solar Radiation		
Global irradiance	Eppley pyranometers with Q, OG1, and RG8 filters	Continuous
Direct irradiance	Eppley pyrheliometer (2) with Q filter*	Continuous
	Eppley pyrheliometer with Q, OG1, RG2, and RG8 filters	3 day^{-1}
	Eppley/Kendall active cavity radiometer	1 mo^{-1}
Diffuse irradiance	Eppley pyranometer with shading disk and Q filter*	Continuous
Turbidity	J-202 and J-314 sunphotometers with 380-, 500-, 778-, 862-nm narrowband filters	3 day^{-1}
	PMOD three-wavelength sunphotometer*: 380, 500, 778 nm; narrowband	Continuous
Ultraviolet radiation	Robinson-Berger UV radiometer (erythema)	Continuous
Meteorology		
Air temperature	Aspirated thermistor*, 2- and 40-m heights	Continuous
	Max.-min. thermometers, 2-m height	1 day^{-1}
	Hygrothermograph	Continuous
Temperature gradient	Aspirated thermistors*, 2- and 40-m heights	Continuous
Dewpoint temperature	Dewpoint hygrometer*, 2-m height	Continuous
Relative humidity	Hygrothermograph	Continuous
Pressure	Capacitance transducer*	Continuous
	Mecurial barometer	5 wk^{-1}
Wind (speed and direction)	Bendix Aerovane*, 8.5- and 40-m heights	Continuous
Planetary boundary layer meteorology (PBL MET)	Wind vane, cup anemometer, and aspirated RTD thermometer (direction, speed, temperature at 3, 5, 10, 20, 30, and 40 m levels)	Continuous
Precipitation	Rain gauge, 8-in	5 wk^{-1}
	Rain gauge, 8-in‡	1 wk^{-1}
	Rain gauge, tipping bucket*	Continuous
Total precipitable water	Foskett IR hygrometer*	Continuous

TABLE 1.1. Summary of Measurement Programs at MLO in 1991—Continued

Program	Instrument	Sampling Frequency
Precipitation Chemistry		
pH	pH meter	Daily
Conductivity	Conductivity bridge	Daily
Chemical components	Ion chromatograph	Daily
Cooperative Programs		
CO_2 (SIO)	Applied Physics IR analyzer	Continuous
CO_2, ^{13}C, N_2O (SIO)	5-L evacuated glass flasks†	1 pair wk^{-1}
CO_2, CO, CH_4, $^{13}C/^{12}C$ (CSIRO)	Pressurized glass flask sample	1 mo^{-1}
CO_2, CH_4, other trace gases (NCAR)	Evacuated stainless steel flasks†	1 pair wk^{-1}
Total suspended particles (DOE)	High-volume sampler (1 filter wk^{-1})	Continuous
Turbidity (AES Canada)	Sonotek sunphotometer no. 5698	1-3 day^{-1}
CH_4 ($^{13}C/^{12}C$) (Univ. of Washington)	35-L evacuated flask	1 mo^{-1}
Ultraviolet radiation (Smithsonian)	8-wavelength UV radiometer: 290-325 nm; narrowband	Continuous
Solar aureole intensity (CSU)	Multi-aperture tracking photometer: 2, 5, 10, 20, 30° fields of view	Continuous
Precipitation collection (DOE)	Exposed collection pails	Integrated monthly sample
Precipitation collection for organic acid analysis (Univ. of Virginia)	Aerochemetric automatic collector	Collection after each rain event
Wet-dry deposition (ISWS, NADP)	Aerochemetric automatic collector and weighing-bucket rain gauge	Integrated 7-day sample
Aerosol chemistry, upslope-downslope discrimination (Univ. of Washington)	Nuclepore filters	Continuous
Aerosol chemistry (Univ. of Calif.-Davis)	Programmed filter sampler	Integrated 3-day sample, 1 continuous and 1 downslope sample (3 days)$^{-1}$
Various trace gases (OGIST)	Stainless steel flasks†	1 set wk^{-1} (3 flasks)
HNO_3, HCl vapor, aerosols (URI)	Filter system	Daily, 2000-0600 LST
Radon (ANSTO)	Aerosol scavenging of Rn daughters	Continuous; integrated 30-min samples
Aerosol surface area (PSI)	Epiphaniometer	Discontinued 6/91
Formation of ^3He (WHOI)	Closed cylinder	Continuous 12-mo ambient exposure from 1/90
Solar spectra (Univ. of Denver)	FTIR spectrometer	1 wk^{-1}
O_2 (NCAR)	Three 5-L glass flasks	1 wk^{-1}
O_2 (URI)	Two 5-L glass flasks	Biweekly

All instruments are at MLO unless indicated.
*Data from this instrument recorded and processed by CAMS.
†MLO and Kumukahi.
‡Kulani Mauka.

TABLE 1.2. Estimated Mauna Loa Venting Episodes (Total Time in Hours) at MLO in 1991*

Jan.	Feb.	March	April	May	June	July	August	Sept.	Oct.	Nov.	Dec.	Year
4	1	1	1	4	4	3	5	2	1	0	0	26

*Criteria: CO_2 SD ≥ 1.0 ppm, wind direction sector 135°-225°, wind speed ≥1.35 m s^{-1}.

Methane

A Carle automated GC system was in continuous operation throughout the year (except for a period mentioned below) providing CH_4 data on the basis of a grab air sample being taken every 24 minutes. The air inlet valve of the Carle 5 GC experienced intermittent alignment problems in midyear which occasionally stopped the air flow. A flame-out problem also developed in this period when the helium carrier gas flow was slightly increased. Thus, the MLO Carle 5 GC was replaced with Boulder's Carle 6 GC in July. The new instrument functioned well for the remainder of the year.

The CH_4 data continued to show clearly defined cycles of varying frequencies. The typical diurnal cycle was well correlated with upslope and downslope winds; the marine boundary layer air had the higher CH_4 concentrations. There were also multiday or synoptic-scale CH_4 cycles observed, which apparently relate to different air mass source regions. Finally, there was still a gradual but persistent upward trend in CH_4 concentrations throughout the year.

Ozone

The 1991 MLO ozone monitoring program consists of three measurement phases: continuous MLO surface monitoring using a Dasibi model 1003-AH UV absorption ozone meter; daily total ozone and Umkehr ozone profile measurements using a computer-based automated Dobson instrument (no. 76); and ozone profile measurements based on weekly ascents of balloonborne ECC ozonesondes from the NWS station at the Hilo airport.

The Dasibi ozone meter performed in a fully satisfactory manner and provided a continuous, high-quality record of station-level ozone concentrations for the entire year.

In addition to the daily automated Umkehr measurements and 5-day-a-week total ozone measurements, 17 special observation periods were undertaken in 1991. Of the 17, 5 were comparisons with Dobson standard instrument no. 83, and the balance were continuous AC-DC direct-sun observations from sunrise to noon. From July 17 to August 20, MLO's Dobson no. 76 was returned to Boulder for maintenance and calibration. On November 27 the Dobson pedestal motor on unit no. 76 was replaced. The new pedestal unit has worked to date without a failure.

There were seven 4A-type sondes flown until February 27, at which time the program was suspended due to alternate research priorities. On June 2, flights were reinstated in response to the unique research opportunity offered by the Mt. Pinatubo eruption and the potential for heterogenous ozone destruction reactions to occur with the stratospheric aerosols introduced by the volcano. Three ozonesonde flights were completed with 4A sondes until July 16, at which time the new type-5A digital sondes were introduced. For the remainder of the year, weekly ozonesonde flights were coordinated with MLO aerosol lidar observations to provide further opportunities to study the effects of the Pinatubo aerosol cloud on ozone chemistry.

Halocarbons and Nitrous Oxide

The RITS system was upgraded during the year to provide hourly ambient air measurements in place of the once-every-3-h samples obtained previously. The RITS sample gas suite was expanded to include CFC-113 as well as N_2O, CFC-11, CFC-12, CCl_4, and CH_3CCl_3. Although this complex gas chromatographic system was not trouble free during the year, those problems that did occur could usually be corrected with little resulting downtime. Two air lines were added to the system (one at mid-tower and the other at the top) along with a pump board, regulators, and flow meters. A floppy drive was replaced in the HP 9133 system, and a redesigned NAFION dryer unit installed. With RITS PLOT it is now possible to obtain a printout of GC results for the past 30 days. Thus the data and performance of the system are regularly reviewed and the RITS gas concentrations correlated with other factors monitored at MLO. This is proving to be a powerful research tool to assist in the tracing of air mass origins.

Aerosols

The TSI unit is a continuous-expansion CNC in which condensation occurs in a butyl alcohol vapor chamber, and single-particle counting statistics are used as a basis for the CN concentration calculation. Drift problems with the TSI started in July, and the instrument was sent for factory repair and recalibration. After the instrument was returned from the company, it displayed higher values compared with the Pollak CNC. This offset is being closely watched to see if a drift will reappear. A TSI inlet orifice cleaning procedure has been instituted once every 6-months instead of yearly as suggested by the manufacturer.

The four-wavelength nephelometer was in continuous service during the year with a minimum of downtime. The aethalometer operated consistently without interruption throughout the year and detected high values of black carbon from February through April.

Radon

The CMDL/DOE radon program completed its first year of operation in 1991, complementing the ANSTO radon monitoring begun in 1989. The new CMDL/DOE instrument experienced several problems in the early stages of its operation at MLO. For instance, unusually heavy rains in March flooded the instrument through its tower intake line, an improperly positioned phosphor screen caused occasional contamination spikes from May to October, and the paper roll mechanism jammed twice in the year.

Several short-term experiments were performed to better define the instrument background. An internal thoron contamination averaging 28 counts per 0.5 h was discovered after a series of pump-off runs and 2-h sampling runs. Radium contamination was shown to be less than one count per 0.5 h, and the instrument background averaged five counts per 0.5 h. Instrument calibrations performed with the ANSTO source gave a sensitivity of 7 mBq m^{-3} count $^{-1}$ with $\sigma = 2$.

A study of the first 100 days of operation in the winter of 1990-1991 showed that periods of high radon during nighttime downslope conditions correlated well with fast transport from Asia, as indicated by back-trajectory calculations. High-radon episodes were also correlated with high residual concentrations of CO_2 and CH_4. Asian transport episodes had radon concentrations as high as 1.2 Bq m^{-3}, and upslope events had radon concentrations reaching 0.6 Bq m^{-3}. Well-aged air had concentrations less than 0.05 mBq m^{-3}.

Solar Radiation

The solar radiation program at MLO continued with the same complement of instruments as in 1989 (see Table 1.1).

Tracking pyrheliometer no.16657 performed well; 11 active cavity comparisons were conducted throughout the year, yielding an average ratio of 1.0012 and standard deviation of 0.0064. This suggests that broadband normal-incidence solar radiation data at MLO in 1991 continued to exhibit a long-term precision of better than 1%.

Thirty-nine instrument calibrations were performed on non-MLO handheld sunphotometers in 1991. The two MLO station handheld sunphotometers were calibrated monthly. Three of four channels exhibited less than 1% drift in their extraterrestrial constants over the last 9 years; the fourth channel drifted by 12% during this time.

Discrete observations of turbidity and three-filter broadband normal-incidence measurements were greatly increased following the eruption of Mt. Pinatubo in June. Optical depths as great as 0.37 and broadband atmospheric transmission values as low as 0.77 were measured in July. During the first 100 days after the eruption, the transmission data exhibited a 19-day periodicity within a 60-day decay constant envelope.

Lidar

An expanded discussion of lidar operations and results is given in section 3.1.2.

Meteorology

There were no major changes in the meteorological observation program. The climatological monitoring of wind speed, wind direction, temperature, dewpoint, and atmospheric pressure were carried out during 1991 with few problems. Semiannual calibrations and weekly dewpoint and temperature comparisons revealed no discrepancies in the data.

Precipitation Chemistry

The MLO modified program of precipitation chemistry collection and analyses was continued throughout 1991 within the basic MLO operational routine. This program consists of a weekly integrated precipitation sample from the Hilo NWS station and the collection of precipitation event samples at MLO. Analyses of these samples are undertaken in the Hilo laboratory for pH, conductivity, and several ions, using currently available equipment.

Cooperative Programs

Table 1.1 lists long-term programs that were operated at MLO for other investigators and organizations under the heading of Cooperative Programs. Most of the listed programs are continuations from 1990 and prior years.

New programs in 1991 are those of NCAR, which began a flask sampling program for oxygen concentration analysis in April, and of the University of Rhode Island, which also began a somewhat similar biweekly oxygen flask sampling program in May. The Keeling O_2 sampling apparatus was returned to NCAR for modification in August because one of the three 5-L glass sampling flasks connected in series exploded at the air intake valve during sampling at MLO. The modified sampling apparatus installed in October has a weaker pressure pump and smaller (0.25 inch-diameter) Dekoban tubing to reduce in-line pressure. No problems have occurred with the new system.

In 1991 MLO was host to at least 178 scientists who came from no less than 11 countries to work on cooperative research projects, calibrate instruments, conduct short-term research projects, or just visit MLO "since they were in the area." NCAR conducted MLOPEX-II, a 1-month-long air chemistry experiment at MLO in September and October. As many as 25 scientists were involved in various stages of this study focused in part on the free troposphere nitrogen cycle. These programs are not listed in Table 1.1 but are included in the tally of visitors to MLO.

1.2. BARROW

D. ENDRES

1.2.1. OPERATIONS

A permanent geomagnetic observatory, separate from the USGS site, was established at the BRW site on March 21, 1991. This geomagnetic observatory was designed and established by the Naval Surface Warfare Center (NAVSWC) as a permanent facility that monitors ambient magnetic noise. In other monitoring program changes, the University of Washington installed equipment to measure precurser gases believed to be causes of summertime Arctic haze events. A special 2-mo project was started in March to provide ground-truth observations for ozone data obtained from satellites. This project was set up to answer questions that have been raised about the calibration performance and comparability of Dobson and satellite instruments operating at high latitudes.

Preliminary plans for a new CMDL observatory building in Barrow were completed in January. Conceptual plans were drafted by MASC personnel as a starting point for letting an architectual and engineering contract that would result in finished plans and construction drawings. In September an architect visited the BRW site to discuss plans and options with local contractors. By early 1992 we should receive 50% completion plans for review and modification.

Electrical power outages occurred at the observatory when the local utility company discovered problems with the city's turbine generators. The generators have a long history of improperly installed modifications that have often caused outages lasting from minutes to hours, sometimes as frequently as three times per day.

An ARCO Alaska exploratory oil rig was established offshore to the east of Point Barrow during the summer. The station is located at 71.3233°N; the test rig is at 71.3240°N. A request for information from ARCO was answered in the form of an Exploration Plan for Cabot Prospect OCS-Y-0747, filed with the Department of Interior, Minerals Management Service. No effect from this operation has been seen in the BRW data to date.

Distinguished visitors this year included Sylvia Earle, the Chief Scientist for NOAA; Walter Massey, Director of NSF;

Jerry Brown from NSF; Menghua Wei from China; and the U.S. Arctic Research Commission.

The 1979 GMC pick-up truck, in continuous service at BRW since 1979, was sold as excess property in November. It was the last of the NOAA agency-owned vehicles. A replacement GSA 1991 Chevy Blazer was acquired in July. The GSA 1985 Chevy Suburban still remains in service; plans are to replace it next year. The process of converting this station's 4-wheel drive and trucks to all GSA vehicles is now complete with a turn-over time of 4 years for each vehicle.

1.2.2. PROGRAMS

Table 1.3 summarizes the 1991 measurement programs at BRW. Operational highlights are as follows:

Carbon Dioxide

The CO_2 system ran all year with minimal down time. The large yearly cycle was noted and working gases changed to bracket the ambient air during the yearly variation. A crack in the drive gear for the strip chart recorder was replaced in August. The chart recorder was replaced with a spare from Boulder in November when the amplifier board malfunctioned. With the installation of a Siemens Ultramat 5E, the BRW CO_2 system was upgraded in September. A modified solenoid panel and updated CAMS program now enable the BRW system to sample in from two sample lines. Each line will alternately sample 25 minutes of ambient air. The working-gas switching scheme remains as before. A sample is collected from the top of the 18.3 m meteorological tower during the first 25 minutes of the hour. At the 25-min mark, a solenoid switches and a sample is collected from half way (9.1 m) up the meteorological tower. At 50 minutes the W1 gas is analyzed, and at 55 minutes the W2 gas is switched in.

Methane

The CH_4 program ran well all year. The major problem was in February when the sample lines became obstructed with ice crystals. The lines were cleared by using a high-pressure pump and forcing air backward through the lines to blow out the ice crystals, and normal air sampling continued. In August the integrator was replaced. The normal late-spring/early-summer increase in the CH_4 mixing ratio was observed. Concentrations higher than 1850 ppmv were seen during these times.

Surface Ozone

There were no major changes in the surface ozone program this year. Dasibi meter no. 1326 ran well all year; it remains the station standard and continues to define the magnitude of the annual cycle and the springtime depletion of surface ozone at BRW.

Total Ozone

The normal Dobson measurement program was supplemented with a period of high-frequency observations during March and April. The extra measurements will be used to help quantify any systematic differences that occur between the TOMS, the SBUV satellite, and Dobson observations taken at high mu during periods of high O_3 concentrations in northern latitudes. The data show that the TOMS instrument recorded values that were 2-3% lower than those obtained from the Dobson during the spring. The TOMS data were also 1% lower at BRW than at MLO during the same time period. The values obtained from the SBUV were about 4% higher than from the Dobson instrument during this same time. AD wavelength versus CD wavelength data were also examined and found to be within the expected range for high O_3.

Halocarbons and Nitrous Oxide

Several times each month the data acquisition system was locked up. The cause in each case was unknown, but the problem was always resolved by doing a powerdown reset. The printer was replaced on March 30, and a new interface card was installed in the printer on December 5. A stream selection valve in the Shimadzu GC began to leak and was replaced during the normal 6-mo site visit by Boulder personnel in June. Soon after that visit the backing screws for the valve became loose and abnormally high gas usage was noted. The screws were tightened, eliminating the leak. Other than abnormal lock ups, the system ran well all year. A set of special flask samples that are used for the LEAPS program were taken during an overpass of the NASA Airborne Arctic Stratospheric Expedition II in October. Once each month flasks are exposed for the LEAPS program in Boulder. These flasks samples are used for the analysis of halons.

Carbon Monoxide

During September Boulder personnel installed the first in situ CO gas chromatograph system for the observatories. The CO detector uses gas reduction to convert CO to CO_2 by H_2O to detect CO levels. The reaction releases H_2, which absorbs UV light in the detector and is converted to CO mixing ratios. Early data show no systematic errors.

Aerosols

The switchover from the GE aerosol counter to the TSI CNC was completed in May after a very favorable 1-year intercomparison between the two instruments. The GE CNC was returned to Boulder after being in continuous operation at BRW since May 1976.

After several episodes of condensation chamber insulation breaking off and entering the focusing cone, the TSI CNC was returned to the factory for repair. The original insulation was fibrous and easily damaged. After new insulation was installed, the TSI CNC worked well with no down time. An intercomparison was performed with a spare TSI unit from Boulder that was then sent to MLO.

The BRW aethalometer was returned to the factory in April for a factory upgrade. The upgrade included a modification to the instrument that allows it to be controlled by an external computer, in this case a Toshiba laptop. The

TABLE 1.3. Summary of Measurement Programs at BRW in 1991

Program	Instrument	Sampling Frequency
Gases		
CO_2	Siemens Ultramat 5E analyzer	Continuous
	3-L glass flasks	1 pair wk^{-1}
	0.5-L glass flasks, through analyzer	1 pair wk^{-1}
CO_2, CH_4, CO	0.5-L glass flasks, P^3 pump unit	1 pair wk^{-1}
CH_4	Carle automated GC	1 sample $(12\ min)^{-1}$
Surface O_3	Dasibi ozone meter	Continuous
Total O_3	Dobson spectrophotometer no. 91	3 day^{-1}
CFC-11, CFC-12, CFC-113, N_2O	300-mL stainless steel flasks	1 pair wk^{-1}
CFC-11, CFC-12, CFC-113, N_2O, CCl_4, CH_3CCl_3	HP5890 automated GC	1 sample $(0.5\ h)^{-1}$
N_2O	Shimadzu automated GC	1 sample $(0.5\ h)^{-1}$
CO	Trace Analytical GC	1 sample $(6\ min)^{-1}$
Aerosols		
Condensation nuclei	Pollak CNC	1 day^{-1}
	TSI CNC	Continuous
Optical properties	Four-wavelength nephelometer	Continuous
Black carbon	Aethalometer	Continuous
Solar and Terrestrial Radiation		
Global irradiance	Eppley pyranometers with Q and RG8 filters	Continuous
Direct irradiance	Tracking NIP	Continuous
	Eppley pyrheliometer with Q, OG1, RG2, and RG8 filters	Discrete
Terrestrial (IR) radiation	Eppley pyrgeometer	Continuous
Albedo	Eppley pyranometer and pyrgeometer	Continuous
Meteorology		
Air temperature	Thermistor, 2 levels	Continuous
	Max.-min. thermometers	1 day^{-1}
Dewpoint temperature	Dewpoint hygrometer	Continuous
Pressure	Capacitance transducer	Continuous
	Mercurial barometer	Discrete
Wind (speed and direction)	Bendix Aerovane	Continuous
Precipitation	Rain gauge, tipping bucket	
Cooperative Programs		
Total surface particulates (DOE)	High-volume sampler (1 filter wk^{-1})	Continuous
Precipitation gauge (USDA)	Wyoming shielded precipitation gauge, Nipher shield, Alter shield, 2 buckets	1 mo^{-1}
Magnetic fields (USGS)	Magnetometer	Continuous
Various trace gases (OGC)	Stainless steel flasks	1 set wk^{-1} (3 flasks set^{-1})
^{13}C, ^{18}O, CO_2 (CSIRO)	5-L glass flasks	1 pair $(2\ wk)^{-1}$
CO_2, ^{13}C, N_2O (SIO)	5-L evacuated glass flasks	1 pair wk^{-1}
CH_4 (Univ. of Calif., Irvine)	Various stainless steel flasks	1 set $(3\ mo)^{-1}$
Earthquake detection (Univ. of Alaska)	Seismograph	Continuous, check site 1 wk^{-1},
$^{13}CH_4$ ($^{13}C/^{12}C$) (Univ. of Washington)	35-L stainless steel flasks	1 $(2\ wk)^{-1}$
Ultralow frequency waves (Univ. of Tokyo)	Magnetometer	Continuous
UV monitor (NSF)	UV spectrometer	1 scan per 0.5 h
Magnetic fields (NAVSWC)	^3He sensors	Continuous
DMS, MSA, SO_2 (Univ. of Washington)	Sample tubes	1 set wk^{-1}

aethalometer was returned to service on May 29 and worked well all year. Episodes of high graphitic carbon amounts were noted during the springtime Arctic haze; normal values returned with the onset of summer. The nephelometer ran well all year, and only minor maintenance was required. Data from BRW show no deviation from the past record *[Ferguson and Rosson*, 1990]. Typical springtime peaks in CN and graphitic carbon were observed; both peaks are associated with Arctic haze.

Solar and Terrestrial Radiation

The solar observational year began in late January with the return of solar instrumentation from Boulder. The station's solar tracker broke down and was replaced in April

with one that required a new stand. Station personnel built the stand with parts supplied from Boulder and installed the tracker during May. No further problems were encountered with the tracker for the rest of the year. A blower ring was installed on the up-facing pyrgeometer in an attempt to keep ice off the dome. Unheated air blowing across the domed surface of the solar instruments sublimates any ice buildup and helps to keep fog from condensing on the domes. Albedo data from 1991 indicate a snow-melt date of June 15. The snow-melt date described in an article by *Dutton and Endres* [1991] is the date when albedo falls below 30%.

Meteorology

A chip was replaced in the meteorology crate when abnormally high dewpoint temperatures were noted. The blower in the dewpoint sensor was replaced when it stopped working in March. Semiannual temperature and wind calibrations were performed as scheduled in March and October. Other than power-related problems, the system ran all year. The highest hourly average winds were noted in January, and the coldest hourly temperatures were noted in February.

Cooperative Programs

All programs ran well during the year and only programs with problems or unusual occurrences are mentioned here. Fluid was changed in the USDA/SCS rain gauges in August. A new type of fluid, with ethanol/propylene glycol as a base, was used and found to be unsuitable for use in the interior of Alaska as well as the colder regions with little precipitation. During the winter the fluid freezes and any precipitation evaporates, giving abnormally low values for precipitation amounts. Automobile gas antifreeze was added on several occasions but did little to help the problem. The older fluid uses methanol and automobile antifreeze as a base.

The NAVSWC geomagnetic instrumentation consists of three ^{3}He magnetometers arranged to form two orthogonal gradiometer axes, north-south and east-west. The sensors are located 152.4 m apart to support the likely magnetic surveillance barrier configurations. The sensors and support electronics are housed in a PVC tube, which is in turn encased in a watertight fiberglass housing. RG-8 cable provides power and sends the signal to a 386 computer. Data are stored on a magnetic tape. A modem phone line is used for instant access by NAVSWC. One of the sensors was found to be noisy and was replaced in October.

The University of Washington installed pumps and mass flow controllers for the summer as part of a project investigating the cause of summertime Arctic haze. Dimethyl sulfide (DMS), SO_2, non-seasalt, and methane sulfonic acid (MSA) are thought to contribute to the haze events seen in previous years. The samples were collected in quartz tubes filled with gold wool and on Teflon filters.

In January the NO, NO_y instrument was removed by the University of Alaska at Fairbanks. The project measured levels of NO and NO_y at BRW as part of a 2-year project. Emissions of NO and NO_y from Prudhoe Bay were thought to be detected.

A UV scanning instrument was installed at the NARL facility in December 1990. BRW personnel calibrate this weekly and provide technical support in cases of malfunctioning equipment. This project is run by Biospherical Instruments Inc., with support from the National Science Foundation. The NSF spectroradiometer network is based on high-spectral-resolution scanning spectroradiometers optimized for UV irradiance measurements. Systems are currently installed at BRW, Palmer, McMurdo, SPO, and Ushuaia, Argentina. Biospherical Instruments operates these instruments and processes data for the use by various researchers. The continuing trend of ozone depletion is of concern because it increases the level of UV irradiance reaching the earth. The purpose of this network is to monitor these increases in UV irradiance for a variety of scientific investigations. After 1 full year of data collection, very few problems were noted. The internal lamp was replaced in April when the old lamp melted two coils together and changed the output of the lamp.

1.3. Samoa

C. Farmer

1.3.1. Operations

Two major events during 1991 affected the operation of the observatory. The eruption of Mount Pinatubo affected the solar radiation and Dobson spectrophotometer measurement programs, and the passage of Hurricane Val in early December affected several of the observatory programs, expecially the continuous CO_2 measurements. The stratospheric haze layer was first noticeable at the observatory on July 16. Changes in various programs associated with the haze layer are mentioned in section 1.3.2. Hurricane Val was a very destructive storm that lasted for 4 days (December 7-10). The eye of the hurricane passed over the southern end of the island, and winds reached as high as 116 mi h^{-1} at the observatory. Rainfall for the period totaled more than 381 mm; an exact total is unknown because both rainfall gauges were disrupted by the storm. The minimum pressure at the observatory was measured at 933 mb by NWS instrumentation. Destruction on the island was widespread, and the roads were partially washed out in several places, making the drive to the observatory somewhat longer than normal. Luckily, the damage at the observatory was not as serious as that from Hurricane Ofa in February 1990. The most significant damage was to the CO_2 sampling mast at the bottom of the stairs. It was a complete loss when it broke about 2.5 m above the surface. Other damage included the door and roof of the storage building, the maximum and minimum thermometer shelter, windows in the main observatory building, the tipping-bucket rain gauge, and the shelter that contained the high-volume sampler operated by EML. Damage that was noticed later, but mostly attributable to the hurricane, was excessive water leaks in the Ekto Building and problems with the backup generator that included a damaged radiator and water in the fuel system.

Several changes were made to the observatory during the year. NWS installed a meteorological tower near the Ekto Building during August and September. Information from this tower goes to the weather station in Tafuna via satellite. Some preliminary comparisons of data have occurred. The location of the tower appears not to be good for wind speed and direction measurements under some conditions. The photovoltaic array and batteries were worked on, and now all panels are again charging the batteries. The batteries for the system continue to decline. A charge equalization procedure was carried out during the year to fully charge the batteries and equalize the charge. This procedure improved the condition of most of the batteries, based on specific gravity checks. Other changes included a new photocopier for the observatory and new air conditioners for the Ekto Building.

A new chief was chosen for Tula village; rent payments are now being made directly to the chief by the station chief. During late July and August extensive periods of brownouts affected the operation of the observatory. These were caused by excessive cooking during the period of mourning (known as the fa'alavelave) for one of the very well known and liked leaders from Tula Village.

The other major occurrence during the year was the breakdown of the backup generator at the observatory. A complete overhaul was completed during January and February. The cost of the overhaul overran the initial estimate by 50%, and several months of negotiations followed in an effort to get the charges adjusted. Oil leaks showed up later in the year and were repaired by observatory personnel.

1.3.2. PROGRAMS

Table 1.4 summarizes the programs at SMO for 1991. Further descriptions of some of the programs follow.

Carbon Dioxide

There were several changes to the sampling system during the year. The water removal system at the point was modified to provide better removal of the water from the traps in February. Back-pressure regulators were installed on the sampling lines in the main building in March to eliminate variations in sample line pressure. This removed a small deviation in the signal at the time of the line switch. New station standards were received and put into use during July. A comparison of the new standards with the old standards was performed prior to returning the old set to Boulder.

The CO_2 program was most affected by the hurricane when the sampling mast at the point area was broken. Measurements were restarted immediately following the hurricane when the sample inlet was reinstalled and located at the top of the remaining portion of the sampling mast, about 2.5 m above the surface. This inlet location remained unchanged for the remainder of the year.

The flask sampling program continued throughout the year without any serious difficulties. The only change was that the regular flask sampling day was switched from Thursday to Monday.

Surface Ozone

There was a problem with condensation in the inlet line to the Dasibi ozone monitor. Moisture got into the unit itself and caused the instrument to act erratically. A heat tape was installed within the insulation and connected to a variable voltage source to provide control over the amount of heating. There was some indication that overheating of the line would cause highly variable ozone levels, possibly a result of hot spots in the heat tape. The temperature of the inlet line was kept at approximately 90°F. The only other problems encountered during the year were the power supply going out on the Dasibi unit and some minor difficulties with the chart recorder.

Total Ozone

No serious difficulties occurred with the operation of Dobson spectrophotometer no. 42 during the year. During the months of July through November special observations were made to try to obtain SO_2 levels in the atmosphere. The entire total ozone program was interrupted for a portion of August and September when the instrument was shipped to Boulder for recalibration. Dobson observations were greatly reduced in November and December as a result of the hurricane and the presence of only one staff member at the station.

Halocarbons and Nitrous Oxide

There were several changes and problems with the halocarbon and N_2O gas chromatographs. However, loss of data was kept to a minimum in most circumstances. All the changes affected both systems. New sample lines were routed from two different levels on the walk-up tower using Decabon tubing. After that, sampling was continued on the one old line and one new line for comparison. However, problems associated with a newly installed water-removal system prevented switching over to the two new lines. At year's end, the system was still being operated in that way. The new water-removal system relies on the subambient temperature within the room to cool the air and remove some of the water vapor from the air stream. The problem involves the accumulation of a fine powdery substance in the water traps that eventually plugs up the water drain. Neither identity nor the source of this substance is known. Also added to the system was a uninterruptable power supply (UPS) to keep the system from being affected so much by the regular low voltages experienced during the evening hours. This has proved to be very successful in improving the quality of the data. It has also provided a means of keeping the N_2O gas chromatograph from being offline after temporary power outages when we automatically switch to the backup generator. The other change for the year was the switch to a newly designed Nafion dryer. Several other problems affected the system in some way during the year. These include failure of the hard disk drive and power supply in the computer, bad diskettes, a shortage of argon

TABLE 1.4. Summary of Measurement Programs at SMO in 1991

Program	Instrument	Sampling Frequency
Gases		
CO_2	Siemens Ultramat 5E analyzer	Continuous
CO_2, CH_4	3-L glass flasks	1 pair wk^{-1}
	0.5-L glass flasks, through analyzer	1 pair wk^{-1}
	0.5-L glass flasks, MAKS pump unit	1 pair wk^{-1}
Surface O_3	Dasibi ozone meter	Continuous
Total O_3	Dobson spectrophotometer no. 42	4 day^{-1}
CFC-11, CFC-12, N_2O	300-mL stainless steel flasks	1 pair wk^{-1}
CFC-11, CFC-12, N_2O, CCl_4, CH_3CCl_3	HP5890 automated GC	1 sample $(h)^{-1}$
N_2O	Shimadzu automated GC	1 pair mo^{-1}
LEAPS Gases H-1301, H-1211, CFC-113, CFC-22	1-L stainless steel flasks	1 pair mo^{-1}
HCOOH, CH_3COOH, HCl, HNO_3, CH_3SO_3H	Condensation sampling with ion chromatographic analysis	Discrete
Aerosols		
Condensation nuclei	Pollak CNC	1 day^{-1}
	G.E. CNC	Continuous
Optical properties	Four-wavelength nephelometer	Continuous
Solar Radiation		
Global irradiance	Eppley pyranometers with Q and RG8 filters	Continuous
Direct irradiance	Eppley pyrheliometer with Q filter	Continuous
	Eppley pyrheliometer with Q, OG1, RG2, and RG8 filters	Discrete
Turbidity	Sunphotometers with 380-, 500-, 778-, and 862-nm narrowband filters	Discrete
Meteorology		
Air temperature	Thermistors (2)	Continuous
	Max.-min. thermometers	1 day^{-1}
Dewpoint temperature	Polished mirror	Continuous
Pressure	Capacitance transducer	Continuous
	Mercurial barometer	1 wk^{-1}
Wind (speed and direction)	Bendix Aerovane	Continuous
Precipitation	Rain gauge, weighing bucket	Continuous
	Rain gauge, tipping bucket	Continuous
	Rain gauge, plastic bulk	1 day^{-1}
	HASL Chemetrics wet-dry collector	1 day^{-1}
Precipitation Chemistry		
pH	Fisher model 805 meter	1 day^{-1} (CMDL); 1 wk^{-1} (NADP)
Conductivity	Beckman model RC-16C meter	1 day^{-1} (CMDL); 1 wk^{-1} (NADP)
Anions (NO_3^-, $SO_4^=$)	Dionex QIC ion chromatograph	1 day^{-1} (CMDL)
Cooperative Programs		
CO_2, ^{13}C, N_2O (SIO)	5-L evacuated glass flasks	3 flasks wk^{-1}
GAGE project: CFC-11, CFC-12, N_2O, CH_3CCl_3, CCl_4 (SIO)	HP5880 gas chromatograph	1 h^{-1}
Various trace gases (OGCIST)	Stainless steel flasks	3 flasks wk^{-1} (3 flasks set^{-1})
Wet deposition (NADP)	HASL Chemetrics wet-dry collector	1 wk^{-1}
Bulk deposition (EML)	Plastic bucket	Continuous (1 bucket mo^{-1})
Hi-vol sampler (EML)	High-volume sampler	Continuous (1 filter wk^{-1})
Hi-vol sampler (SEASPAN Project)	High-volume sampler	Continuous (1 filter wk^{-1})
CH_4 ($^{13}C/^{12}C$ ratio) (Univ. of Wash.)	30-L pressurized cylinder	Biweekly
Light hydrocarbons (UCI)	1-L evacuated stainless steel flasks	3-4 flasks qtr^{-1}

and methane, the failure of two valve actuators, and the breakdown of the air compressor used to activate the valve changes.

Flask air sampling continued on a weekly basis when flasks were available. Either 300-mL (weekly) or 1-L (monthly) flasks were used.

Aerosols

The aerosol program experienced a major change during the middle of the year when the nephelometer was shipped back to Boulder and it was decided that it would not be returned until the inlet problem was solved. The solution may be more than a year away. The other component of the aerosol program, the GE CNC, ran throughout most of the year, experiencing problems typical of past years.

Solar Radiation

The arrival of the Pinatubo haze increased the activity with this program. All continuous measurements were more closely monitored; e.g., the normal-incidence pyrheliometer alignment was checked twice a day and the pyranometer domes were cleaned more frequently. The filter-wheel NIP measurements were increased when possible, although the meteorological conditions somewhat hampered this activity. The sunphotometer measurements that were discontinued during the previous year were restarted for a short-time period as well.

Meteorology

The aerovane was replaced in September, and the maximum/minimum thermometers were relocated to the carport after the hurricane destroyed the shelter. The tipping-bucket rain gauge was slightly damaged when it blew over during the hurricane but was easily repaired, and the cracked plastic rain gauge was replaced after the hurricane. All other instruments performed well during the year.

Precipitation Chemistry

Daily precipitation samples continued to be collected during the year. The major change in the program is that now all analyses are being performed at the observatory. Samples are no longer being shipped to MLO for further analyses. Analyses are performed using a Dionex QIC ion chromatograph that belongs to the station chief. A Dionex AS4A separator column and a AMMS-1 micro-membrane suppressor column are being used. Standards in the range of the expected concentrations are prepared from 1000 ppm solutions.

Cooperative Programs

The cooperative program that involved the most time during the year was operation of the SIO gas chromatographs. The problems included a bad electrometer board, a contamination peak in the standard, loss of calibration gas flow, a faulty board and battery in the UPS, and water in the inlet. A site visit in September resulted in the system being completely down for about 2 weeks for repair by station personnel. The system was running well by the end of the year. Most all other programs operated without difficulty for the year. Two exceptions were the EML programs, which were affected by the hurricane. The high-volume sampler was still down at the end of the year, and the bulk deposition sample collected prior to and during the hurricane was lost. The NADP wet-dry collector had a few problems that required adjustment of the clutch, and some samples were affected when the backup generator was down.

1.4. South Pole Observatory

J. Lowell

1.4.1. Operations

The Amundsen-Scott South Pole Station is located a few hundred meters grid southeast from the geographic South Pole. It is an NSF-sponsored Antarctic research station operated year-round by scientific and support personnel. The basic station was constructed in 1974-1975, and although still usable, it is showing signs of age.

At the Amundsen-Scott station, NOAA's SPO is housed in the NSF Clean Air Facility (CAF), which is approximately 90 m upwind of the northernmost archway attached to the main station. Because the winds at the South Pole blow in a highly regular direction, a Clean Air Sector (CAS) has been designated upwind of the CAF. The winds blow 98% of the time from a predescribed area of the CAS. To maintain data integrity, the CAS is a controlled space closed to personnel, vehicles, and aircraft.

SPO operations are compressed into the short summer season: resupply, major repairs, and many scientific projects. Normally SPO "opens" on or about November 1 and "closes" on or about February 14. The rest of the year the station is in the hands of the winterover crew. With the exception of a midwinter air drop on or about June 25, there is no direct outside contact with the South Pole station and the crew.

CMDL's SPO program is supported logistically by three separate organizations: NSF, U.S. Navy, and ASA. NSF is the main-line federal agency that is currently overseeing all U.S. federally-funded operations on the continent of Antarctica. It funds and oversees both scientific projects and support operations. The U.S. Navy is contracted by NSF to staff and maintain the NSF-owned LC130 cargo planes and helicopters. The U.S. Navy gives this task to the VXE-6 Squadron located at Pt. Magoo, California. ASA is the primary contractor for all other support activities. These activities include, but are not limited to, cargo handling, cafeteria, meteorology, computer support, heavy-equipment operation and maintenance, and communications. Other stationwide ASA responsibilities are station management, station electrical requirements, plumbing, construction, etc. CAF station facilities, electrical, and carpentry needs, etc., all receive the same ASA support.

With the addition of the second 300-kW generator installed in the 1990-1991 summer season, station power for the year was excellent. In fact, only two power outages due

to station generator problems occurred all year. The CAF is a 5 m × 10 m building built in 1975-1976. Mounted on stilts, the building was and is the best design for all structures built on the polar plateau. Although the CAF has been one of the more durable structures at the South Pole, it too is showing signs of age.

The Balloon Inflation Tower (BIT) continues to be a critical facility for the CMDL balloonborne sonde projects. This year three balloon programs were run from this facility (ozone, water vapor, and backscatter); almost 100 flights were attempted. An enlargement of the cargo arch doors improved the balloon programs substantially by allowing plastic balloons to be inflated on the ground and sustain little if any damage before launch. This in turn allowed a more regular schedule to be maintained and much improved heights reached for the balloons.

Communications are maintained throughout the year using several communication satellites. E-mail, Polarmail, data transmissions, and phone calls can be made during certain times of the day when one or more of the satellites are visible over the horizon. A computer log was implemented in an effort to improve the communication between the SPO/CAF and Boulder. This electronic log consisted of three main parts: (1) a maintenance and repair log, which was kept and transmitted to Boulder biweekly; (2) a time log, which was kept for use on station; and (3) an inventory control system.

The CAMS, which has collected data since 1984, generally functioned well for the year with only a few board failures. All of these except for the meteorological A/D board were repaired with a minimum of down time.

1.4.2. PROGRAMS

Table 1.5 summarizes the programs at SPO, and Table 1.6 summarizes the statistics for the 1990-1991 winterover year. Further discussion of some of the programs follows:

Carbon Dioxide

The Seimans continuous infrared CO_2 analyzer was new this year. It replaced the URAS infrared analyzer. No problems were encountered with the new hardware. The flask sampling program continued; through-analyzer and independent outside samples were collected. The P^3 system was replaced by a modified (for cold weather) MAKS system to collect the exterior samples. The new system proved easy to operate and had much improved heat retention over the P^3.

Surface Ozone

The Dasibi meter continues to operate without any major down time. There were very few occurrences of the Dasibi-CAMS interface problem.

Total Ozone

The Dobson spectrophotometer no. 80 continued this year with a new expanded observation schedule. During the summer months all observational types that could be taken were as weather allowed. Moon observations continued as before. With the onset of the ozone depletion season, the observation schedule was started earlier (October 5). A problem with the power supply occurred during the moon observation period. Spares kept this project 100% operational. No other problems were encountered with the equipment.

Ozone Profiles

A very aggressive balloon program was attempted this year. The improvements in training, upgrading the telemetry, shifting to a digital system, and the enlargement of the cargo arch doors each helped produce a successful year. The new ozonesonde telemetry system installed is a 403-MHz system using the Vaisala radiosonde attached to the ECC ozonesonde. In general the system was reliable, simple, and easy to operate. The problem of static discharges causing radiosonde failures continues. Antistatic mats have been installed in all sonde workplaces, and the problem is much reduced over previous years. The year's final statistics were 69 successful flights out of 75 attempted.

Nitrous Oxide and Halocarbons

This program had more than its share of problems for the year. Both GC's ran well over the summer, but following closing, GC2 stopped working and was off line for the rest of the season. A significant amount of repair time was spent but no improvement resulted. GC1 worked all year at an increased sensitivity setting. Flasks were exposed on the normal summer schedule.

Water Vapor Profiles

The water vapor sondes had an on/off year. During the summer, two launches crashed; after that, all launches went well. The major problem encountered was the loss of Freon. One of the cylinders sent down at the start of the year arrived empty. This was not noticed until after closing. Two more cylinders arrived at air drop and things proceeded well. The year's final statistics were six successful flights out of eight attempted.

Aerosols

The aerosol programs ran very well this year. The nephelometer had some problems early in the year; for 2 weeks at the start of the season, the machine was off line for repairs. After that, everything worked smoothly until the end of August when the fourth channel had a problem with continuing signal dropouts. The aethalometer had sporadic problems at the start of the year. A lost program tape delayed getting this program back on line. From March on, no problems were encountered. No major problems were encountered with the TSI CNC. It replaced the GC CNC this season. The Pollak CNC had a continuing problem of unstable readings after any maintenance. After a few days, the readings return to normal.

Solar Radiation

The solar equipment all ran as expected. Continued icing problems with the lines blowing air over the domes persisted

TABLE 1.5. Summary of Measurement Programs at SPO in 1991

Program	Instrument	Sampling Frequency
Gases		
CO_2	Siemans IR analyzer	Continuous
CO_2, CH_4	0.5-L glass flasks, through analyzer	1 pair weekly
	0.5-L glass flasks, MAKS pump unit	1 pair twice mo^{-1}
Surface O_3	Dasibi ozone meter	Continuous
Total O_3	Dobson spectrophotometer no. 82	2 day^{-1}
Ozone profiles	Balloonborne ECC sonde	1 wk^{-1}, summer, autumn, winter; 1 $(3\ day)^{-1}$, spring
CFC-11, CFC-12, CFC-113, N_2O, CH_3CCl_3, CCl_4	Shimadzu automated mini-2 GCs	1 sample $(3\ h)^{-1}$
CFC-11, CFC-12, N_2O, CFC-113, CCl_4, CH_3CCl_3	300-mL stainless steel flasks	3 pair mo^{-1}, summer
CFC-11, CFC-12, N_2O, CFC-113, CCl_4, CH_3CCl_3, H-1301, H-1211, F-22, F113	850-mL stainless steel flasks	1 pair mo^{-1}, summer
Water vapor	Balloonborne sonde	9 times yr^{-1}
Aerosols		
Condensation nuclei	Pollak CNC	1 day^{-1}
	TSI CNC	Continuous
Optical properties	Four-wavelength nephelometer	Continuous
Carbon aerosols	Aethalometer	Continuous
Solar Radiation		
Global irradiance	Eppley pyranomters with Q and RG8 filters	Continuous, summer
	Eppley pyranometer with Q filter	Continuous, summer
	Net radiometer	Continuous, summer
Direct irradiance	Eppley pyrheliometer with Q, OG1, RG2, and RG8 filters	Discrete, summer
	Eppley pyrheliometer with Q and RG8 filters	Continuous, summer
Albedo	Eppley pyranometers with Q and RG8 filters, downward facing	Continuous, summer
Terrestrial Radiation		
Global irradiance	Eppley pyrgeometer	Continuous
Albedo	Eppley pyrgeometer, downward facing	Continuous
Meteorology		
Air temperature	Platinum resistor, 2- and 20-m heights	Continuous
Pressure	Capacitance transducer	Continuous
	Mercurial barometer	1 time wk^{-1}
Wind (speed and direction)	Bendix aerovane	Continuous
Frost-point temperature	Hygrometer	Continuous
Cooperative Programs		
CO_2, ^{13}C, N_2O (SIO)	5-L evacuated glass flasks	2 mo^{-1} (3 flasks $sample^{-1}$)
Total surface particulates (DOE)	High-volume sampler	Continuous (4 filters mo^{-1})
Various trace gases (OGCIST)	Stainless-steel flasks	Twice mo^{-1} (3 flasks set^{-1})
^{14}C (NOAA/ARL)	3,000 psi spheres	500 psi day^{-1}
Interhemispheric $^{13}C/^{14}C$ (CSIRO)	5-L glass flasks	1 or 2 flasks mo^{-1}
Polar stratospheric clouds (Univ. of Rome)	Optical lidar	Instrument inoperative
Polar stratospheric clouds (Univ. of Wyoming)	Balloonborne sonde	9 times yr^{-1}

TABLE 1.6. NOAA Yearly Summary Statistics for the 1990-1991 Winterover Year

Month	Dobson Obs.	Ozone Flts.	W/V Flts.	B/S Flts.	CMDL CO_2 Flasks	CSIRO Flasks	OGC Flasks	SIO Flasks	NOAA ^{14}C Spheres	DOE Filters	CMDL NOAH Flasks	Lidar Obs.
Nov. 1990	433	11/11	1/1		12	1	4/8	6	3	4	6	
Dec. 1990	264	6/6	0/2		14	1/2	10	6	2/3	4		
Jan. 1991	161	5/5	1/1		8/12	1	8	0/6	3	4		
Feb. 1991	113	4/5			10	1/2	8	15	0*	4		17
March 1991	0	4/4			16	1	10	6	3	4		7
April 1991	10	4/4			12	2	8	6	4	4		3
May 1991	123	4/6		2/2	12	1	6	6	3	4		9
June 1991	59	4/5		2/4	12	2	8	6	4	4		14
July 1991	30	4/4		1/1	14	1	8	6	3	4		10
Aug. 1991	63	5/5	1/1	2/2	12	2	8	6	3	4		15
Sept. 1991	0	7/8	1/1		12	1	8	6	3	4		7
Oct. 1991	175	11/12	2/2		12	2	8	6	3	4		10
Totals	1431	69/75	6/8	7/9	146/150	16/18	86/90	75/81	34/35	48/48	6/6	92/92
Quantity possible	100%	92%	75%	77.8%	97.3%	88.9%	95.5%	92.6%	97.2%	100%	100%	100%

W/V is water vapor; B/S is backscatter. The notation 4/8, e.g., means four successes out of eight attempts. The number possible is an estimate to derive some sort of quantity measurement.

*No spheres were exposed due to the planned move of the project to McMurdo.

all year. Several air pump failures occurred over the winter months. A side-by-side comparison with several solar radiation collectors from the Soviet Union was started this year.

Meteorology

The meteorology program ran fairly well this year. One problem with the windbird recurred during the winter. One analog-to-digital converter board did go out in October 1991. The digital storing of the data is missing, but the analog collection continued.

Cooperative Programs

Several changes in the cooperative programs occurred this year. The NSF-sponsored, BSI-operated UV-B program was transferred to the ASA contractor to run and maintain. A second science technician position was created to support this project. The structure housing the equipment was upgraded and enlarged with the addition of an attic ladder to allow access to the unit through the roof of the CAF.

The ^{14}C program was originally scheduled to be relocated to McMurdo during the summer. At the last minute the program move was canceled and reinstallation at SPO was required. Samples for 1 month were lost due to the shutdown/reinstallation of the program (February 1991).

Major changes to the University of Rome lidar occurred this year. Two persons from the URM visited the station during the summer season. They reduced the complexity of the equipment and succeeded in simplifying operations. The other major change was the addition of one of the ASA science technicians to the team conducting operations. During the NOAA balloon launches, the ASA technician operated the lidar. During the meteorological synoptic launches, NOAA personnel operated the equipment. In direct contrast to earlier years, this program ran well; there was no down time due to maintenance or repair. The optics stayed in alignment the entire year. Some trouble developed in transferring data to Rome. At the end of the year, data transfer problems still occurred regularly.

The University Of Wyoming backscatter balloon sonde experiment S-117 finished its final year at the pole. The year went well for the backscatter program; seven successful flights were made, and two not so successful flights were also attempted. One flight crashed on launch and one flight launched well, but only went up 1000 m, turned around, and floated back to the ice.

A problem with the SIO flask sampling program was noted during the winter. SIO was informed of the potential problem, but no changes were recommended.

The other cooperative programs continued as in the past and without notable incident.

1.5. REFERENCES

Bodhaine, B.A., J.M. Harris, J.A. Ogren, and D.J. Hofmann. Aerosol optical properties at Mauna Loa Observatory: Long-range transport from Kuwait? *Geophys. Res. Lett., 19(6)*, 581-584, 1992.

Dutton, E.G., and D. J. Endres, Date of snowmelt at Barrow, Alaska, U.S.A., *Arctic Alpine Res., 23(1)*, 115-119, 1991.

Ferguson, E.E., and R.M. Rosson (Eds.), *Climate Monitoring and Diagnostics Laboratory, No. 19: Summary Report 1990*, 133 pp., NOAA Climate Monitoring and Diagnostics Laboratory, Boulder, CO, 1991.

2. Carbon Cycle Division

P.P. TANS (EDITOR) T.J. CONWAY, E.J. DLUGOKENCKY, K.W. THONING
P.M. LANG, K.A. MASARIE, P. NOVELLI, AND L. WATERMAN

2.1. CONTINUING PROGRAMS

2.1.1. IN SITU CARBON DIOXIDE MEASUREMENTS

The concentration of atmospheric CO_2 was measured with continuously operating NDIR analyzers at the four CMDL observatories during 1991 as in previous years. Monthly and annual mean CO_2 concentrations are given in Table 2.1. These values are provisional, pending final calibrations of station standards. Preliminary selected daily average CO_2 concentrations for 1991 are plotted versus time for the four observatories in Figure 2.1. A striking aspect of the 1991 data was that the annual mean concentration difference between BRW and SPO remained as large as it has been since 1988. This is a striking departure from the period 1980-1987, when the difference remained close to 3.0 ppm. This year the (provisional) difference was 5.1 ppm.

Modifications to the BRW system were made in September. Air is now sampled from two parallel sampling lines on the meteorological tower, similar to the MLO and SMO systems. On September 11 the CO_2 NDIR analyzer was changed from a Hartmann-Braun URAS 2T to a Siemens ULTRAMAT 5F.

2.1.2. FLASK SAMPLE CARBON DIOXIDE MEASUREMENTS

Measurements of the global distribution of atmospheric CO_2 by flask sampling continued in 1991. Samples were collected at 32 sites of the CMDL cooperative flask sampling network (Table 2.2) and CO_2 mixing ratios were measured in the Boulder Carbon Cycle Group laboratory. Provisional annual mean CO_2 mixing ratios for 1991 and revised values for 1989 and 1990 are given in Table 2.2 and Table 2.3.

As part of the continuing effort to improve the ability of the sampling network to quantify the sources and sinks of global atmospheric carbon, we began sampling at four new sites in 1991. These are: (1) Tae-ahn Peninsula, South Korea (TAP), a coastal location downwind of the potentially large CH_4 source due to rice production in eastern Asia; (2) Qinghai Province, China (QPC), a continental high mountain location that is to become a background station as part of the Global Atmospheric Watch (GAW) program of the World Meteorological Organization (WMO); (3) Mace Head, Ireland (MHT), a coastal site that samples both North Atlantic marine air masses and air masses that have passed over Europe; (4) Izana Observatory, Tenerife, Canary Islands (IZO), an island mountain top site that samples North Atlantic, Saharan, and European air masses.

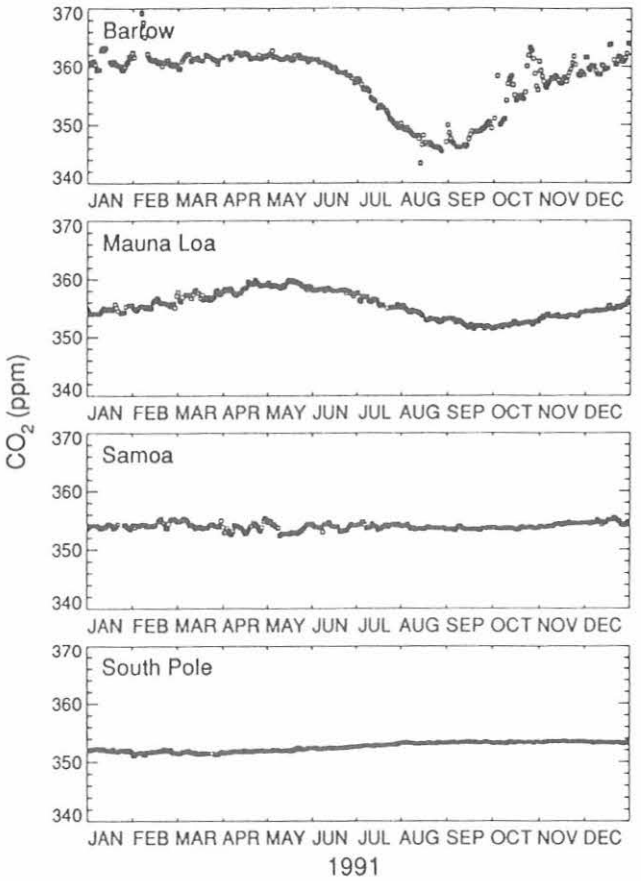

Fig. 2.1 Preliminary selected daily mean mixing ratios of CO_2 at the four CMDL observatories.

TABLE 2.1 Provisional Monthly Mean CO_2 Concentrations From Continuous Analyzer Data (ppmv, Relative to Dry-Air WMO X85 Mole Fraction Scale)

	BRW	MLO	SMO	SPO
Jan.	360.82	354.64	353.84	351.97
Feb.	362.09	355.53	354.52	351.66
March	361.16	357.05	354.17	351.50
April	361.73	358.42	353.55	351.77
May	361.52	358.98	353.48	352.03
June	359.80	357.99	353.95	352.38
July	353.69	356.07	353.91	352.81
Aug.	347.44	353.77	353.58	353.22
Sept.	348.28	352.20	353.54	353.37
Oct.	356.21	352.20	353.65	353.32
Nov.	358.34	353.64	354.26	353.46
Dec.	360.87	354.93	354.69	353.33
Year	357.66	355.45	353.93	352.57

TABLE 2.2 Provisional 1989-1991 Annual Mean CO_2 Concentrations From the Flask Network Sites

Code	Station	CO_2 (ppm) 1989	1990	1991
ALT	Alert, N.W.T., Canada	355.1	355.5	357.2
AMS	Amsterdam Island	350.5	[ ]	[ ]
ASC	Ascension Island	351.6	352.9	353.9
AVI	St. Croix, Virgin Islands	353.5	[ ]	
AZR	Terceira Island, Azores	351.0	353.2	355.8
BME	Bermuda (east coast)		355.2	356.1
BMW	Bermuda (west coast)		355.1	356.6
BRW	Barrow, Alaska	355.0	356.0	357.5
CBA	Cold Bay, Alaska	354.4	355.3	357.3
CGO	Cape Grim, Tasmania	350.3	351.5	352.8
CHR	Christmas Island	353.3	354.3	355.6
CMO	Cape Meares, Oregon	354.4	355.4	356.7
GMI	Guam, Mariana Islands	353.5	354.2	356.2
HBA	Halley Bay, Antarctica	[ ]	[ ]	[ ]
IZO	Izaña Observatory Tenerife			[ ]
KEY	Key Biscayne, Florida	354.4	356.3	356.5
KUM	Cape Kumukahi, Hawaii	352.9	354.3	355.8
MBC	Mould Bay, Canada	355.5	356.0	357.6
MHT	Mace Head, Ireland			[ ]
MID	Midway Island	354.1	355.2	357.1
MLO	Mauna Loa, Hawaii	352.8	354.1	355.6
NWR	Niwot Ridge, Colorado	353.3	354.7	355.8
PSA	Palmer Station, Antarctica	350.9	351.9	353.2
QPC	Qinghai Province, China			[ ]
RPB	Ragged Point, Barbados	352.9	354.7	355.9
SEY	Mahé Island, Seychelles	352.2	353.3	353.9
SGI	South Georgia Island	[ ]	[ ]	[ ]
SHM	Shemya Island, Alaska	354.5	355.0	356.9
SMO	American Samoa	351.7	352.8	354.2
SPO	South Pole, Antarctica	350.6	351.8	353.1
STM	Ocean Station M	354.0	354.8	356.5
SYO	Syowa Station, Antarctica	[ ]	352.2	353.3
TAP	Tae-ahn Peninsula, S. Korea			360.2

Square brackets indicate insufficient data to calculate annual mean.

TABLE 2.3 Provisional Annual Mean CO_2 Concentrations From Shipboard Flask Sampling

Latitude	1987	1988	1989	1990	1991
			Southland Star (PAC)		
30°N	349.8	352.2	353.4	354.8	356.6
25°N	349.7	351.9	353.3	354.5	356.3
20°N	349.6	351.9	353.3	355.5	356.2
15°N	349.2	352.6	354.2	354.9	356.2
10°N	349.3	352.3	353.5	355.4	356.3
5°N	349.8	352.4	353.8	355.3	356.2
0	349.3	352.3	354.0	355.1	355.9
5°S	349.7	352.2	353.5	354.9	355.5
10°S	348.6	351.4	352.9	354.2	355.3
15°S	347.5	350.4	352.5	353.4	354.3
20°S	347.7	349.7	351.5	352.7	353.9
25°S	347.4	349.7	351.2	352.6	353.6
30°S	347.5	349.8	351.2	352.8	353.5
35°S	347.7	349.6	351.2	352.1	353.5
			Wellington Star (PAW)		
30°N					356.6
25°N					356.0
20°N					356.0
15°N					355.9
10°N					356.3
5°N					355.8
0					355.5
5°S					355.5
10°S					354.8
15°S					354.5
20°S					353.8
25°S					353.6
30°S					353.7
35°S					353.7

Sampling on regular voyages of the containerships *Southland Star* and *Wellington Star* continued in 1991. In 1991 we began sampling aboard a third ship, the refined product carrier *Carla A. Hills*. This project, carried out with the cooperation of Chevron Shipping, Inc., consists of sampling at 3° latitude intervals from 3 to 21°N in the South China Sea between Hong Kong and Singapore, relatively close to the large CH_4 source due to rice production in southeast Asia. Provisional annual mean CO_2 mixing ratos for the two oldest shipboard programs are presented by latitude in Table 2.3.

Our efforts to further improve the flask sampling network include detecting the atmospheric signal of biomass burning. Potential sites for this are the Cape Verde Islands and a site in Brazil. In order to better understand the terrestrial biosphere, additional continental desert sites are also planned. Possible sites in the western U.S. deserts and the Mongolian Peoples Republic are being evaluated.

The CMDL atmospheric CO_2 data for 1981-1991 have been smoothed and combined into the 3-dimensional representation of the atmospheric CO_2 field shown in Figure 2.2. The selected data for each site have been smoothed in time using the method described by *Thoning et al.* [1989], and then the station curves were combined and smoothed in space to obtain a uniform grid at 2 week by 10° latitude intervals. For the first time we have included the shipboard data in producing this figure. This representation conveniently displays many of the major features of the global CO_2 cycle: the globally averaged secular increase in CO_2 of ~1.4 ppm yr^{-1}; the seasonality due to the northern hemispheric terrestrial biosphere; and the northern hemisphere to southern hemisphere CO_2 gradient that reverses in summer, but on an annual mean basis shows higher mixing ratios in the north than in the south. The increased difference between BRW and SPO that was seen in the continuous analyzer data, is also evident in the flask data. The preliminary data show a difference of about 4.4 ppm.

In addition to optimizing the network site distribution, we are continuing to refine the sample collection and storage methods to increase the precision and accuracy of our measurements and to obtain higher percentages of acceptable samples. In 1991, 18 sampling sites were using the 2.5-L Teflon O-ring stopcock flasks. This flask type is needed to obtain adequate precision for measurements of CO and isotopic ratios. The conversion to 2.5-L flasks will continue in 1992 and will begin to include the slow turn-around sites in the southern hemisphere that require more flasks per site.

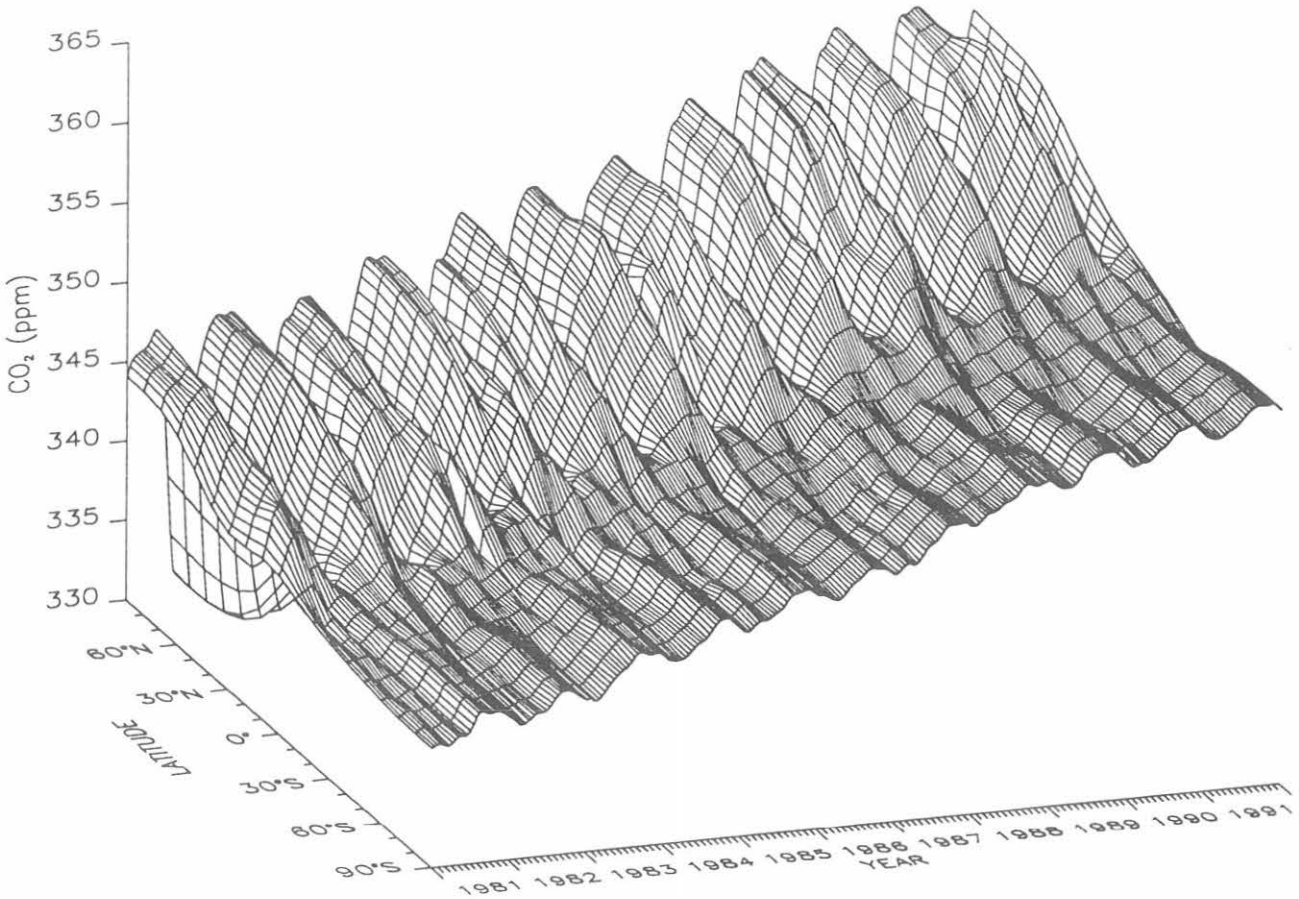

Fig. 2.2 Three-dimensional representation of the global distribution of atmospheric CO_2 in the remote lower troposphere generated by smoothing flask data collected as part of the cooperative flask sampling network. Data from the high altitude sites at MLO and NWR were not used. Smoothing is accomplished by first fitting curves to the flask data which account for the long-term trend, the seasonal cycle, and interannual variations in each. From these curves, biweekly values are extracted, and a smooth curve as a function of latitude is drawn through each set of bi-weekly values.

The deployment of the MAKS sampler (the replacement for the original P^3 sampler) was nearly completed in 1991. Thirty of the 32 sites were using MAKS samplers by the end of 1991. The remaining sites will be converted in 1992. The shipboard programs use evacuated 3-L flasks filled by simply opening the stopcocks. This method is used to simplify sample collection for the ship personnel, and sampling from ships using this method is generally effective.

Finally, to increase the probability of getting properly collected, uncontaminated air samples, we have intensified our training program. In 1991 ten sample collectors were trained in Boulder. On-site training was conducted in South Korea (TAP), aboard the *Carla A. Hills* (SCS), and in the Mongolian Peoples Republic. The flask data clearly show the benefits of this face-to-face training.

2.1.3. In Situ Methane Measurements

Quasi-continuous in situ measurements of atmospheric CH_4 were continued at BRW and MLO during 1991. The measurement apparatus consists of a custom built multi-port sampling system and a Carle Series 400 gas chromatograph (GC) with flame ionization detection (FID) of CH_4. Quantification of CH_4 is based on secondary standards that are intensively calibrated against the NOAA/CMDL primary CH_4 standards in Boulder before and after deployment at the observatories. The measurement frequency is 60 ambient air samples per day. Raw data are returned to Boulder where they are processed by a rule-based expert system [AMIE; see *Masarie et al.*, 1991]. All data obtained when the analytical system was operating less than optimally are flagged and excluded from further analysis. In 1991, 7.7% of the BRW data and 21.3% of the MLO data were flagged by AMIE. The larger percentage of flagged data at MLO has been traced to a minor problem with the integration technique used and has been corrected. In the last 3 months of the year (since the correction was made), only 6% of the data were flagged at MLO.

Daily mean CH_4 mixing ratios in ppb (1 ppb = 1 part in 10^9 by volume) for 1991 are shown in Figures 2.3*a* (BRW) and 2.3*b* (MLO). These daily means exclude all data flagged by the expert system, but they are not constrained for wind speed and direction. Local contamination, observed as large spikes in the

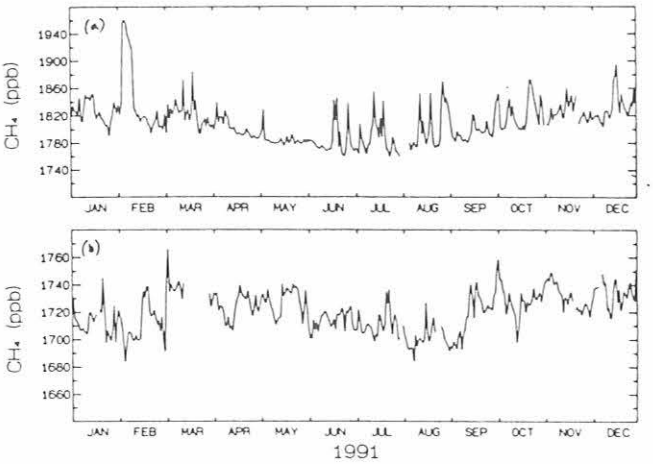

Fig. 2.3 Unselected, daily average, CH_4 mixing ratios for 1991: (*a*) BRW and (*b*) MLO. Gaps in the data are due to instrument malfunction.

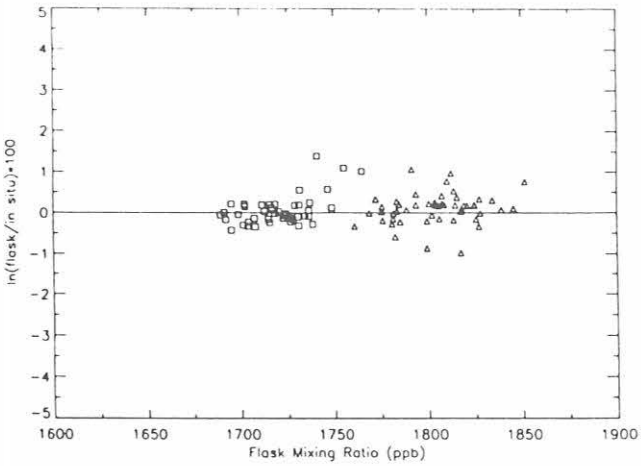

Fig. 2.4 Comparison of flask data with in situ hourly means for MLO (□) and BRW (Δ). The y-axis is equivalent to percent difference between the flask value and the hourly mean in situ value.

record, are nearly completely removed when the wind speed is constrained to a clean air sector defined as 20 to 110°. Preliminary analysis of the large CH_4 spike at the beginning of February at BRW suggests that this was an arctic haze event. The wind was predominantly from the north, and CH_4 was highly correlated with CO_2 giving a linear regression slope of 17 ppb CH_4/ppm CO_2. This value is consistent with other values obtained during arctic haze events [*Conway and Steele*, 1989].

In addition to the in situ measurements, flask samples are collected approximately weekly at BRW and MLO. Figure 2.4 is a comparison of flask samples and hourly average CH_4 values from the in situ measurement system for 1991. The ordinate axis, plotted as ln(flask/in situ) × 100 is equivalent to percent difference between the two samples. Agreement between the two data sets is excellent, with most pairs agreeing to within ± 0.5%.

2.1.4. Flask Measurements of Methane

The determination of the global distribution of atmospheric CH_4 in the remote troposphere continued in 1991 through analysis of flask samples collected as part of the Carbon Cycle Group cooperative flask sampling network. Samples were obtained approximately weekly from the 32 fixed sites and from two different commercial ships, while sampling from a third ship was begun (see section 2.1.2.). Provisional annual mean mixing ratios in ppb are shown in Tables 2.4 and 2.5. Flasks collected during 1991 have not yet been received in Boulder from Halley Bay and South Georgia Island.

The purpose of these measurements is to document trends, seasonal variations, and the spatial distribution of atmospheric CH_4 with a goal towards understanding the global CH_4 budget. Since south and southeast Asia are postulated to be significant, and yet poorly determined CH_4 source regions, the shipboard

TABLE 2.4. Provisional 1991 Annual Mean CH_4 Mixing Ratios Concentrations From the Flask Network Sites

Code	Station	CH_4 (ppb)
ALT	Alert, N.W.T., Canada	1795.3
ASC	Ascension Island	1669.4
AZR	Azores	[ ]
BME	Bermuda (east coast)	1761.7
BMW	Bermuda (west coast)	1760.4
BRW	Barrow, Alaska	1802.3
CBA	Cold Bay, Alaska	1787.9
CGO	Cape Grim, Tasmania	1651.4
CHR	Christmas Island	1678.6
CMO	Cape Meares, Oregon	1767.0
CRO	Crozet	[ ]
GMI	Guam, Mariana Islands	1718.4
HBA	Halley Bay, Antarctica	[ ]
IZO	Tenerife, Canary Islands	[ ]
KEY	Key Biscayne, Florida	1740.1
KUM	Cape Kumukahi, Hawaii	1732.9
MBC	Mould Bay, Canada	1801.7
MHT	Mace Head, Ireland	[ ]
MID	Midway Island	1751.9
MLO	Mauna Loa, Hawaii	1719.8
NWR	Niwot Ridge, Colorado	1749.6
PSA	Palmer Station, Antarctica	1652.2
QPC	Qinghai Province, P.R.C.	[ ]
RPB	Ragged Point, Barbados	1724.1
SEY	Mahe Island, Seychelles	1673.1
SGI	South Georgia Island	[ ]
SHM	Shemya Island, Alaska	1790.7
SMO	American Samoa	1661.4
SPO	South Pole, Antarctica	1652.9
STM	Ocean Station M	1788.8
SYO	Syowa Station, Antarctica	[ ]
TAP	Tae-ahn Peninsula, S. Korea	1817.0

Square brackets indicate insufficient data to calculate annual mean.

TABLE 2.5 Provisional 1991 Annual Mean CH_4 Mixing Ratios From the *Southland Star* and *Wellington Star* Shipboard Flasks

Latitude	PAC (ppb)	PAW (ppb)
35°S	1660.5	1658.3
30°S	1655.3	1654.8
25°S	1654.5	1657.1
20°S	1656.5	1658.1
15°S	1660.3	1660.9
10°S	1668.5	1663.1
5°S	1671.2	1675.0
Equator	1673.7	1675.9
5°N	1689.2	1686.7
10°N	1708.7	1716.9
15°N	1721.5	1723.7
20°N	1728.4	1739.8
25°N	1743.3	1747.5
30°N	1762.3	1757.7

samples that we have begun to collect in the South China Sea and the samples from QPC and TAP should provide exciting new data which, when combined with a model of tropospheric transport and chemistry, will provide new constraints on the global CH_4 budget.

Measurements of CH_4, CO, and H_2 continue to be made with the Carle 7 analytical system. A change in the flask analysis procedure was instituted in October 1991. Prior to that time, two aliquots were measured from one member of a pair of flasks collected simultaneously. A total of 4990 aliquots were measured in 1991 with this procedure, and the difference between corresponding aliquots was -0.08 ±3.2 ppb. A total of 1284 flasks were measured using the new procedure, where both flasks of a pair were analyzed, one aliquot each. Over many years of running the analytical systems measuring two aliquots per flask, the excellent precision of the measurements was established. We feel the additional information obtained by looking at pair agreement between flasks collected simultaneously more than compensates for the information we lose concerning the instrumental reproducibility. Monthly intercomparisons of primary standards still provide information on Carle 7 performance.

Annual mean CH_4 values for each marine boundary layer site, including shipboard data, are plotted versus sine of latitude in Figure 2.5 for 1984 through 1991. Unlike CO_2, the curves are remarkably similar from one year to the next. Evident in this plot is the strong north-south gradient demonstrating the greater CH_4 source strength in the northern latitudes, the average annual increase in the global burden of atmospheric CH_4 of 34 Tg yr^{-1}, and the homogeneity of CH_4 in the high southern latitudes. There is excellent agreement between data from shipboard (small symbols starting in 1987) and fixed sampling sites. The two sites at 13°N are reproducibly different from year to year by about 10 ppb. This difference appears to be related to differences in transport between the two sites. The Atlantic site at RPB receives air masses with more northern hemisphere influence than the Pacific site at GMI due to differences in the position of the ITCZ at these two locations. The CH_4 signal at RPB may also be influenced by biomass burning in South America. We also see an offset between the two sites in Bermuda. The two sites are separated by ~22 miles (the length of the island), but the eastern end of the island (BME) may be influenced by a higher population density there. In particular, the pumping of sewage from cesspits may lead to elevated CH_4 values even when the wind is blowing off the ocean (D. Connelly, private communication).

The global distribution of atmospheric CH_4 in the marine boundary layer is shown in Figure 2.6. The grid spacing is 10° in latitude and 2 weeks in time. This 3-dimensional distribution is generated by smoothing the flask data in time and latitude. It assumes no variation in CH_4 mixing ratio with longitude. This is a somewhat safe assumption in the southern hemisphere, but in the northern hemisphere, particularly in continental areas close to strong sources of CH_4 [see *Fung et al.*, 1991], this assumption breaks down. Based on the modeling study of *Fung et al.* [1991], longitudinal gradients up to 3% may exist, but the CH_4 "hot spots" cover relatively small geographical regions. They have only a relatively small effect on the zonally averaged values shown in Figure 2.6.

Figure 2.6 is a smoothed representation of the flask data, and its validity relies on the methods used to smooth the flask data in time and latitude. The ability of Figure 2.6 to properly represent our flask data has been evaluated by calculating the difference between actual flask values and their corresponding values interpolated from the grid for the appropriate day and latitude. The result is shown in Figure 2.7, where the mean difference is 0.6 ± 13.7 ppb. There is significantly more scatter in the northern hemisphere which is in agreement with our observations from individual sampling sites there. This comparison gives us confidence that Figure 2.6 is an accurate representation of our data, and that this grid may be used when comparing NOAA/CMDL methane data to other data sets.

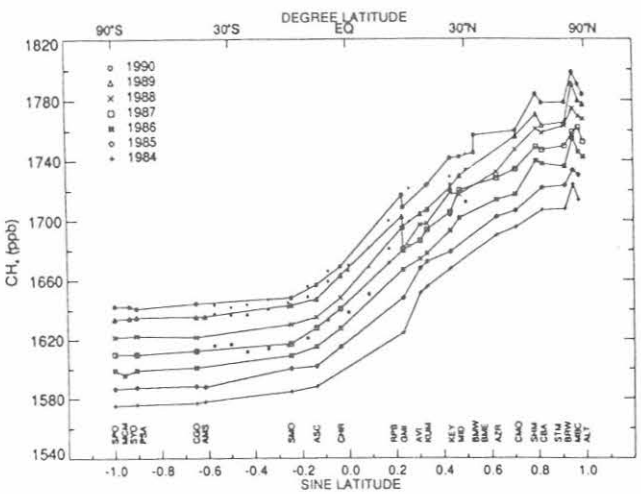

Fig. 2.5 Latitudinal distribution of the annual mean CH_4 mixing ratio for 1984-1991. Annual means are determined from flask samples. Data from the high altitude sites MLO and NWR are excluded. The small symbols denote shipboard data from the *Southland Star* and the *Wellington Star*.

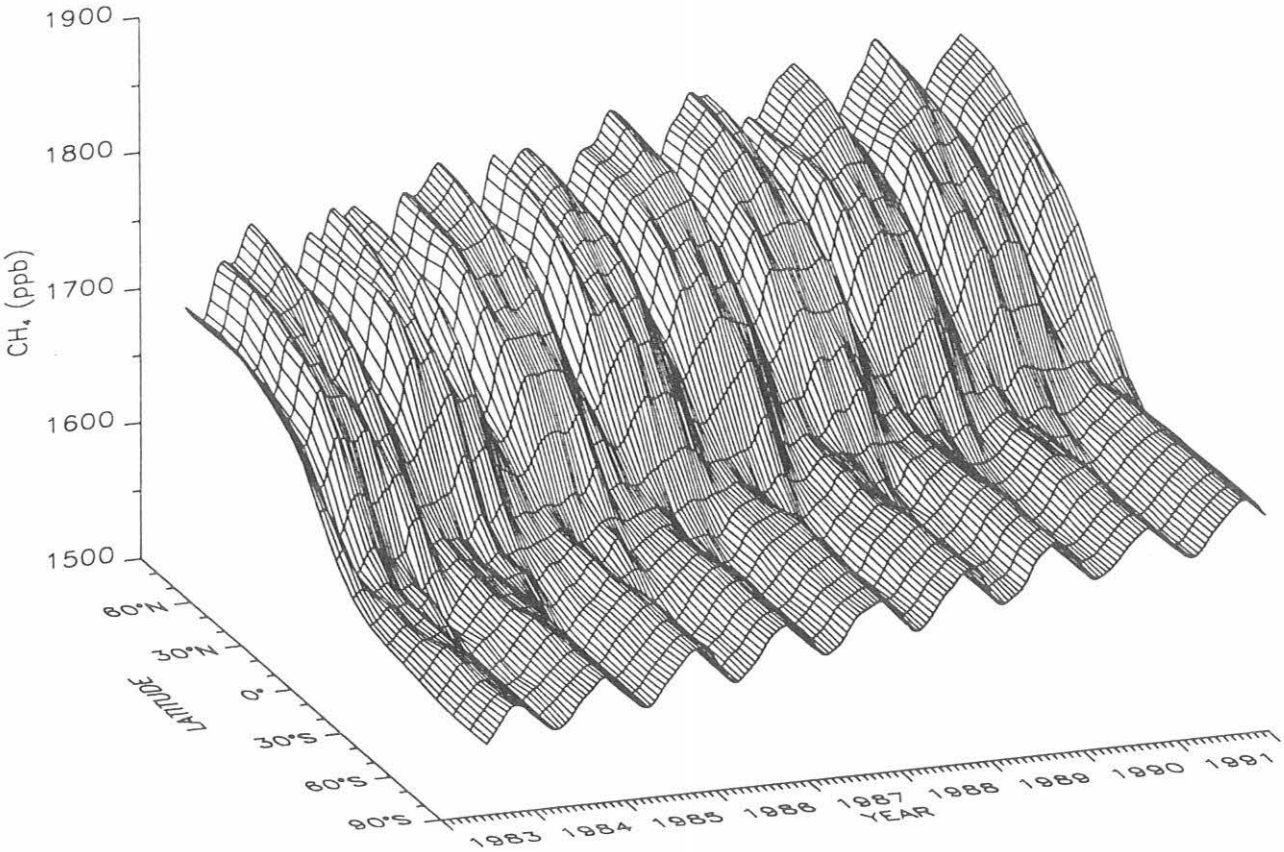

Fig. 2.6 Three-dimensional representation of the global distribution of atmospheric CH_4 in the remote lower troposphere, generated in a way similar to Figure 2.2.

The data in Figure 2.6 have been averaged using proper weighting factors to determine hemispheric annual means, and these are shown graphically in Figure 2.8. The plot indicates that the interhemispheric difference has increased over the period of the measurements, suggesting that the northern hemisphere growth rate has been larger than the southern hemisphere growth rate. The decrease in the interhemispheric gradient in 1989 followed by a recovery in 1990 appears to be related to the La Niña event of that time. During La Niña events, meteorological conditions are conducive to enhanced transport between hemispheres [see *Prinn et al.*, 1992]. Remembering that CH_4 mixing ratios are always larger in the northern hemisphere, any enhanced exchange of air between the hemispheres will decrease the interhemispheric difference. The interhemispheric difference recovered in 1990, because the normal exchange time between hemispheres of about 1 year restored the original quasi-steady-state distribution with latitude.

2.1.5. In Situ Carbon Monoxide Measurements

In September 1991, a Trace Analytical Reduction Gas Analyzer (RGA) was installed at BRW to measure CO mixing ratios. The RGA was configured to make quasi-continuous measurements of CO at a frequency of approximately 20 measurements per hour. The analysis of CO by this instrument is based upon the chromatographic separation of atmospheric trace gases and the subsequent reaction of reduced gases such as CO and H_2 with hot mercuric oxide (HgO) contained in a stainless steel "bed" ($CO + HgO \rightarrow CO_2 + Hg$). The elemental mercury generated by this reaction is detected by resonance absorption. Control of the analytical and data retrieval systems are initiated by a program residing in a HP3396B integrator which commands actions of a HP3421A Data Acquisition and Control System through HPIL/HPIB communications. Air samples are introduced to the instrument through one of two alternating intake lines, a two-port eight-position valve introduces an air sample or one of two standards to the 3 cm^3 sample loop. The analysis requires about 3 minutes. Chromatographic data is stored on a diskette. In Boulder, Colorado, mixing ratios were calculated from the raw data using a two-point, linear calibration scheme. Standards were referenced to the NOAA/CMDL CO standard scale (prepared by gravimetric methods and described in detail by *Novelli et al.* [1991]). All CO mixing ratios presented here are reported in units of parts per billion (ppb) by mole fraction in dry air. Precision of the instrument, as estimated from the ratio of the

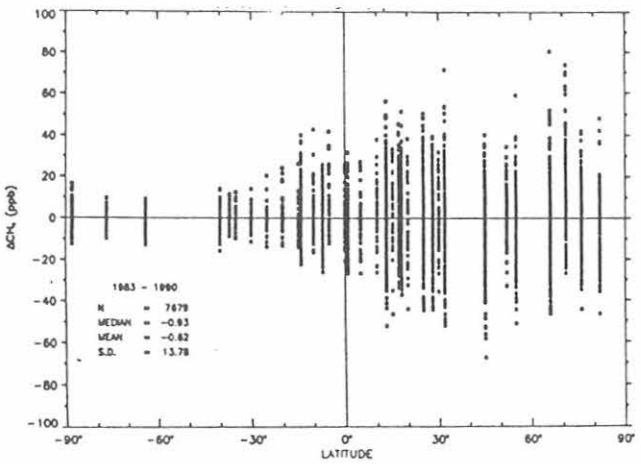

Fig. 2.7 Comparison of network flask data to the CH_4 surface in Figure 2.6.

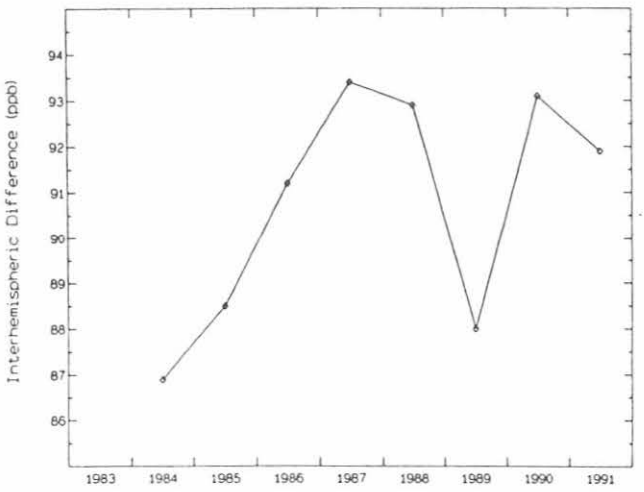

Fig. 2.8 Difference between the annually averaged CH_4 mixing ratio in the northern and southern hemispheres.

two standards over periods of several hours, was approximately 0.5 ppb.

Hourly averaged CO mixing ratios from September to December 1991 are shown Figure 2.9*a*. The data have not been constrained for wind speed or direction. CO mixing ratios over the period of study show a gradual increase punctuated by periods of higher CO levels and short term variability. Mixing ratios in September were approximately 100 ppb, compared to December levels of about 175 ppb. Three periods of elevated CO suggesting synoptic events are evident in the time series: in late October, mid-December, and again at the end of December. Each of these events is reflected in the hourly-averaged record of CH_4 measured in situ at BRW (Figure 2.9*b*). This suggests a common source for the two gases. However, there are events in the CH_4 record, most notably two events in early-mid October and a period of elevated variability in November, that are not

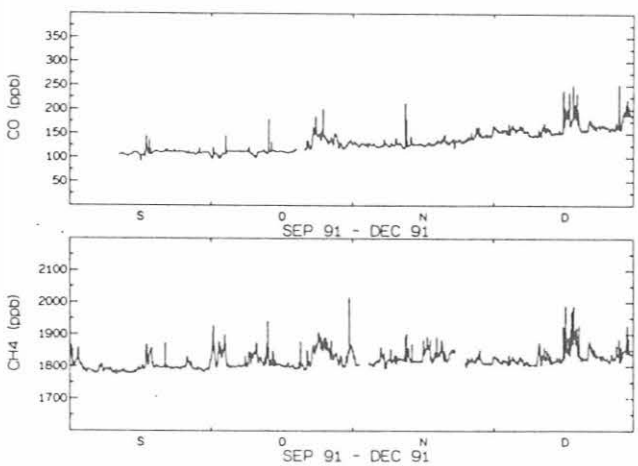

Fig. 2.9 (*a*) Hourly average CO mixing ratios measured in situ at BRW in units of ppb by mole fraction in dry air. (*b*) Hourly average CH_4 mixing ratios measured in situ at BRW in units of ppb by mole fraction in dry air.

correlated with CO levels. This suggests that while the sources of high CO usually occur in air parcels having high CH_4, there may be a source of CH_4 influencing BRW which does not contain high CO.

2.1.6. FLASK MEASUREMENTS OF CARBON MONOXIDE

CO mixing ratios were measured in a subset of flasks collected as part of the cooperative flask sampling program. Measurements were made only in air from sites where glass flasks with Teflon O-ring stopcocks were used. Table 2.6 provides the sites where CO was measured in 1991 and the date of the first sample. Analysis of air for CO and H_2 were made on a semi-automated trace analytical RGA. This instrument shared a common flask sampling carousel, data collection and analysis system, and a valve switching control with a Carle gas chromatograph used for flask measurements of CH_4. From January 1 to September 20, two aliquots of air from a single flask were analyzed; after that date one aliquot of air from each of two simultaneously collected flask samples were analyzed. This approach, long used for CO_2 analysis, is believed to permit better estimation of the uncertainties associated with the complete air collection and analysis procedure—rather than solely an estimate of analytical precision as represented by analysis of two aliquots from a single flask. CH_4, CO and H_2 analyses used a common reference gas. Each sample analysis was bound before and after by analysis of the standard gas. This reference gas, identification number AAL-17269, was filled at Niwot Ridge with chemically-dried air and was calibrated against the primary CMDL CO standards. H_2 was referenced to an arbitrary scale awaiting the preparation of accurate standards. The precision of the CO method, estimated as the difference of mixing ratios determined for each flask in a simultaneously collected pair of flasks, was 1 ppb or better.

TABLE 2.6. Locations of Flask Sites Used for CO Analyses

Code	Station	Month/Year of first Sample*
ASC	Ascension Island	Feb. 1989
BWE	Bermuda (East)	June 1991
BWE	Bermuda (West)	July 1991
BRW	Point Barrow, AK	July 1988
CGO	Cape Grim, Tasmania	June 1991
CHR	Christmas Island	Dec. 1989
GMI	Marianas Island, Guam	Oct. 1989
IZO	Izana, Tenerife	Nov. 1991
KEY	Biscaine, FL	Aug. 1991
KUM	Cape Kumukahi, HI	June 1989
MHT	Mace Head, Ireland	June 1991
MLO	Mauna Loa, HI	July 1989
NWR	Niwot Ridge, CO	Dec. 1988
QPC	Qinghai Province, China	July 1991
SEY	Seychelles	Sept. 1990
SMO	Samoa	Sept. 1988
TAP	Tae-ahn Peninsula, Korea	Nov. 1990

*Month in which air samples were first collected in a glass flask fitted with Teflon O-ring stopcocks and analyzed for CO.

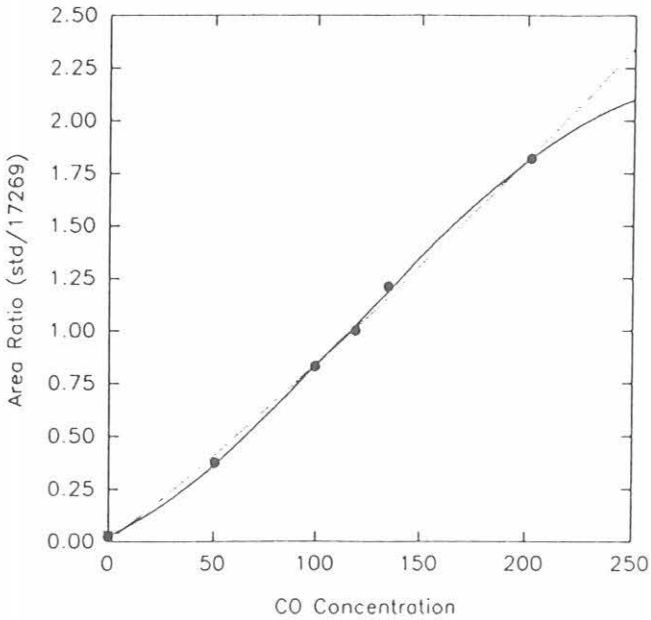

Fig. 2.10 Carbon monoxide calibration curve determined on the combined CO/CH_4 analysis system used for analysis of flask samples. Instrument response is expressed as the ratio of the area response of the standards used to generate the curve to that of one standard (AAL-17269). The solid line is a third-order polynomial fit to the data; the dotted line is a quadratic fit.

The response characteristics of the CO instrument were evaluated by running a series of standards with CO mixing ratios (50-200 ppb) in the range of background tropospheric levels. At least ten aliquots from each of five standards and one sample of zero air were analyzed for CO. One of these standards was AAL-17269. The mean area responses of the standards were then divided by that of AAL-17269. It was clear the response characteristics for this instrument were non-linear (Figure 2.10) and the CO mixing ratios needed to be calculated using a multi-point calibration curve. We have observed, as have other researchers who use this instrument for measuring CO, that non-linear responses are common and appear to be HgO bed dependent. The area response ratio data were fit with both a quadratic and a third-order polynomial curve (Figure 2.10). These calibration curves served as the basis of the approach used to calculate mixing ratios. The data from eight calibration experiments performed between March 1991 and March 1992 were pooled and used to generate time-averaged second- and third-order polynomial curves. The coefficients from the mean curve were used to calculate flask CO mixing ratios. For a given area response, the mean value of the mixing ratios calculated using each of the eight individual curves varied by less than 1% among themselves. Mixing ratios calculated with the mean curve parameters also differed less than 1% from the mean value from the individual calibration curves. The very small variation between curves indicates it is appropriate to calculate mixing ratios using time-averaged curve fit parameters.

Preliminary CO mixing ratios measured in flask samples were determined by first calculating the ratio of the sample area response to the mean response of the standard analyzed immediately before and after it. Using the calibration curve and these ratios, a mixing ratio for each sample was calculated by an iterative approach that uses the quadratic function to estimate the first approximation to the CO concentration. Because standards above 200 ppb were not used for the calibration curves, it was necessary to calculate mixing ratios above this level using the quadratic fit only.

In 1991 CO mixing ratios at BRW were measured in air collected weekly in 2.5-L glass flasks. The preliminary time series data are shown in Figure 2.11. A dramatic seasonal cycle is evident, with highest CO levels in the winter and lowest in summer. Seasonal cycles of trace gases are caused by the temporal imbalance of their sources and sinks. The changes in CO at BRW reflect, in part, the rate of CO oxidation by hydroxyl (OH) radical (CO + OH ---> CO_2 + H). This reaction accounts for most of the loss of CO in the troposphere. The lifetime (τ) of CO can be calculated as $\tau = (k[OH])^{-1}$, where k is the first order reaction rate constant ($k_{(298\ K,\ 1\ atm)} = 2.39 \times 10^{-13}$ cm^3 $molecule^{-1}$ s^{-1}, calculated from data presented in *NASA*, 1987 and [OH] is the concentration of hydroxyl radical. Using a cubic spline fit to the model-derived OH data presented in *Spivakovsky et al.* [1990], we estimated seasonal OH levels at our flask sampling sites. At BRW the calculated average lifetime for a CO molecule in January is on the order of thousands of years, in April it is 8 months, in July 1.7 months, and in October the lifetime is again on the order of many years.

One test of the accuracy of the CO data discussed above is by comparing measurements made using different approaches. The flask data were measured in Boulder using discreet air samples after about 1 week of storage, and mixing ratios were calculated using a multi-point curve fit. In contrast to the flask samples, in situ CO mixing ratios were drawn into the sample loop off a tower intake line and were immediately analyzed; mixing ratios

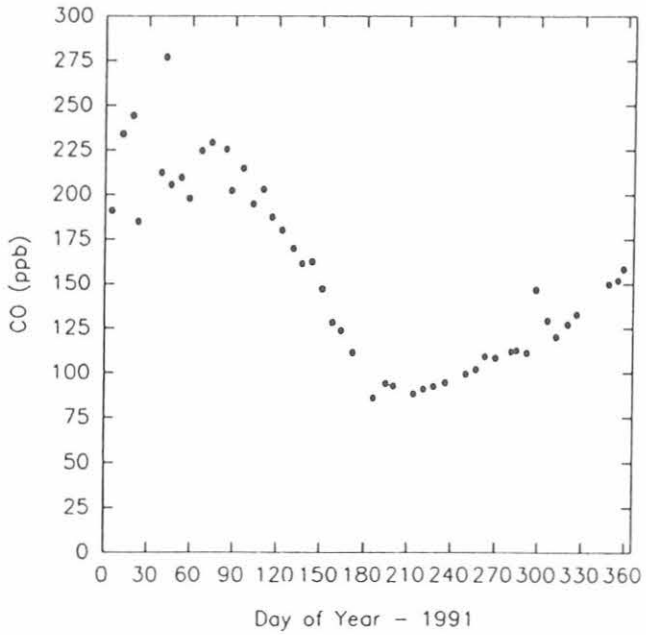

Fig. 2.11 Time series of preliminary CO mixing ratios measured in air collected at Point Barrow using 2.5-L glass flasks. Mixing ratios were calculated as described in the text and are reported in units of ppb by mole fraction in dry air.

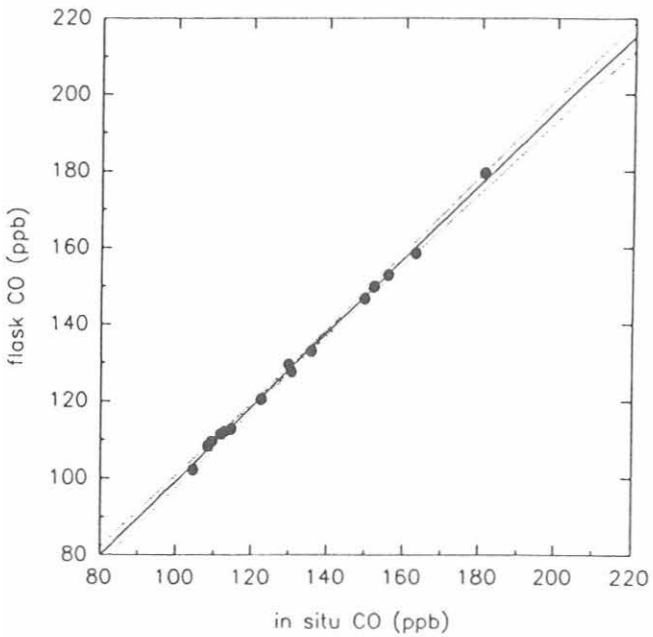

Fig. 2.12 Scatter plot of CO mixing ratios measured in flask samples collected at BRW to those determined using the in situ analyzer. The best fit linear regression to the data is Y = 0.98 (±0.02) X + 2.42 (±0.34), where X = mixing ratio measured in situ, and Y = mixing ratio determined in flask sample. Dotted lines represent the 95% confidence intervals.

were calculated using a two-point calibration. Figure 2.12 presents a scatter plot of preliminary CO mixing ratios measured in air collected in flask samples versus air analyzed in situ at the time of flask sample collection. A linear regression fit to the data indicates that within the measurement uncertainity there was no difference between the two data sets. The high correlation of the two independent data sets (r^2 = 0.996) suggests the high quality and accuracy of the measurements.

During 1991 a complete year of flask measurements were made at 10 sites (Table 2.6). The preliminary annual mean CO mixing ratios at these stations are presented in Table 2.7. The annual mean mixing ratios were calculated by first averaging the aliquots from a single sample or pairs of samples. From these values the monthly mean CO mixing ratio was determined, and these monthly means were used to calculate the annual mean. For comparison, when available, annual mean values for previous years are presented. The uncertainty of the mean value is approximately 1.5%.

The preliminary 1991 mean CO_2 mixing ratios measured at CMDL flask sites are shown as a function of latitude in Figure 2.13. The general trend in mixing ratios is a decrease from north to south. However, regional influences are noted at some stations. Annual mean CO levels at ASC (7°S) and SEY (4°S) are somewhat greater than would be predicted from levels observed at stations to the north and south (SMO and CHR). At ASC, this apparent elevation of CO probably reflects, in part, the transport of effluent from biomass burning in Africa, which are expected to reach ASC during September and October [*Fishman et al.*, 1991]. At SEY, a site in the northern Indian Ocean, transport during the austral spring and summer from the Indian subcontinent elevates CO levels. Mixing ratios in the winter were lower: 50-70 ppb.

The mean annual CO mixing ratio at TAP is quite high compared to stations to the north and south. CO levels at TAP (36°N) are much greater than those observed at NWR (40°N). TAP is located on the Korean peninula and is clearly effected by regional anthropogenic trace gas sources. Elevated levels of CH_4 and CO_2 have also been observed at this location.

TABLE 2.7. Preliminary 1991 Annual Mean CO Mixing Ratios: Comparison to Previous Years*

	Arithmetic Annual Mean CO Mixing Ratios		
Site	1989	1990	1991
BRW	156.9	153.0	151.0
NWR	125.2	120.5	128.2
TAP			230.6
KUM		109.9	108.9
MLO		101.6	100.0
GMI		104.9	110.0
CHR		79.6	77.8
SEY			88.6
ASC	82.8	86.2	84.6
SMO	64.8	64.6	68.3

*Mean annual CO mixing ratios were calculated as described in the text. Units are ppb by mole fraction.

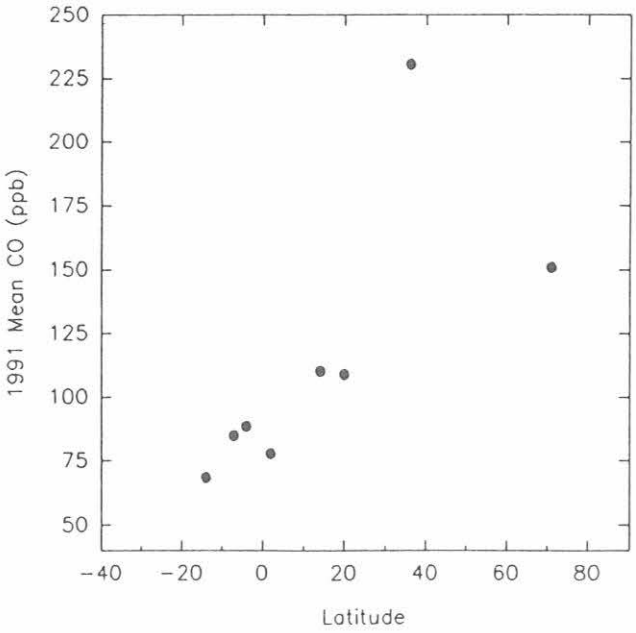

Fig. 2.13. Preliminary annual mean CO mixing ratios plotted as a function of latitude.

2.2. Reference Gas Standards

The calibrations of CO_2-in-air reference gas tanks continued in 1991; on 121 days, 258 tanks were calibrated. One-hundred and eight high-pressure cylinders were filled at NWR in 1991 with dry air for use as reference standards. The set of 15 reference gases stored in large aluminum cylinders and which will eventually become the NOAA/CMDL primary CO_2 standards were sent to the SIO for calibration in 1991.

Construction of a system for making manometric measurements of the mole fraction of CO_2 in standard gases continued in 1991. Extensive modifications to the system were made. The original 12-L sample volume was replaced with a 6-L volume in order to decrease the amount of time needed to extract the CO_2 from the air sample in the system. Possible linearity and calibration problems with the pressure gauges were observed. These gauges will be calibrated using a dead weight pressure gauge purchased by the Carbon Cycle Group in 1992.

2.3. Special Projects

Four continuous CO_2 analyzer systems were built for the AOML and PMEL NOAA laboratories under a cooperative arrangement with CMDL. These systems will measure both atmospheric CO_2 and the CO_2 partial pressure (pCO_2) of the surface water during expeditions conducted by these laboratories on NOAA ships. CMDL also provided CO_2 reference gases and calibrations for that purpose.

2.4. References

Conway, T.J., and L.P. Steele, Carbon dioxide and methane in the Arctic troposphere, *J. Atmos. Chem., 9*, 81-99, 1989.

Fishman, J., K. Fakhruzzaman, B. Cros, and D. Ngarga, Identification of widespread pollution in the southern hemisphere deduced from satellite analysis, Science, 252, 1693-1696, 1991.

Fung, I., J. John, J. Lerner, E. Matthews, M. Prather, L.P. Steele, and P.J. Fraser, Three-dimensional model synthesis of the global methane cycle, *J. Geophys. Res., 96*, 13,033-13,065, 1991.

Masarie, K.A., L.P. Steele, and P.M. Lang, A rule-based expert system for evaluating the quality of long-term, in situ, gas chromatographic measurements of atmospheric methane, *NOAA Tech. Memo. ERL CMDL-3*, 37 pp., NOAA Climate Monitoring and Diagnostics Laboratory, Boulder, CO, 1991.

Novelli, P.C., L.P. Steele, and J.W. Elkins, The development and evaluation of a gravimetric reference scale for use in measurements of atmospheric carbon monoxide, *J. Geophys. Res., 96*, 13,109-13,121, 1991.

NASA, Chemical kinetics and photochemical data for use in stratospheric modeling, Evaluation number 8, *JPL Publication 87-41*, 196 pp., California Institute of Technology, Pasadena, California, 1987.

Prinn R., D. Cunnold, P. Simmonds, F. Alyea, R. Boldi, A. Crawford, P. Fraser, D. Gutzler, D. Hartley, R. Rosen, and R. Rasmussen, Global average concentration and trend for hydroxyl radicals deduced from ALE/GAGE Trichloroethane (methyl chloroform) data for 1978-1990, *J. Geophys. Res., 97*, 2445-2461, 1992.

Spivakovsky, C.M., R. Yevich, J.A. Logan, S.C. Wofsy, and M.B. McElroy, Tropospheric OH in a three-dimensional chemical tracer model: An assessment based on observations of CH_3CCl_3, *J. Geophys. Res., 95*, 18,441-18,471, 1990.

Thoning, K.W., P.P. Tans, and W.D. Komhyr, Atmospheric Carbon Dioxide at Mauna Loa Observatory 2. Analysis of the NOAA GMCC Data, *J. Geophys. Res. 94*, 8549-8565 (1989).

3. Aerosol, Radiation, Ozone, and Water Vapor Division

J. OGREN (EDITOR), B BODHAINE, J. DELUISI, E. DUTTON, R. EVANS, R. GRASS, J. HARRIS, D. HOFMANN, W. KOMHYR, D. NELSON, , AND S. OLTMANS

3.1. CONTINUING PROGRAMS

3.1.1. SURFACE AEROSOLS

Operations

The aerosol monitoring program at BRW, MLO, SMO, and SPO continued during 1991 as in previous years. CN concentration was measured continuously with TSI (butanol-based) CN counters at BRW, MLO, and SPO, and with a G.E. CN counter at SMO. Daily calibration points were provided by Pollak CN counters at all stations. TSI CN counters have been operated at BRW since March 1990, MLO since May 1988, and at SPO since January 1989. A TSI CN counter will be installed at SMO in 1992. Aerosol scattering extinction coefficient (σ_{sp}) at the 450-, 550-, 700-, and 850-nm wavelengths was measured continuously at each station with a four-wavelength nephelometer. Aerosol absorption coefficient has been measured continuously using aethalometers at BRW since April 1988, MLO since April 1990, and at SPO during December 1986-December 1991. A more sensitive instrument for measuring aerosol absorption will be developed for use at SPO. There are currently no definite plans for measuring aerosol absorption at SMO.

Figure 3.1 shows daily geometric means of CN concentration (lower portion of each plot), σ_{sp} (middle portion of each plot), and Ångström exponent (upper portion of each plot) at the CMDL stations for 1991. Two independent values of Ångström exponent (α) were calculated from the 450, 550, and 700-nm channels of σ_{sp} data using the relation

$$\alpha = -\frac{\Delta \log \sigma_{sp}}{\Delta \log \lambda}$$

where α is Ångström exponent and λ is wavelength. Previous *Summary Reports* showed all four wavelengths of σ_{sp} data; however, this report shows only daily and monthly averages of the three shortest wavelengths in order to improve the presentation of α. These averages are calculated only if data for all three wavelengths are available. The interpretation of α in terms of aerosol size distribution was discussed by *Bodhaine and DeLuisi* [1985]. Monthly geometric means of the 1991 aerosol data are listed in Table 3.1. A graphical presentation of the monthly geometric means of the entire data record for the four stations is shown in Figure 3.2. Because of instrument problems at SMO, CN and σ_{sp} data are missing for part of the year. The SMO nephelometer operation will be resumed in the future after a new aerosol intake system has been designed and installed.

Discussion

The BRW data in Figure 3.1 show a σ_{sp} maximum of about $3 \times 10\text{-}5$ m^{-1} during winter and spring, typical of the well-known Arctic Haze. The peak normally occurs in March; however, because of missing data during that month, it is not known when the actual springtime peak occurred. Minimum values of σ_{sp} below 10^{-6} m^{-1} occurred in June. The BRW long-term record shown in Figure 3.2 clearly shows this annual cycle in σ_{sp}, with springtime monthly means exceeding 10^{-5} m^{-1} and summertime monthly means below about 10^{-6} m^{-1}. The BRW CN record shows a more variable semiannual cycle with a maximum that usually coincides with the maximum in σsp, and another maximum in late summer or early fall. The secondary maximum in late summer is thought to be caused by local oceanic emissions of DMS gas that are eventually converted to sulfate aerosol [*Radke et al.*, 1990]. The annual mean for CN is 152 cm^{-3} and the annual mean for σ_{sp} (550 nm) is $3.76 \times 10\text{-}6$ m^{-1}. Note that the G. E. counter CN record is shown as a solid line and the TSI counter CN record is shown as a dashed line. The individual squares plotted on the CN graph are monthly means of Pollak counter observations. These are shown separately because the TSI and Pollak counter give independent data sets, whereas the G. E. counter was calibrated using the Pollak counter data. The BRW data set was presented by *Quakenbush and Bodhaine* [1986].

The MLO σ_{sp} data shown in Figure 3.1 are fairly typical with the highest values in March, April, and May, and lower values in fall and winter. Large events in the springtime, caused by the long-range transport of Asian desert dust in the upper troposphere to the vicinity of Hawaii, dominate the record. As discussed in the *1988 Summary Report* [*Elkins and Rosson*, 1989], σ_{sp} values have been generally higher since the installation of the new nephelometer in 1985 and have not reached the low values expected in winter. The increasing trend in σ_{sp} at MLO is obviously caused by higher winter values in the latter part of the record and the reason is believed to be instrumental. The MLO CN record shown in Figure 3.1 is fairly typical, giving an annual geometric mean concentration of 190 cm^{-3}; the annual mean of σ_{sp} (550 nm) is $9.74 \times 10\text{-}7$ m^{-1}. Note that all MLO aerosol data presented here are in the form of geometric means during

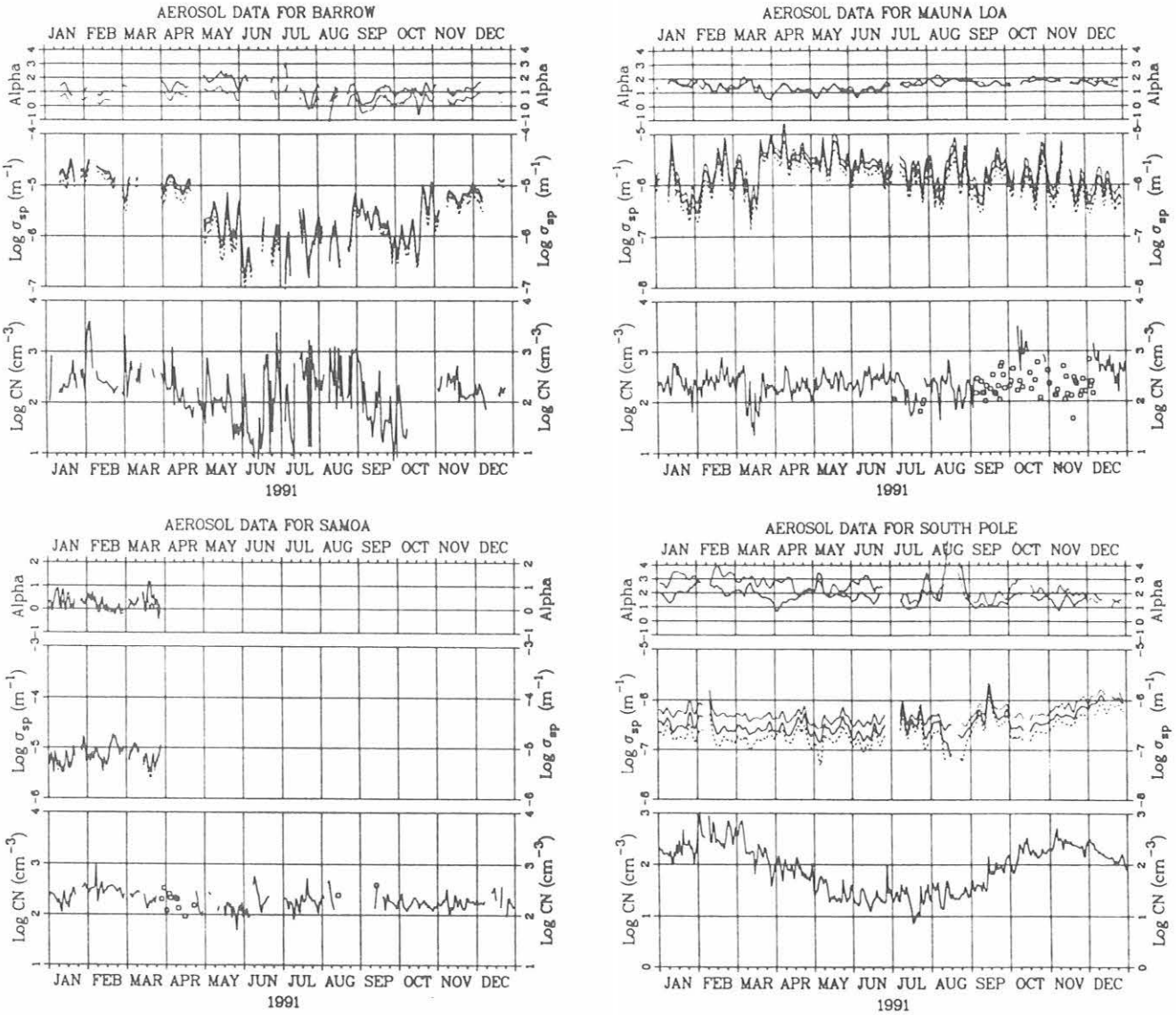

Fig. 3.1. Daily geometric means of σsp and CN data at BRW, MLO, SMO, and SPO for 1991. Data for MLO are included only for 0000-0800 LST. For each station, CN concentration (lower) is shown as a solid line, and daily mean Pollak counter data are shown as small squares. σ_{sp} data (middle) are shown for 450 (dotted), 550 (solid), and 700 nm (dashed). Ångström exponents (Alpha) were calculated from 450- and 550-nm (dotted), and 550- and 700-nm (solid) σ_{sp} data.

0000-0800 HST (1000-1800 UT) in order to include data for nighttime downslope wind conditions only. The MLO data set was presented by *Massey et al.* [1987].

The SMO σ_{sp} and CN data continue as in previous years with no significant annual cycle or long-term trend. The SMO 1991 annual means are about 197 cm^{-3} for CN concentration and about 7.34×10^{-6} m^{-1} for σ_{sp} (550 nm), representative of the background marine boundary layer in that region. The SMO nephelometer was removed from service at the end of March, therefore, the annual mean is not representative of the entire year. A detailed analysis of the entire SMO data record was presented by *Bodhaine and DeLuisi* [1985].

The SPO σ_{sp} and CN data are shown in Figure 3.1. These data show a strong annual cycle reaching a maximum of about 300 cm-$^{-3}$ in the austral summer and a minimum of about 10 cm^{-3} in the winter, similar to previous years. The σ_{sp} data show fairly clean values in the fall, events due to the transport of sea salt particles in July and September, and a general increase in the spring. Referring to the long-term data set for SPO shown in Figure 3.2, the σ_{sp} data generally show intermediate values in the austral summer and fall, and large events, sometimes exceeding 10-6 m^{-1}, in late winter. These large

TABLE 3.1. Monthly Geometric Means of CN concentration (cm^{-3}) and σ_{sp} (m^{-1}) at 450, 550, and 700 nm for BRW, MLO, SMO, and SPO During 1991

	Jan.	Feb.	March	April	May	June	July	Aug.	Sept.	Oct.	Nov.	Dec.
						BRW						
CN	283	354	365	138	84	54	172	357	77	51	169`	164
σ_{sp} (450)	1.78-5	1.81-5	1.30-5	8.85-6	2.27-6	1.05-6	1.04-6	1.23-6	2.28-6	2.05-6	5.15-6	1.03-5
σ_{sp} (550)	1.58-5	1.66-5	1.14-5	7.43-6	1.86-6	8.71-7	9.78-7	1.19-6	2.26-6	1.96-6	4.65-6	9.26-6
σ_{sp} (700)	1.16-5	1.28-5	8.19-6	5.09-6	1.17-6	5.57-7	7.31-7	9.44-7	1.90-6	1.50-6	3.48-6	6.88-6
						MLO						
CN	177	189	118	160	195	192	122	167	130	481		394
σ_{sp} (450)	7.37-7	1.09-6	1.98-6	3.98-6	2.99-6	1.75-6	1.16-6	1.43-6	1.04-6	1.01-6	7.62-7	7.32-7
σ_{sp} (550)	5.44-7	8.07-7	1.50-6	3.10-6	2.40-6	1.39-6	8.35-7	9.69-7	7.41-7	6.96-7	5.13-7	4.99-7
σ_{sp} (700)	3.67-7	5.92-7	1.12-6	2.32-6	1.87-6	1.10-6	5.98-7	6.40-7	5.13-7	4.71-7	3.41-7	3.46-7
						SMO						
CN	232	322	223	165	162	164	179	243	196	162	172	194
σ_{sp} (450)	6.58-6	8.55-6	7.84-6									
σ_{sp} (550)	6.16-6	8.50-6	7.56-6									
σ_{sp} (700)	5.65-6	8.18-6	6.94-6									
						SPO						
CN	182	382	179	81	30	23	21	27	64	161	253	156
σ_{sp} (450)	5.81-7	6.37-7	4.62-7	4.67-7	4.10-7	3.95-7	4.85-7	3.73-7	7.63-7	4.85-7	7.97-7	1.29-6
σ_{sp} (550)	3.10-7	3.35-7	2.61-7	2.82-7	2.59-7	2.29-7	3.34-7	2.37-7	5.52-7	2.97-7	5.23-7	9.93-7
σ_{sp} (700)	1.94-7	1.89-7	1.61-7	1.93-7	1.58-7	1.51-7	2.39-7	1.29-7	4.19-7	1.94-7	3.73-7	6.68-7

A compact exponential format is used for σ_{sp} such that $1.78\text{-}5 = 1.78 \cdot 10^{-5}$.

aerosol events are caused by the transport of sea salt in the upper troposphere from stormy regions near the Antarctic coast to the interior of the continent. The SPO 1991 annual means are about 86 cm^{-3} for CN and 3.47×10^{-7} m^{-1} for σ_{sp} (550 nm). Analyses of the SPO data were presented by *Bodhaine et al.* [1986, 1987]. The complete data set was presented by *Bodhaine and Shanahan* [1990].

The least-squares trend lines shown in Figure 3.2 were calculated using the common logarithms of the monthly means of the entire data record, and the results are given in Table 3.2. Similar trend lines have been calculated and presented in previous CMDL *Summary Reports*.

3.1.2. Lidar Observations of Aerosols

Lidar observations were successfully completed on 72 evenings during 1991. In order to measure possible enhanced backscatter resulting from the oil fires in Kuwait, observation procedures were modified to extend backscatter measurements into the troposphere. April 1 through April 18 aerosol backscatter profiles were measured down to at least 8 km (MSL), and beginning April 23, measurements were again modified to provide aerosol profile data down to 5.3 km. Because of improvements in normalization as well as quality of stratospheric data, this last procedure which typically incorporates 200 laser shots performed using five different system configurations, was adopted for routine observations.

While considerable structure in the tropospheric aerosol backscatter was measured through June, it was not possible to separate Asian dust from possible Kuwait oil fire contribution because of the lack of baseline data.

The first evidence of enhanced backscatter from the June 15-16, 1991, eruption of Mt. Pinatubo was measured by

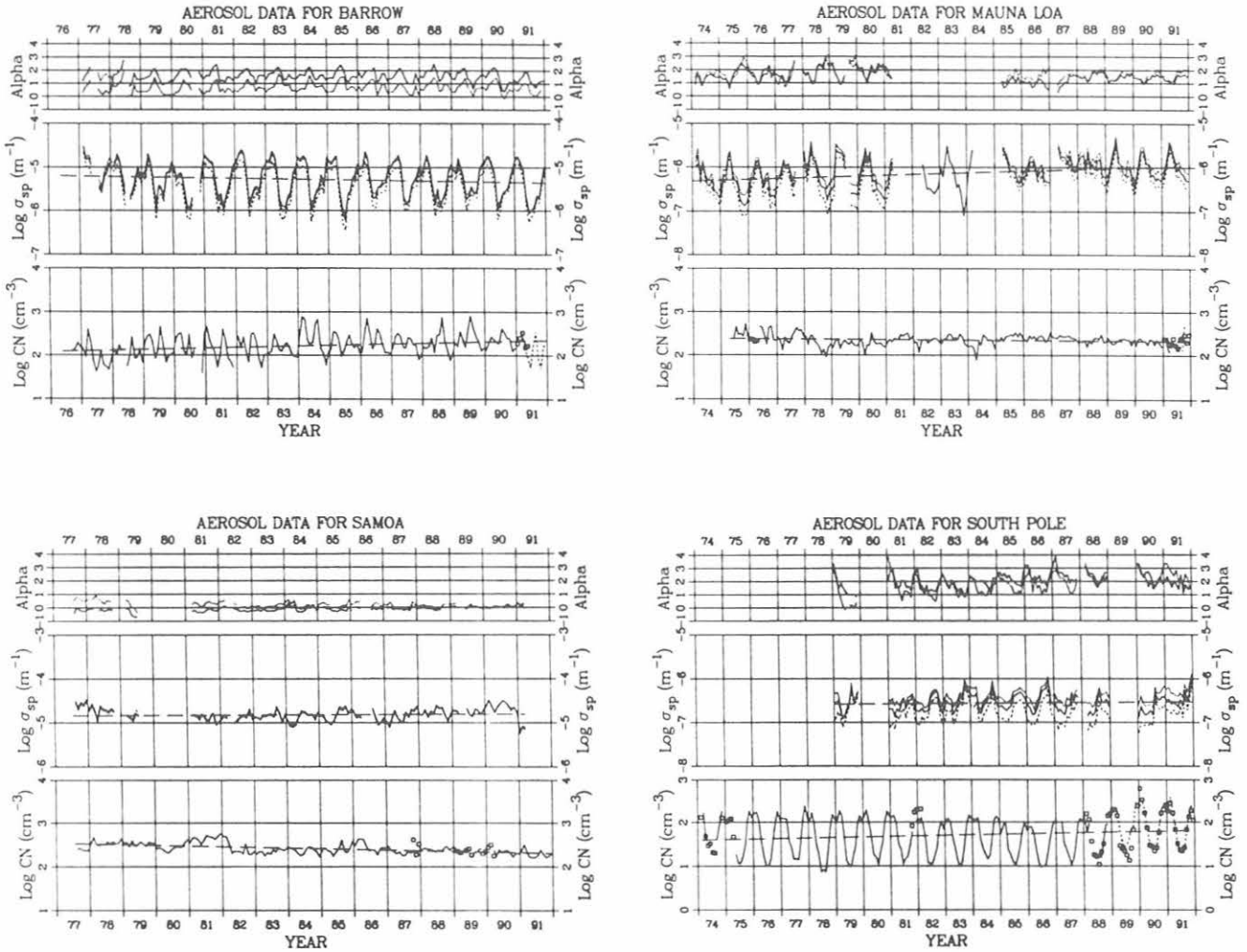

Fig. 3.2. Monthly geometric means of σ_{sp} and CN data for the entire data record. Data for MLO are included only for 0000-0800 LST. σ_{sp} data (middle) are shown for 450 (dotted), 550 (solid), and 700 nm (dashed). Ångström exponents (alpha) were calculated from 450- and 550-nm (dotted), and 550- and 700-nm (solid) σ_{sp} data. Note that G. E. CN counter data are shown as a solid line, TSI CN counter data are shown as a dashed line, and Pollak CN counter data are shown as small squares. Details of the trend lines are given in Table 3.2.

the MLO lidar system on July 1. Although the stratospheric impact from Mt. Pinatubo has been estimated to be 2-3 times that of El Chichon [*Bluth et al.*, 1992; *McCormick and Veiga*, 1992], MLO lidar backscatter measurements of the stratospheric aerosol from the two eruptions at MLO, as seen in Figures 3.3 and 3.4, are quite comparable. As shown in Figure 3.5, the most significant difference between the early El Chichon and Mt. Pinatubo stratospheric aerosol cloud is the median backscatter height.

3.1.3. Total Ozone Observations

Total ozone observations were continued throughout 1991 at 15 of 16 stations that comprise the U.S. Dobson spectrophotometer network (Table 3.3). Of the 15 stations, 5 were operated by CMDL personnel, 4 are operated by the NWS, 2 are domestic cooperative stations, and 4 are foreign cooperative stations. The Dobson spectrophotometer operated at Florida State University in Tallahassee until November 1989 will be relocated in 1992 to the Municipal Airport in Tallahassee and will be operated by NWS staff.

Provisional, daily 1991 total ozone amounts applicable to local noon for stations listed in Table 3.3 have been archived at the World Ozone Data Center, 4905 Dufferin Street, Downsview, Ontario M3H 5T4, Canada, in *Ozone Data for the World.* Table 3.4 lists the provisional mean monthly total ozone amounts measured at the various stations. (Monthly means are derived for stations where

TABLE 3.2. Least Squares Trend Analysis of the Common Logarithms of the Data Shown in Figure 5.2*

	Parameter	Slope	Intercept	S.E.	Trend (% yr^{-1})
BRW	CN	0.0165	0.830	0.264	3.87%
	σ_{sp}	-0.00992	-4.44	0.397	-2.26%
MLO	CN	-0.00992	2.65	0.131	-0.77%
	σ_{sp}	0.0193	-7.74	0.313	-4.54%
SMO	CN	-0.0153	3.71	0.107	-3.46%
	σ_{sp}	0.00278	-5.06	0.141	0.64%
SPO	CN	0.0118	0.720	0.435	2.75%
	σ_{sp}	0.00422	-6.92	0.195	0.98%

*The time axes in Figure 3.2 are in fractional years, with a data point centered at the enter of a month; e.g., January 1974 = 74.042, February. = 74.125, etc.

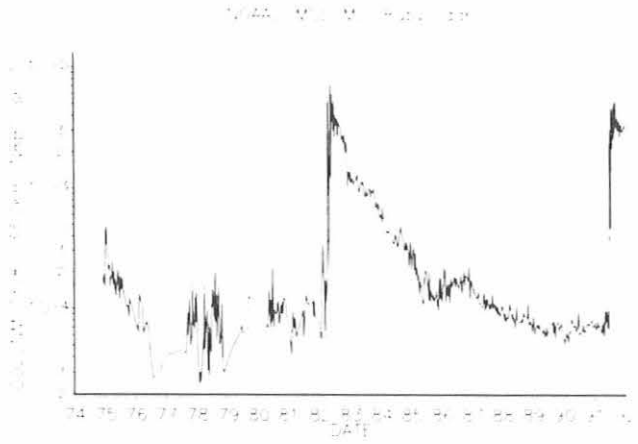

Fig. 3.3. Stratospheric column aerosol backscatter from Mt. Pinatubo eruption.

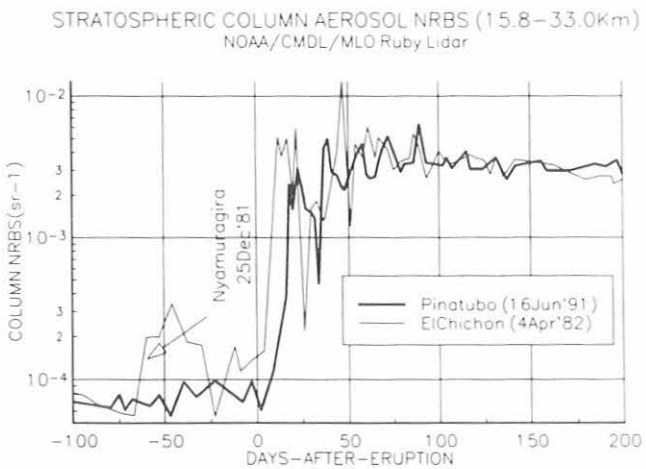

Fig. 3.4. Comparison of stratospheric column aerosol backscatter from El Chichon and Mt. Pinatubo eruptions.

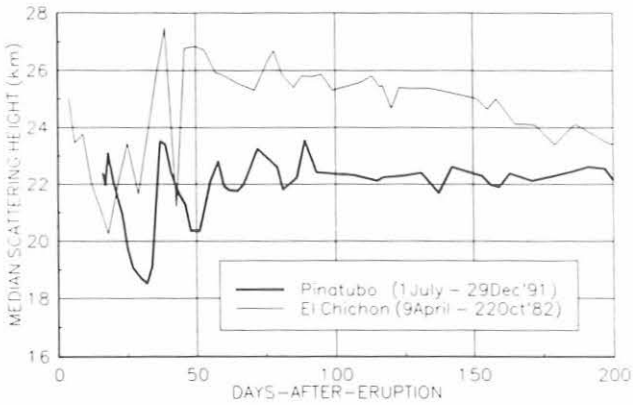

Fig. 3.5. Comparison of median heights of stratospheric aerosol layers from El Chichon and Mt. Pinatubo eruptions.

observations were made during at least 10 days each month.) A correction of about 1.7% has been applied to the Wallops Island data on the basis of recalibration of the Wallops Island Dobson instrument in September 1991. Ozone values in Table 3.4 are expressed in the *Vigroux* [1957] ozone absorption coefficient scale. To convert to the new *Bass-Paur* [1985] ozone absorption scale that became effective world-wide in January 1992 [*Komhyr et al.*, 1992], the ozone values in Table 3.4 should be multiplied by 0.9743.

Figures 3.6 and 3.7 plot provisional total ozone anomaly data (i.e., monthly mean ozone deviations from monthly normals) for 12 of the 15 operating CMDL ozone stations for 1979-1991. Data used in the analysis are provisional, archived at the World Ozone Data Center, Downsview, Canada, except as follows: Bismarck May-December 1986 data were corrected by increasing ozone value by about 3.5%. Corrections of 0 to -1.7% were linearly applied to Wallops Island data for May 1985-September 1991; MLO and SMO data were reprocessed in the past through July 1987; and minor corrections were recently applied to the Fresno data.

Least-squares linear regression lines fitted to the ozone anomaly data through 1991 exhibit several interesting features. The two most northerly stations, Barrow and Poker Flat, show nonsignificant downward ozone trends of -0.32 and -0.37% yr^{-1}, respectively, based on sparse data obtained during spring-to-autumn seasons of years when observations were made. Stations Caribou, Bismarck, Boulder, Haute Provence, and Wallops Island (located between 47° and 38°N latitudes) exhibit downward ozone trends ranging from -0.43 to -0.29% yr^{-1}. Essentially zero ozone trends are evident for Fresno, MLO, Huancayo, SMO, and Lauder (located between 37°N and 45°S latitudes). Note that the trend data are not strictly

TABLE 3.3. U.S. Dobson Ozone Spectrophotometer Station Network for 1991

Station	Period of Record	Instrument No.	Agency
Bismarck, ND	Jan. 1, 1963-present	33	NOAA
Caribou, ME	Jan. 1, 1963-present	34	NOAA
Wallops Is., VA	July 1, 1967-present	38	NOAA; NASA
SMO	Dec. 19, 1975-present	42	NOAA
Tallahassee, FL	May 2, 1964-Nov. 30, 1989	58	NOAA; Florida State University
Boulder, CO	Sept. 1, 1966-present	61	NOAA
Poker Flat, AK	March 6, 1984-present	63	NOAA; University of Alaska
Lauder, New Zealand	Jan. 29, 1987-present	72	NOAA; DSIR
MLO	Jan. 2, 1964-present	76	NOAA
Nashville, TN	Jan. 2, 1963-present	79	NOAA
Perth, Australia	July 30, 1984-present	81	NOAA; Australian Bureau Meteorology
SPO	Nov. 17, 1961-present	82	NOAA
Haute Provence, France	Sept. 2, 1983-present	85	NOAA; CNRS
Huancayo, Peru	Feb. 14, 1964-present	87	NOAA; IGP
BRW	June 6, 1986-present	91	NOAA
Fresno, CA	June 22, 1983-present	94	NOAA

TABLE 3.4. Provisional 1991 Monthly Mean Total Ozone Amounts (m-atm-cm)

Station	Jan.	Feb.	March	April	May	June	July	Aug	Sept.	Oct.	Nov.	Dec.
Bismarck, ND	366	361	395	386	343	332	324	300	301	293	304	317
Caribou, ME	385	396	397	397	376	366	361	338			292	342
Wallops Is., VA	316	347	370	349	334	346	328	319		294	285	299
SMO	243	247	246	249	250	252	258	256		252	254	268
Tallahassee, FL												
Boulder, CO	337	320	379	362	333	326	303	303	295	287	290	301
Poker Flat, AK			450	414	401							
Lauder, New Zealand	276	270	264	283	308	313	328	367	376	364	351	306
MLO	246	239	279	299	299	292	279		273	262	252	248
Nashville, TN	325	332	354	349	335	348	324		310	305	286	295
Perth, Australia	276	264	278	275	281	298	308	317	337	328	322	298
SPO	280	268			251	253	262	245		166	297	309
Haute Provence, France	351	394	359	402	399	369		329		307	291	279
Huancayo, Peru	248	253	257	251	246	245	252	254	255	261	257	253
BRW			461	428	395	353	338	310	310			
Fresno, CA	319	318	385	359	381	350	328	324	307	285	279	295

comparable, since they are not representative in all instances of the same time interval.

Numbers in brackets in the upper right hand corner of each plot of Figures 3.6 and 3.7 are the ozone trends in % yr^{-1} computed from data ending December 31, 1990. Note that through 1990, computed trends are in most cases considerably more negative than trends determined through 1991, implying that ozone increased over many parts of the globe during 1991. The large downward ozone trends of -0.77% yr^{-1} at Haute Provence during 1984-1990 and -0.63% yr^{-1} at Lauder during 1987-1991 resulted largely from unusually low ozone values at Haute Provence in February 1990 and during the latter one-half of 1990 at Lauder. Most stations (see especially Fresno and Lauder) show more ozone in 1991 than in 1990.

Figure 3.8 plots mean total ozone amounts measured at SPO during October 15-31 time intervals of 1962-1991. (Mid-October is when Dobson spectrophotometer total

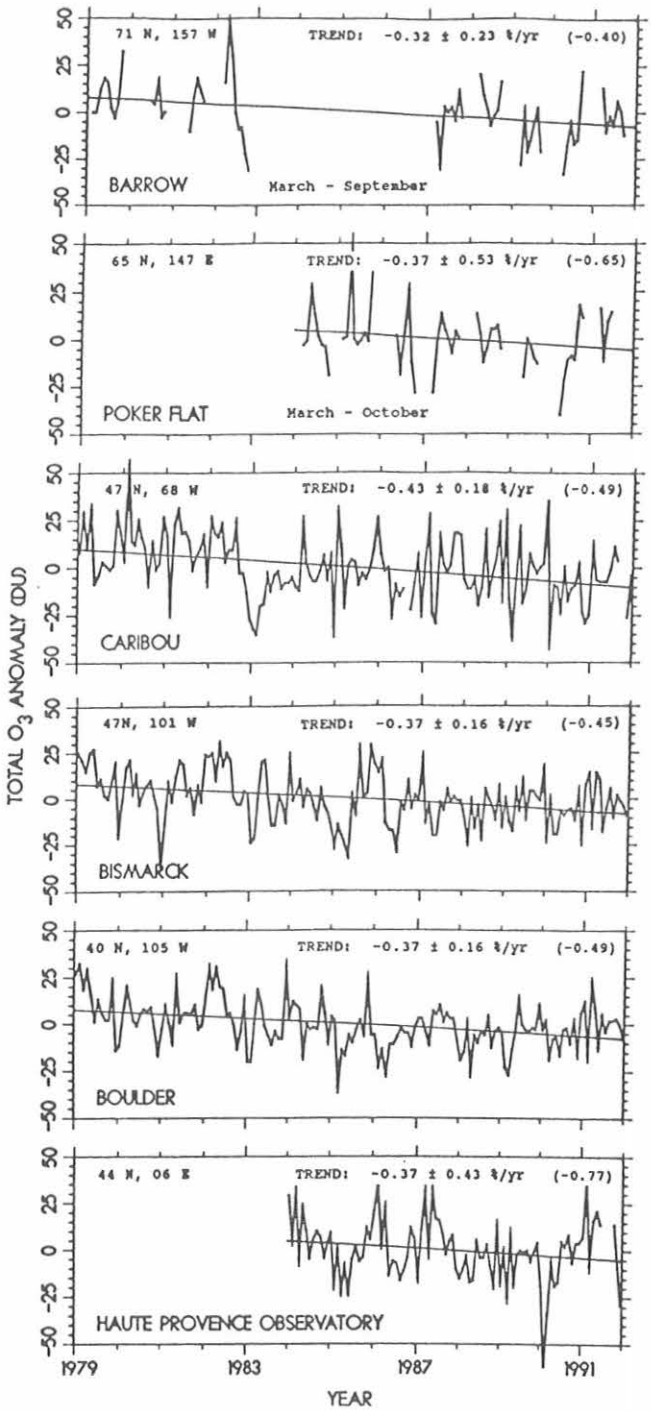

Fig. 3.6. Provisional total ozone anomaly data derived from Dobson spectrophotometer observations made at BRW, Poker Flat, Caribou, Bismarck, Boulder, and Haute Provence observatories. Least-squares linear regression lines are fitted to data obtained through 1991. Uncertainties in indicated ozone trends are 95% confidence intervals (t-statistic). The values in brackets in the upper right hand corner of each plot is the ozone trend derived from data obtained only through 1990.

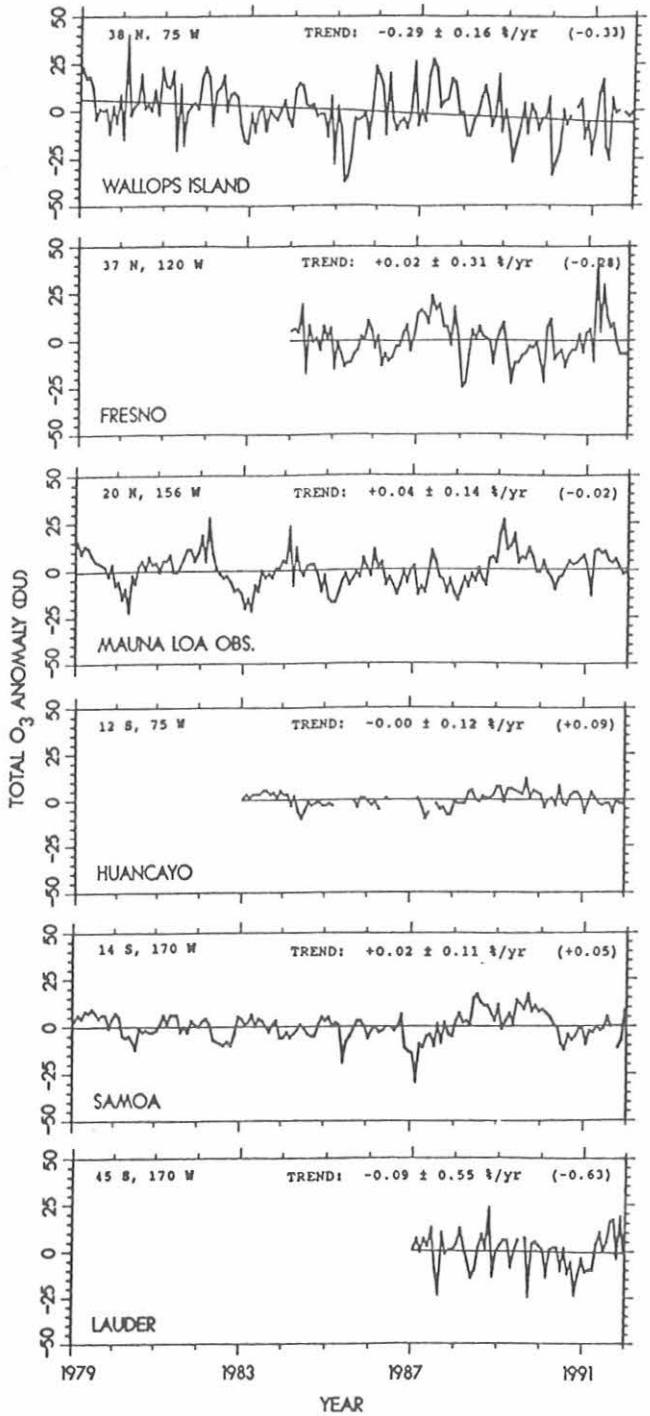

Fig. 3.7. Provisional total ozone anomaly data obtained from Dobson spectrophotometer observations made at Wallops Island, Fresno, MLO, Huancayo, Samoa, and Lauder. Least-square linear regression lines are fitted to the data obtained through 1991. Uncertainties in indicated ozone trends are 95% confidence intervals (t-statistic). The value in brackets in the upper right hand corner of each plot is the ozone trend derived from data obtained only through 1990.

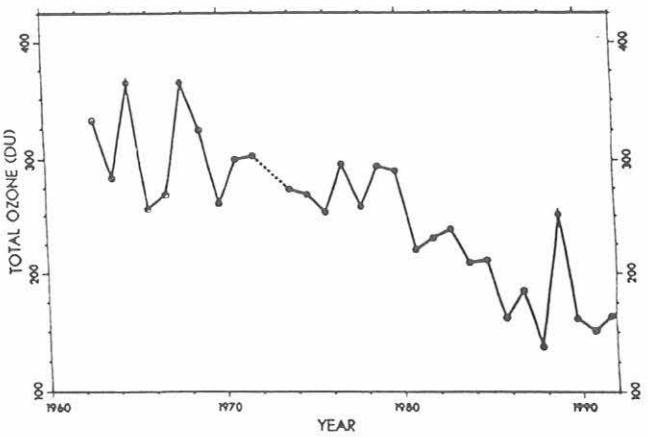

Fig. 3.8. SPO mean total ozone amounts for October 15-31 time intervals of 1962-1991.

ozone observations first became possible each year at South Pole following the polar night.) The October 1991 mean ozone value was only slightly higher than the previous year's value and comparable to mean total ozone amounts measured in 1985 and 1989. Thus far, the record October mean monthly ozone low at SPO appeared in 1987.

3.1.4. Umkehr Observations

Umkehr observations with automated Dobson ozone spectrophotometers were continued during 1991 at Boulder, Haute Provence, Lauder, MLO, Perth, and Poker Flat. Table 3.5 lists the number of observations that yielded useful data. Observations exhibiting excessive cloud interference were not useful. Umkehr data quality was degraded during the second half of 1991 following the eruption of Mt. Pinatubo in the Philippines in June, which heavily contaminated the stratosphere with aerosol particles.

TABLE 3.5. Umkehr Observation Frequency During 1991

Station	Station Coordinates	Total No. Obs. Made	Total No. Useful Obs.*
Boulder	40°N, 105°W	489	227
Haute Provence	43°N, 6°E	402	208
Lauder	45°S, 170°E	568	158
MLO	20°N, 156°W	585	387
Perth	32°S, 116°E	539	293
Poker Flat	65°N, 147°W	255	54

*Number of useful observations may increase following re-examination of data obtained after the eruption of Mt. Pinatubo in June 1991.

TABLE 3.6. CMDL Dobson Spectrophotomters Calibrated in 1991

Station	Instrument No.	Calibration Date	Calib. Corr. Needed (%)
Bismarck	3	July 30	+0.76
Boulder	61	Aug. 14	+1.50
Caribou	34	Sept. 9	-0.12
MLO	76	June 8	+1.59
Nashville	79	July 30	+1.20
Tallahassee	58	Aug. 22	-1.99
SMO	42	Sept. 9	-0.54
Wallops Island	38	Sept. 16	-1.72

*Applicable to μ = 2 and 300 DU ozone.

All provisional 1990 Umkehr data have been archived at the WMO World Ozone Data Center in Canada from where they may be obtained by NOAA-NESDIS (and other users) for comparison with NOAA-11 and SBUV-2 satellite ozone profile measurements. Umkehr layer aerosol corrections [*DeLuisi*, 1989], as a function of latitude and time, are routinely provided to NESDIS. C.L. Mateer (Scarborough, Ontario, Canada) is continuing work on improving existing Umkehr data reduction algorithms by incorporating into them improved ozone absorption and primary scattering coefficients.

3.1.5. Calibration of CMDL Dobson Spectrophotometers

A major effort was undertaken during 1991 to calibrate CMDL-operated Dobson ozone spectrophotometers. Table 3.6 lists the instruments calibrated and the resulting calibration corrections expressed in terms of percent ozone for average ozone and air mass values of 300 DU and μ = 2, respectively. Except for Dobson instrument 76, which was calibrated at MLO, the calibrations were performed in Boulder relative to NOAA's World primary standard Dobson spectrophotometer 83 and to secondary standard Dobson spectrophotometer 65.

Because of the considerable workload involving the NOAA instrument calibrations, no foreign Dobson Spectrophotometers were calibrated in 1991.

3.1.6. Validation of TOMS and Satellite Instrument Ozone Data

World primary standard Dobson spectrophotometer 83 was operated in June-August 1990 at MLO in an ongoing program to maintain the instrument in calibration.

Another objective of the program is to assess the quality of total ozone data obtained with NASA's TOMS and SBUV spectrometers aboard the Nimbus 7 satellite as well as with NOAA's SBUV-2 spectrometers aboard the NOAA-9 and NOAA-11 satellites.

Relative to Dobson instrument 83, whose long-term ozone measurement precision has been maintained at about ±0.5% [*Komhyr et al.*, 1989], the calibration of the TOMS instrument has continued to drift (Figure 3.9*a*) at a rate now approaching 0.9% yr^{-1}.

Dobson instrument 83 has been used since the mid-1970's to calibrate Dobson instruments of the global Dobson spectrophotometer station network. While in the past the TOMS and SBUV data have been corrected by normalization to Dobson spectrophotometer total ozone values [*World Meteorological Organization*, 1988], a pair wavelength justification technique has been recently developed by NASA scientists as an independent means of correcting the satellite data. Data thus corrected are referred to as version 6 data. As shown in Figure 3.9*b* [see also *McPeters and Komhyr*, 1991], the agreement between the corrected TOMS data and Dobson instrument 83 data is now highly satisfactory.

To investigate the possibility of instrument stray light affecting the MLO Dobson instrument 83 observations that involve A-wavelength (305.5/325.0-nm) observations, an analysis was conducted in 1990 using longer, C-wavelength (311.5/332.4-nm) observations made at MLO since 1979. Stray light effects at the longer wavelengths are negligible. As shown in Figure 3.9*c* relative to TOMS data, observations with Dobson instrument 83 on AD and C wavelengths yield highly similar results, lending credence to the validity of the MLO Dobson instrument 83 and the TOMS and SBUV instrument comparisons.

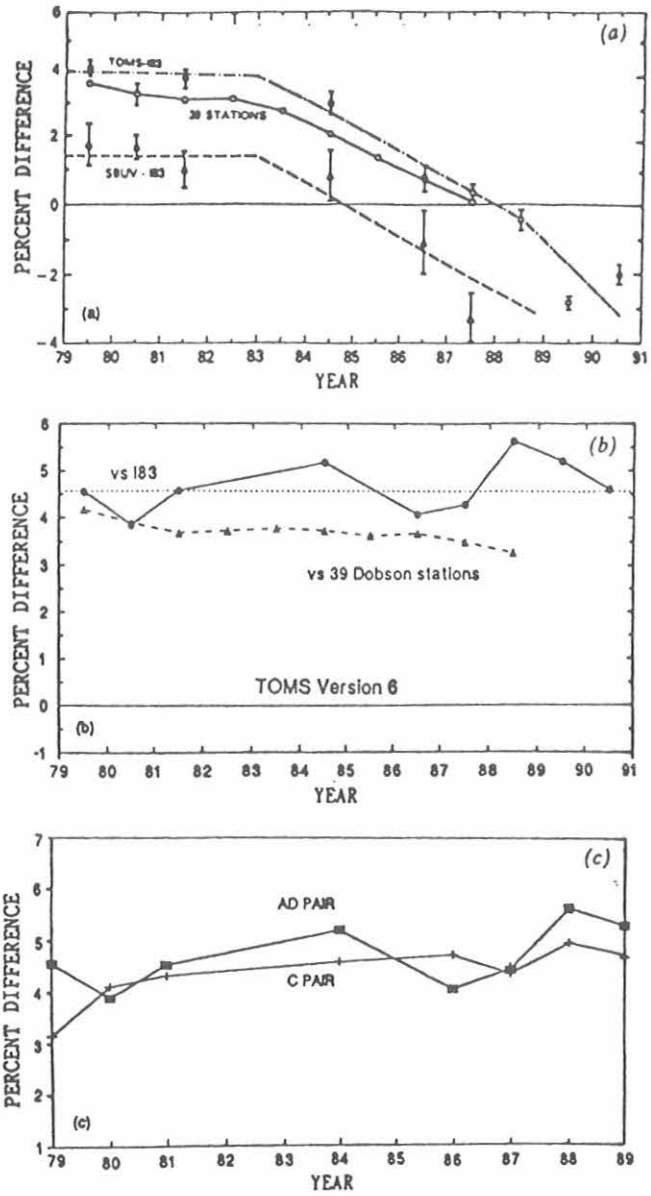

Fig. 3.9. (*a*) TOMS and SBUV total ozone data compared with Dobson instrument 83 total ozone data at MLO and total ozone data from 39 select Dobson instrument stations showing calibration drift with time of the satellite instruments due to diffuser plate degradation. (*b*) TOMS version 6 total ozone data corrected by means of a pair-wavelength justification technique, compared with Dobson instrument 83 data and data from 39 select Dobson instrument stations. (*c*) Corrected TOMS total ozone data, compared with Dobson instrument 83 data derived from observation on AD as well as C wavelengths.

3.1.7. Tropospheric Ozone

Surface ozone measurements continued at the four CMDL sites as well as from the AEROCE sites at Bermuda; Barbados; Mace Head, Ireland; and Niwot Ridge, Colorado. In September 1991 a surface ozone monitor was installed at Reykjavik, Iceland, with funds provided by the NOAA Climate and Global Change Atmospheric Chemistry Program. Because of nearby pollution sources, the site in Reykjavik is not an optimal one. A second site in Iceland on Westmann Island is planned for 1992. Table 3.7 gives the mean monthly ozone mixing ratio for each site for 1991. For MLO the values are the average for downslope flow only and at Reykjavik, the averages are based on the period from 03 to 07 LST.

Figure 3.10 presents the averaged monthly data for these sites as well as data from Izaña in the Canary Islands. At Reykjavik data for only a few months are available. At most of the northern hemisphere sites, there is a spring maximum. At BRW boundary layer depletion gives a minimum during the spring [*Oltmans et al.*, 1989]. At Barbados the cut-off by spring of high latitude flow result in a winter maximm [*Oltmans and Levy*, 1992*a*].

TABLE 3.7. Monthly Mean Surface ozone Mixing Ratios (ppbv) During 1991

Station	Jan.	Feb.	March	April	May	June	July	Aug.	Sept.	Oct.	Nov.	Dec.
BRW	31.8	30.2	16.7	14.2	29.3	25.5	24.5	31.7	28.4	27.6	30.0	27.1
Reykjavik, Iceland									(22.1)	31.0	32.6	34.3
Mace Head, Ireland	30.6	32.7	32.4	44.2	39.5	36.9	35.4	34.7	37.3	32.2	35.8	27.0
NWR	44.0	46.0	48.4	55.6	54.4	48.9	47.8	41.6	42.0	42.8	39.4	40.9
Bermuda	35.0	38.5	46.0	46.3	45.1	(30.7)	18.1	17.7	17.9	31.4	40.8	41.4
MLO	45.3	41.8	48.4	56.9	55.5	41.5	39.2	33.1	31.5	33.9	32.6	33.3
Barbados	(29.0)	24.6	24.0	23.8	21.0	18.4	17.6	15.2	15.7	14.7	21.2	24.6
SMO	6.7	8.7	6.6	7.9	13.8	14.3	20.8	20.1	23.2	15.1	12.2	15.4
SPO	23.8	19.9	18.9	23.8	26.8	30.9	31.8	34.1	27.7	27.2	22.8	22.1

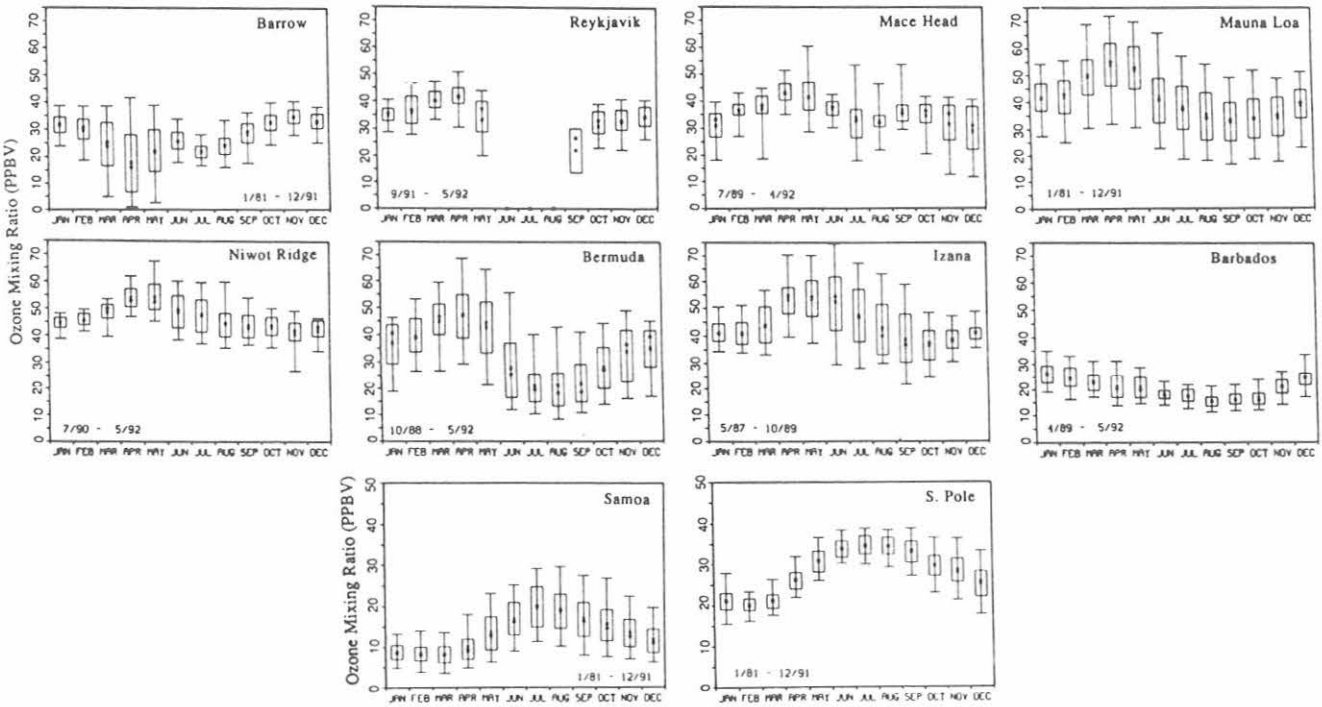

Fig. 3.10. Monthly surface ozone mixing ratio (ppbv). The dot is the median, the x is the mean, the box the inner 50th percentile, and the whiskers the inner 90th prcentile.

In the southern hemisphere, there is a rather ubiquitous winter maximum and summer minimum [*Oltmans and Levy*, 1992*b*].

At the four CMDL sites, the long-term data series has been analyzed for a linear trend (Figure 3.11). At BRW there has been an overall increase of 0.70% yr^{-1} for the 20 years of measurements. Almost all of this is a result of the large summer (May-September) increase of over 25% since the measurements began. This increase may be the result of the increase in nitrogen oxide emissions on the north slope of Alaska associated with petroleum extraction activities [*Jaffe*, 1991]. At MLO there has been a relatively small but significant increase that has taken place primarily in the winter and spring. Since 1983 the overall change has been near zero. At SPO the large significant decrease during the summer was discussed in the *1990 Summary Report* [*Ferguson and Rosson*, 1991, *Schnell et al.*, 1991].

3.1.8 Ozonesonde Observations

By the beginning of 1991, the only continuing ozonesonde program was at SPO where measurements began in 1986. With the eruption of Mt. Pinatubo,

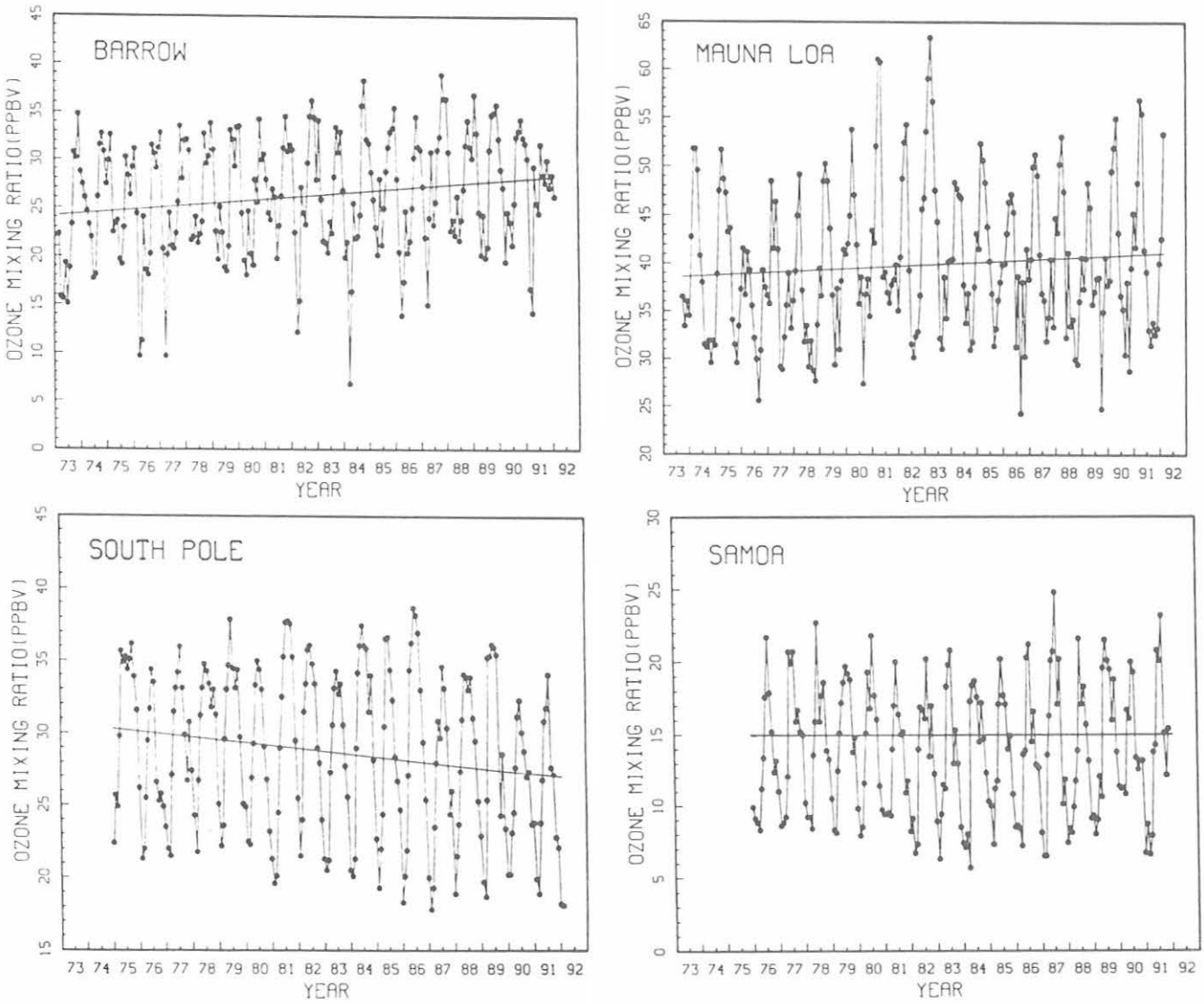

Fig. 3.11. Monthly mean surface ozone mixing ratios with the linear least-squares trend line from monthly anomalies superimposed.

programs were reinstituted at Hilo and Boulder using the digital ozonesonde system described in the *1991 Summary Report* [*Ferguson and Rosson*, 1991]. At Hilo there is only a 3-month gap from the termination of the earlier program that started in 1985, to the beginning of the recent set of observations. At Boulder on the other hand, there are only occasional soundings from mid-1989 to mid-1991. The results of these special measurements are described in section 3.2.2 of this report.

For the period 1986-1991, the 2 km average ozone mixing ratio at SPO for each sounding is shown in Figure 3.12 for the altitude range from 4-26 km. For the layer centered at 12 km the 1991 values are noticeably lower. This will be discussed in a later section on volcanic effects. In the layers from 14-20 km, the development in the spring of a deep minimum is the striking feature. During 1988, and to a lesser extent in 1986, there is a tendency for the decline to near zero ozone amounts in some layers to be interrupted in early October. In other years—notably 1987, 1989, and 1990—low ozone values persist well into November or even December. In 1991 values dipped very low but recovered by early November. The onset of the higher ozone values is closely tied to the breakdown of the polar vortex [*Komhyr et al.*, 1986]. This modulation of the timing of the vortex breakdown in the region from 14 to 26 km is the mechanism responsible for the approximate quasi-biennial variation in the magnitude of the ozone hole [*Garcia and Solomon*, 1987].

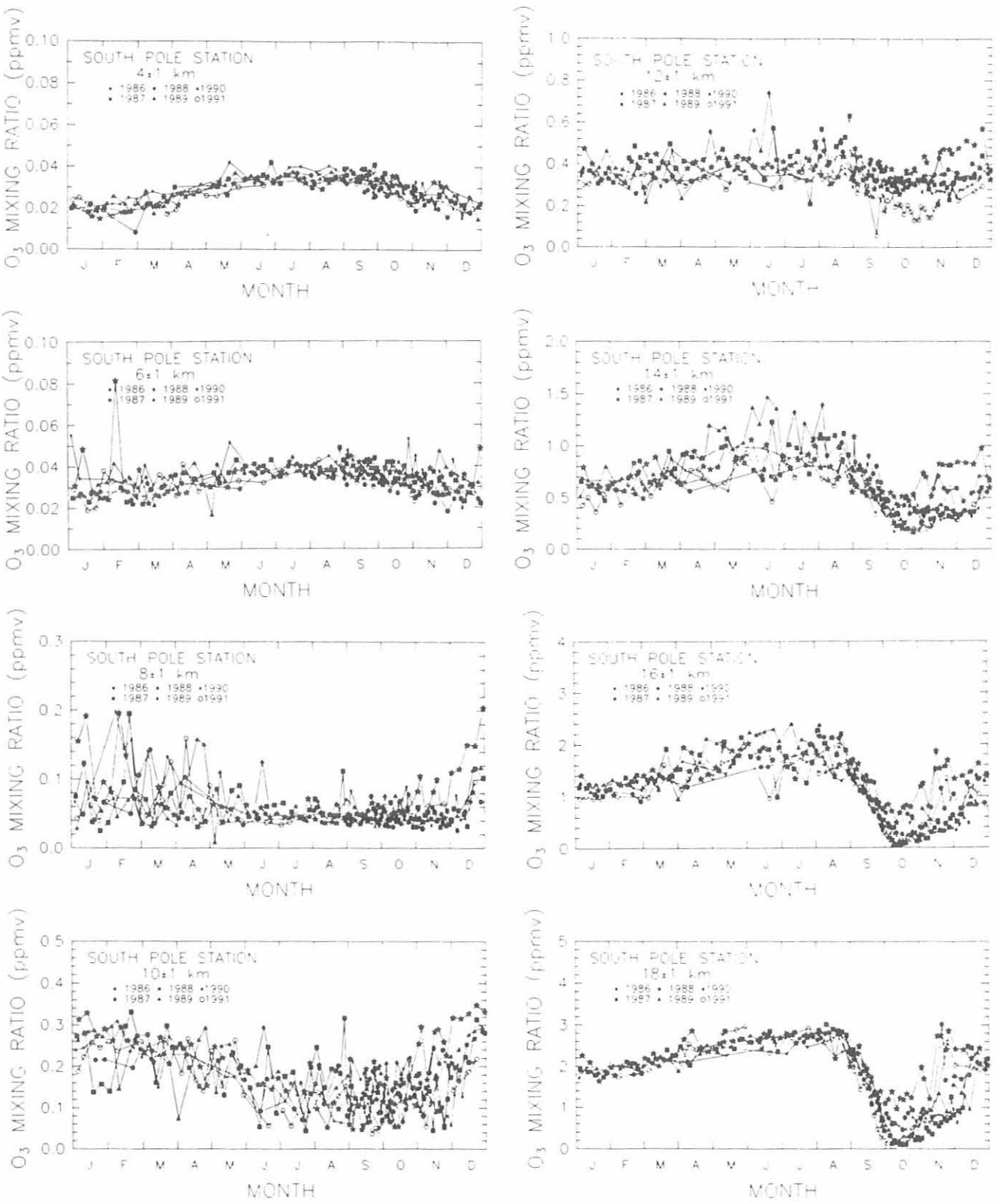

Fig. 3.12. Average ozone mixing ratios at SPO in 2 km layers from 4-26 km. Each point represents a single ozonesonde sounding.

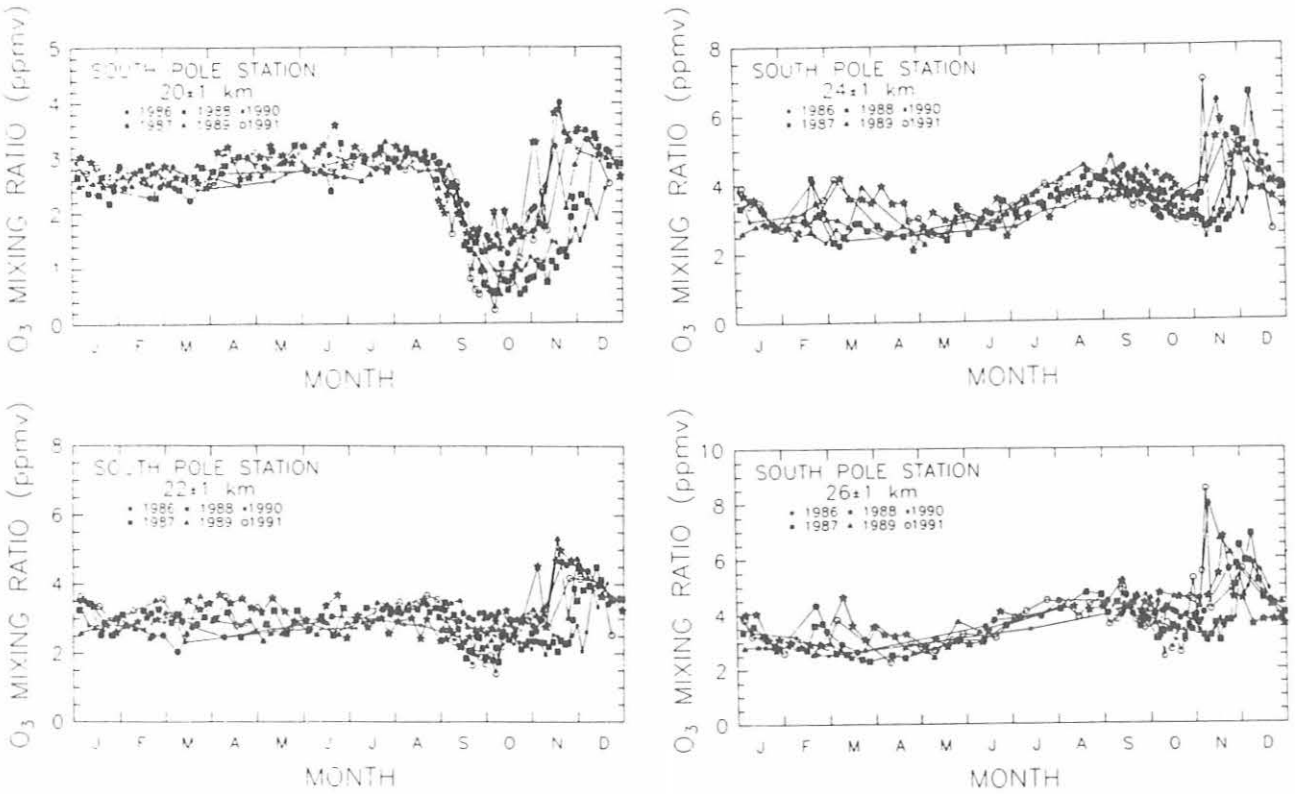

Fig. 3.12. Average ozone mixing ratios at SPO in 2 km layers from 4-26 km. Each point represents a single ozonesonde sounding.

3.1.9. Stratospheric Water Vapor

Monthly water vapor soundings continued in Boulder on an approximate monthly schedule. Beginning in 1991, the frostpoint hygrometer soundings were made using a digital data system. The system is identical to that used with the ozonesondes [*Ferguson and Rosson*, 1991]. The system uses the TMAX digital interface and the Vaisala radiosonde. Since the radiosonde provides relative humidity as well as pressure and temperature data, the new system provides an opportunity to compare a widely used sensor in meteorological soundings with the cryogenic frost-point instrument.

During February 1991, a series of four water vapor soundings were carried out at Edwards Air Force Base, as part of an intercomparison campaign with the Lyman alpha hygrometer flown on the ER-2 aircraft. These soundings also coincided with overpasses of the SAGE II satellite. The stratospheric mixing ratios for each of the four profiles are shown in Figure 3.13. At altitudes greater than 18 km, most of the differences are probably instrumental. The standard deviation is 0.2 ppmv or approximately 5% of the mean value. In the region from 12 to 18 km, there were significant changes in the flow pattern from February 25 to February 26 that are responsible for the differences from 1 day to the next.

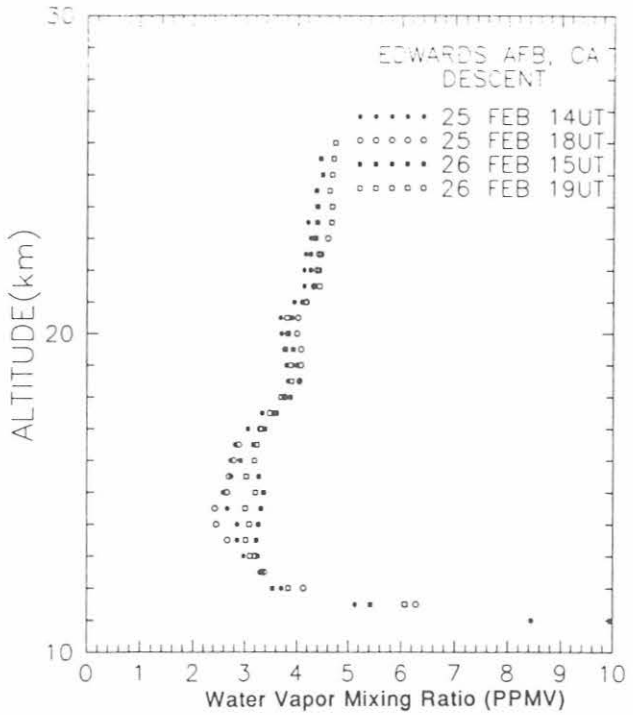

Fig. 3.13. Stratospheric water vapor mixing ratios from four balloon soundings made in California during February 1991. Each symbol represents a 0.5 km average.

3.1.10. SURFACE RADIATION

Global Baseline Surface Radiation Monitoring

Surface based radiation monitoring projects are currently being carried out at seven CMDL locations: Barrow, Alaska (BRW), Erie, Colorado (BAO), Bermuda (BRM), Mauna Loa, Hawaii (MLO), Kwajalein, Marshall Islands (KWJ), American Samoa (SMO), and the South Pole (SPO). Measurements include downward and upward, broadband solar and thermal infrared irradiances which comprise the surface radiation budget. The surface radiation budget (SRB) is a basic and critically important climate variable that has long been inadequately observed because of insufficient global coverage and inherent instrumental limitations. Extensive SRB observations are made at CMDL sites where the measurements have been determined to be at least regionally representative. In order to make the CMDL data more useful to the general scientific community, irradiances observed at those representative sites, BRW, BAO, KWJ, BRM, and SPO are being incorporated into an international data base sponsored by the WMO and NASA under the Baseline Surface Radiation Network (BSRN). All data from CMDL sites are stored as part of the long-term CMDL surface radiation record that exists for the past 15 years at BRW, MLO, SMO, and SPO. Previous *CMDL* (and *GMCC*) *Summary Reports* have discussed the wide ranging and useful applications of these data to scientific questions. In the past year several projects were begun and/or completed utilizing the observational results from the CMDL field sites, including: comparison of BAO and satellite-derived SRB under clear and cloudy conditions [*Cess et al.*, 1991; *Cess et al.*, 1992], detection of intermediate-term trends in cloudiness related to radiation perturbations [*Dutton et al.*, 1991; *Schnell et al.*, 1991], a technique for monitoring long-term climate variability using surface albedo records [*Dutton and Endres*, 1991; *Foster et al.*, 1992], identification of a strong statistical coherence between the QBO and the MLO long-term transmission record as seen in Figure 3.14 [*Dutton*, 1992*a*], a surprisingly good agreement between modeled and observed thermal infrared irradiances over the range of globally extreme conditions, see Figure 3.15 from *Dutton* [1992*b*], and a determination of the radiative effects of the Mt. Pinatubo volcanic eruption [*Russell et al.*, 1992; *Dutton et al.*, 1992].

Updated results on late summer cloudiness and irradiance trends at SPO reported by *Dutton et al.* [1991] are shown in Figure 3.16. As suggested by *Dutton et al.* [1991], the previously observed trends during January and February between 1977 and 1988 should not project into the future. The current levels are at or near the mean for the 15-year record for all months.

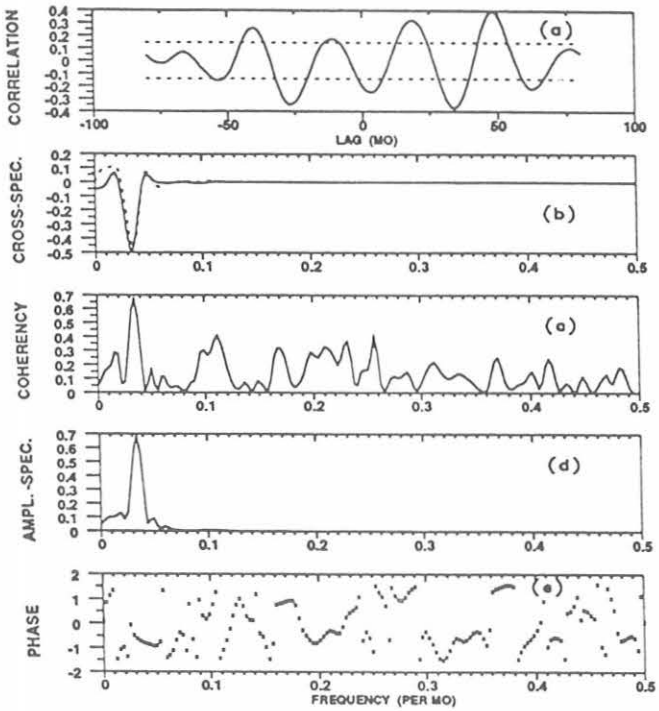

Fig. 3.14. Coherency analysis of the spectral relationship between the Singapore zonal wind field and the amplitude of the MLO atmospheric transmission annual cycle. (*a*) Lag correlations; the 99% confidence intervals are shown by the dashed line. (*b*) Cross-spectral plot showing the co-spectrum and quadrature spectrum. (*c*) Coherency (coherence squared) spectrum. (*d*) Amplitude spectrum. (*e*) Phase spectrum.

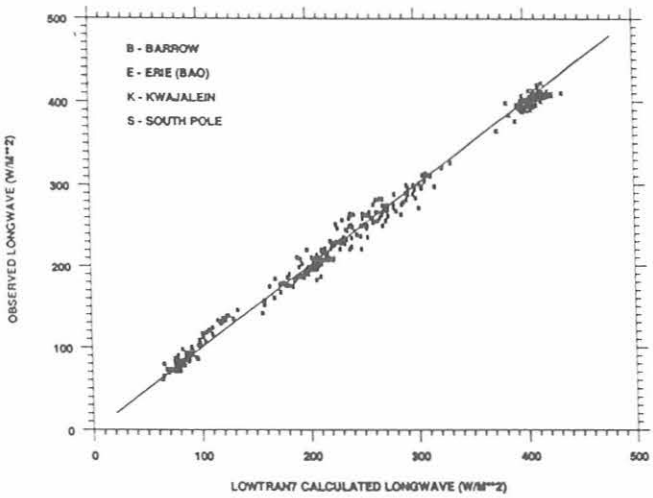

Fig. 3.15. An overall comparison between computed and observed downward infrared irradiance for clear-sky conditions at the four CMDL sites indicated on the plot. The straight line is a 1:1 line for reference purposes.

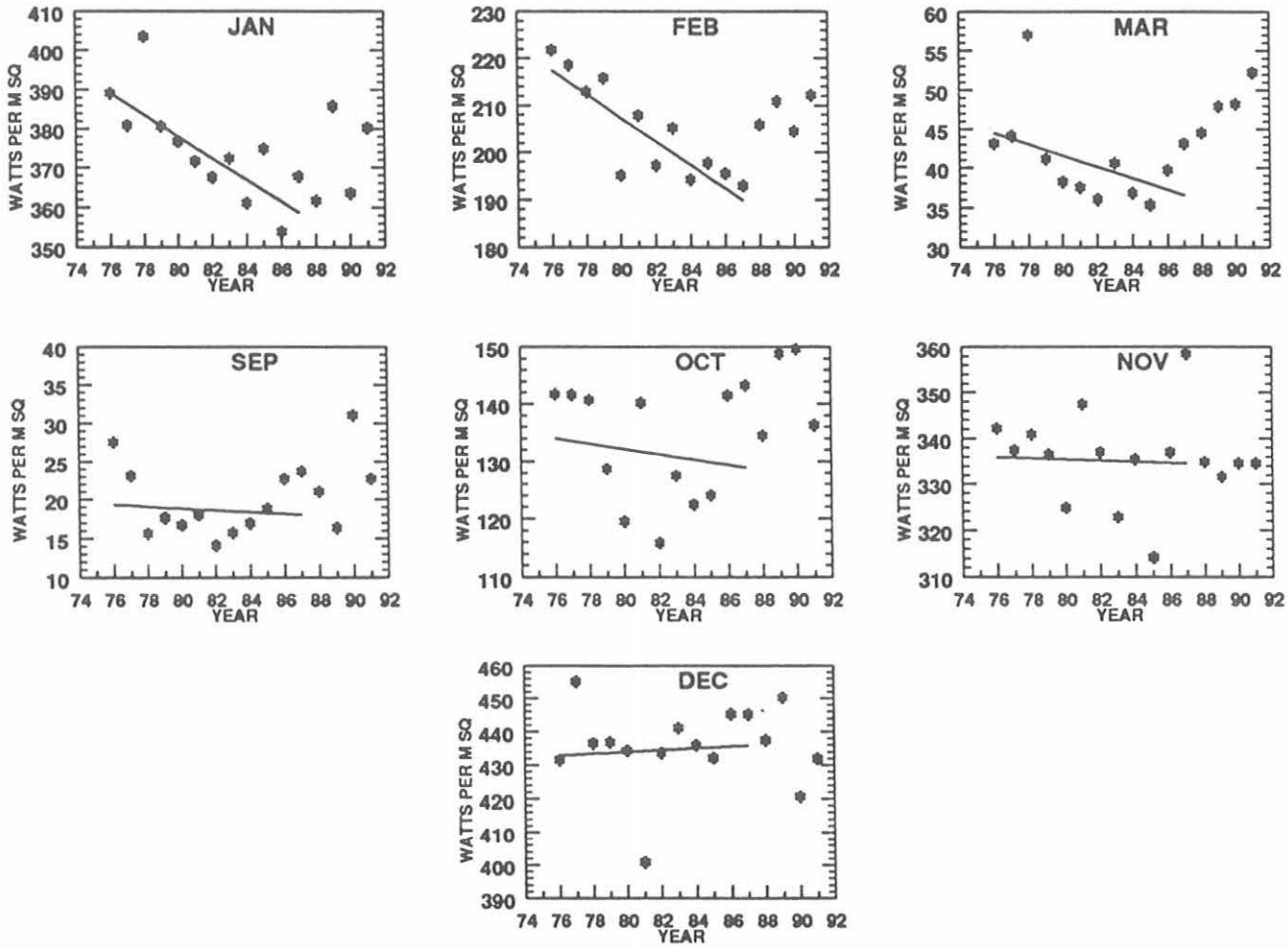

Fig. 3.16. Monthly mean total (direct plus diffuse) solar irradiance at SPO. The plotted line are for linear least-squares fits for 1976 through 1987.

Observatory operations continued during the year without many significant changes. Additional levels of the 300 m BAO tower were instrumented with radiometers to measure upwelling irradiance in addition to the measurements made the last 5 years at the top level. Russian counterpart instruments were on loan and operated for 1 year at SPO. An Eppley Smartracker was installed and operated at BRW. The solar tracker and radiometers at KWJ were replaced after various mechanical and electronic failures. Blowers at BRW and SPO designed to keep ice and snow from accumulating on the pyrgeometer and pyranometer domes, continue to be a problem because of limited effectiveness and pump failures. The tracker mounting stand at SPO was replaced with a permanently mounted rigid pedestal on the roof of the CAF.

Data processing for the three newer sites, KWJ, BAO, and BRM, was largely incorporated into the system used to process raw data from the other older sites. Incoming data are presently processed and edited as received from the site within 2-4 weeks. Final processing is completed about 1 calendar year after the data are available for processing. Final assignment of calibration information is ongoing as updated radiometer calibration data are made available. Data editing, processing, and final storage have been moved to medium-sized and personal computers directly under the control of CMDL, thereby eliminating the dependence of outside computer expertise and resources.

Remote Sensing of Aerosol Optical Properties and Water Vapor

Other than clouds, aerosols and water vapor are the main contributors to thermal-infrared and solar radiation variations and subsequent radiative climate forcing. The potential climate variations resulting from such variations are extensive and varied. The observed and potential radiative variations may be due to either anthropogenic causes, increased industrial production of aerosols and

water vapor feedback resulting from increasing greenhouse gases, or from natural causes such as volcanic, biogenic, or surface wind generated aerosols and inherently varying water vapor. CMDL has a long history of exploratory and operational projects relating to the remote sensing of aerosols and water vapor as related to climate variations. Since 1977 wide-band spectral observations of direct solar irradiance using a filter wheel NIP at BRW, MLO, SMO, and SPO have been used to infer aerosol optical depth and column water vapor amounts. These measurements have proven to be durable and stable over time thereby excelling in a monitoring effort even though their accuracy is less than can be obtained by more sophisticated but less robust instrumentation. Results from this project were last reported 4 years ago in this publication and the updated results are shown in Figure 3.17. Additional and exceptional effort has been put into high-precision, narrow-spectral band, optical depth measurements at MLO. Several narrowband (0.005 μm) sunphotometers are routinely operated at MLO, and because of the nearly ideal atmospheric conditions and the existence of automated observing platforms, they have produced reliably consistent long-term data sets. Results from the MLO aerosol optical depth measurement project are reported by *Dutton et al.* [1992] and *Russell et al.* [1992] and in previous *CMDL Summary Reports*.

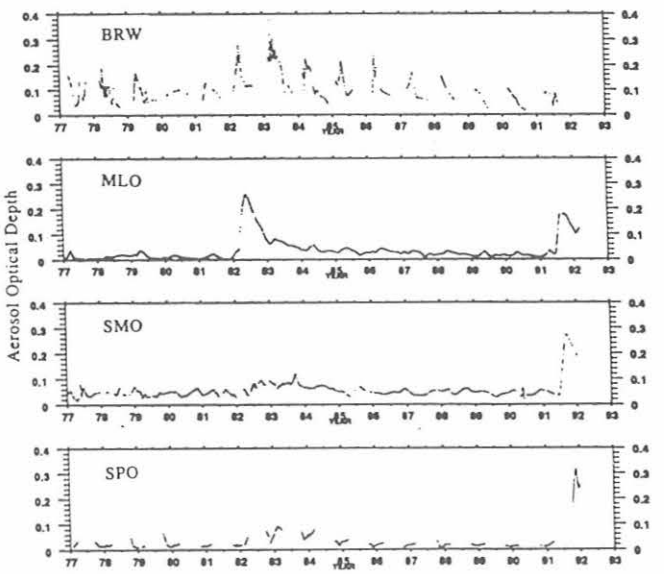

Fig. 3.17. Aerosol optical depth determined from the CMDL filter wheel NIP measurement project. The plotted points result from a 6-month statistical (lowess) smoother and emphasize the effects of the eruptions of El Chichon (1982) and Pinatubo (1991).

3.1.11. Solar Radiation Facility

Operational and support functions for CMDL observatories, BSRN sites, NWS SOLRAD sites as well as other ERL laboratories continued during 1991. Additional activities included substantial development, preparation and deployment efforts associated with the FIRE II field experiment in Coffeyville Kansas, for which the SRF designed, fabricated, and installed an array of pyrgeometer sensor supports incorporating ventilation and shading from direct sun. Information about the effects of solar heating of pyrgeometer domes during operation was obtained and summarized in a separate report. An array of global and direct beam, broadband solar sensors was maintained at Boulder along with the rotating shadowband radiometer system developed at Battelle Laboratory that has been in operation since June 1989. The rotating shadowband system proved useful in monitoring the effects of the June 1991 Mount Pinatubo volcanic eruption. The results were also summarized and incorporated in *Larson et al.* [1992].

Archiving and analysis capabilities were enhanced during 1991. Two new disk drives were added to the SRF computer system that allowed larger archived data sets to be put online for access by researchers. Additionally, a project was initiated in June 1991 that will reprocess all the historic 1-minute data collected at the SRF since it first became operational in early 1977. These data will be reformatted for compatibility with a newer SRF data system that began operation in early 1987. The goal is to have a continuous research data set online that will incorporate the time period from 1977 to present.

Standards activities during 1991 were focused on the procurement of two new active cavity radiometers that will be automated and controlled by an IBM-compatible computer system. They will also be equipped with optional windows that will allow all weather operation. A continuously-operated, window-equipped cavity radiometer, together with a diffuse measurement obtained from a continuously shaded pyranometer, achieves the highest accuracy broadband solar measurements using currently available sensors. These systems will be deployed at selected sites in the CMDL network.

3.1.12. Atmospheric Trajectory Analysis

An Analysis of 5-Day Midtroposphere Flow Patterns for the South Pole: 1985-1989

A study was completed whose goal was to describe common midtropospheric flow patterns for SPO. The results will be published in a special Antarctic issue of *Tellus*. Some of the highlights of this paper are presented here.

Isobaric 5-day back trajectories on the 500-hPa surface were calculated twice daily at 0000 and 1200 UT for 5 years, 1985-1989. The 500-hPa level was chosen to represent flow in the midtroposphere above the surface inversion. In addition, selected isentropic trajectories were computed to determine the effects of vertical motions on typical transport paths.

The trajectory models were documented by *Harris* [1982] and *Harris and Bodhaine* [1983]. Meteorological data was provided by ECMWF in the form of global gridded analyses from the WMO archive. Cluster analysis, a multivariate technique, was applied to the trajectories to summarize transport patterns by year and by month. The technique is documented in detail in *Harris and Kahl* [1990]. Factors contributing to uncertainty in SPO trajectories include interpolation errors in the trajectory calculations, uncertainty in the derived wind field caused by the sparsity of observations over Antarctica, and errors introduced by the isobaric approximation. The magnitude of these errors is probably similar to that estimated by *Kahl et al.* [1989] for trajectories in the Arctic. They estimated the uncertainty in trajectories to be 800-1000 km after 5 days. Some random trajectory errors may average out where large numbers of trajectories are summarized over years and seasons, as in this study. However, the flow patterns presented here should still be viewed as rough estimates of the actual transport to SPO.

Trajectories for each year were grouped into "transport clusters" consisting of trajectories having similar wind speed and direction. Figure 3.18 shows the mean trajectories or "cluster means" representing these transport clusters, determined for 2 selected years, 1987 and 1989. Plus signs indicate 1-day upwind intervals along the cluster means. At 5-days upwind of SPO, each cluster mean is marked with two numbers: (top) the percentage of all trajectories falling in that cluster and (bottom) an arbitrary number (1-6) identifying the transport cluster.

Cluster means produced for all 5 years indicated that easterly flow occurred 8-18% of the time. Flow from the east was most often anticyclonic, but sometimes weakly cyclonic. Winds were usually light enough that flow originated on the continent 5 days back. Westerly flow patterns were the strongest and most frequent (37-51% occurrence). They were also consistently cyclonic, usually reflecting flow from storms in the Ross Sea area, the average center of the circumpolar vortex. Strong northerly flow occurred more often in some years than in others. For example, cluster means show that 1987 (Figure 3.18*a*) had more vigorous northerly transport than other years, particularly 1989 (Figure 3.18*b*). Year-to-year variability was also apparent in other flow patterns. For example, the strength of southwesterly flow was

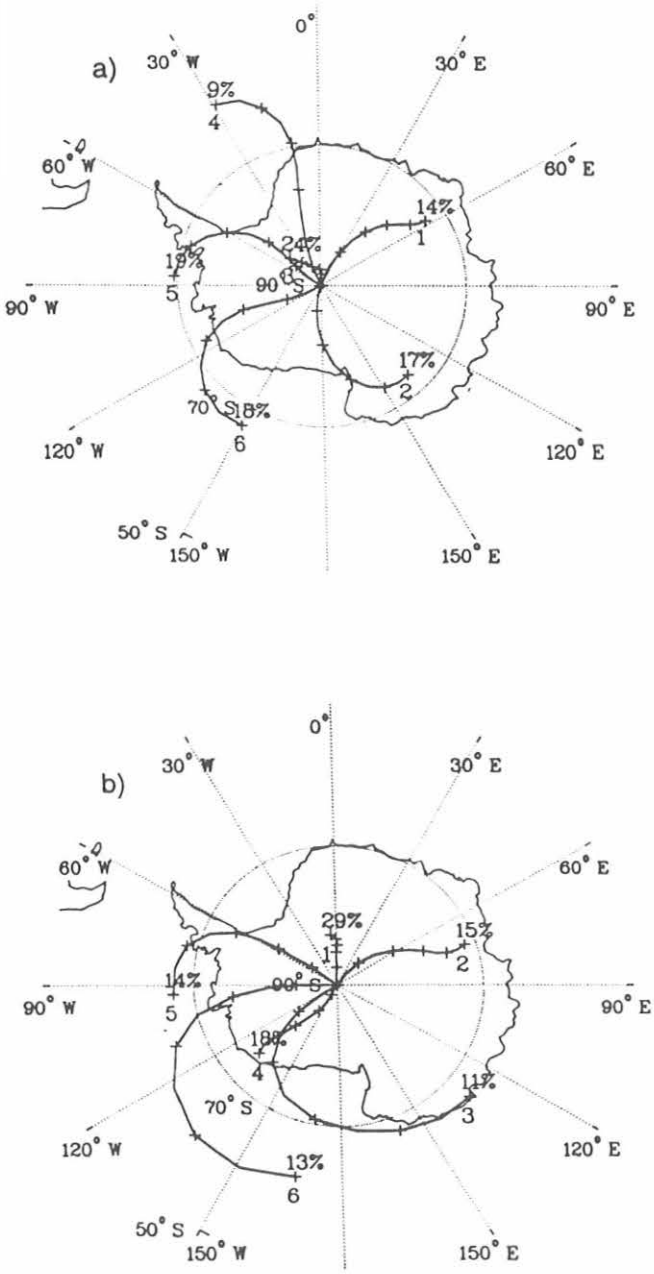

Fig.3.18. Yearly atmospheric flow patterns for SPO depicted by cluster-mean back trajectories at 500 hPa for (*a*) 1987 and (*b*) 1989. Plus signs indicate 1-day upwind intervals. The numbers 5 days upwind of SPO show (top) the percentage of trajectories occurring in that cluster and (bottom) the arbitrary cluster number used for identification.

reduced in 1987 (Figure 3.18*a*), and enhanced in 1988 (not shown) compared with other years.

Trajectories were also clustered by month to determine seasonal changes in flow pattern. Figure 3.19 shows the two extremes in seasonal flow: (a) January cluster means

indicating the lightest winds and (b) October cluster means indicating the strongest flow patterns of the year. Cluster means for the other months showed minimal long-range transport occurred within 5 days during November, December, and February. During April through September cluster means showed strong transport 9-29% of the time. The most vigorous long-range transport occurred during July through October.

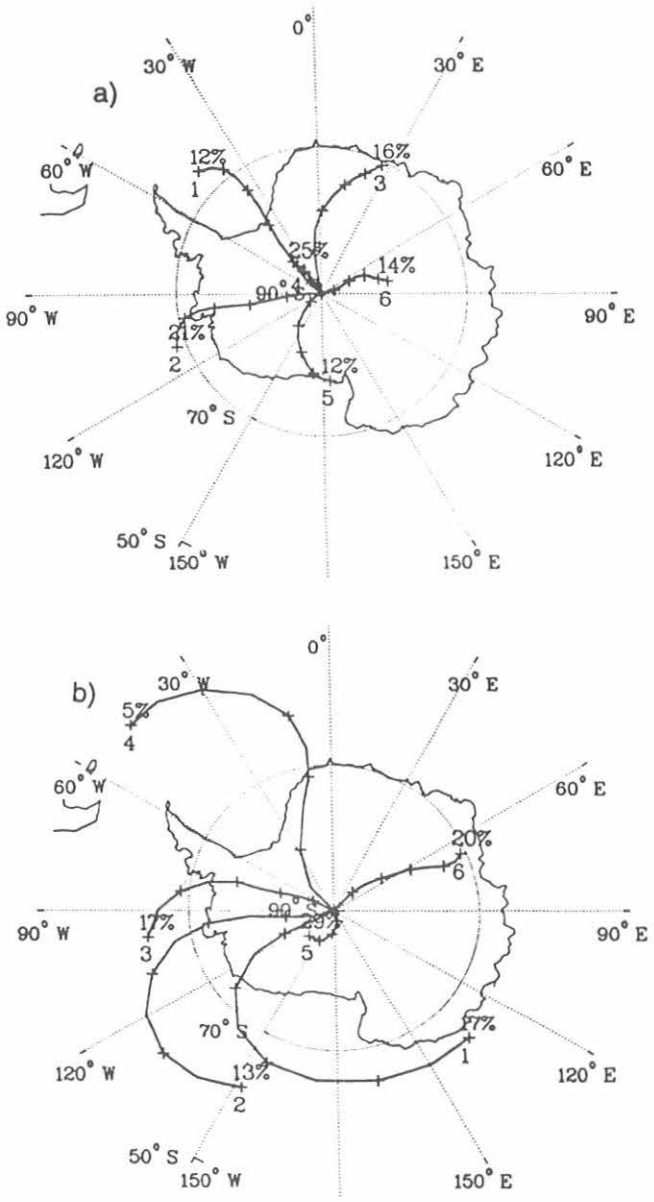

Fig.3.19. Atmospheric flow patterns for SPO, for (*a*) January and (*b*) October, depicted by cluster-mean back trajectories at 500 hPa for the period 1985—1989. Plus signs indicate 1-day upwind intervals. The numbers 5 days upwind of SPO show (top) the percentage of trajectories occurring in that cluster and (bottom) the arbitrary cluster number used for identification.

Isentropic trajectories were computed to investigate how typical transport patterns change when adiabatic vertical motions are taken into account. Figure 3.20 presents an example from a case study which compared isobaric to isentropic trajectories. Figure 3.20*a* shows 500-hPa isobaric trajectories and Figure 3.14*b* shows 275-K

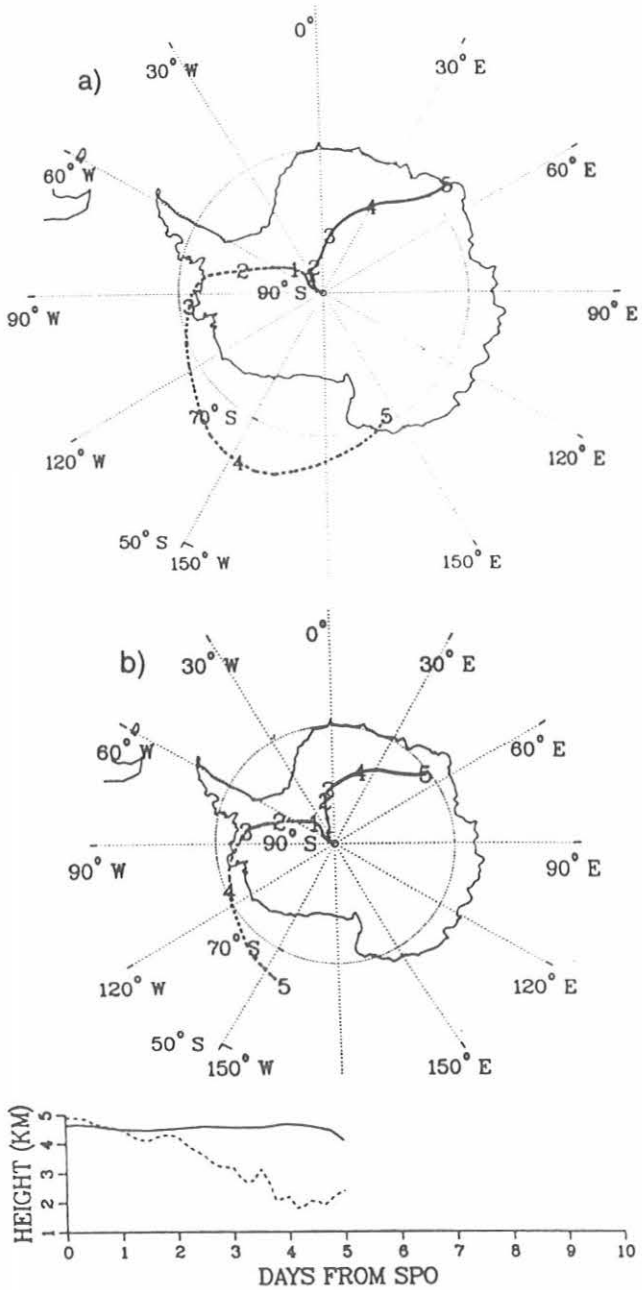

Fig.3.20. (*a*) 500-hPa isobaric trajectories and (*b*) 275-K isentropic trajectories arriving at SPO on August 21, 1989. Trajectories are marked at 1-day upwind intervals with a numeral showing the days back. The plot below the isentropic trajectories shows the heights of the air parcels. Line type distinguishes arrival time (solid = 0000 UT; dashed = 1200 UT).

isentropic trajectories, both arriving at SPO on August 21, 1989. The trajectories are marked at 1-day upwind intervals with a numeral showing the days back. A solid line is used for the trajectory arriving at 0000 UT, and a dashed line is used for the trajectory arriving at 1200 UT. A plot showing the heights of the air parcels is below the isentropic trajectories.

The height plot in Figure 3.20*b* reiterates the pattern seen frequently in the case study examples of ascent over west Antarctica, and steady heights over northeast Antarctica. The main reason that this pattern is revealed by the isentropic trajectories is that, on average, air is colder over the plateau east of SPO than over west Antarctica. The mean 500-hPa isotherms, though nearly circular, are offset to the east of the Pole by about 8° of latitude [*Schwerdtfeger*, 1970]. This asymmetry of the isotherms may be largely controlled by the elevation of the ice sheet and the extent of the radiation temperature inversion. In addition, SPO is much nearer to comparatively warm open water to the west than to the east. The result is that air parcels approaching SPO from the west cross larger temperature gradients than those from the east. The positive vertical motion seen in isentropic trajectories from the west is consistent with the fact that isentropes slope upward toward cold air [*Carlson*, 1981; *Harris and Bodhaine*, 1983].

Danielson [1961] described the systematic error in isobaric trajectories caused by warm-air advection associated with rising motion and (in the southern hemisphere) counterclockwise turning of the wind with height. The expected result over western Antarctica is more cyclonic curvature and higher wind speeds in the 500-hPa isobaric flow patterns, especially beyond the coast. This error is evident in Figure 3.20*a* in the trajectory arriving at 1200 UT.

The case study determined that the isobaric flow patterns are useful in these respects: (1) The direction in which the an air parcel arrives at SPO agrees with isentropic estimates. (2) Most isobaric trajectories over east Antarctica do not differ appreciably from isentropic ones because of limited vertical motion. (3) Isobaric trajectories over west Antarctica are usually too long and exhibit too much cyclonic curvature near and beyond the coast because of failure to account for ascent of the air parcels approaching SPO. However, the speed and curvature of the isobaric flow over west Antarctica is indicative of the vigor of the storms along the coast and their ability to transport marine air to the interior of Antarctica. (4) Because of the steep ascent of the isentropic surfaces over west Antarctica caused by the strong temperature gradient, air parcels probably originate in the boundary layer over open water around the coast. Any transport from farther northward within the boundary layer cannot be diagnosed by the isentropic model, but would be slower than that depicted by the isobaric model.

The knowledge gained from the isobaric transport clusters can thus be refined by the isentropic case study. This process leads to the conclusion that the source of aerosols, heat, and moisture that is episodically transported to SPO within 5 days is usually the marine boundary layer over open waters off the west coast of Antarctica. Transport from the Weddell Sea area is also possible, but occurs less frequently. The most vigorous transport occurs in 2-4 days, during July through October. Preferred transport with warm-air advection from the west reflects the fact that the circumpolar vortex is asymmetric, the average isotherms are offset to the east of the pole, and the continent itself is not symmetric in shape or elevation with respect to the pole.

3.2. Special Projects

3.2.1. Effects of Mt. Pinatubo Eruption on Strato-spheric Ozone

The ozonesonde programs at Boulder, Colorado, and Hilo, Hawaii, were reinstated following the eruption of Mt. Pinatubo in the Philippines in June 1991 to study the effects of the volcanic effluent on stratospheric ozone. Monthly average ozone concentrations in 2 km-thick layers at both sites are shown in Figures 3.21*a* and *b*. Post-eruption ozone concentrations were no lower than one standard deviation below the average. In light of the relatively short length of the record, this slight decrease is not statistically significant, although concentrations were consistently near the lowest values found for that season. Because of their locations at approximately 20°N and 40°N, Hilo and Boulder would not, however, be expected to show large depletion.

At SPO, on the other hand, there was a significant reduction of ozone in the lower stratosphere [*Hofmann et al.*, 1992]. This reduction, however, was probably primarily a result of the eruption of Mt. Hudson in southern Chile in August 1991 rather than an effect of Mt. Pinatubo. By late September the ozone mixing ratio in the 11-13 km layer was nearly 50% lower than any of the previous 5 years. This contributed to late September column amounts 10-15% lower for this period than during any previous year since soundings began in 1986.

3.2.2. Aerosol Absorption Measurements at MLO

Introduction

Smoke clouds associated with burning oil wells in Kuwait have been seen in satellite observations since early February 1991 [*Limaye et al.*, 1991]. Because of speculation concerning long-range transport of these pollution materials and their possible effect on global

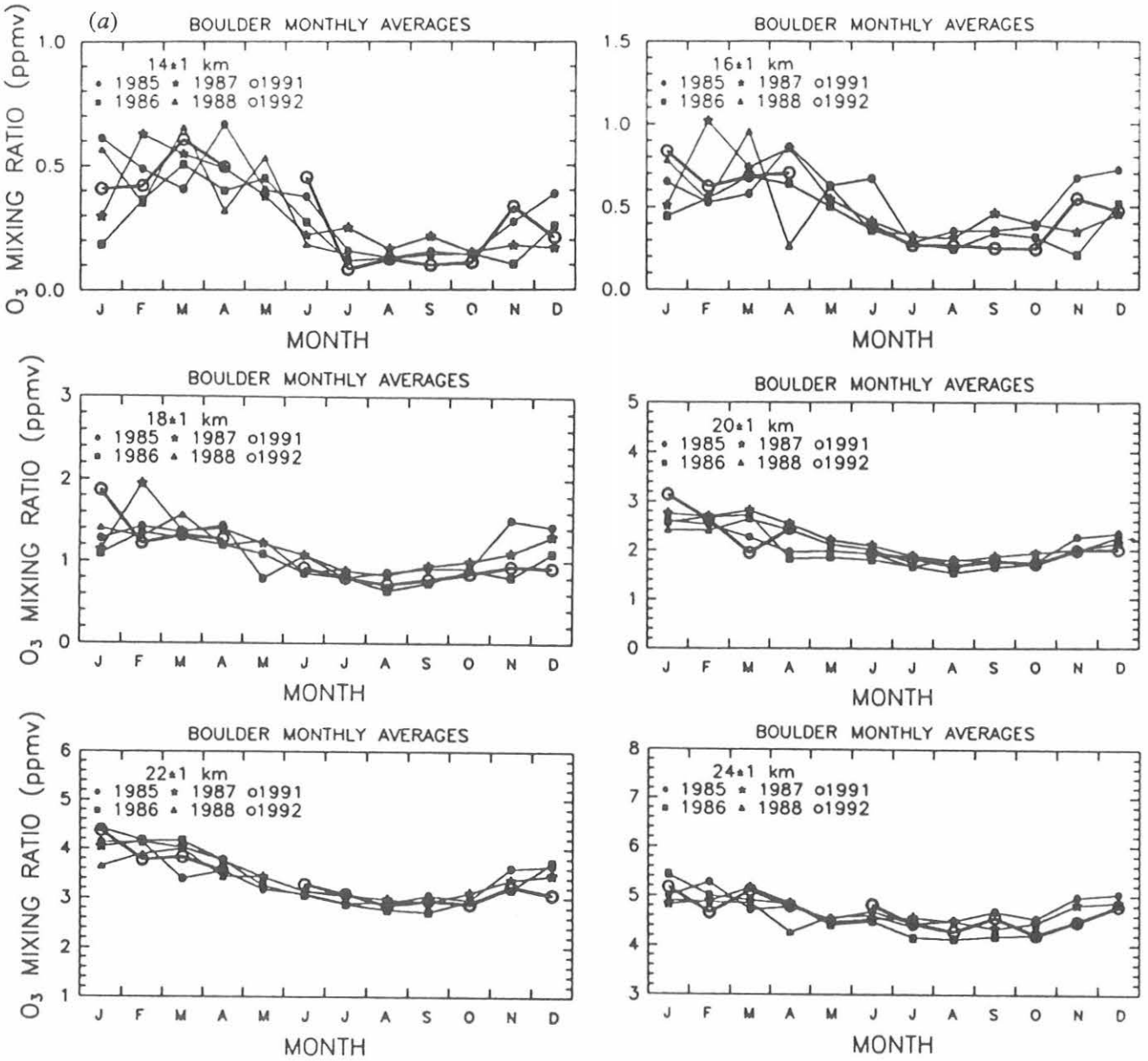

Fig. 3.21. Monthly average ozone mixing ratio in 2 km layers from (*a*) Boulder, and (*b*) Hilo, Hawaii. Approximately four soundings make up each monthy average.

climate, we examined the aerosol absorption record at MLO in order to detect any events that may have originated in Kuwait. Also, we calculated large-scale air-mass trajectories at the 500-hPa level in order to estimate the general direction of air-mass flow and approximate transport times from Kuwait to Hawaii. The results of this study were presented by *Bodhaine et al.* [1992].

The well-known annual cycle in aerosol concentrations at MLO has been discussed by *Bodhaine et al.* [1981] and is known to be caused by the long-range transport of dust from Asia during the spring [*Shaw*, 1980; *Darzi et al.*, 1982]. Trajectories calculated backwards from MLO [*Miller*, 1981; *Harris and Kahl*, 1990] show frequent long-range transport during winter and spring. The aerosol maximum at MLO in April and May occurs when strong westerly flow coincides with dust storms over Asian deserts [*Merrill et al.*, 1989].

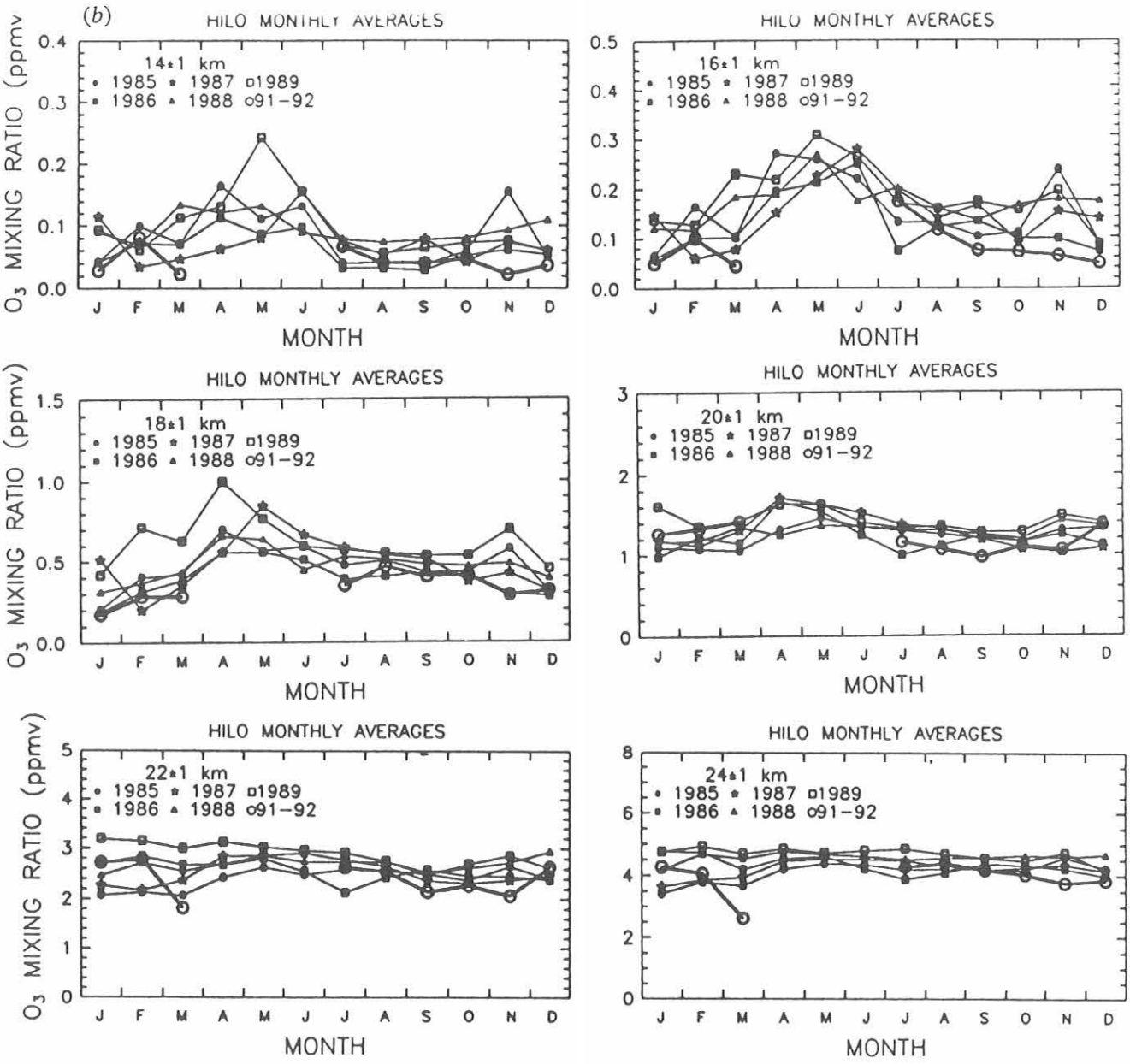

Fig. 3.21.—Continued. Monthly average ozone mixing ratio in 2 km layers from (*a*) Boulder, and (*b*) Hilo, Hawaii. Approximately four soundings make up each monthy average.

Instrumentation

Continuous measurements of the aerosol light absorption coefficient (σ_{ap}) were initiated at MLO in April 1990 using an aethalometer [*Hansen et al.*, 1982]. The aethalometer measures the attenuation of light transmitted through particles accumulating on a quartz-fiber filter in real time. The MLO instrument has an incandescent light source and a broadband detector; the spectral response for elemental carbon particles peaks at 830 nm [A.D.A. Hansen, personal communication, 1991]. We calculated σ_{ap} using the equation:

$$\sigma_{ap} = -\frac{1}{1.9}\frac{A\ln(I_2/I_1)}{Q(t_2-t_1)}$$

where A is the area of the spot on the filter (about 1 cm^2), Q is the volumetric sample flow rate (16.4 LPM), and I_1 and I_2 are the normalized intensities of the sample beam at times t_1 and t_2. The value 1.9 in the above equation combines the manufacturer's calibration factor of 19 m^2 g^{-1}, relating BC (black carbon) concentration to light attenuation on the filter, and an assumed value of 10 m^2 g^{-1}, relating BC concentration to light absorption in the atmosphere.

The stability of the aethalometer optics allows detection of changes in transmitted light intensity of 1 part in 10^4, corresponding to a light absorption coefficient of about 1.5×10^{-8} m^{-1} for a 1-hour mean. The corresponding detection limit for BC is 1.5 ng m^{-3} for a 1-hour mean. Since carbon is usually the dominant absorber in the atmospheric aerosol, the measurement of σ_{ap} is often used as a surrogate for BC [*Rosen et al.*, 1978]. Although hematite (Fe_2O_3) is a fairly strong absorber, about 200 times as much hematite as black carbon is needed for equivalent absorption.

Trajectory Calculations

Ten-day, 500-hPa isobaric trajectories [*Harris*, 1982] were calculated backwards from MLO twice daily for the period April 1990-June 1991. The average station pressure at MLO is 680 hPa; however, 500-hPa trajectories were chosen to represent midtropospheric transport in conjunction with nighttime downslope conditions at MLO [*Mendonca*, 1969]. The specification of a 10-day trajectory duration was made to facilitate the identification of potential source regions as far upwind as Kuwait, a distance of about 15,000 km. We have denoted a 10-day of Kuwait as a Kuwait (K) trajectory, and a 10-day trajectory that passes over Japan or the coast of China as a China (C) trajectory. All Kuwait trajectories also passed over southern China.

Discussion

Light absorption coefficient and BC concentrations are shown in Figure 3.22 (top), along with σ_{sp} (550 nm) and calculated single scatter albedo [$\omega = \sigma_{sp}/(\sigma_{sp} + \sigma_{ap})$] (bottom) for April 1990-June 1991. Each point is a 9-hour mean calculated from the hourly means between 1000-1800 GMT (0000-0800 LST). This time period is considered to be the best for sampling the nighttime downslope wind flow most representative of background tropospheric conditions at MLO. The time periods shown at the top of the graph indicate arrival times for air parcels that originated near Kuwait (K) or over China (C) within the previous 10 days. One annual cycle of σ_{ap} with numerous events superimposed on a slowly changing baseline is shown. The average of the baseline is of the order of 0.1-1 $\times$ 10^{-7} m^{-1} (1-10 ng m^{-3} BC) during summer and fall, and 1-3 $\times$ 10^{-7} m^{-1} (10-30 ng m^{-3} BC) during spring. Events in aerosol absorption exceeding 3 $\times$ 10^{-7}

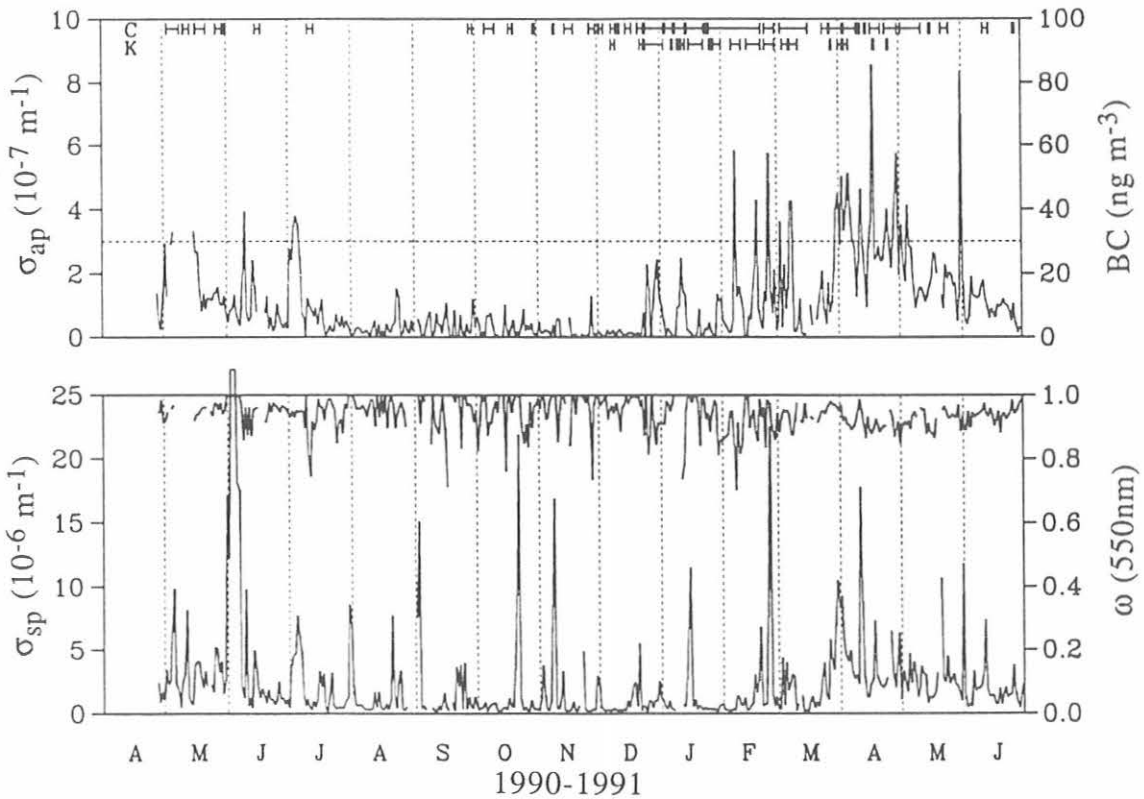

Fig. 3.22. Daily mean σ_{ap} (top) and σ_{sp} at 550 nm (bottom) at MLO during the time period April 1990-June 1991. The right-hand scale on the top graph shows calculated BC concentration. Also, ω at 550 nm is shown in the upper portion of the bottom graph (right-hand scale). The upper portion of the top graph shows time periods during which 500-hPa trajectories arriving at MLO passed over China (C) and/or Kuwait (K) within the previous 10 days.

trajectory that comes within 10° latitude and 20° longitude m^{-1} (30 ng m^{-3} BC), shown by the horizontal dashed line in Figure 3.22 (top), were considered to be candidates for long-range transport, possibly from Kuwait. Figure 3.23 shows an example of rapid transport from Kuwait to Hawaii on February 7, 1991. This trajectory was in the vicinity of Kuwait 5.5 days earlier, corresponding to an average speed of about 32 m s^{-1}. This is relatively fast transport for the 500-hPa level (about 5.5 km altitude), and is below the jet stream. Note the absence of BC events in mid-March during the absence of Kuwait trajectories.

Conclusion

Large peaks in the MLO σ_{ap} record coincide with rapid transport events from Kuwait to Hawaii as shown by large-scale back-trajectory calculations. These measurements set an upper limit on expected BC concentrations in the free troposphere due to Kuwaiti oil fires because Kuwait trajectories also pass over southern China and could contain particles originating in China. The envelope of average concentrations appears to be about 15-30 ng m^{-3} during conditions of maximum long-range transport, with some events exceeding 50 ng m^{-3}. This may be compared to BC concentrations exceeding 1 μg m^{-3} during an Arctic haze event [*Hansen and Rosen*, 1984] in a layer about 500 m above Barrow, Alaska, and the much higher concentrations found in urban areas.

The climatic effect of aerosol particles depends on the optical properties of the particles and on the albedo of the underlying surface. Absorbing particles will cause a localized heating of the atmosphere, while backscattering essentially reduces the amount of incoming solar energy. The concentrations found in this study will have a negligible effect on the earth's climate.

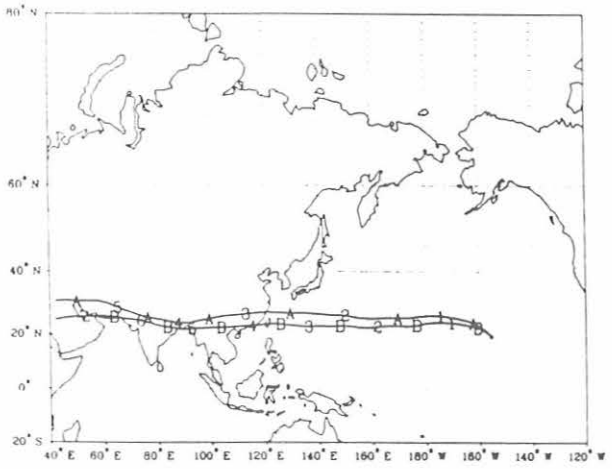

Fig. 3.23. Trajectories calculated backwards from MLO at the 500-hPa level at 0000 GMT (A) and 1200 GMT (B) on February 7, 1991. The numbers on the trajectories indicate days backward from MLO; the A and B labels appear at the 0.5-day points.

3.2.3. Umkehr Ozone Profile Analysis (1979-1990)

Introduction

Umkehr ozone profile data from five stations situated in the northern hemisphere were corrected for stratospheric aerosol errors and analyzed for short-term trend (using simple linear regression) between, and including, the years 1979 to 1986 by *DeLuisi et al.* [1989]. The primary reason that the short-term analysis was performed was that a profound downward trend in upper stratospheric ozone was reported to have been observed by the Solar Backscatter UltraViolet (SBUV) satellite ozone profiler. The SBUV was known to have a problem with a calibration drift of the diffuser plate that periodically reflects solar UV into the view of the instrument. The sun observation then becomes the calibration reference. Not knowing whether the trend was real or an artifact of the SBUV instrument, a panel of experts (Ozone Trends Panel) was formed to investigate the situation. The Umkehr measurement was of interest to the panel because of its sensitivity to ozone profile in the upper stratosphere and, therefore, Umkehr measurements could be compared with the SBUV results for verification. The short-term Umkehr analysis by *DeLuisi et al.* [1989] revealed a trend of -1.1% per year at 40 km, whereas the SBUV trend was approximately twice this value after corrections for the diffuser were applied [*Fleig et al.*, 1989]. The Umkehr result was in agreement with photochemical predictions of ozone depletion and effects of the solar cycle, although this result does not necessarily verify whether the fluorocarbon ozone depletion theory is correct.

In June 1991, a workshop was held by the World Meteorological Organization (WMO) at Geneva, Switzerland, to update the status of stratospheric ozone research. This report briefly summarizes the features of the updated CMDL's Umkehr ozone trends findings that were provided for the workshop report. This report also contains a comparison of the Umkehr results with results from a recent calibration of the SBUV by a carefully calibrated SBUV instrument (the SSBUV) carried aboard the Space Shuttle [*Hilsenrath et al.*, 1992].

Procedure

Umkehr observations obtained by five northern midlatitude stations comprised the basic data set for analysis. The five stations are: Tateno, Japan; Boulder, Colorado; Lisbon, Spain; Arosa, Switzerland; and Belsk, Poland. These stations range in latitude from 36°N to

observations from 1979 to 1984, after which SAGE II aerosol and ozone data were used because of the extended global coverage and high frequency data rate. Corrections to Umkehr ozone profiles were also calculated for 10° wide latitude bands centered on 10° latitudes, overlapping the regions where Umkehr measurements are made. Monthly averages of the entire set of Umkehr data from all five stations were then calculated. This approach gives greater weight to the stations providing the greater numbers of Umkehr data. The method used for correcting the Umkehr data was reported by *DeLuisi et al.* [1989].

Results

Figure 3.24 is an update of Umkehr measurements from the five stations mentioned in the previous section. Umkehr layers 7 (35.1 km) and 8 (40.1 km) are shown. The Umkehr layer system is tabulated in Table 3.8. To remove the annual cycle, the monthly averaged Umkehr data are averaged and then subtracted from each month. The result is a departure from a mean. Inspection of the resulting data reveals a period of high ozone concentration from 1979 to 1982. Shortly after this period, the ozone concentration decreased rather dramatically until 1985. After this, the concentrations remained nearly constant until the present. It is worthy to note that the solar cycle maxima occurred in 1980 and 1991. By now, the ozone concentrations should be up to the levels of 1980 if only solar cycle effects control the ozone concentrations in the upper stratosphere.

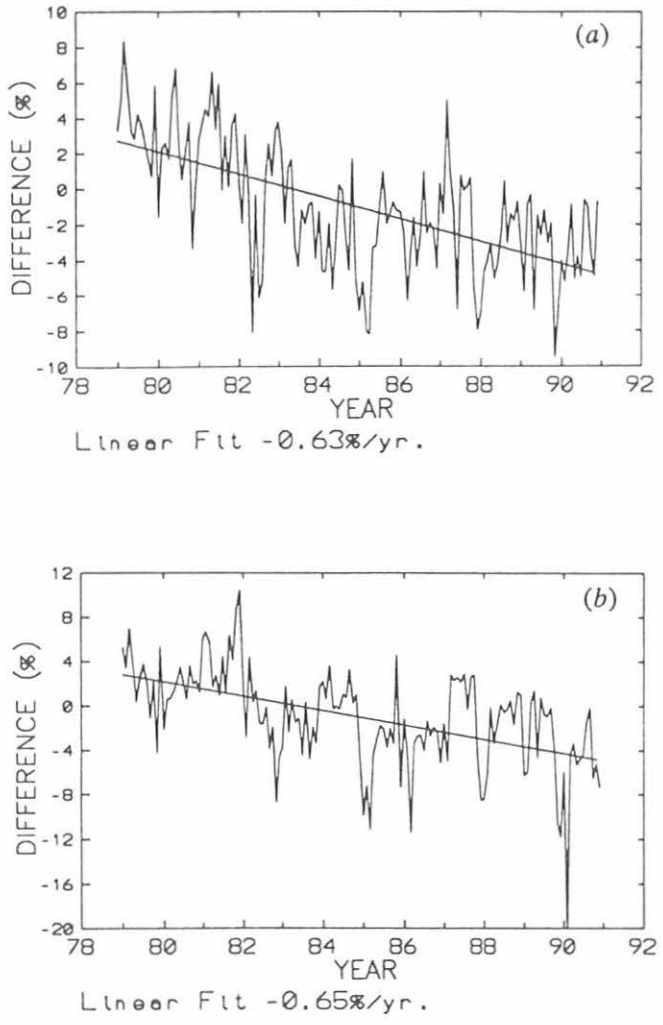

Fig. 3.24. Plots of deseasonalized ozone concentration in Umkehr layers 7 and 8 are shown as departures from the mean of all months for each month. Note the line representing the linear least-square fit to the data.

TABLE 5.8. Layers Used for Umkehr Ozone Profile Retrievals

Layer Number	Layer-Base Pressure (atm)	Layer-Base Height (km)
0	1.00E + 0	0.0
1	5.00E − 1	5.5
2	2.50E − 1	10.3
3	1.25E − 1	14.7
4	6.25E − 2	19.1
5	3.12E − 2	23.5
6	1.56E − 2	28.0
7	7.81E − 3	32.6
8	3.91E − 3	37.5
9	1.95E − 3	42.6

Figure 3.24 also shows a linear least-squares fit to the ozone concentrations in layers 7 and 8, serving as an example of the procedure used to obtain a measure of the changes that occurred during the period of time being examined. Figure 3.25 summarizes results of the least-squares analyses for layers 4 through 9. It is clear from the results in Figure 3.25 that ozone has been decreasing in most Umkehr layers. The exception is perhaps layer 5 (26.2 km) in which ozone changes, in percent, appear to be minimal.

Figure 3.26 shows a comparison of Umkehr ozone changes with those determined by the SSBUV. The SSBUV flew in October 1989, and the area of the earth covered by the satellite ranged from 30°S to 30°N; whereas, the Umkehr stations and the changes were calculated for October and November combined. In general the agreement is quite good. Note, however, that the magnitudes of the changes are less than those for all years shown in Figure 3.25. These changes are consistent with seasonally-dependent negative changes noted in the total ozone, which were shown to be smallest in the fall season.

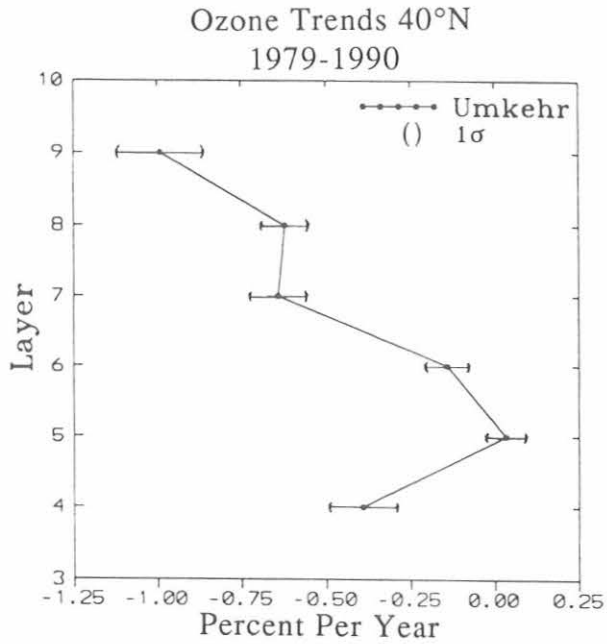

Fig. 3.25. Summary of the least-square fit analysis, similar to Figure 3.24, of ozone for Umkehr layers 4-9.

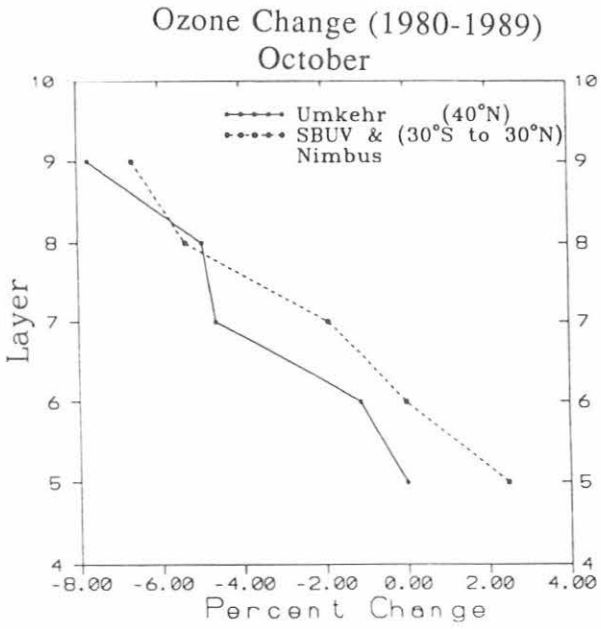

Fig. 3.26. Comparison of SSBUV ozone changes with those determined by Umkehr. These results are representative of changes occurring in the fall season.

Conclusion

Umkehr measurements for 1979 through 1990 obtained at five stations situated near 40°N, have been showing a general decline in atmospheric ozone at practically all altitudes, with the possible exception of Umkehr layer 5. The decline does not appear to be manifested as a steadily decreasing change. Rather, it appears to be primarily due to a step change occurring mainly during 1982 through 1984. A comparison of linear least-square fit to fall-season Umkehr ozone profile data with a change in ozone profile observed by the SBUV and the SSBUV in the fall of 1980 and 1989 shows generally good agreement. In the photochemical region, a change of approximately -5% is noted for 1979-1990, according to Umkehr observations and SBUV observations made in 1980 through 1989. During the present period of solar activity maximum starting in 1990, the Umkehr ozone concentrations near 40 km do not appear to be increasing to the level observed in 1980 during the time of solar activity maximum.

3.3. References

Bass, A.M., and R.J. Paur, The ultraviolet cross-sections of ozone, in *Atmospheric Ozone*, edited by C.S. Zerefos and A. Ghazi, pp. 606-610, Reidel, Boston, 1985.

Bluth, G.J.S., S.D. Doiron, C.C. Schnetzler, A.J. Krueger, L.S. Walter, , Global Tracking of the SO_2 Clouds from the June 1991 Mount Pinatubo Eruption, *Geophys. Res. Lett. 19*, 151-154, 1992.

Bodhaine, B.A., and J.J. DeLuisi, An aerosol climatology of Samoa, *J. Atmos. Chem., 3*, 107-122, 1985.

Bodhaine, B.A., and M.K. Shanahan, Condensation nucleus and aerosol scattering extinction measurements at the South Pole Observatory: 1979-1988, *NOAA Data Rep. ERL CMDL-1*, NOAA Climate Monitoring and Diagnostics Laboratory, Boulder, CO, 148 pp., 1990.

Bodhaine, B.A., B.G. Mendonca, J.M. Harris, and J.M. Miller, Seasonal variations in aerosols and atmospheric transmission at Mauna Loa Observatory, *J. Geophys. Res., 86*, 7395-7398, 1981.

Bodhaine, B.A., J.J. DeLuisi, J. M. Harris, P. Houmere, and S. Bauman, Aerosol measurements at the South Pole, *Tellus, 38B*, 223-235, 1986.

Bodhaine, B.A., J.J. DeLuisi, J. M. Harris, P. Houmere, and S. Bauman, 1987, PIXE analysis of South Pole aerosol, *Nuclear Instr. Meth., B22*, 241-247, 1987.

Bodhaine, B.A., J.M. Harris, J.A. Ogren, and D.J. Hofmann, Aerosol optical properties at Mauna Loa Observatory: Long-range transport from Kuwait? *Geophys. Res. Lett., 19*, 581-584, 1992.

Carlson, T.N., Speculations on the movement of polluted air to the Arctic, *Atmos. Environ., 15*, 1473-1477, 1981.

Cess, R.D., E.G. Dutton, J.J. DeLuisi, and F. Jiang, Determining surface solar absorption from broadband satellite measurements for clear skies: Comparison with surface measurements. *J. Climate, 4*, 236-247, 1991.

Cess, R.D., S. Nemesure, E.G. Dutton, J.J. DeLuisi, G.L. Potter, and J.J. Morcrette, The impact of clouds on the shortwave radiation budget of the surface-atmosphere system: Interfacing measurements and models, *J. Climate*, in press, 1992.

Danielson, E.F., Trajectories: Isobaric, isentropic and actual, *J. Meteorol., 18*, 479-486, 1961.

Darzi, M., and J.W. Winchester, Aerosol characteristics at Mauna Loa Observatory, Hawaii, after east Asian dust storm episodes, *J. Geophys. Res., 87*, 1251-1258, 1982.

DeLuisi, J.J., D.U. Longenecker, and C.L. Mateer, An objective method of correcting Umkehr measurements for volcanic aerosol error, *Proceedings, Quadrennial Ozone Symposium 1988 and*

Tropospheric Ozone Workshop, Göttingen, Germany, August 8-13, 1988, edited by R.D. Bojkov and P. Fabian, pp. 100-104, A. Deepak, Hampton, VA, 1989.

DeLuisi, J.J., D.U. Longenecker, C.L Mateer, and D.U. Wuebbles, An analysis of northern middle-latitude Umkehr measurements corrected for stratospheric aerosols for 1979-1986, *J. Geophys. Res. 94(D7)*, 9837-9846, 1989.

Dutton, E.G., An extended comparison between LOWTRAN7-computed and observed broadband thermal irradiance: Global extreme and intermediate surface conditions. *J. Atmosph. Oceanic Tech.*, submitted, 1992*a*.

Dutton, E.G., A coherence between the QBO and the amplitude of the Mauna Loa atmospheric transmission annual cycle. *Int. J. Climatol.*, in press, 1992*b*.

Dutton, E.G., and D.J. Endres, Date of snowmelt at Barrow, Alaska, U.S.A., *Arctic and Alpine Res., 23*, 115-119, 1991.

Dutton, E.G., R.S. Stone, D.W. Nelson, and B.G. Mendonca, Recent interanual variations in solar radiation, cloudiness, and surface temperature at the South Pole, *J. Climate, 4(8)*, 848-858, 1991.

Dutton, E.G., S. Ryan, P. Reddy, and J. DeLuisi, Clear sky aerosol optical depth at Mauna Loa, 1982—1991, unpublished manuscript, 1992.

Elkins, J.W., and R.M. Rosson (Eds.), *Geophysical Monitoring for Climatic Change, No. 17: Summary Report 1988*, 142 pp., NOAA Air Resources Laboratory, Boulder, CO, 1989.

Ferguson, E.E. and R.M Rosson (Eds.), *Climate Monitoring and Diagnostics Laboratory, No. 19: Summary Report 1990*, pp. 34-54, NOAA Environmental Research Laboratories, Boulder, CO, 1991.

Fleig, A.J., D.S. Silberstein, C.G. Wellemeyer, P.K. Bhartia, and J.J. DeLuisi, An assessment of the SBUV/TOMS ozone data quality, based on comparison with external data, *Proceedings, the Quadrennial Ozone Symposium 1988 and Tropospheric Ozone Workshop*, edited by R.D. Bojkov and P. Fabian, 822 pp., A. Deepak, Hampton, VA, 1989.

Foster, J.L., J.W. Winchester, and E.G. Dutton, The date of snow disappearance on the Arctic tundra as determined from satellite, meteorological station, and radiometric in-situ observations, *IEEE Trans. Geosci. Remot. Sens.*, in press, 1992.

Garcia, R.R., and S. Solomon, A possible relationship between interannual variability in Antarctica ozone and the quasi-biennial oscillation, *Geophys. Res. Lett., 14*, 848-851, 1987.

Hansen, A.D.A., and H. Rosen, Vertical distribution of particulate carbon, sulfur, and bromine in the Arctic haze and comparison with ground-level measurements at Barrow, Alaska, *Geophys. Res. Lett., 11*, 381-384, 1984.

Hansen, A.D.A., H. Rosen, and T. Novakov, Real-time measurement of the absorption coefficient of aerosol particles, *Appl. Opt., 21*, 3060-3062, 1982.

Harris, J.M., The GMCC atmospheric trajectory program, *NOAA Tech. Memo. ERL ARL-116*, 32 pp., NOAA Environmental Research Laboratories, Boulder, CO, 1982.

Harris, J.M., and B.A. Bodhaine (Eds.), *Geophysical Monitoring for Climatic Change, No. 11: Summary Report 1982*, pp. 67-75, NOAA Environmental Research Laboratories, Boulder, CO, 1983.

Harris, J.M., and J.D. Kahl, A descriptive atmospheric transport climatology for the Mauna Loa Observatory using clustered trajectories, *J. Geophys. Res., 95(D9)*, 13,651-13,667, 1990.

Hilsenrath, E., R.P. Cebula, and C.H. Jackman, Ozone depletion in the upper stratosphere etimated from satellite and space shuttle data, *Nature, 358*, 131-133, 1992.

Hofmann, D.J., S.J. Oltmans, J.M. Harris, S. Solomon, T. Deshler, and B.J. Johnson, Observation and possible causes of new ozone depletion in Antarctica in 1991, *Nature, 359*, 283-287, 1992.

Jaffe, D.A., Local sources of pollution in the Arctic: From Prudhoe Bay to the Taz Peninsula, in *Pollution of the Arctic Atmosphere*, edited by W.T. Sturges, pp. 255-287, Elsevier, New York, 1991.

Kahl, J.D., J.M. Harris, G.A. Herbert, and M.P. Olson, Intercomparison of three long-range trajectory models applied to Arctic haze, *Tellus, 41(B)*, 524-536, 1989.

Komhyr, W.D., R.D. Grass, and R.K. Leonard, Total ozone decrease at South Pole, Antarctica, 1964-1985, *Geophys. Res. Lett., 13*, 1248-1251, 1986.

Komhyr, W.D., R.D. Grass, and R.K. Leonard, Dobson spectrophotometer 83: A standard for total ozone measurements, 1962-1987, *J. Geophys. Res., 94(D7)*, 9847-9861, 1989.

Komhyr, W.D., C.L. Mateer, and R.D. Hudson, Effective Bass-Paur 1985 ozone absorption coefficients for use with Dobson ozone spectrophotometers, *J. Geophys. Res.*, submitted, 1992.

Larson, N.R., E.W. Kleckner, J.J. Michalsky, and L.C. Harrison, Mount Pinatubo stratospheric aerosol perturbation measured by northern mid-latitude solar photometers, *EOS, 73(14)*, 67, 1992).

Limaye, S.S., V.E. Suomi, C. Velden, and G. Tripoli, Satellite observations of smoke from oil fires in Kuwait, *Science, 252*, 1536-1539, 1991.

Massey, D.M., T.K. Quakenbush, and B.A. Bodhaine, Condensation nuclei and aerosol scattering extinction measurements at Mauna Loa Observatory: 1974-1985, *NOAA Data Rep. ERL ARL-14*, 174 pp., Air Resources Laboratory, Silver Spring, MD, 1987.

McCormick, M.P., R.E. Veiga, SAGE II Measurements of early Pinatubo aerosols, *Geophys. Res. Lett. 19*, 155-158, 1992.

McPeters, R.D., and W.D. Komhyr, Long-term changes in SBUV/TOM relative to World Primary Standard Dobson Spectrophotometer 83, *J. Geophys. Res., 96(D2)*, 2987-2993, 1991.

Mendonca, B.G., Local wind circulation on the slopes of Mauna Loa, *J. Appl. Meteorol., 8*, 533-541, 1969.

Merrill, J.T., M. Uematsu, and R. Bleck, Meteorological analysis of long range transport of mineral aerosols over the North Pacific, *J. Geophys. Res., 94*, 8584-8598, 1989.

Miller, J.M., A five-year climatology of back trajectories from the Mauna Loa Observatory, Hawaii, *Atmos. Environ., 15*, 1553-1558, 1981.

Oltmans, S.J., W.D. Komhyr, P.R. Franchois, and W.A. Matthews, Tropospheric ozone: Variations from surface and ECC ozonesonde observations, in *Proceedings, Quadrennial Ozone Symposium 1988 and Tropospheric Ozone Workshop*, edited by R.D. Bojkov and P. Fabian, 539-543, A. Deepak, Hampton, VA, 1989*a*.

Oltmans, S.J., R.C. Schnell, P.J. Sheridan, R.E. Peterson, S.M. Li, J.W. Winchester, P.P. Tans, W.T. Sturges, J.D. Kahl, and L.A. Barrie, Seasonal surface ozone and filterable bromine relationship in the high Arctic, *Atmos. Environ., 23*, 2431-2441, 1989*c*.

Oltmans, S.J., and H. Levy II, Seasonal cycle of surface ozone over the western North Atlantic, *Nature, 358*, 392-394, 1992*a*.

Oltmans, S.J. and H. Levy II, Ozone measurements from a global network of surface sites, *Proceedings, 1992 Quadrennial Ozone Symposium*, Charlottesville, VA, June 4-13, 1992, A. Deepak, Hampton, VA, in press, 1992*b*.

Quakenbush, T.K., and B.A. Bodhaine, Surface aerosols at the Barrow GMCC Observatory: Data from 1976 through 1985, *NOAA Data Rep. ERL ARL-10*, 230 pp., Air Resources Laboratory, Silver Spring, MD, 1986.

Radke, L.F., C.A. Brock, R.J. Ferek, and D.J. Coffman, Summertime arctic hazes, paper A52B-03 presented at the AGU Fall Annual Meeting, San Francisco, December 3-7, 1990.

Rosen, H., A.D.A. Hansen, L. Gundel, and T. Novakov, Identification of the optically absorbing component in urban aerosols, *Appl. Opt., 17*, 3859-3861, 1978.

Russell, P.B., E.G. Dutton, R.F. Pueschel, J.M. Livingston, T. DeFoor, D. Allen, P. Pilewskie, M.A. Box, J.A. Reagan, B.M. Herman, S.A. Kinne, and D.J. Hofmann, Pinatubo and prePinatubo optical depth spectra: Mauna Loa measurements, comparison, inferred particle size distributions, radiative effects, and relationship to lidar, *J. Geophys. Res.*, submitted 1992.

Schnell, R.C., S.C. Liu, S.J. Oltmans, R.S. Stone, D.J. Hofmann, E.G. Dutton, T. Deshler, W.T. Sturges, J.W. Harder, S.D. Sewell, M. Trainer, and J.M. Harris, Decrease of summer tropospheric ozone concentrations in Antarctica, *Nature, 351*, 726-729, 1991.

Schwerdtfeger, W., The climate of Antarctica, in *World Survey of Climatology, 14*, edited by S. Orvig, 253-355, New York, Elsevier, 1970.

Shaw, G. E., Transport of Asian Desert aerosol to the Hawaiian islands, *J. Appl. Meteorol., 19*, 1254-1259, 1980.

Vigroux, E., Détermination des coefficients moyens d'absorption de l'ozone en vue des observations concernant l'ozone atmosphèrique a l'aide du spectromètre Dobson, *Ann. Phys., 2*, 209-215, 1967.

WMO, Report of the International Ozone Trend Panel-1988, *World Meteorological Organization Global Ozone Research and Monitoring Project-Report No. 18, 1*, 193-197, 1988.

4. Acquisition and Data Management Division

G. HERBERT (EDITOR), M. BIENIULIS, T. MEFFORD, AND K. THAUT

4.1. CONTINUING PROGRAMS

4.1.1. STATION CLIMATOLOGY

The climatology of surface weather observations at the CMDL observatories is based on hourly-average measurements of the wind direction, wind speed, station pressure, air and dewpoint temperature, and precipitation amount. The 15-year station climatologies are an important record for the interpretation of measured values of aerosols, trace gases, and climatic change. The sensors currently in use were selected not only for high accuracy, but also for ruggedness, to minimize failures in the extreme conditions of the polar region (Table 4.1). To the extent that it is practical, WMO siting standards were followed.

Table 4.1 describes the disposition of the sensors as of January 1, 1991. The following changes were made throughout the year: at BRW, there were no changes in the instruments throughout 1991. At MLO, the secondary anemometer, 782 was replaced with anemometer 1829 on DOY 145. On DOY 166, the primary anemometer 931 was replaced with 782. Then on DOY 346, the two anemometers were switched such that 1829 was the primary anemometer while 782 became the secondary anemometer. In SMO, anemometer 458 was replaced with 883 on DOY 271. At SPO anemometer 168 was replaced with 577 on DOY 150. Thermometer 701 was replaced with 704 on DOY 325. Also on DOY 325, thermometer 703 was moved from a height of 2.2 m to 2.0 m. On DOY 327, thermometer 704 was moved to a height of 19.2 m while thermometer 835 and hygrometer 3720 were moved to a height of 2.0 m. A week later, thermometer 704 was again moved to a height of 21.2 m. On DOY 338, anemometer 168 was replaced with 826.

Barrow

Descriptions of the BRW station and its climate are given in previous *CMDL Summary Reports* [e.g., *DeLuisi*, 1981]. Wind roses of hourly averages resultant wind direction and speed are presented in 16 direction classes and 4 speed classes (Figure 4.1). Winds from the "clean-air" sector, north-northeast-southeast directions occurred 59% of the time as compared to 63% for the 14-year climatology. In 1991, 20% of the winds came from the east-northeast as compared to 17% for the 14-year climatology. The year's maximum hourly average wind speed of 22 m s^{-1} occurred on January 30, which set a new all time record for the month. A new maximum wind speed was measured during May as well.

The average temperature for 1991 was within 0.5°C of the climatological average of –12.7°C (Table 4.2). A record maximum temperature of 18.0°C was reported for June. Like 1990, the monthly mean temperatures and pressures were not significantly different from normal.

Mauna Loa

In this report, the climatology of MLO is regarded as consisting of two distinct regimes because the bimodal distribution of the wind direction changes with the time of day. The night (downslope) period (1800-0600 LST) and the day (upslope) period (0600-1800 LST) define the two regimes. The 14-year night and day wind roses illustrate the two distinct wind patterns (Figure 4.2).

TABLE 4.1. CMDL Meteorological Sensor Deployment 1991

Sensor	BRW		MLO		SMO		SPO	
	Serial No.	Elevation, m	Serial No.	Elevation, m	Serial No.	Elevation, m	Serial No.	Elevation, m
Primary anemometer*	576	16.7	931	8.5	458	13.7	168	11.8
Secondary anemometer*			782	38.5				
Pressure transducer†	2366	9	225	3403	752	30	8	2840
Mercurial barometer	641	9	278	3403	961	30		
Air temperature A‡	8801	2.5	8805	1.7	8803	9.8	703+	2.2
Air temperature B§	8802	15.3	8809	37.8	8806	2.3	701+	23.2
Air temperature C‡	8	3.1	46	2.0	50	9.8	835+	2.2
Dewpoint temperature hygrometer**	8	3.1	46	2.0	50	9.8	3720	2.2

*Aerovane, Bendix, Inc., model no. 141, Baltimore, MD.

† Pressure transducer, Rosemount, Inc., model no. 1201F1b, Minneapolis, MN. Heights of all pressure sensors are given with respect to MSL.

‡Linearized thermistors, Yellow Springs Inst. Co., model no. 44212, Yellow Springs, Ohio, except at SPO.

Platinum resistance thermometer, Yellow Springs Inst. Co., model no. RTD-385, Yellow Springs, Ohio

§Thermometer, positioned at the top of the local sampling tower to facilitate an estimation of boundary layer stability.

**Hygrothermometer, Technical Services Laboratory model no. 1063, Fort Walton Beach, FL.

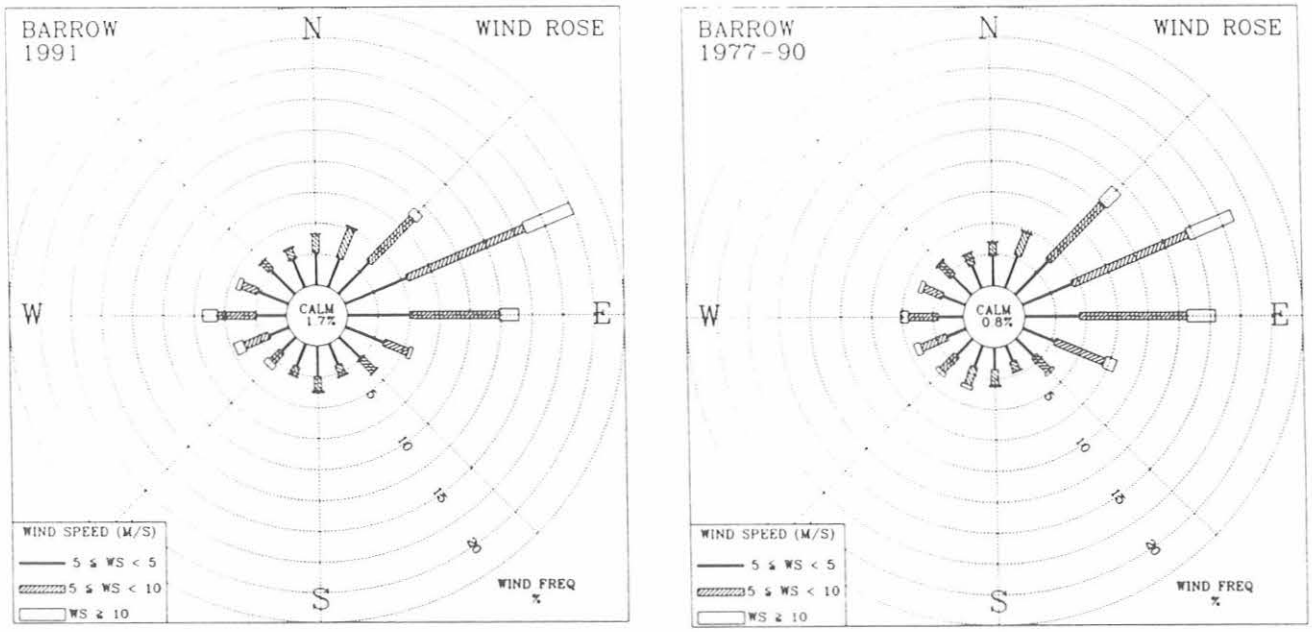

Fig. 4.1. Wind rose of surface winds for BRW for 1991 (left) and 1977-1990 (right)

TABLE 4.2. BRW 1991 Monthly Climate Summary

	Jan.	Feb.	March	April	May	June	July	Aug.	Sept.	Oct.	Nov.	Dec.	1991
Prevailing wind direction	W	ENE	W	ENE	ENE	E	E	ENE	ENE	E	ENE	ENE	ENE
Average wind speed (m s^{-1})	7.0	6.2	4.9	5.1	6.0	5.4	5.0	6.6	7.2	6.2	5.4	6.0	5.9
Maximum wind speed* (m s^{-1})	22	17	13	13	17	10	16	18	17	17	13	14	22
Direction of max. wind* (deg.)	257	63	44	61	54	75	218	263	78	227	329	61	257
Average station pressure (hPa)	1020.6	1020.0	1013.1	1014.7	1012.7	1015.8	1014.1	1011.1	1014.8	1013.1	1020.8	1008.1	1014.9
Maximum pressure* (hPa)	1047	1044	1033	1027	1029	1024	1030	1023	1031	1031	1038	1045	1047
Minimum pressure* (hPa)	992	998	997	1003	998	1004	993	987	997	988	1001	986	986
Average air temperature (°C)	−27.9	−28.7	−28.3	−16.6	−3.1	1.2	2.2	1.6	−1.3	−7.4	−22.1	−26.5	−12.4
Maximum temperature* (°C)	−11	−13	−13	−6	2	18	12	16	11	1	−4	−17	18
Minimum temperature* (°C)	−40	−44	−42	−36	−11	−5	−2	−4	−6	−20	−35	−36	−44
Average dewpoint temperature (°C)	−28.4	−29.4	−31.1	−18.9	−4.4	−0.7	0.8	0.2	−2.6	−8.6	−24.5	−29.2	−14.4
Maximum dewpoint temperature (°C)	−2	−14	−15	−7	0	11	9	9	6	1	−5	−19	11
Minimum dewpoint temperature (°C)	−45	−45	−46	−39	−12	−6	−3	−5	−7	−21	−38	−40	−46
Precipitation (mm)	0	1	0	2	4	2	5	5	5	1	0	0	24

Instrument heights: wind, 16.7 m; pressure, 9 m (MSL); air temperature, 2.5 m; dewpoint temperature, 3.1 m. Wind and temperature instruments are on tower 25 m northeast of the main building.

*Maximum and minimum values are hourly averages.

TABLE 4.3. MLO 1991 Monthy Climate Summary

	Jan.	Feb.	March	April	May	June	July	Aug.	Sept.	Oct.	Nov.	Dec.	1991
						Night							
Prevailing wind direction	SSW	SW	SSE	SSE	SSE	SSW	SSE	SSE	SSE	SSE	SSE	SSE	SSE
Average wind speed (m s^{-1})	5.5	5.9	5.0	5.1	3.3	2.2	4.1	4.0	4.4	2.7	5.5	3.8	4.3
Maximum wind speed* (m s^{-1})	19	13	13	16	13	7	14	13	11	8	13	10	19
Direction of max. wind* (deg.)	249	165	236	189	159	163	164	151	154	155	157	156	249
Average station pressure (hPa)	679.0	678.9	679.2	680.1	680.5	680.6	681.2	681.6	680.4	679.8	680.6	679.7	680.1
Maximum pressure* (hPa)	683	682	682	684	684	684	684	684	685	682	684	683	685
Minimum pressure* (hPa)	672	675	675	677	677	678	679	679	675	677	676	676	672
Average air temperature (°C)	3.3	4.0	2.1	3.6	5.5	5.8	7.1	6.0	5.8	6.0	5.8	4.2	4.9
Maximum temperature* (°C)	9	11	7	9	12	13	14	13	12	11	11	9	14
Minimum temperature* (°C)	−1	−1	−2	−1	0	1	3	2	2	1	2	−1	−2
Average dewpoint temperature (°C)	−11.3	−15.5	−10.2	−15.5	−16.0	−12.2	−13.2	−5.9	−7.4	−9.4	−9.3	−8.1	−11.2
Maximum dewpoint temperature (°C)	5	4	4	5	7	6	7	10	7	6	7	6	10
Minimum dewpoint temperature (°C)	−27	−36	−33	−32	−34	−26	−33	−25	−28	−29	−26	−27	−36
Precipiation (mm)	0	1	9	1	0	0	0	3	23	1	0	0	39
						Day							
Prevailing wind direction	NNW	NW	SE	N	N	N	NNE	NNW	NNE	NNE	SE	ENE	N
Average wind speed (m s^{-1})	5.3	5.6	5.2	4.8	3.7	3.0	4.2	3.8	4.1	3.0	4.5	3.6	4.2
Maximum wind speed* (m s^{-1})	24	14	17	13	11	6	12	11	10	8	11	10	24
Direction of max. wind* (deg.)	198	249	247	187	155	332	155	102	149	2	170	140	198
Average station pressure (hPa)	678.8	678.9	679.2	680.3	680.7	680.8	681.4	681.8	680.5	679.8	680.6	679.6	680.2
Maximum pressure* (hPa)	684	683	683	684	684	684	684	684	684	683	684	683	684
Minimum pressure* (hPa)	669	675	675	677	678	678	679	679	676	677	676	676	669
Average air temperature (°C)	7.3	8.2	5.6	8.7	10.5	10.5	11.9	10.3	10.5	10.5	10.0	8.0	9.3
Maximum temperature* (°C)	15	18	13	14	17	17	19	17	16	17	16	15	19
Minimum temperature* (°C)	−1	−1	−2	0	2	3	4	2	3	1	2	−1	−2
Average dewpoint temperature (°C)	−4.6	−11.1	−5.8	−10.0	−7.8	−3.8	−5.0	−0.5	−2.9	−1.8	−3.4	−5.3	−5.2
Maximum dewpoint temperature (°C)	8	5	6	6	7	8	9	11	8	14	10	8	14
Minimum dewpoint temperature (°C)	−24	−34	−34	−32	−31	−25	−32	−27	−27	−23	−25	−27	−34
Precipitation (mm)	5	5	41	7	1	12	13	49	8	1	1	11	153

Instrument heights: wind, 8.5 m; pressure, 3403 m (MSL); air temperature, 1.7 m; dewpoint temperature, 2.0 m. Wind and temperature instruments are on a tower 15 m southwest of the main building.

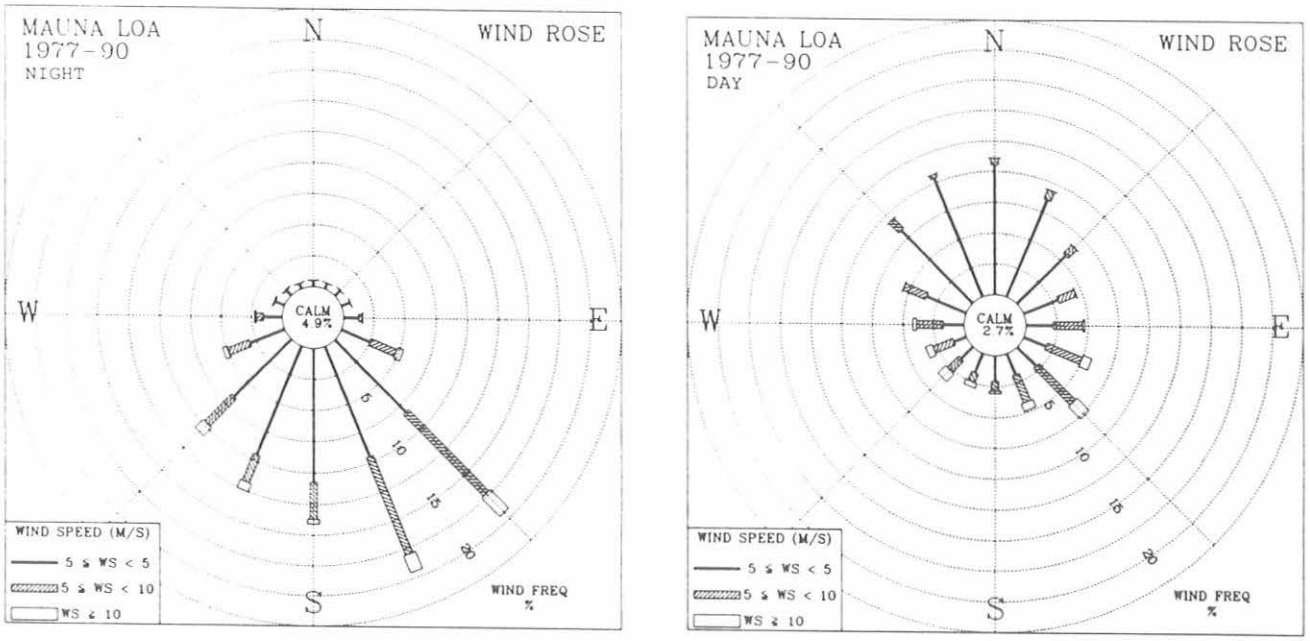

Fig. 4.2. Wind roses of the surface winds for MLO for 1977-1990 night (left) and day (right). The distribtuion of resultant wind direction and speed are given in units of percent occurence for the 14-year period. Wind speed is displayed as a function of direction in three speed classes.

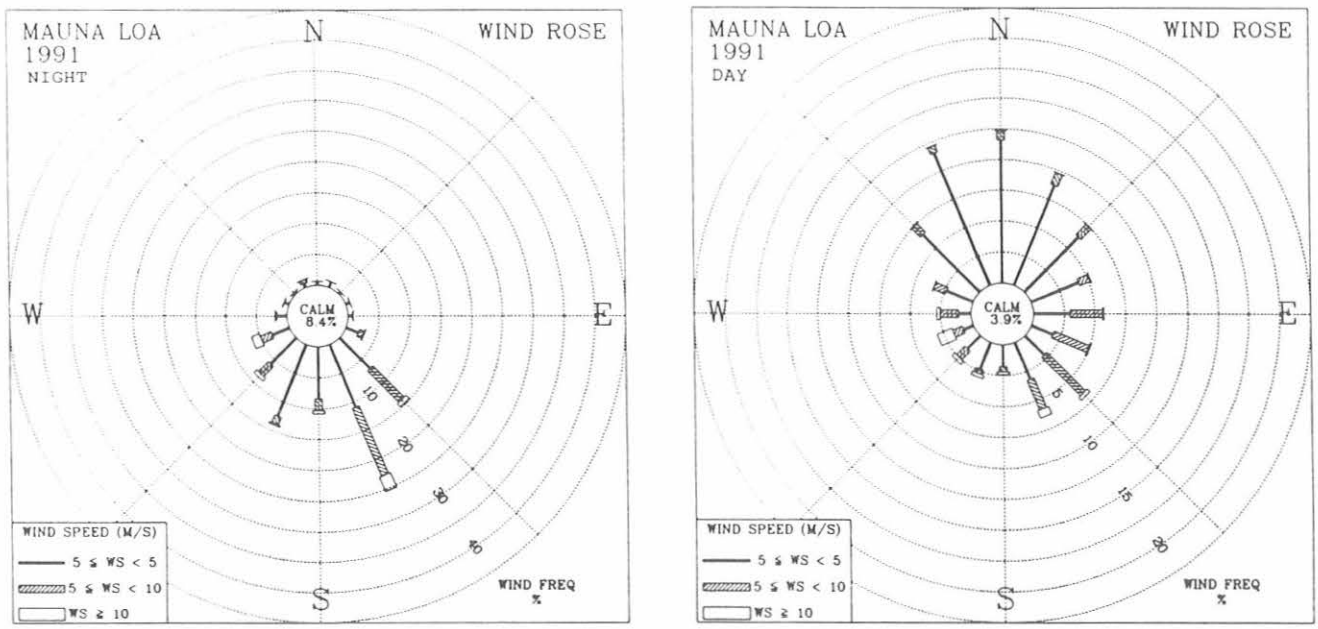

Fig. 4.3. Wind roses of the surface winds for MLO for 1991 night (left) and day (right). The distribtuion of resultant wind direction and speed are given in units of percent occurrence for the year. Wind speed is displayed as a function of direction in three speed classes.

Night Regime. The 14-year wind rose (Figure 4.2), shows that 91% of all the winds observed had a southerly component with south-southeast dominating. The 1991 wind rose (Figure 4.3) shows a slightly higher percentage of southerly winds (94%) than does the 14-year rose. Storm related winds (WS $\geq$10 m s^{-1}) with westerly and easterly components are evident in both the 1991 and 14-year wind rose in equal proportion, 6.7% and 7.1% respectively. The upslope or northerly component winds (north-northwest–east-northeast) about 5% of the time, are primarily the results of the daytime, upslope flow extending into the evening hours.

TABLE 4.4. SMO 1991 Monthly Climate Summary

	Jan.	Feb.	March	April	May	June	July	Aug.	Sept.	Oct.	Nov.	Dec.	1991
Prevailing wind direction	E	NNW	NNW	SSE	SSE	SSE	SSE	SE	SSE	SE	SE	SSE	SSE
Average wind speed (m s^{-1})	3.2	4.4	3.7	3.1	4.1	4.5	6.4	6.4	4.7	4.4	2.4	5.6	4.4
Maximum wind speed* (m s^{-1})	9	17	12	9	13	11	12	13	12	9	9	32	32
Direction of max. wind* (deg.)	325	325	325	328	161	121	144	149	159	152	8.8	12	12
Average station pressure (hPa)	999.2	997.3	1000.1	999.5	1000.9	1001.7	1002.2	1002.5	1002.0	1001.0	999.3	994.5	1000.1
Maximum pressure* (hPa)	1004	1003	1005	1004	1006	1005	1006	1006	1007	1005	1003	1001	1007
Minimum pressure* (hPa)	996	991	996	995	997	996	998	998	998	997	995	944	944
Average air temperature (°C)	28.2	27.7	28.4	28.3	27.4	27.0	26.7	26.6	26.4	27.1	27.1	27.1	27.3
Maximum temperature* (°C)	33	33	33	33	33	32	31	32	31	31	32	32	33
Minimum temperature* (°C)	22	23	23	24	24	23	23	23	23	24	21	22	21
Average dewpoint temperature (°C)	24.2	24.3	24.2	24.3	23.6	23.6	23.5	†	22.7	22.8	23.8	23.1	23.7
Maximum dewpoint temperature (°C)	26	27	28	26	26	26	25	†	26	25	25	26	28
Minimum dewpoint temperature (°C)	21	22	22	21	18	20	20	†	21	20	21	19	18
Precipitation (mm)	205	404	146	159	209	183	192	55	39	89	238	578	2497

Instrument heights: wind, 13.7 m; pressure, 30 m (MSL); air temperature, 9 m. Wind and temperature instruments are on Lauagae Ridge, 110 m northeast of the main building. Pressure sensors are in the main building.

*Maximum and minimum values are hourly averages.

†Missing Data

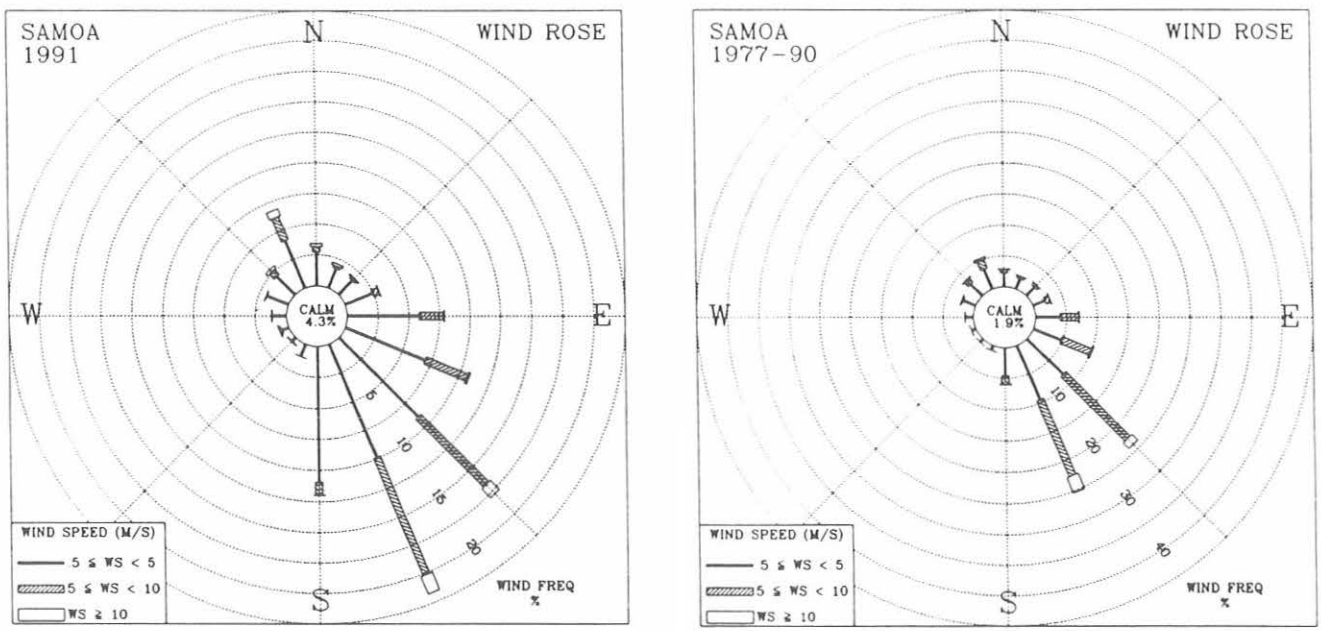

Fig. 4.4. Wind roses of the surface wind for SMO for 1991 (left) and 1977-1990 (right). The distribution of the resultant wind direction and speed are in units of percent occurrence for the year and 14-year period, respectively. Wind speeed is displayed as a function of direction in three speed classes.

Table 4.5. SPO 1991 Monthly Climate Summary

	Jan.	Feb.	March	April	May	June	July	Aug.	Sept.	Oct.	Nov.	Dec.	1991
Prevailing wind direction	N	ENE	NNE	ENE	E	E	NNE	E	N	E	NNE	NNE	NNE
Average wind speed (m s^{-1})	4.3	5.6	5.7	5.3	5.8	6.0	7.0	5.1	5.2	5.6	5.2	4.0	5.4
Maximum wind speed* (m s^{-1})	8	13	12	12	12	13	13	15	13	15	12	9	15
Direction of max. wind* (deg.)	348	354	343	359	359	3	31	22	359	6	12	8	22
Average station pressure (hPa)	683.9	689.6	675.6	680.3	676.9	682.4	679.9	673.2	680.5	674.2	682.2	696.5	681.2
Maximum pressure* (hPa)	690	710	689	692	706	695	694	682	703	701	696	705	710
Minimum pressure* (hPa)	677	674	665	669	658	668	666	664	656	661	668	690	656
Average air temperature (°C)	−26.8	−36.5	−55.9	−57.6	−59.0	−58.1	−56.0	−59.0	−53.5	−51.9	−38.4	−25.1	−48.2
Maximum temperature* (°C)	−20	−23	−42	−29	−33	−37	−39	−42	−36	−33	−23	−20	−20
Minimum temperature* (°C)	−37	−48	−67	−69	−74	−73	−72	−71	−77	−63	−48	−33	−77

Instrument heights: wind, 12.2 m; pressure 2841 m (MSL); air temperature, 2.2 m. The anemometer and thermometer are on a tower 100 m grid east-southeast of CAF. Pressure measurements are made inside CAF.

*Maximum and minimum values are hourly averages.

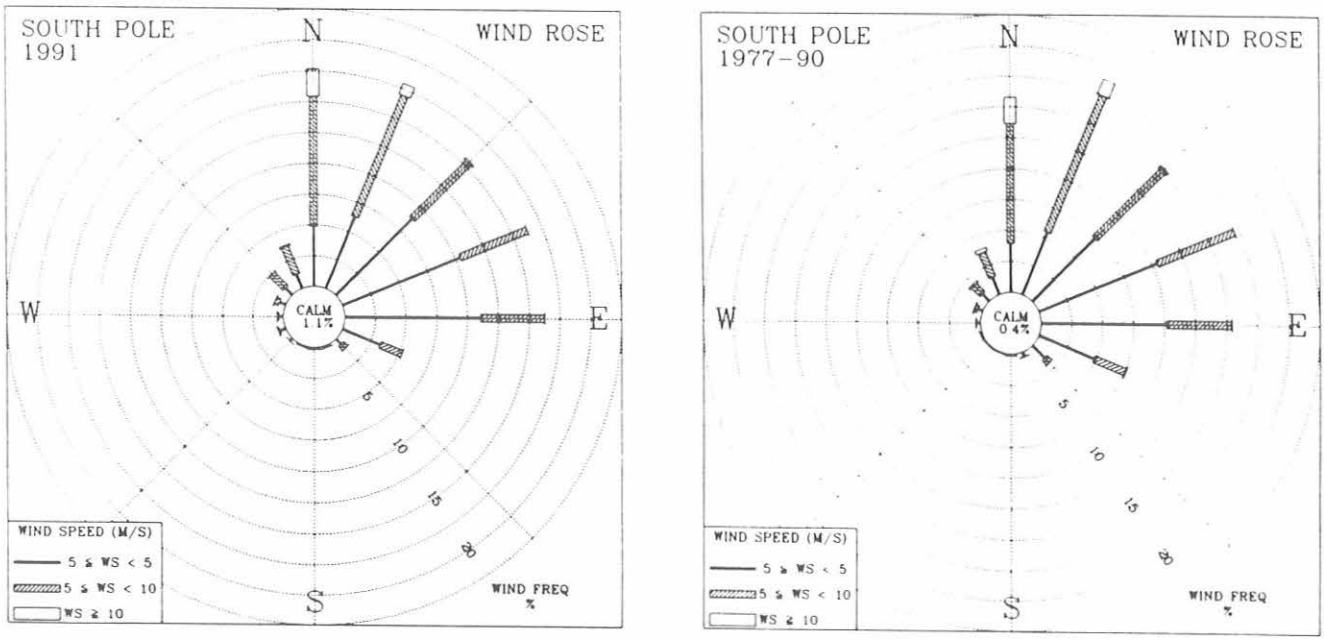

Fig. 4.5. Wind roses of the surface wind for SPO for 1991 (left) and 1977-1990 (right). The distribution of the resultant wind direction and speed are in units of percent occurrence for the year and 14-year period, respectively, Wind speeed is displayed as a function of direction in three speed classes.

TABLE 4.6*a* CMDL CAMS Operations Summary, 1991

Individual CAMS	Expected No. of Blocks 1991	Percent Data Capture			
		BRW	MLO	SMO	SPO
ASR	8760	99.87% [11]	99.49% [45]	99.55% [127]	99.78% [19]
CO_2	8760	98.98% [89]	90.16% [74]	99.76% [21]	96.58% [300]
MO3	4380	99.84% [7]	99.93% [3]	99.33% [29]	99.47% [23]
Total	21900	99.51% [107]	99.44% [122]	99.19% [177]	98.44% [342]

TABLE 4.6*b* CMDL CAMS Operations Summary, 1991

Block Type	Description	Expected No. of Blocks 1991	Blocks Recorded and [Blocks Missing]			
			BRW	MLO	SMO	SPO
A	Hourly aerosol data	2190	2170 [3]	2180 [10]	2161 [29]	2186 [4]
B	Secondary aerosol data	2190	887 [1303]	624 [1566]	0*	2186 [4]
C	Hourly CO_2 data	8396†	8311 [85]	8326 [70]	8376 [20]	8109 [287]
D	Daily CO_2 data	365	364 [1]	368	365 [0]	364 [1]
E	Hourly CO_2 calibration data	364‡	421	389	380	432
F	CO_2 calibration report	52	61	55	54	61
H	Daily aerosol data	365	365	364 [1]	363 [2]	368
I	Meteorological calibration	365	365	365	363 [2]	358
M	Hourly meteorological data	4380	4373 [7]	4377 [3]	4351 [29]	4357 [23]
N	Surface ozone calibration	52	57	58	38 [14]	0
O	Daily surface ozone data	365	365	365	363 [2]	411
S	Hourly solar radiation data	8760	8749 [11]	8716 [44]	8633 [127]	8741 [19]
T	Daily solar radiation data	365	364 [1]	363 [2]	359 [6]	364 [1]
W	Daily meteorological data	365	365	363	363 [2]	412

*Secondary aerosol channels are not used in Samoa
†Nominal block count equal to total hours in year less 52 7-hr calibration periods.
‡Nominal block count equal to 52 7-hr calibration periods.

Day Regime. The 14-year day wind rose (Figure 4.2) indicates that light wind speeds in the west-northwest–east-northeast sectors were observed 57% of the time. (Only 49 hours with wind speeds greater than 10 m s^{-1} were reported from 1977-1990.) This represents the upslope flow attributed to the daytime heating of MLO. The 1991 day wind rose (Figure 4.3) compares well with the 14-year rose, in that the northerly wind components prevail 57% of the time. The day wind rose was more uniformly distributed in the light wind classes than that of the night wind rose which was due to the occurrence of variable wind directions during the transition periods of dawn and dusk, most of which were included in this regime. The percent frequency of occurrence of wind in the 10 m s^{-1} or greater wind class for 1991 was about 2% less than the 14-year average.

The 1991 average day-night temperature difference was 4.4°C, and the average dewpoint temperature for 1991 was -8.2°C (Table 4.3). The year's maximum temperature of 19.0°C occurred on July 16, and the minimum of –2.0°C occurred on March 12. The minimum station pressure for 1991 occurred on January 27 when it reached 669 mb, which ties the all-time record low. The year 1991 was a very dry year with only 192 mm of precipitation, which is only 28% of the 14-year average of 678 mm. Only the months of March, August, and September had amounts that were equal to or above normal.

Samoa

A comparison of SMO's 1991 wind rose (Figure 4.4) with that of the 14-year period shows a slightly lower percentage (56%) of "clean air" sector winds (north-northwest–southeast) in 1991 than for the 1977-1990 period (58%). (If air passing over the offshore island of Aunu'u is to be avoided, the south-southeast wind sector (26%) cannot be considered in the "clean air" sector.) The peak hourly-average wind speed of 32 m s^{-1} occurred on December 9 during the passage of Typhoon Val.

During the encounter with Typhoon Val, a number of station records were established. The anemometer was operational throughout the storm and recorded a peak gust of over 45 m s^{-1}.

At its minimum, the hourly average station pressure reached an estimated 944 hPa, a new record. (The estimate was determined by correcting the minimum pressure observed at NWS in Tafuna for the height difference. The station pressure was deleted due to windowing.) A total of 491 mm of precipitation was reported for the storm..

While a new station pressure record low was being set on December 9, the remaining 11 months were above the 14-year normal (Table 4.4). The average wind speed for the year was 0.6 m s^{-1} below normal. The average temperature for 1991 of 27.3°C is consistent with the 14-year average of 27.0°C. The average pressure of 1000.1 hPa is 0.7 hPa above the 14-year average. The precipitation total for the year measured 2497 mm, which was 250 mm above the 14-year normal.

South Pole

The distribution of the surface wind direction in 1991 (Figure 4.5) is nearly identical to that of the 14-year pattern with "clean air" sector winds (grid north-northwest–east-southeast) occurring 93.7% in 1991 compared to the 14-year average of 94.1%. A slightly higher percentage of winds in the 0.5 m s^{-1} to 5 m s^{-1} range (49.9%) was observed in 1991 than the long term average of 47.3%. The average wind speed for 1991 very closely follows that of the 14-year average. The maximum hourly average wind speed was 15 m s^{-1} on August 1 and 2 and then again on October 6.

While the 1991 annual average temperature was within 0.8°C of the 14-year average, the annual average station pressure was 2.2 hPa above normal (Table 4.5). During 1991, February, September, and December set new maximum pressure records of 710 hPa, 703 hPa, and 705 hPa respectively, while October tied the record of 701 hPa. Seven monthly average pressures were above normal. The average pressure for July-December was 4.4 hPa above normal. The maximum temperature was -20°C while the minimum was -77°C.

4.1.2. Data Management

During 1991, the CAMS operated 99.15% of the time. The 2.04% increase over 1990 is attributed to the equipment operating most of the year without any power outages caused by storms. In particular, the overall performance at SMO increased by almost 9% (Table 4.6*a*). CAMS gathers data from sensors that operate continuously at each of the four CMDL observatories. The CAMS performance was monitored by comparing the number of data files recorded against those expected for the year. In CAMS, there are data files regularly recorded 12 or 24 times a day. In the summary table (Table 4.6*b*), the hourly solar radiation file was used to monitor the ASR CAMS. The hourly CO_2 data files were used for the CO2 CAMS. The hourly average meteorological data file was used for the MO3 CAMS.

Due to the remoteness of the observatories, power outages are common and are the main reason for data loss. Another reason for data loss is hardware failure. During 1991, CAMS had five boards fail, four at SPO and one at MLO.

4.2. Reference

DeLuisi, J.J. (Ed.), *Geophysical Monitoring for Climatic Change, No. 9: Summary Report 1980*, 163 pp., NOAA Environmental Research Laboratories, Boulder, CO, 1981.

5. Nitrous Oxide and Halocarbons Division

S.A. MONTZKA (EDITOR), J.W. ELKINS, J.H. BUTLER, T.M. THOMPSON, W.T. STURGES, T.H. SWANSON, R.C. MYERS, T.M. GILPIN, T.J. BARING, S.O. CUMMINGS, G.A. HOLCOMB, J.M. LOBERT, AND B.D. HALL

5.1. CONTINUING PROGRAMS

5.1.1. FLASK SAMPLES

During 1991 air sample pairs continued to be collected and analyzed for CFC-11 (CCl_3F), CFC-12 (CCl_2F_2), and nitrous oxide (N_2O). The collection sites were BRW, NWR, MLO, SMO, SPO, and ALT; their locations are shown in Figure 5.1. In May 1991, Cape Grim (CGO) Baseline Air Pollution Station, Tasmania (Latitude: 40.6822°S, Longitude: 144.6883°E) a part of CSIRO/DAR, was added to the NOAH flask sampling network making it the most southern, year round sampling site. ALT was upgraded to the higher pressure (3 atm) pump in May. All the sites are now equipped with this pump that provides sufficient pressure for the samples to be analyzed on four different instruments for numerous chemical constituents.

The automated flask analysis system has been routinely used throughout the year. This system greatly reduces the amount of operator time required for flask analyses. The old flask system requires manual sample injection and at most three pairs of flasks can be analyzed in an 8-hour day. The new system is capable of analyzing six pairs of flasks with only 1.5 hours of operator setup time. Once the setup is complete, the system automatically injects sample and calibration gases, and records results. Data comparison between the old and new systems will continue into 1992 when the old system will be phased out.

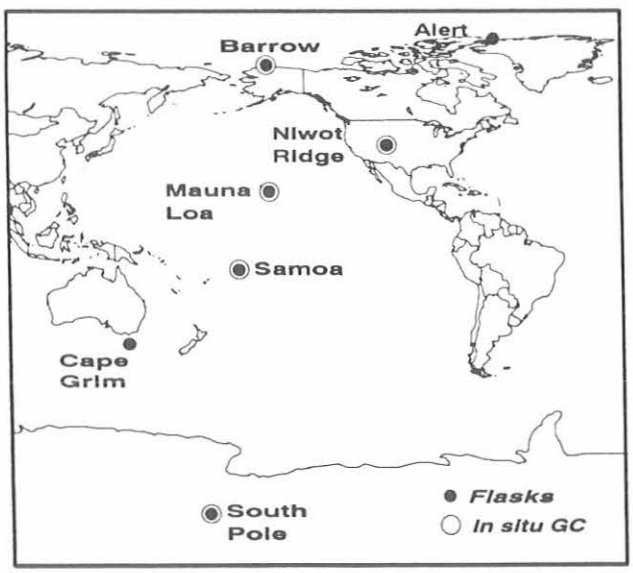

Fig. 5.1. Location of flask (solid circles) and in situ (open circles) sampling locations for nitrous oxide and selected halocarbons.

Final NOAA scale mixing ratios for CFC-11, CFC-12, and N_2O have been assigned to the three calibration tanks used since 1977. The historic intercomparisons have been carefully checked and small drift corrections applied on the data from 1977 to 1985 as discussed in the standards section. The monthly mean mixing ratios calculated for the sample sites are presented in Tables 5.1-5.3. These values supersede all previous preliminary data.

The station time series have been combined into monthly global means and are graphed in Figure 5.2. The same GC was used throughout the entire sampling period, the only major modifications were automating the EC-GC, adding a pre-column, and replacing a gas sampling valve to permit backflushing and more rapid sampling in 1987. The gap in the CFC-12 record during 1984-1985 was due to a GC problem that only affected that compound.

Both CFCs, particularly CFC-11, showed a decrease in growth rate during the past few years that is apparent at all flask-sampling locations as a consequence of reduced production and release (Figure 5.3). Previous reports [*Rasmussen and Khalil*, 1986; *Cunnold et al.*, 1986; *Elkins et al.*, 1988] showed that the mean global growth rates between 1977 and 1984 were increasing linearly, and our results give rates of 9 ± 1 ppt yr^{-1} (one standard deviation; by mole fraction) for CFC-11 and 17 ± 3 ppt yr^{-1} for CFC-12. After a period of peak growth rates of 11 ± 1 ppt yr^{-1} for CFC-11 and 19.5 ± 2 ppt yr^{-1} for CFC-12 from 1985 to 1988, the growth rates have been decreasing rapidly, reaching levels in late 1991 of 4 ± 1 ppt yr^{-1} for CFC-11 and 14 ± 2 ppt yr^{-1} for CFC-12. The global slowdown of the growth rates observed after 1989 are also supported by estimates of reduced emissions [*AFEAS*, 1991; *McFarland and Kaye*, 1992] made by the CFC producers and are directly attributed to the international efforts of the Montreal Protocol [*UNEP*, 1987] and voluntary reductions from producers and users to reduce stratospheric ozone depletion. If the observed slowdown in growth rates continues at 1990-1991 levels, global atmospheric CFC-11 and -12 mixing ratios will reach a maximum well before the turn of the century, and thereafter begin to decline [*Elkins et al.*, 1992].

In contrast to the CFCs, the mean growth rate of N_2O has almost doubled from ~0.6 ppb yr^{-1} from the 1977-1985

Table 5.1. Monthly Means of the Mixing Ratios of N_2O in ppb from the Flask Program

Year	Jan.	Feb.	March	April	May	June	July	Aug.	Sept.	Oct.	Nov.	Dec.
						ALT N_2O						
1988	—	307.7	307.9	308.2	308.8	308.3	308.2	308.1	308.7	309.5	308.7	309.5
1989	—	308.0	312.3	309.0	309.2	309.0	308.2	309.0	308.8	308.0	308.0	308.9
1990	309.2	309.3	310.4	310.3	312.1	311.1	311.6	310.4	309.7	309.7	310.7	309.9
1991	310.2	310.6	311.8	310.4	312.7	311.9	311.7	311.5	311.4	310.6	311.2	315.1
						BRW N_2O						
1977	—	—	—	—	—	—	—	—	298.5	304.6	300.6	304.7
1978	303.9	302.8	301.7	301.9	302.2	302.2	302.4	301.8	303.3	302.1	301.7	301.5
1979	301.1	301.5	302.1	302.2	303.1	302.9	304.0	303.7	304.0	302.6	301.6	302.9
1980	302.6	303.1	302.0	301.8	303.1	302.7	302.4	304.9	302.9	300.9	301.5	302.9
1981	302.9	302.4	303.1	304.0	303.7	304.0	303.8	306.1	303.1	302.8	302.5	303.3
1982	301.8	304.2	303.9	304.7	304.8	304.2	305.2	305.3	304.7	303.7	304.1	304.3
1983	304.2	305.0	304.3	303.9	304.8	304.1	306.5	305.0	302.7	304.6	303.7	304.0
1984	304.5	304.0	303.7	304.5	305.2	305.5	305.1	306.5	305.2	305.4	305.8	306.1
1985	307.9	306.4	305.1	304.9	306.3	305.8	303.8	304.4	305.6	305.8	305.5	305.1
1986	305.2	305.3	305.2	306.2	306.6	307.7	309.0	308.8	307.1	306.4	306.5	305.7
1987	306.9	307.0	307.2	306.6	308.9	308.0	308.2	308.0	308.5	308.2	307.0	308.2
1988	307.5	307.0	308.6	307.5	307.3	307.0	307.3	306.2	308.4	307.5	307.7	308.2
1989	308.5	309.7	307.8	309.2	309.4	308.8	310.9	309.0	309.0	308.2	309.6	309.4
1990	308.7	309.2	309.3	310.1	309.9	309.7	308.8	310.5	312.2	310.5	309.4	309.8
1991	310.2	310.5	311.7	311.4	311.1	311.9	311.4	310.6	311.2	311.2	310.5	311.2
						NWR N_2O						
1977	—	—	—	—	—	—	—	303.5	300.3	299.7	301.7	—
1978	—	302.3	302.1	302.8	303.3	301.9	301.7	301.9	302.9	302.5	302.9	303.6
1979	303.4	301.4	303.3	302.2	302.7	303.3	303.8	303.9	301.6	302.6	305.0	304.1
1980	306.7	304.3	303.2	303.8	304.0	305.3	302.8	306.2	304.2	303.3	304.1	303.0
1981	304.1	303.2	304.4	305.0	303.8	304.5	303.5	305.2	303.6	303.7	303.5	303.5
1982	304.8	303.4	304.2	306.1	305.6	305.4	306.2	307.5	305.6	304.9	306.3	305.9
1983	305.9	306.8	306.0	305.6	306.7	305.8	308.1	308.2	305.5	305.0	304.8	306.1
1984	305.2	305.0	304.4	305.2	306.0	307.7	308.1	309.1	307.1	306.9	307.3	308.1
1985	307.8	308.6	304.9	305.8	306.8	306.2	306.7	306.2	306.6	306.3	306.7	305.9
1986	306.0	306.0	306.0	306.1	306.4	306.3	307.8	306.8	306.9	307.4	306.5	306.8
1987	307.5	306.5	307.9	307.2	307.7	308.2	306.4	307.4	305.6	307.9	309.2	310.0
1988	309.6	308.0	309.7	306.7	307.5	307.0	309.8	309.7	307.6	308.7	309.4	309.6
1989	308.7	312.2	308.4	309.3	310.7	310.4	310.1	310.9	310.1	310.5	309.6	309.4
1990	311.3	310.4	310.0	309.5	310.1	310.4	309.5	312.9	313.0	311.7	311.4	311.1
1991	310.3	311.1	310.9	311.3	308.4	312.0	313.1	312.7	312.8	312.1	310.8	310.9
						MLO N_2O						
1977	—	—	—	—	—	—	—	—	301.1	302.5	300.1	303.1
1978	302.4	301.5	303.1	300.5	299.5	301.1	300.1	300.8	301.5	300.9	301.2	300.8
1979	301.3	302.4	302.1	302.6	302.3	301.6	302.4	302.0	302.2	304.4	302.6	303.5
1980	303.4	302.3	304.3	301.8	303.2	303.3	301.9	301.0	302.7	304.0	301.8	302.6
1981	302.0	303.0	303.9	034.8	303.4	304.8	303.6	303.1	303.8	304.0	303.8	303.0
1982	304.3	303.9	304.4	305.2	304.7	304.7	304.7	307.0	304.7	306.0	305.0	304.3

Table 5.1. Monthly Means of the Mixing Ratios of N_2O in ppb from the Flask Program—Continued

Year	Jan.	Feb.	March	April	May	June	July	Aug.	Sept.	Oct.	Nov.	Dec.
						MLO N_2O						
1983	304.3	305.0	305.1	304.8	305.2	304.1	304.4	304.7	305.4	304.6	304.2	304.9
1984	305.2	304.5	304.3	306.4	305.6	304.9	307.8	306.4	305.6	306.7	307.3	306.3
1985	307.4	307.4	306.6	305.6	305.1	306.8	305.1	305.0	307.1	307.6	307.7	307.6
1986	306.7	306.3	308.2	306.9	307.5	307.0	308.9	308.5	308.8	308.9	308..0	307.6
1987	307.1	307.5	308.2	305.7	308.2	307.1	306.7	307.7	306.5	307.9	307.2	307.7
1988	306.8	307.8	306.4	307.9	307.3	307.3	308.2	307.1	306.9	308.0	309.8	307.2
1989	308.1	309.0	308.6	309.7	308.9	309.5	308.4	309.3	309.8	309.6	308.7	309.6
1990	310.8	310.0	311.2	309.4	308.5	308.3	309.1	312.2	311.0	311.03	311.4	311.4
1991	312.5	310.2	311.0	311.1	310.1	311.0	310.6	311.0	311.1	312.0	311.6	311.8
						SMO N_2O						
1977	—	—	—	—	—	—	297.6	—	—	298.0	297.4	—
1978	297.2	298.9	299.1	299.8	300.7	300.1	299.6	298.8	299.1	298.9	300.1	299.5
1979	300.7	299.7	298.6	299.0	300.0	299.5	299.8	300.7	300.8	302.3	299.7	301.4
1980	301.5	302.0	300.5	299.4	299.5	300.4	299.0	299.5	300.3	300.1	298.2	299.2
1981	301.4	300.4	300.7	298.4	301.2	300.8	301.7	300.4	301.7	301.3	302.3	301.4
1982	299.4	299.8	300.6	302.5	302.7	303.0	301.8	302.2	303.3	302.6	302.6	302.3
1983	303.7	302.9	302.7	303.0	302.1	302.7	304.0	304.4	302.3	304.0	302.8	303.6
1984	304.2	304.0	303.9	303.7	303.1	303.7	303.7	304.0	304.0	303.7	303.2	304.8
1985	304.5	305.8	303.6	304.6	303.7	304.3	303.9	304.4	303.4	304.8	304.4	304.8
1986	303.9	305.0	304.5	305.0	303.9	305.5	305.0	305.4	305.4	304.5	305.9	305.1
1987	304.2	303.0	303.9	307.4	305.3	302.5	304.6	302.3	305.6	305.8	306.1	306.3
1988	306.9	306.4	305.3	304.5	305.4	305.1	305.4	305.6	305.7	305.2	306.4	308.1
1989	305.8	308.5	307.8	306.6	306.4	307.7	306.0	309.2	308.1	306.8	307.5	307.4
1990	—	309.5	308.5	307.6	307.0	307.2	307.4	308.1	310.9	309.0	307.1	309.6
1991	309.8	—	309.9	310.4	311.5	309.6	309.9	310.2	309.9	307.8	310.5	308.5
						CGO N_2O						
1991	—	—	—	—	309.4	310.0	309.3	310.1	310.8	309.5	311.0	—
						SPO N_2O						
1977	—	—	—	—	301.3	—	—	—	301.5	—	—	300.5
1978	300.5	302.3	—	302.4	298.5	301.4	301.8	301.7	299.5	—	300.5	300.9
1979	300.8	299.8	—	—	—	—	—	—	—	301.2	301.6	301.8
1980	301.6	—	301.8	301.3	303.5	300.0	300.0	302.7	—	300.5	300.8	300.1
1981	300.9	301.4	302.2	304.6	302.7	304.4	302.5	303.0	303.6	305.3	303.2	302.7
1982	304.1	—	—	—	—	—	—	—	—	—	302.8	303.5
1983	303.3	—	—	—	—	303.6	—	—	302.7	—	—	303.4
1984	303.5	303.8	—	—	—	—	—	—	—	—	304.7	305.7
1985	307.7	—	—	—	—	—	—	—	—	—	304.4	305.3
1986	306.6	—	—	—	—	—	—	—	—	—	305.4	305.1
1987	307.2	—	—	—	—	—	—	—	—	—	305.6	305.8
1988	307.0	306.8	—	—	—	—	—	—	—	—	—	306.1
1989	306.3	—	—	—	—	—	—	—	—	—	—	308.5
1990	309.9	—	—	—	—	—	—	—	—	—	—	309.3
1991	309.1	307.9	—	—	—	—	—	—	—	—	—	310.0

Table 5.2. Monthly Mixing Ratios of CFC-12 in ppt From the Flask Program

Year	Jan.	Feb.	March	April	May	June	July	Aug.	Sept.	Oct.	Nov.	Dec.
						ALT CFC-12						
1988	—	458.6	453.4	464.0	466.7	461.0	—	465.2	468.5	—	473.1	477.8
1989	—	472.9	—	477.2	488.8	—	475.8	483.4	484.9	489.4	488.3	494.4
1990	490.8	492.2	493.1	498.2	495.6	—	493.2	492.0	487.8	495.7	497.4	497.3
1991	501.6	501.2	504.5	507.0	502.0	497.1	506.4	509.3	508.4	508.4	510.2	526.5
						BRW CFC-12						
1977	—	—	—	—	—	—	—	—	—	—	—	—
1978	—	—	—	290.7	—	—	287.8	—	292.7	296.4	299.7	296.8
1979	298.0	296.1	299.9	295.8	295.2	299.4	300.9	299.8	307.7	303.8	309.1	311.2
1980	312.8	308.2	310.7	316.5	316.3	314.3	310.7	314.7	320.0	318.8	327.6	335.9
1981	323.1	323.5	327.2	330.8	333.3	328.9	335.7	345.6	336.1	339.9	341.7	344.5
1982	344.7	345.6	347.1	349.4	350.4	345.6	350.1	351.4	353.1	358.2	361.5	361.2
1983	363.9	364.4	363.4	363.9	366.1	363.2	364.0	366.5	374.6	378.8	375.9	375.2
1984	381.3	385.3	375.5	—	—	—	—	—	—	—	—	—
1985	—	405.1	390.5	392.8	397.7	405.5	391.2	394.1	406.8	414.6	417.9	419.9
1986	419.1	421.1	422.6	424.0	421.1	423.7	422.0	419.7	421.8	430.3	433.3	437.3
1987	435.5	436.3	444.1	442.5	441.4	439.1	447.4	443.1	452.9	456.2	458.3	458.9
1988	457.8	459.1	461.5	461.8	458.6	460.8	461.1	462.9	468.9	470.8	482.7	476.5
1989	479.0	473.7	475.3	476.4	477.7	474.5	482.9	478.8	482.1	485.5	492.2	493.2
1990	495.3	503.1	491.1	490.4	490.4	493.4	486.7	490.7	490.9	496.4	497.4	497.8
1991	501.2	501.9	505.1	501.5	496.2	502.2	501.0	502.7	507.5	510.9	512.0	519.0
						NWR CFC-12						
1977	—	—	—	—	260.5	268.1	255.8	263.6	287.0	288.7	281.6	279.3
1978	285.0	269.6	275.4	—	—	292.5	298.2	301.4	—	286.7	294.1	290.3
1979	285.0	287.2	296.6	304.9	292.3	294.2	294.5	296.4	310.9	294.4	300.0	304.3
1980	309.9	312.5	316.2	311.1	315.2	308.9	308.7	309.7	313.0	312.3	312.8	317.3
1981	317.5	315.3	323.7	324.8	326.8	328.4	331.9	333.5	334.3	339.5	331.0	334.2
1982	338.2	335.6	339.9	349.4	342.4	346.8	353.3	349.6	349.6	353.0	353.6	352.9
1983	354.3	357.5	359.5	360.1	362.2	363.5	377.0	364.4	372.1	373.2	373.8	377.1
1984	374.7	371.1	368.9	—	—	—	—	—	—	—	—	—
1985	—	—	383.8	383.3	390.6	391.2	388.2	395.9	405.3	405.8	414.8	408.6
1986	408.8	408.7	411.9	410.4	418.2	418.6	416.4	421.3	415.7	422.8	422.2	424.6
1987	427.2	425.4	438.2	435.5	—	443.2	441.9	441.6	450.7	453.6	452.7	452.7
1988	454.7	450.8	450.8	459.0	459.8	456.4	468.6	469.8	465.0	462.5	474.2	466.6
1989	465.7	473.9	461.1	469.8	473.7	476.8	480.6	483.0	482.5	478.8	485.9	482.8
1990	482.5	491.3	485.7	483.0	489.4	494.1	491.0	490.8	502.4	494.0	497.0	497.0
1991	495.3	493.4	492.1	500.8	492.3	501.0	504.4	504.6	509.5	511.1	503.4	505.7
						MLO CFC-12						
1977	—	—	—	—	272.4	—	261.8	—	260.6	267.1	267.9	277.6
1978	277.7	272.8	276.7	284.4	—	287.8	282.8	284.9	282.6	282.7	287.2	293.6
1979	295.9	288.9	291.3	289.4	295.6	296.3	299.8	—	304.7	—	304.8	306.3
1980	311.8	321.1	305.9	311.4	300.0	307.9	309.0	309.9	308.7	318.6	317.1	314.1
1981	311.7	318.5	318.4	329.1	332.8	330.8	335.9	334.6	339.2	338.2	337.2	348.6
1982	341.7	342.4	338.6	339.9	340.8	341.7	339.8	343.8	347.8	349.3	349.7	352.9
1983	347.1	354.3	353.5	354.1	353.9	356.3	363.9	358.2	367.6	367.5	372.6	370.5
1984	368.4	376.3	363.9	—	—	—	—	—	—	—	—	—

Table 5.2. Monthly Mixing Ratios of CFC-12 in ppt From the Flask Program—Continued

Year	Jan.	Feb.	March	April	May	June	July	Aug.	Sept.	Oct.	Nov.	Dec.
						MLO CFC-12						
1985	—	381.3	383.3	378.7	387.9	398.6	385.5	387.0	403.0	409.2	403.6	409.8
1986	407.2	404.2	411.4	413.8	413.5	415.1	412.2	417.7	419.6	428.9	426.9	427.5
1987	428.7	420.2	441.0	431.6	—	432.9	432.6	437.5	447.7	448.2	448.9	442.3
1988	441.7	446.7	444.4	452.7	452.0	452.9	456.0	456.3	459.7	460.7	—	468.0
1989	467.9	461.2	465.0	468.8	468.0	468.5	468.3	472.8	475.6	478.9	477.6	474.2
1990	482.9	480.1	482.2	487.5	484.1	483.8	482.7	486.1	489.9	488.7	489.4	491.4
1991	492.4	485.5	491.9	496.6	495.0	498.4	497.3	498.9	498.7	503.3	505.5	504.0
						SMO CFC-12						
1977	—	—	—	—	234.8	232.3	237.4	242.7	241.4	243.9	244.2	250.9
1978	251.1	255.9	249.3	—	259.3	259.4	257.2	258.6	262.0	262.9	266.9	266.8
1979	273.7	273.2	272.8	273.8	271.8	272.4	275.2	276.7	280.1	280.1	283.5	280.6
1980	284.9	284.6	284.6	287.9	286.0	288.6	288.8	288.2	292.2	293.5	293.0	296.9
1981	299.2	302.7	303.5	306.1	306.8	305.7	312.1	313.1	311.7	315.3	317.7	318.5
1982	322.7	326.0	323.7	326.1	322.9	324.9	328.1	329.8	330.0	333.4	332.6	333.0
1983	338.1	339.2	342.8	342.1	341.5	341.8	342.0	348.1	351.7	354.6	356.1	357.4
1984	356.9	362.8	358.6	—	—	—	—	—	—	—	—	—
1985	—	373.1	369.8	371.0	379.2	379.1	375.1	373.8	387.6	389.5	389.6	392.8
1986	395.1	399.2	397.3	397.8	398.2	403.0	401.6	403.4	405.3	405.2	405.3	409.1
1987	411.6	414.2	420.9	414.3	418.4	409.8	418.2	—	—	421.7	425.6	426.3
1988	428.7	432.3	429.1	437.5	434.6	432.9	440.7	441.1	440.7	445.2	449.4	447.8
1989	450.5	454.1	448.2	451.4	453.8	445.4	457.5	457.3	459.7	461.8	460.6	465.2
1990	474.4	4€ 8	469.9	468.4	467.6	471.5	469.2	471.4	473.8	475.7	478.6	481.9
1991	486.7	—	486.7	487.9	491.8	485.8	488.3	490.4	493.1	493.5	494.6	492.8
						CGO CFC-12						
1991	—	—	—	—	480.3	481.4	485.2	486.7	490.1	492.0	488.8	—
						SPO CFC-12						
1977	—	234.6	—	—	—	232.4	—	—	—	—	—	253.1
1978	—	—	—	—	—	—	—	—	—	255.3	257.1	263.3
1979	263.7	259.3	—	—	—	—	—	—	—	—	290.8	280.9
1980	280.8	—	—	283.6	284.4	289.0	287.0	—	304.3	295.2	291.8	294.2
1981	294.0	299.7	—	—	302.9	—	—	—	—	—	—	320.0
1982	317.3	—	—	—	—	—	—	—	—	—	344.5	—
1983	343.7	—	—	—	—	—	—	—	—	—	—	343.8
1984	—	357.1	—	—	—	—	—	—	—	—	—	—
1985	—	—	—	—	—	—	—	—	—	—	386.1	389.0
1986	392.9	—	—	—	—	—	—	—	—	—	401.9	404.8
1987	408.1	—	—	—	—	—	—	—	—	—	420.4	419.9
1988	417.6	—	—	—	—	—	—	—	—	—	436.6	435.6
1989	439.6	—	—	—	—	—	—	—	—	—	—	459.6
1990	464.7	—	—	—	—	—	—	—	—	—	—	472.6
1991	474.8	472.1	—	—	—	—	—	—	—	—	486.7	488.5

Table 5.3. Monthly Mean Mixing Ratios of CFC-11 in ppt from the Flask Program

ar	Jan.	Feb.	March	April	May	June	July	Aug.	Sept.	Oct.	Nov.	Dec.
						ALT CFC-11						
1988	—	256.3	—	258.1	—	255.8	—	—	—	—	264.6	263.0
1989	—	—	—	—	267.8	268.7	—	267.2	—	272.5	270.7	276.1
1990	273.9	277.2	276.8	275.5	—	274.6	272.1	275.9	273.6	276.6	274.9	277.4
1991	279.2	277.4	275.1	279.0	282.9	278.9	278.0	275.2	275.5	276.0	281.0	282.6
						BRW CFC-11						
1977	145.5	148.1	144.1	145.5	150.8	143.6	—	147.3	148.2	154.9	155.0	157.9
1978	156.5	155.6	156.7	159.0	156.9	157.3	158.3	159.0	163.7	163.3	167.9	165.9
1979	164.8	165.3	167.9	167.4	166.4	166.1	166.9	166.4	168.9	172.4	173.3	175.0
1980	175.8	174.6	176.6	175.2	174.8	176.2	175.7	176.7	177.5	178.5	176.4	181.3
1981	181.1	185.1	182.5	183.6	182.8	184.2	184.2	184.9	183.7	188.0	190.1	192.3
1982	190.6	193.2	193.7	192.3	190.5	190.2	191.7	192.5	194.2	195.4	197.0	198.0
1983	199.6	199.0	199.1	200.8	—	201.8	202.6	200.5	204.2	204.5	207.6	205.8
1984	209.2	209.7	208.8	206.9	208.9	208.2	209.7	209.7	211.5	214.1	215.6	218.5
1985	219.2	224.9	220.6	223.1	221.1	218.4	219.4	222.8	223.2	227.9	229.9	230.2
1986	230.9	230.6	231.7	237.8	232.3	232.3	232.0	234.6	232.9	239.0	239.3	243.0
1987	242.2	242.3	243.7	245.3	245.9	245.2	247.8	247.3	249.0	253.1	255.4	256.3
1988	254.3	256.4	256.6	258.6	256.1	256.5	256.4	257.6	258.8	261.5	266.4	265.4
1989	263.9	265.6	266.4	267.0	265.7	264.7	265.3	264.1	266.9	272.0	276.9	275.6
1990	275.7	277.4	274.1	272.6	271.0	272.6	269.5	271.7	271.1	272.6	273.8	276.1
1991	277.3	277.8	278.6	275.2	274.6	274.6	273.7	274.8	274.7	277.0	277.0	279.8
						NWR CFC-11						
1977	151.6	149.4	143.7	146.6	148.1	140.4	144.2	146.6	145.2	151.6	148.8	155.6
1978	150.1	154.2	152.0	—	159.0	152.9	157.4	160.0	164.9	160.6	162.0	159.5
1979	159.3	157.6	163.1	161.3	160.8	163.4	163.4	165.3	163.0	168.6	169.9	168.6
1980	169.0	168.8	177.6	172.3	176.3	173.2	175.1	—	173.3	175.3	177.7	174.5
1981	177.3	177.1	179.3	176.8	180.9	181.1	180.7	182.2	183.4	185.2	182.9	183.8
1982	184.9	183.7	187.2	189.1	188.5	188.8	191.9	189.3	190.9	190.6	194.8	195.0
1983	193.0	195.9	196.2	199.5	199.0	198.4	199.2	199.3	201.3	202.8	201.9	205.0
1984	203.5	201.5	206.7	204.8	206.3	206.6	206.5	206.0	208.8	212.7	210.6	214.2
1985	213.8	212.2	215.9	216.3	218.2	215.9	215.6	218.9	223.6	224.5	225.1	223.9
1986	223.3	227.5	225.9	226.5	228.2	230.0	226.9	231.2	228.9	233.7	237.0	233.5
1987	234.0	236.4	237.1	238.0	240.7	242.2	240.8	243.7	246.1	251.3	249.6	251.3
1988	251.5	250.7	252.2	253.1	258.2	254.5	257.3	258.7	255.1	254.5	262.5	258.9
1989	258.2	262.6	257.9	260.7	260.8	262.0	268.6	266.1	267.3	264.8	269.3	265.7
1990	267.1	268.8	270.6	267.0	267.6	268.8	267.7	269.0	269.1	270.2	272.0	270.6
1991	269.2	273.0	269.2	273.8	270.1	273.2	274.5	273.0	274.6	273.4	273.9	275.4
						MLO CFC-11						
1977	140.0	139.3	140.3	135.8	135.6	142.1	140.0	143.3	145.7	144.7	145.3	147.0
1978	149.0	148.7	148.7	149.4	150.1	150.3	151.4	152.1	155.4	153.4	155.1	154.9
1979	157.1	158.9	159.1	158.6	157.6	157.9	160.3	—	164.0	168.2	166.9	165.4
1980	167.5	167.1	168.8	170.2	166.4	170.5	171.9	171.5	170.6	173.6	174.6	173.3
1981	172.4	175.6	176.6	177.6	177.1	178.2	180.6	179.8	180.6	182.6	182.1	184.0
1982	182.3	182.1	183.6	184.0	185.6	185.4	184.7	187.2	188.7	189.6	189.6	188.5
1983	190.0	191.3	193.0	193.2	194.7	196.9	198.0	197.9	198.4	199.0	198.8	201.5
1984	200.9	202.0	200.9	202.5	202.2	202.8	204.1	204.9	206.6	208.9	213.2	210.9

Table 5.3 Monthly Mean Mixing Ratios of CFC-11 in ppt from the Flask Program—Continued

Year	Jan.	Feb.	March	April	May	June	July	Aug.	Sept.	Oct.	Nov.	D
						ALT CFC-11						
1985	212.6	212.6	217.4	214.8	215.7	216.3	215.5	217.9	218.4	222.1	220.2	224.7
1986	219.6	222.3	225.2	228.4	227.1	226.2	228.5	227.6	233.2	234.0	232.2	233.5
1987	233.2	—	236.3	238.1	—	236.8	238.5	239.1	242.3	245.0	244.9	242.4
1988	241.5	246.4	242.7	247.9	248.5	249.6	249.3	250.5	252.8	253.3	257.9	—
1989	257.7	255.0	256.5	259.6	259.0	260.4	258.9	261.4	263.4	262.7	262.2	264.0
1990	265.0	263.5	264.9	263.4	263.8	267.5	265.5	265.4	264.9	267.8	267.3	270.5
1991	270.4	265.8	269.1	271.2	271.4	268.6	270.3	270.5	269.6	269.7	271.8	274.4
						SMO CFC-11						
1977	130.6	130.2	125.0	130.0	129.6	130.2	131.8	133.7	134.5	135.2	134.5	133.5
1978	138.3	137.7	139.2	141.1	141.3	141.1	141.1	143.3	143.2	144.9	147.7	146.6
1979	149.3	152.0	149.9	151.2	149.9	149.6	151.6	152.2	152.0	156.2	155.3	155.4
1980	157.9	158.7	158.8	158.7	159.2	160.8	159.5	159.8	163.2	162.0	161.6	163.1
1981	165.2	166.4	165.4	167.5	167.4	167.8	168.5	170.4	171.5	171.9	174.1	173.7
1982	175.4	175.1	175.7	177.3	177.1	176.1	178.5	180.2	179.8	181.2	181.2	180.8
1983	185.3	182.7	186.5	186.0	185.6	187.2	187.3	186.2	187.8	190.6	189.0	193.4
1984	194.7	196.5	193.2	196.1	195.3	193.6	194.5	195.2	199.3	199.1	197.6	203.9
1985	204.4	206.9	206.8	207.7	206.8	205.3	207.0	208.0	209.7	210.2	209.5	212.9
1986	216.5	210.5	213.9	216.9	219.2	219.5	219.1	220.7	221.0	220.9	221.1	223.5
1987	223.2	229.0	226.6	225.6	230.1	226.6	227.5	—	233.0	231.0	233.8	234.7
1988	236.1	237.3	235.0	239.6	237.4	239.1	239.4	242.1	239.1	242.4	244.2	248.6
1989	248.9	248.7	247.4	249.6	249.7	249.4	250.0	252.3	253.8	253.6	253.5	255.1
1990	258.0	254.2	258.0	257.0	255.5	258.0	258.6	260.7	260.5	258.8	261.3	265.3
1991	263.8	—	264.9	264.9	265.4	264.3	265.8	267.2	267.9	267.7	267.8	266.8
						CGO CFC-11						
1991	—	—	—	—	—	269.9	264.4	—	265.8	267.5	—	—
						SPO CFC-11						
1977	134.3	125.9	—	—	—	—	—	—	—	—	—	—
1978	143.2	—	—	—	—	—	—	151.9	—	—	158.3	150.3
1979	147.6	149.5	—	—	—	—	—	—	—	—	155.1	164.0
1980	156.7	—	—	157.2	169.7	158.1	—	—	—	170.5	160.1	164.9
1981	164.2	164.8	—	—	178.1	—	—	—	—	186.5	167.6	178.4
1982	181.5	—	—	—	—	—	—	—	—	—	192.9	193.7
1983	192.9	—	—	—	—	—	—	—	—	—	—	187.5
1984	—	190.5	—	—	—	—	—	—	—	—	198.5	205.1
1985	206.5	—	—	—	—	—	—	—	—	—	211.0	216.1
1986	—	—	—	—	—	—	—	—	—	—	222.3	—
1987	222.8	—	—	—	—	—	—	—	—	—	232.4	231.0
1988	—	—	—	—	—	—	—	—	—	—	239.8	237.0
1989	—	—	—	—	—	—	—	—	—	—	—	251.1
1990	253.4	—	—	—	—	—	—	—	—	—	—	260.6
1991	261.4	258.3	—	—	—	—	—	—	—	—	—	264.6

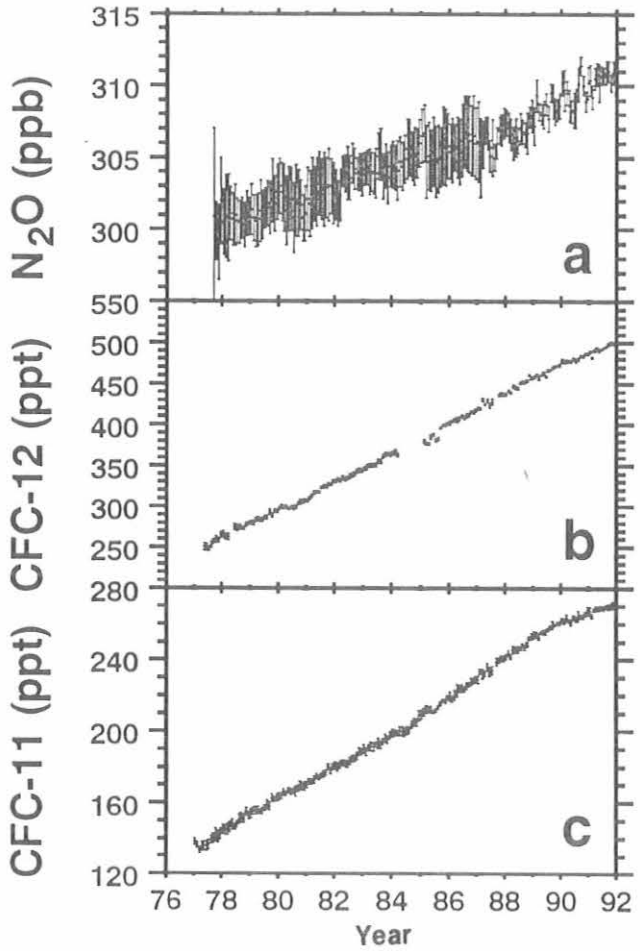

Fig. 5.2. Global monthly mean mixing ratios of (*a*) N_2O in ppb, (*b*) CFC-12 in ppt, and (*c*) CFC-11 in ppt. The standard deviation for each monthly mean is also shown. The global mean is determined from the monthly data at ALT, BRW, NWR, MLO, SMO, CGO, and SPO when available. Tic marks on the abscissa are the beginnning of the year, January 1.

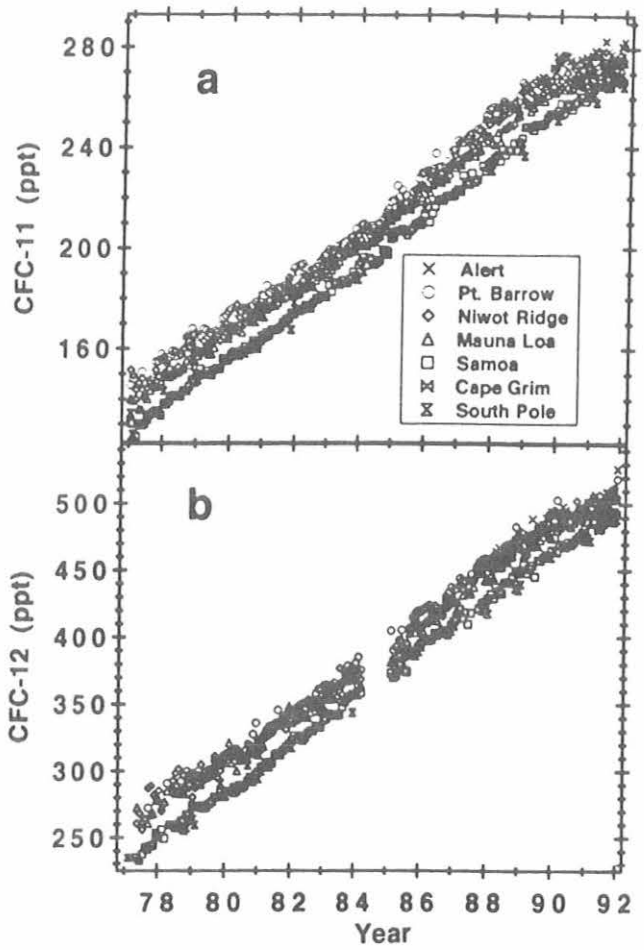

Fig. 5.3. Monthly means of the observed mixing ratio (ppt) measured in flask pairs from CMDL and cooperative stations for (*a*) CFC-11 and (*b*) CFC-12. Upon request, a color version of this figure is available from the NOAH Division.

time period to ~1.1 ppb yr^{-1} in recent years (1988-1992). The reason for this apparent rise in growth rate is unknown since the magnitudes of sources from human activities and oceans are uncertain.

5.1.2. RITS Continuous Gas Chromatograph Systems at CMDL Stations and Niwot Ridge

In situ analysis of air continued at BRW, MLO, NWR, SMO, and SPO using EC-GC. The schematic of the in situ GC system is shown in Figure 5.4. There are three separate channels on each system: (1) N_2O, (2) CFC-12, and (3) CFC-11, CFC-113 (CCl_2F-$CClF_2$), methyl chloroform (CH_3CCl_3), and carbon tetrachloride (CCl_4). Each channel has a 10-port gas sampling valve that is configured for backflushing the analytical column after the peaks of interest are detected by the ECD. These automated systems analyze one sample of air every hour, 24 times each day.

During scheduled maintenance trips in May and June, a new air sampling inlet system was installed at BRW, MLO, and SMO. Figure 5.5 is a diagram of this system. It consists of 0.93 cm outside diameter, Dekabond tubing running from the top of the meteorological tower to a continuously operating pump mounted near the gas chromatographs. A stream select valve allows air to be sampled either from this line or from the normal gas sampling stack and calibration gas cylinders. A comparison of the two air streams is underway in an effort to understand sources of contamination and boundary layer gradients.

Analysis of N_2O measurements at SMO in 1990 and early 1991 indicated chromatographic problems associated with

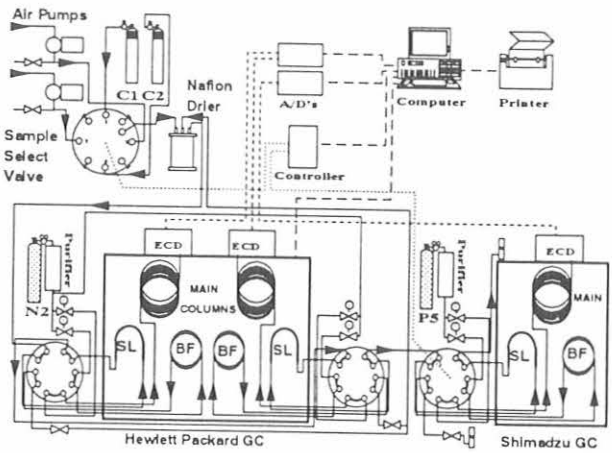

Fig. 5.4. Schematic layout of the RITS GC system. A/Ds are analog to digital convertors (PE-Nelson), BF is a backflush column, C1 and C2 are calibration tanks, N2 is nitrogen carrier gas, P5 is 95% argon-5% methane carrier gas, and SL is a sample loop (~2.5 mL).

electric power fluctuations. Although the station power is augmented by a backup generator, adequate station power continued to be a problem. The generator would turn on during blackouts but not during brownout situations. In May 1991, a 4.1 kVA UPS was installed at SMO. This unit has enough capacity to maintain power for the entire chromatographic system during power disruption before the generator turns on and also conditions both voltage and frequency during brownout conditions. Figure 5.6 shows the residual N_2O mixing ratios averaged for the hours of

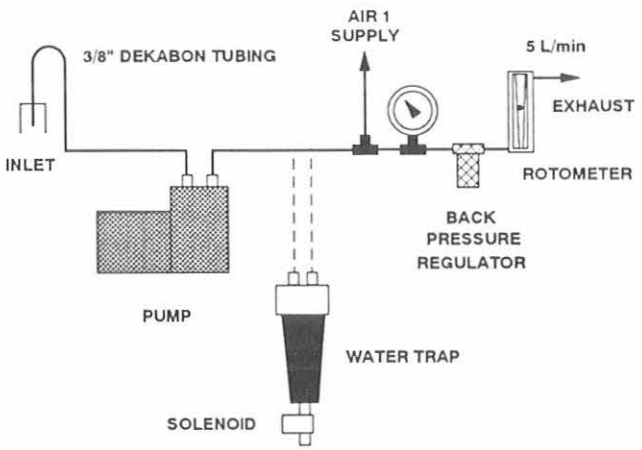

Fig. 5.5. New inlet system installed at BRW, MLO, and SMO. The water trap is installed only at SMO and MLO. At the end of the trap is a solenoid valve that periodically releases water that has accumulated in the trap.

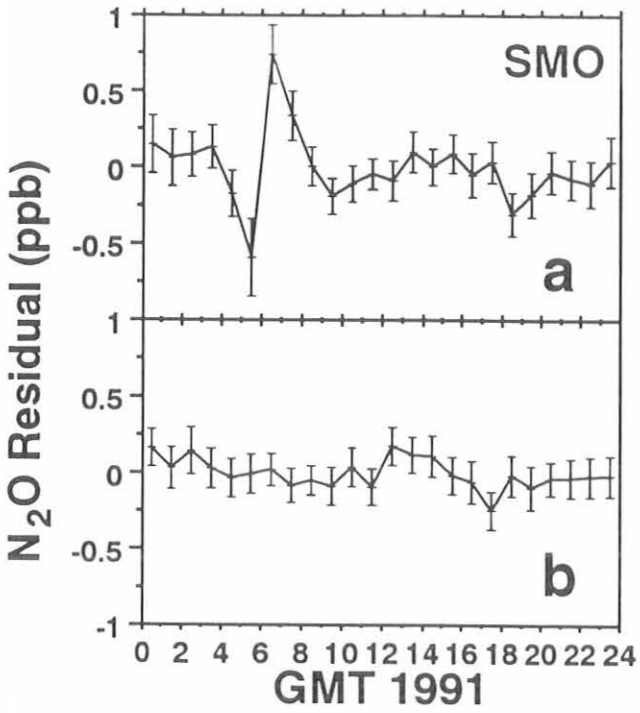

Fig. 5.6. Residual N_2O mixing ratios in ppb at SMO during 1991 before the UPS was installed (*a*) and after (*b*). The residuals were averaged for each hour of the day and the bars represent the 95% confidence interval of the mean.

day before and after the UPS was installed. It appears that the voltage fluctuations in the island power did affect a few of the N_2O measurements, and, with the addition of the UPS, the problem has been resolved.

Late in 1991, a new data collection system was purchased for SPO to be installed in January 1992. This system consists of a 386 IBM PC with IEEE-488 card, PE-Nelson interface box, and printer. The computer runs the same controlling software as the other sites and allows the storing of raw chromatograms, not just reported results. This allows for data reprocessing in Boulder, should the need arise.

The daily means for N_2O, CFC-12, CFC-11, and CCl_4 from the in situ systems are shown in Figures 5.7-5.10, respectively. Additional support for the deceleration of atmospheric growth rates of CFC-11 and CFC-12 is confirmed from in situ EC-GC measurements [*Swanson et al.*, 1992].

5.1.3. Low Electron Attachment Potential Species (LEAPS)

One objective of the LEAPS program has been to estimate recent trends in the growth of H-1211 and H-1301

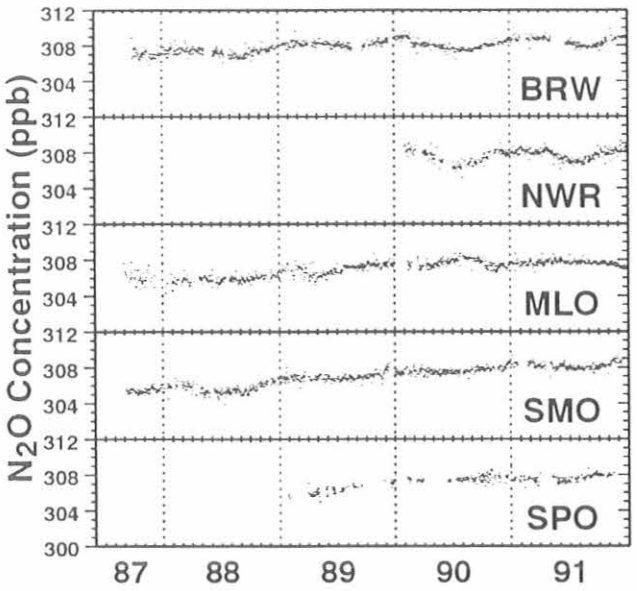

Fig. 5.7. Daily average N_2O mixing ratios in ppb from the in situ GCs.

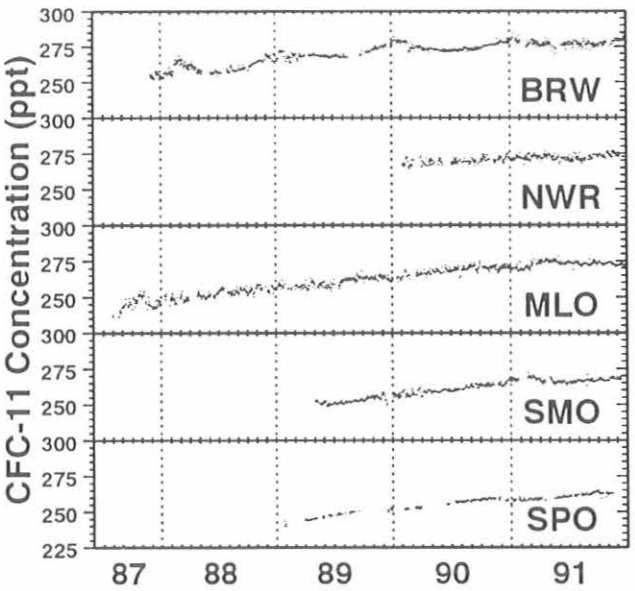

Fig. 5.9. Daily average CFC-11 mixing ratios in ppt from the in situ GCs.

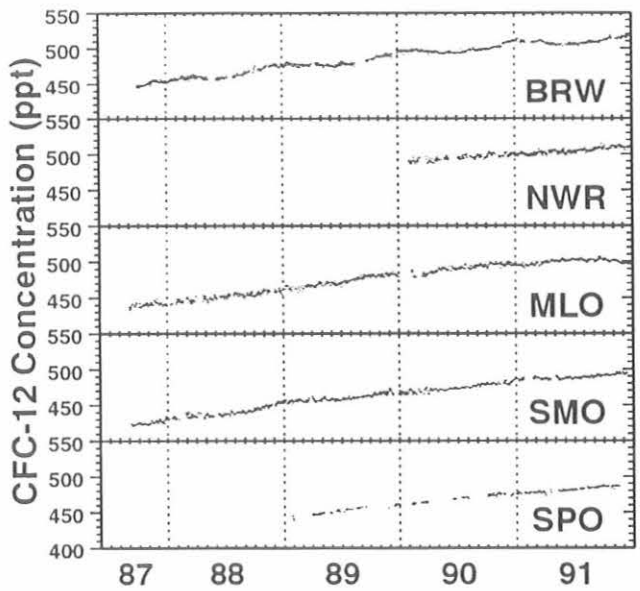

Fig. 5.8. Daily average CFC-12 mixing ratios in ppt from the in situ GCs.

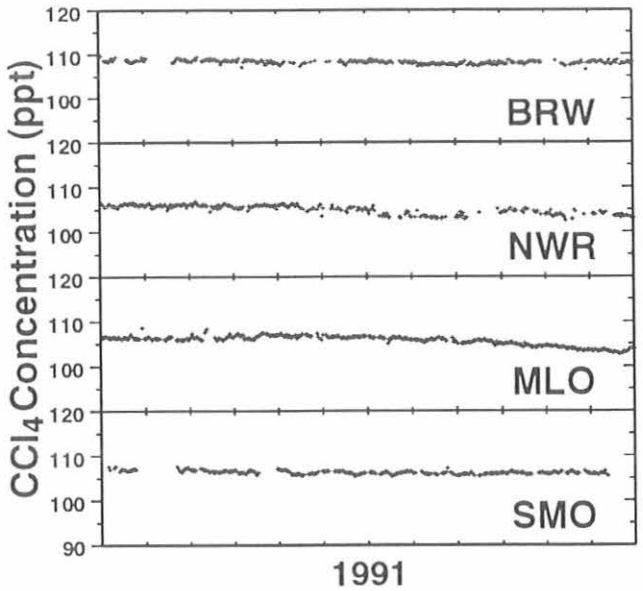

Fig. 5.10. Daily average CCl_4 mixing ratios in ppt from the in situ GCs.

from flask samples collected at NOAA's climate monitoring stations and cooperative flask sampling sites (Table 5.4), and on research cruises in the Pacific Ocean (Table 5.5).

Halons H-1211 ($CBrClF_2$) and H-1301 ($CBrF_3$) are introduced into the atmosphere almost solely as fire extinguishants; other uses, such as etching with H-1301 and dispersing from towers as atmospheric tracers, are currently minimal. These trace gases are of interest because they have very high ozone depletion potentials [*Solomon et al.*, 1992]. Although each of the halons is present at only 1-2 ppt, both are persistent in the troposphere with estimated mean lifetimes of about 65

Table 5.4. Atmospheric Measurements of Halon-1301 and Halon-1211 [*Butler et al.*, 1992]

Station	Year	H-1301	SE-1301*	H-1211	SE-1211*	Station	Year	H-1301	SE-1301*	H-1211	SE-1211*
ALT	91.359	2.23	0.15	2.44	0.08	MLO	90.200	1.70	0.07	2.53	0.19
ALT	91.529	1.77	0.09	1.91	0.16	MLO	90.444	1.78	0.06	1.67	0.03
ALT	91.759	1.89	0.07	2.27	0.04	MLO	90.523	1.48	0.03	—	0.01
ALT	91.874	1.92	0.04	—	—	MLO	90.679	1.80	0.07	1.94	0.11
BRW	89.589	1.62	0.32	—	—	MLO	90.830	1.88	0.12	2.07	0.07
BRW	89.668	1.64	0.09	2.56	0.19	MLO	90.942	2.03	0.02	2.52	0.15
BRW	89.767	1.82	0.10	1.86	0.09	MLO	91.227	1.59	—	2.15	—
BRW	90.304	1.86	0.02	2.12	0.16	MLO	91.038	1.60	0.09	2.14	0.05
BRW	90.455	1.77	0.04	2.14	0.05	MLO	91.184	1.67	0.08	2.26	0.20
BRW	90.455	1.90	0.03	2.12	0.09	MLO	91.230	1.58	0.22	2.03	0.09
BRW	90.589	1.85	0.01	2.11	0.05	MLO	91.518	1.55	0.11	2.28	0.17
BRW	90.704	1.99	0.03	2.28	0.01	MLO	91.690	1.82	0.04	2.00	—
BRW	90.858	2.01	0.02	2.55	0.05	MLO	91.781	1.86	0.03	—	—
BRW	91.126	2.08	0.02	—	—	MLO	91.866	1.82	0.03	2.26	0.05
BRW	91.173	1.79	0.00	2.30	—	MLO	91.921	1.89	0.02	2.32	0.07
BRW	91.225	2.22	0.02	—	—	SMO	89.515	1.51	0.03	2.26	0.36
BRW	91.225	2.01	0.02	2.32	0.16	SMO	89.515	1.27	0.03	—	—
BRW	91.449	1.96	0.05	2.64	0.12	SMO	89.767	1.45	0.03	2.00	0.07
BRW	91.625	1.79	0.05	2.00	0.08	SMO	89.693	1.38	0.04	1.87	0.04
BRW	91.770	2.02	0.07	1.95	0.31	SMO	90.282	1.83	0.03	1.74	0.03
BRW	91.855	1.83	0.05	—	—	SMO	90.112	1.92	0.11	2.53	0.21
BRW	91.953	2.08	0.04	2.57	0.19	SMO	90.512	1.58	0.01	2.02	0.03
NWR	89.641	1.56	0.07	1.96	0.07	SMO	90.438	1.63	0.04	2.11	0.08
NWR	89.756	1.54	0.03	1.88	0.01	SMO	90.690	1.55	0.02	1.94	0.05
NWR	89.852	1.60	0.01	1.99	0.03	SMO	90.833	1.72	0.03	2.51	0.03
NWR	90.101	1.50	0.02	1.96	0.21	SMO	90.956	1.84	0.08	2.64	0.16
NWR	90.178	1.77	0.07	2.03	0.04	SMO	91.112	1.55	0.04	1.90	0.08
NWR	90.449	1.65	0.03	1.92	0.09	SMO	91.233	1.84	—	2.18	—
NWR	90.523	1.85	0.17	2.03	0.28	SMO	91.447	1.77	0.07	2.35	0.11
NWR	90.526	1.71	0.10	1.92	0.08	SMO	91.405	1.72	0.02	—	—
NWR	90.871	2.07	0.03	1.95	0.01	SMO	91.619	1.43	0.03	1.99	0.11
NWR	90.945	1.75	0.04	2.32	0.05	SMO	91.699	1.66	0.14	1.87	—
NWR	91.022	1.59	0.07	2.03	0.12	SMO	91.866	1.69	0.06	2.16	0.08
NWR	91.148	1.79	0.00	2.45	0.32	CGO	91.359	1.65	0.03	2.10	0.15
NWR	91.214	1.73	0.03	2.06	0.04	CGO	91.452	1.68	0.05	—	—
NWR	91.521	1.74	0.07	2.26	0.05	CGO	91.537	1.59	0.10	1.86	0.03
NWR	91.616	1.85	0.02	1.96	0.07	CGO	91.696	1.67	0.04	—	—
NWR	91.712	2.28	0.09	2.28	0.05	CGO	91.825	1.73	0.03	—	—
NWR	91.901	1.96	0.02	2.53	0.04	SPO	90.068	1.56	0.04	1.80	0.03
MLO	89.504	1.14	0.11	—	—	SPO	90.008	1.50	0.03	2.04	0.09
MLO	89.600	1.28	0.02	—	—	SPO	90.213	1.38	0.02	2.10	0.08
MLO	89.677	1.60	0.02	1.92	0.03						

*The error in the measurement is reported as the standard error, SE-1301 and SE1211.

years for H-1301 and 16 years for H-1211 [*Burkholder et al.*, 1991]. Because of the long atmospheric lifetimes, these gases carry a significant amount of bromine up to the stratosphere where it can destroy O_3 catalytically. Recent reports indicate that reactions involving BrO and ClO may be responsible for 20-25% of the springtime depletion of

Table 5.5. Mean Atmospheric Measurements of Halon-1301(H-1301) and Halon-1211(H-1211) From Research Expeditions in the Pacific Ocean [*Butler et al.*, 1992]

Expedition	Year	H-1301	H-1211
SAGA-2	87.5	0.96	1.91
RITS 89	89.2	1.45	2.01
SAGA-3	90.3	—	1.89

stratospheric O_3 over the Antarctic [*Anderson et al.*, 1989]. The manufacture of both gases is to be discontinued globally by the end of the year 2000 according to the Montreal Protocol on Substances that Deplete the Ozone Layer [*UNEP*, 1987], and perhaps sooner, owing to unilateral action by users, manufacturers, and producing countries.

Paired samples have been collected every 1-2 months in electropolished, stainless-steel flasks since mid-1989 at four of the five CMDL flask network sites: BRW, NWR, MLO, and SMO. The fifth station, SPO, was sampled only during the summers of 2 years; hence the record from that station is not continuous. In 1991 sample collection for halons was begun at ALT and CGO. Flasks were also filled on research cruises from SAGA-2 in 1987 (45°N to 30°S), RITS-89 in 1989 (50°N to 60°S), and SAGA-3 in 1990 (20°N to 15°S) in the remote Pacific Ocean.

The mean difference in H-1301 mixing ratio between samples collected within the same latitudinal bands on the first two cruises suggests a growth rate of 0.29 ± 0.04 ppt yr^{-1} for 1987-1989 (Figure 5.11*a*). This high growth rate is also supported by the mean interhemispheric difference of 0.28 ppt in the cruise samples. Because the atmospheric lifetime of 65 years for H-1301 is long compared to the interhemispheric exchange time of about 1 year and because it is highly likely that most of the H-1301 is emitted in the northern hemisphere, the mean latitudinally weighted, interhemispheric difference should approximate the annual growth rate (Table 5.6). Strictly calculated, this would represent a growth rate of about 0.25 ppt yr^{-1} during this interval.

Data from the CMDL flask network show a significantly lower rate of growth for H-1301 from 1989 through 1991 (Figure 5.11*a*, Table 5.6). The rate of increase varied among individual stations from 0.11 to 0.19 ppt yr^{-1}, with a mean of 0.17 ± 0.06 ppt yr^{-1}. The mean interhemispheric difference during this time was 0.18 ppt, which represents an atmospheric growth rate of 0.15 ppt yr^{-1}, consistent with the observed trends.

The growth rate of atmospheric H-1211 was relatively constant at 0.08 ± 0.02 ppt yr^{-1} for 1987-1991 (Figure 5.11*b*). Although the mean interhemispheric difference for H-1211 of 0.11 ppt supports an atmospheric growth rate

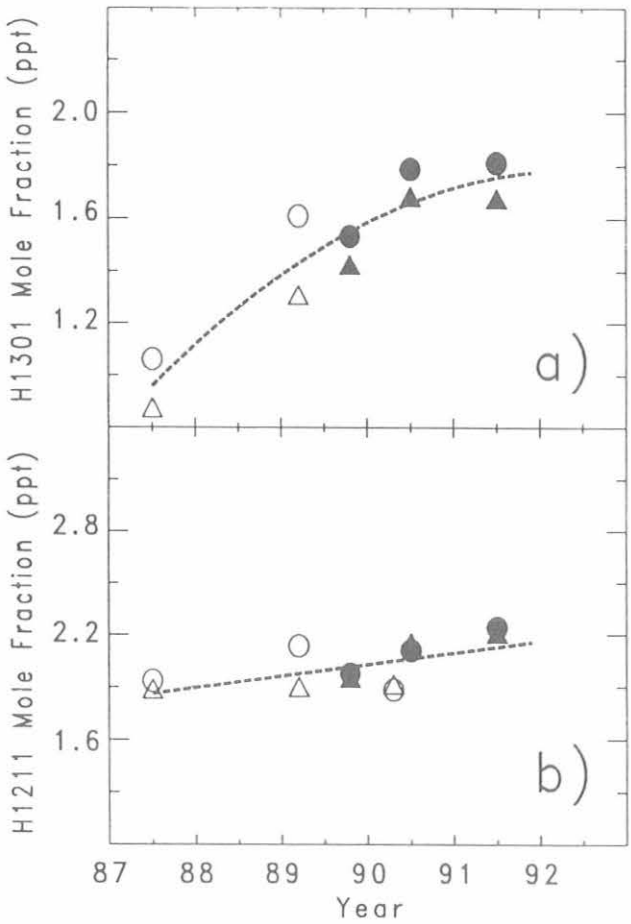

Fig. 5.11. Dry atmospheric mixing ratios of (*a*) H-1301 and (*b*) H-1211 from 1987 to 1992 [*Butler et al.*, 1992]. Circles denote the northern hemisphere and triangles represent the southern hemisphere. Open symbols are latitudinally weighted means of data from cruises in the remote Pacific Ocean; and filled symbols are latitudinally weighted, calendar-year averages of monthly measurements from fixed sites. (Measurements of H-1301 were not obtained for the 1990 cruise.)

much closer to zero, H-1211 is not as well-suited to this calculation as is H-1301; the lifetime of H-1211 is much shorter and its emission pattern may be more variable. The mean growth rate of 0.08 ppt yr^{-1}, however, is much less than those reported by other investigators for earlier periods (Table 5.6). It is clear from these data that the atmospheric growth rates of both halons have decreased dramatically in recent years, both in absolute and relative terms.

Production of both halons began declining after 1988; however, it is more uncertain exactly when, and to what extent, releases started dropping off. Annual growth rates for 1960-1990 were calculated from emission data in *McCulloch* [1992] with a simple, one-box, finite-increment model:

Table 5.6. Atmospheric Growth Rates of H-1301 and H1211 (ppt yr^{-1}) 1978-1992

Year	Location	H-1301		H-1211	
		(ppt yr^{-1})	(% yr^{-1})	(ppt yr^{-1})	(% yr^{-1})
1981	Pacific Ocean* [*Singh et al.*, 1983]	0.1	13%	—	
1982-1984	Upper troposphere [*Lal et al.*, 1985]	—		0.12	20%
1979-1985	South Pole† [*Khalil and Rasmussen*, 1985]	—		0.16	21%
1979-19987	Upper troposphere‡ [*Singh et al.*, 1988]	0.05	4.5%	0.16	12%
1978-1987	Oregon coast [*WMO*, 1988]	0.05 - 0.21	18%	0.16 ± 0.01	7-15%
1987-1989	Pacific Ocean	0.29 ± 0.04	16%	0.08 ± 0.02	3%
1989-1991	CMDL observatories	0.17 ± 0.06	10%	0.08 ± 0.02	3%

*Growth rate estimated from interhemispheric difference:

$$\frac{dX}{dt} = \frac{\Delta X}{\tau_e} - \frac{X}{\tau}$$

where X is the halon mixing ratio in the southern hemisphere (ppt), ΔX is the latitudinally weighted interhemispheric difference in mixing ratio (ppt), τ_e is the interhemispheric exchange time, and τ is the atmospheric lifetime of the halon. This equation requires that emissions in the southern hemisphere are insignificant.

†Because data from the various studies were not standardized by intercalibration, the absolute growth rates have been adjusted to match the NOAA scale, where possible. Relative growth rates (% yr^{-1}), however, are not affected by differences in calibration scales.

‡Based upon only three data points; large relative uncertainty in mixing ratios.

$$\Delta X(t+1) = \frac{\Delta t}{\tau}\left[(t-0.5)\frac{fE(t+1)}{M_a}\right] - X(t)$$

where $\Delta X(t+1)$ is the mean change in tropospheric mixing ratio for time increment $t+1$, Δt is 1 year, τ is the mean lifetime in the atmosphere, f is the fraction of total atmospheric halon in the troposphere divided by the fraction of total atmospheric mass in the troposphere, $E(t+1)$ is the total annual emission, M_a is the mass of the atmosphere, and $X(t)$ is the average tropospheric mixing ratio in a given year. The fraction, f, was calculated as 1.13 for H-1301 and 1.17 for H-1211 from data given in *Lal et al.* [1985] and *Singh et al.* [1988]. The emission scenarios predict 1990 mixing ratios to within 6% of the measured values, indicating excellent agreement between NOAH measurements, emission rates from *McCulloch* [1992], and lifetimes from *Burkholder et al.* [1991]. The recent downward trends in the growth rates of both halons are also supported by emission data, although there is some disagreement in the absolute rates (Figure 5.12, Table 5.6). Growth rates calculated from atmospheric data are associated with some error, but the uncertainties in estimating annual emissions are much greater. This is particularly true for the late 1980s and early 1990s, when mandatory and voluntary reductions in use of the halons have dramatically reduced their release to the atmosphere. *McCulloch* [1992] simply estimated emissions as fractions of production over three intervals from 1960 through 1990. Today, considerable effort is being made to limit releases, and much of the halon already produced remains in extinguishers or has been stockpiled. Hence, recent growth rates calculated from measurements of atmospheric mixing ratios are probably more reliable than estimates from release scenarios.

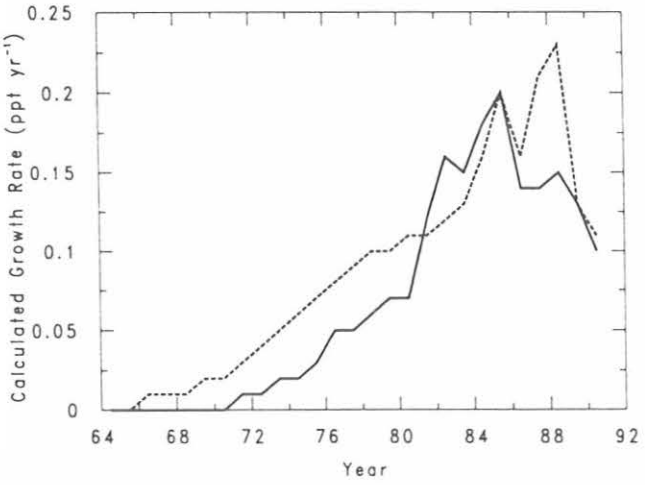

Fig. 5.12. Tropospheric growth rates for H-1301 (solid line) and H-1211 (dashed line), calculated from emission data given in *McCulloch* [1992].

5.1.4. ALTERNATIVE HALOCARBON MEASUREMENTS

Chlorine-mediated ozone destruction in the stratosphere has provided the impetus for eliminating the use of CFCs within the next decade. The Montreal Protocol for Substances that Destroy Ozone [*UNEP*, 1987] was the first treaty in which target dates were set for reduction and gradual elimination of different CFCs such as CFC-12, CFC-11, CFC-113, CFC-114 (CCl_2F-CCl_2F), CFC-115 (CCl_2F-CF_3), methyl chloroform, carbon tetrachloride, and the halons. Additional agreements and individual nations have pushed these target dates even earlier.

A combination of different compounds are expected to replace the CFCs, including hydrochlorofluorocarbons (HCFCs) and hydrofluorocarbons (HFCs). HCFCs contain chlorine, but less of this chlorine will be released in the stratosphere than that released by CFCs. One HCFC, HCFC-22 ($CHClF_2$), is readily available as it has been used extensively in refrigeration and air conditioning applications since the 1970s. The ozone depletion potential (ODP) of HCFC-22 is much less than the CFCs that it replaces, however, models suggest that its impact on stratospheric ozone could be significant if its use is allowed to continue unabated [*Solomon et al.*, 1992]. As a result, the HCFCs are viewed as temporary replacements for CFCs until better alternatives are developed, such as the HFCs. HFCs contain no chlorine and are expected to have ODPs of zero. Until recently, however, these compounds were not readily available and the hazards associated with their use were unknown. Within the last year, one of these compounds, HFC-134a, has been introduced in automobile air conditioners.

Global measurements of HCFC-22, other HCFCs, and HFCs allow for monitoring the buildup of these compounds in the atmosphere. Such measurement programs help validate models used to understand chemical and dynamic processing within the atmosphere on a global scale.

The alternative halocarbon measurement program at CMDL is based on two different approaches (1) flask sampling of air from around the globe, and (2) the use of absorbent tubes to collect large volumes of air at remote sites. Both of these approaches require that samples be analyzed in Boulder. In 1991 techniques were developed using gas chromatography with mass spectometric detection (GC-MS) to measure HCFC-22 and other compounds in flasks. Further developmental work was undertaken to optimize the collection of large amounts of ambient air on various absorbent materials and to screen different alternative halocarbons for their response by ECD and oxygen-doped ECD.

GC-MS Measurements of Hydrohalocarbons

Techniques were developed in 1991 for the analysis of ambient air by GC-MS. One to two hundred cm^3 of dry air are cryogenically collected onto an uncoated length of fused silica tubing at reduced pressure and directly injected onto a capillary chromatography column. This method affords good precision (relative standard deviation of ~1%) for measurements of compounds present at sub-ppb levels in background tropospheric air. For compounds present at levels as low as 1-10 ppt, collection of larger volumes of air is often necessary and will be accomplished with larger flasks and/or the use of absorbents.

Routine analysis of air from the CMDL stations, NWR, CGO, and ALT, using the GC-MS instrument, was begun in November 1991 by sampling air from flasks that are currently collected and analyzed by our LEAPS program (Table 5.7). Measurements of nine compounds were performed on each flask sample including HCFC-22. Tests conducted in this laboratory indicate that the integrity of HCFC-22 is maintained in these flasks for periods of at least 2 months.

Preliminary results indicate that the global average mixing ratio of HCFC-22 at the end of 1991 was approximately 100 ppt. The northern hemisphere contained 10-15 ppt more HCFC-22 than the southern hemisphere (after latitude weighting). These results are fairly consistent with calculations that use emission and lifetime estimates to generate global mixing ratios [*Midgley and Fisher*, 1992]. However, these results are substantially lower than have been reported previously for ground-based chromatographic measurements [*WMO*, 1988]. It is likely that this difference is due to a discrepancy in calibration scales. We believe that our current scale is accurate to within 5%, and further work in 1992 will help define these uncertainties further.

In an attempt to describe the growth of HCFC-22 in the past, archived air collected from SAGA-2 (Table 5.8) and NWR (Table 5.9) and stored at CMDL has been analyzed by GC-MS. Although rigorous testing of the stability of compounds such as HCFC-22 in different containers has not yet been completed, results of these analyses are reported in

Table 5.7. Atmospheric Measurements of HCFC-22 Reported as Dry Mixing Ratios in ppt (by Mole Fraction)

Station	Collection Date	No. of Flasks	HCFC-22 (ppt)
ALT	1991.87397	2	110.2
BRW	1991.95342	1	109.2
NWR	1991.98082	2	103.3
MLO	1991.99726	2	102.9
SMO	1991.90411	2	96.2
SMO	1991.99726	2	94.2
CGO	1991.88767	2	93.0
CGO	1991.91233	2	91.9
SPO	1991.95068	1	92.0

Table 5.8. Atmospheric Levels of HCFC-22 Measured in Flasks Collected During SAGA-2

Date	Latitude	Longitude	HCFC-22 (ppt)
1987.3836	36.8	-160.0	79.0
1987.3918	23.3	-160.0	75.5
1987.4027	1.7	-160.0	71.5
1987.4247	-22.2	-160.0	67.9
1987.4301	-29.4	-170.0	67.2

Figure 5.13 for air collected at NWR after mid-1988 in a number of different types of containers, with and without drying agents in line. For unknown reasons, contamination of these samples is a problem for air collected prior to mid-1988. However, for samples collected after this time, a growth rate of 6.4 ppt yr^{-1} (or 7.0% yr^{-1}) can be estimated from these data. This is very similar to growth rates that have been reported in the literature for HCFC-22 for the years 1985-1990 [*WMO*, 1988, *Rinsland et al.*, 1990] and calculated from emission estimates [*Midgley and Fisher*, 1992]. This is an indication that the growth of HCFC-22 has been fairly constant over the past 2 years despite the drastic reduction in use and emission of CFC-11 and CFC-12 during this time [*Elkins et al.*, 1992].

Table 5.9. Atmospheric Levels of HCFC-22 Measured in Archived Gas Cylinders*

Collection Date	HCFC-22 (ppt)	Type of Container and Method	Moisture
1988.8932	85.0	0	0
1988.8932	84.5	0	0
1989.2986	86.2	1	0
1990.3863	95.7	2	0
1990.9123	98.3	3	0
1991.1616	99.7	2	0
1991.7781	109.5	3	1
1991.942	107.9	2	2

*All cylinders were pumped at NWR. The types of sample containers are described by the following types: 0 = electropolished, stainless steel, 33-L container initially filled to 300 psig with ambient air; 1 = Aculife treated (Scott Specialty Gases, Plumsteadville, Pennsylvania), 49.9-L steel gas cylinder filled to 2000 psi with ambient air; 2 = Aculife treated, 29.5-L aluminum gas cylinder filled to 2000 psi with ambient air; and 3 = Aculife treated, 5.9-L aluminum gas cylinder filled to 2000 psi with ambient air. The moisture was removed with either Aquasorb (moisture = 0, support coated P_2O_5, Mallinockrodt, Paris, Kentucky) or Sicapent (moisture = 1, support coated P_2O_5, EM Science, Gibbstown, New Jersey) to dewpoints below -80° C. Ome cylinder was filled without a dryer (moisture = 2).

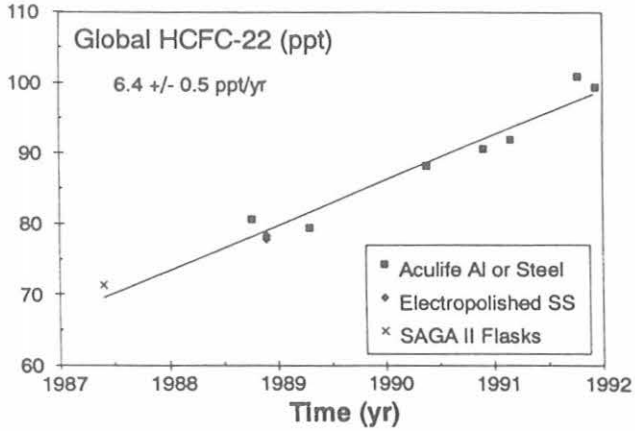

Fig. 5.13. Global estimates of HCFC-22 (by GC-MS) in archived air samples collected at NWR and during the SAGA-2 cruise. For the NWR samples, mixing ratios were divided by 1.086 to aproximate the global average of HCFC-22 at that time. Five samples taken during the SAGA-2 cruise between 30°S and 37°N and between 160°E and 170°E were latitudinally weighted to determine a global mean (Table 5.8).

Absorbent Tube and O_2-Doped ECD Measurement of Hydrohalocarbons

Further screening of potential absorbent materials for concentrating halocarbons and hydrohalocarbons from large air samples was continued in 1991. The present design for an absorbent trap consists of a 35 cm long, 0.63 cm outside diameter steel tube packed with a 9 cm length of Carbosieve S-II (Supelco), 5 cm of Carboxen 1000 (Supelco), and 16 cm of HayeSep D_B (Hayes Separations). Samples were collected on the tube at ambient temperature (25-30°C), and desorbed at 200°C. The desorbed compounds were cryogenically refocused and analyzed with the LEAPS GC. The LEAPS GC has two ECDs in series; the second detector is doped with oxygen-in-nitrogen to 0.2% O_2.

Analytical precision for some halocarbons and HCFC-22 are shown in Table 5.10. Peak areas showed standard errors (1σ, n = 3) of about 2-4%. Normalizing to CFC-12 improved precision to ~1% or less.

Figure 5.14 shows a calibration curve for CFC-12 collected on the trap from a range of NOAH gas standards. Two measurements of CFC-12 in a cylinder filled at NWR are also shown in this figure. Using the standard curve shown gave a CFC-12 mixing ratio of 479 ±6 ppt. An earlier analysis using our flask GC system gave a CFC-12 mixing ratio of 461 ± 3 ppt for this cylinder.

The ECD responds only weakly to HFCs and some HCFCs. We have determined, however, that a number of HCFCs and HFCs can be detected using O_2-doping of an ECD. When used in conjunction with absorbent tubes,

TABLE 5.10. Analytical Precision for Some Halocarbons and HCFC-22 in NOAA-191 (1-16 ppb Mixture in Air)*

Compound	Precision (Sample Standard Error, n = 3), %	
	Peak Area	Ratio to CFC-12
CFC-12	2.8	—
CFC-11	3.3	0.47
CFC-113	3.7	1.26
CH_3CCl_3	2.2	0.57
CCl_4	2.5	0.28
HCFC-22 (O_2-doped ECD)	4.3	0.86

*Loops were swept onto an absorbent trap (Carbosieve S-II, Carboxen 1000, HayeSep D_B) with 400 mL of N_2 at 30°C, and then desorbed with backflush at 200°C.

detection of these compounds using an O_2-doped ECD should be possible at the ppt level. Figure 5.15 illustrates the measurement of the only HFC currently used by industry: HFC-134a (CH_2FCF_3). While HFC-134a is not detected in the undoped ECD, oxygen doping enhances the response of this compound dramatically. Measurement of lower level standards suggests that a detection limit (three times the RMS noise) of around 3 ppt is possible in a 10-L air sample.

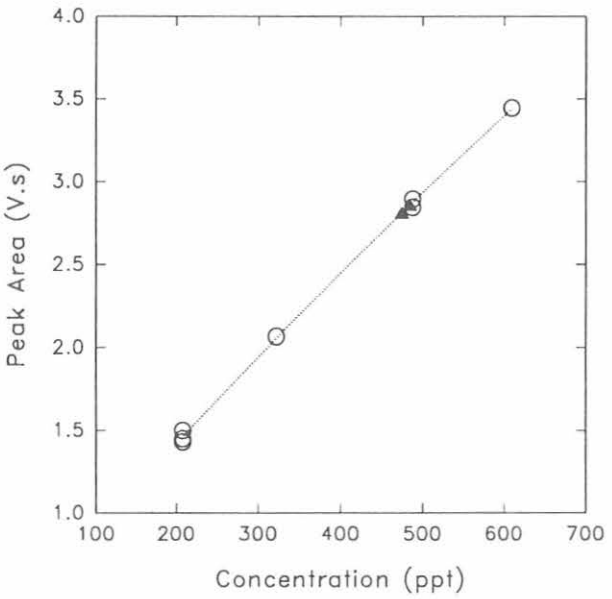

Fig. 5.14. CFC-12 gas standards (open circles) of varying concentrations trapped on an absorbent tube (10 mL of standard and 550 ml of N_2) and then desorbed at 200 °C into the LEAPS GC. Also shown (solid triangles) are two similar analyses of air from a cylinder filled at NWR.

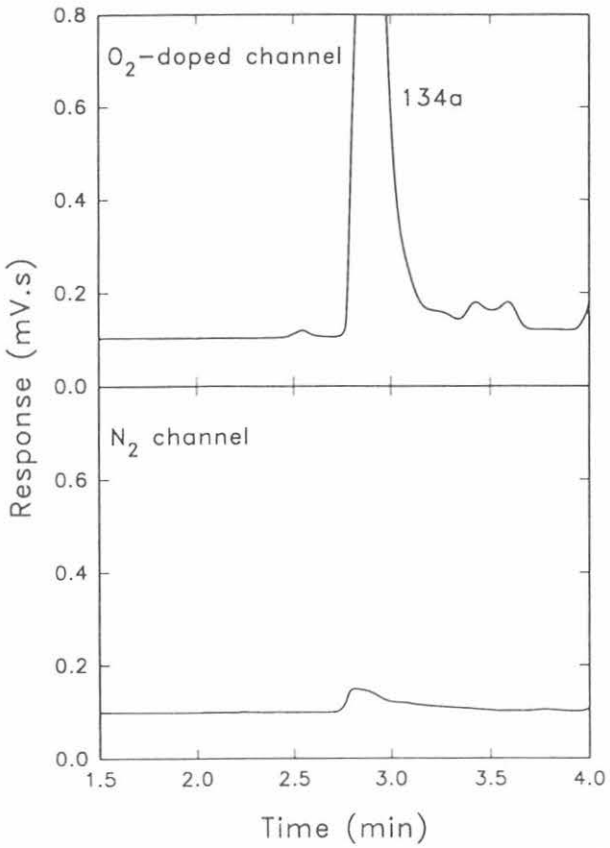

Fig. 5.15. Chromatograms from non-doped and O_2-doped ECDs in series from the same injection of 10 mL of a 156 ppm HFC-134a standard (balance air).

Figure 5.16 shows the chromatograms obtained from a 1 µL injection of "pure" HCFC-142b ($CClF_2CH_3$). This compound has already been detected in the atmosphere at the ppt level. As is the case with HFC-134a, a high degree of signal enhancement is possible with O_2-doping. The bulk sample contains CFC-11 and HCFC-141b (CCl_2FCH_2) as impurities. The HCFC-141b is also clearly visible in the O_2-doped ECD response. We do not as yet have standards for this compound to determine detection limits, but from the response observed in Figure 5.16 for high concentrations, we expect to be able to detect ppt levels with sample enrichment using absorbent tubes.

HCFC-123 (CF_3CHCl_2) has a similar response on both the doped and non-doped detector. The inherently lower noise of the non-doped channel makes this the choice for lowest detection limit. The detection limit was estimated to be 0.06 ppt in a 10-L air sample.

The LEAPS GC program has already established that O_2-doping enhances the response of HCFC-22 in an ECD. Therefore, it will be possible to measure HCFC-22, HCFC-123, HCFC-142b, HCFC-141b, and HFC-134a using O_2-

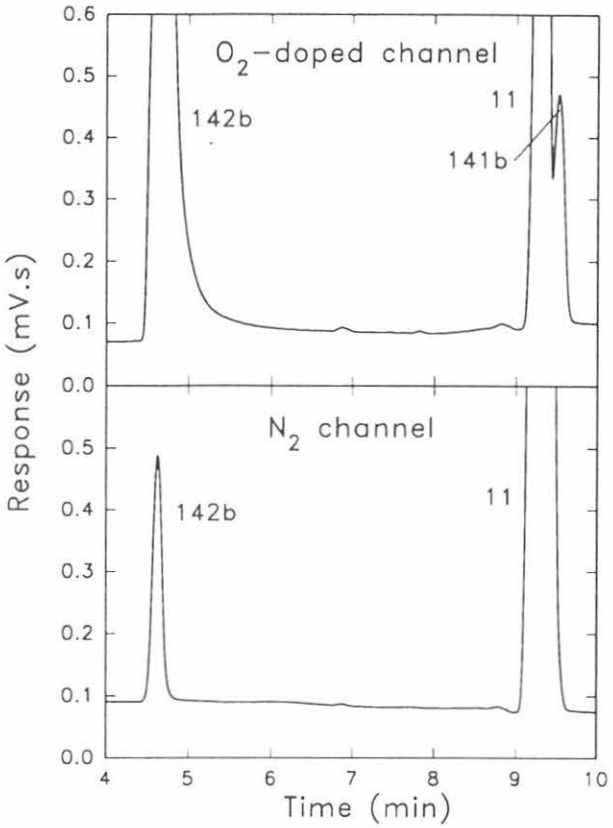

Fig. 5.16. Chromatograms from non-doped and O_2-doped ECDs in series from the same injection of 1 µL of "pure" HCFC-142b. CFC-11 and HCFC-141b are present as impurities.

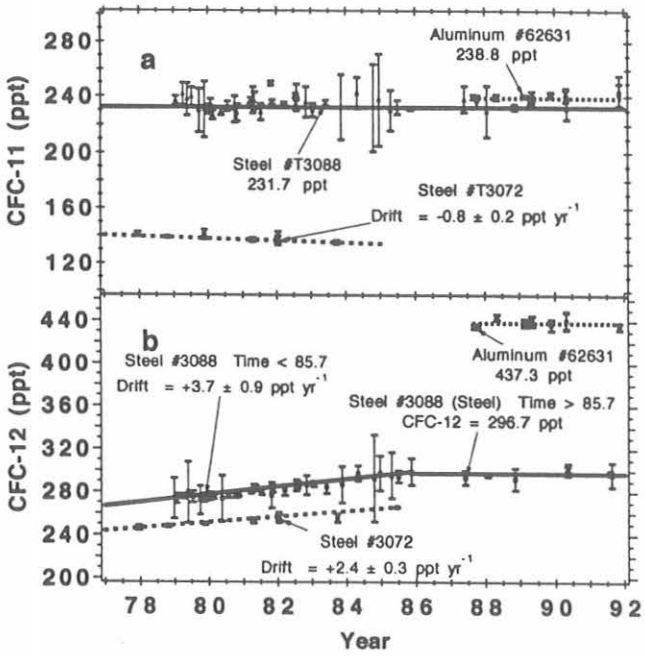

Fig. 5.17. History of NOAA calibration scale for (*a*) CFC-11 and (*b*) CFC-12. Steel cylinder no. 3072 was the only cylinder used for calibration from 1977 to 1985 and it drifted in mixing ratio starting in 1977 to 1985 for both CFC-11 and -12. However, cylinder no. 3088 has not drifted significantly since 1985 for CFC-12. Cylinder no. 3072 was emptied accidently in 1985; therefore, only cylinder no. 3088 and no. 62631 have been used to calibrate the flask measurements. Error bars are 95% C.I.

doped ECD and absorbent tube sample concentration. This gives us another viable technique, along with mass selective detection, for monitoring hydrohalocarbons. In addition, absorbent tube technology can enhance sampling flexibility of other detection methods, including mass selective.

5.1.5. Gravimetric Standards

A major effort was placed on refining our calibration of CFC-11 and CFC-12 over the past year because of the observed slowdown in their growth rates. Primary calibration of flask measurements involved only three gas standards throughout the entire period. These standards, filled with air from the NWR region, were recalibrated recently on a NOAA scale based on gravimetric standards prepared in our laboratory since 1986. All gravimetric standards agreed to better than 1%. The analysis of long-term drift of the three working standards revealed that only one standard (cylinder no. 3072), which was used from 1977 to 1985, had a statistically significant drift rate for both CFC-11 and CFC-12 (Figure 5.17). On the basis of comparisons with primary standards maintained by OGIST [*Rasmussen and Khalil*, 1986], we have estimated that the mixing ratio of CFC-12 was increasing at 2.4 ± 0.3 (one standard deviation) ppt yr^{-1} and CFC-11 was decreasing at 0.8 ± 0.2 ppt yr^{-1} in that first standard. In last year's report [*Ferguson and Rosson*, 1991], the three working standards were put on the NOAA scale, and the drift was incorrectly assumed to be insignificant for all cylinders at all times. Although we recently have corrected our data, the effect of drift in standards during 1977-1985 does not affect the more recent slowdowns of CFC growth rates that are reported here. Our absolute values for CFC-12 are about 3.4 ± 1.5% higher, and for CFC-11 about 3.2 ± 1.3% lower than those measured by the ALE/GAGE [*Cunnold et al.*, 1986] based on a comparison of data from a jointly occupied station at SMO. Results from a recent laboratory intercomparison of two cylinders showed that our scale for CFC-12 is 1.3% higher and for CFC-11 is 0.1% higher than the SIO scale [*Bullister and Weiss*, 1988].

Twenty-seven primary calibration standards were prepared during 1991 in the standards laboratory (see Table 5.11). Sixteen of the standards were prepared as multi-

Table 5.11. Summary of Gravimetric Standards Prepared in 1991

Compounds	Qty	Concentration Range	Prepared For
CFC-11, CFC-113, CFC-12, CH_3CCl_3, CCl_4, HCFC-22, N_2O	16	ppm, ppt	ACATS and NOAH
HCFC-22	2	ppm, ppb	NOAH
HCFC-123	3	ppm, ppb	NOAH
HFC-134a	1	ppb	NOAH
CH_4	3	percent, ppm	CC
CH_4, N_2O	2	ppm, ppb	JPL

component mixtures specifically for the ACATS project, but were also used in other NOAH projects. Six standards were prepared for use in the Alternative Halocarbon Measurements' project. Three methane standards were prepared for the Carbon Cycle Division including two at the percent-level and one at ambient levels. The percent-level standards will be used to generate a suite of primary standards above and below atmospheric mixing ratios for future use as a primary calibration scale. Two standards, one containing N_2O and the other CH_4, were prepared for JPL. Four NWR air secondary standards were prepared and analyzed for the RITS project. Two were used to replace GC calibration standards at SMO, and two were used to replace the GC calibration standards at NWR.

A nickel oxide catalyst was installed on the Shimadzu FID-GC model GC-8 for the measurement of CO and CO_2. The addition of the GC-MS to the NOAH group has greatly enhanced the standards laboratory capabilities to evaluate impurities of reagents used in preparing standards and also in detecting contamination problems in cylinders and in the blending manifold. A new manifold heated to 300°C has been built for transferring pure gases. After each use, it is purged with high-purity N_2 while placed inside an oven. An additional manifold currently being built, has been designed for preparing ppt level standards.

During 1991, we continued to develop a primary calibration scale for HCFC-22. Earlier measurements by chromatographic techniques (*WMO*, 1988) have suggested substantially higher mixing ratios than observed here at CMDL or by long-path infrared (*Rinsland et al.*, 1990), or expected from estimates of emissions (*Midgley and Fisher*, 1992). The GC-MS has been used to verify linearity of the standards from ppt to ppb levels. Further work is planned to expand this result to the high ppm level in 1992.

Accurate standard preparation also hinges on knowing the purity of reagent materials. Analysis of pure HCFC-22 from two different manufacturers was performed by GC-MS and FT-IR. Small amounts (1-2 μL) of pure material were injected directly onto a capillary column and analyzed. The chromatograms are presented in Figure 5.18 and indicate, when combined with the results of FT-IR analysis (performed by the AL), that the purity of both of these reagents is better than 99.9%.

One of the special projects that required the preparation of numerous standards was the ACATS project where trace gases (CFC-11 and CFC-113) were measured real-time via a gas chromatograph installed on one of NASA's ER-2 aircraft. In-flight calibrations were performed with a gravimetrically prepared calibration gas mixture. Two standards were initially prepared using pure aliquots of CFC-11, CFC-12, CFC-113, methyl chloroform, carbon tetrachloride, and HCFC-22. The resulting mixing ratios of the gases ranged from high parts per billion to low parts per million levels. Eight standards were then prepared from these two standards to provide a suite of calibration standards that contained mixing ratios above and below the atmospheric levels of these gases. Four additional standards were prepared as bulk mixtures contained in 46.4-L cylinders. The mixing ratios of components in these standards were targeted to approximate the range of levels expected from the lower troposphere to the upper stratosphere. A listing of the standards and their gravimetrically assigned mixing ratios are shown in Table 5.12. The suite of eight calibration standards and one of the bulk standards were intercompared using the ACATS GC. Figures 5.19 and 5.20 show a plot of response versus gravimetric mixing ratio of CFC-11 and CFC-113 respectively.

5.2. Special Projects: Airborne Chromatograph for Atmospheric Trace Species (ACATS)

Measurement of vertical profiles of trace gases, in particular CFCs, has gained more importance in the research activities of CMDL. Expanding our program to

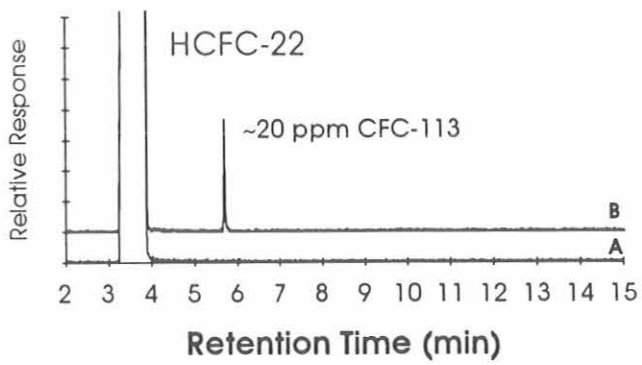

Fig. 5.18. GC-MS chromatograms of "pure" HCFC-22 from two different manufacturers, (*a*) Scott Specialty Gas and (*b*) PCR Inc.

Table 5.12. Gravimetrically Prepared Standards Used for ACATS Project

Standard Number	CFC-11	CFC-113	CFC-12	CH_3CCl_3	CCl_4	HCFC-22	N_2O
NOAA-192	478 ppb	132 ppb	1.58 ppm	761 ppb	754 ppb		
NOAA-190	282 ppb	119 ppb	1.46 ppm	599 ppb	954 ppb	469 ppb	
NOAA-191	3.02 ppb	1.28 ppb	15.7 ppb	6.42 ppb	10.2 ppb	5.03 ppb	
NOAA-215	4.33 ppb	1.83 ppb	22.5 ppb	9.21 ppb	14.7 ppb	7.23 ppb	4.83 ppm
NOAA-204	303 ppt	128 ppt	1.57 ppb	644 ppt	1.03 ppb	505 ppt	
NOAA-203	235 ppt	99.3 ppt	1.22 ppb	499 ppt	795 ppt	391 ppt	
NOAA-202	118 ppt	50.1 ppt	615 ppt	252 ppt	401 ppt	197 ppt	
NOAA-196	136 ppt	37.5 ppt	451 ppt	217 ppt	215 ppt		
NOAA-193	55.6 ppt	23.5 ppt	289 ppt	118 ppt	188 ppt	92.9 ppt	
NOAA-194	69.2 ppt	19.1 ppt	229 ppt	110 ppt	109 ppt		
NOAA-195	49.5 ppt	13.6 ppt	164 ppt	78.7 ppt	78.0 ppt		
NOAA-197	23.5 ppt	6.48 ppt	77.8 ppt	37.5 ppt	37.1 ppt		
BULK-1	33.5 ppt	14.2 ppt	173.8 ppt	71.2 ppt	113 ppt	55.7 ppt	
BULK-2	131 ppt	55.6 ppt	682 ppt	279 ppt	445 ppt	219 ppt	
BULK-3	77.2 ppt	32.6 ppt	400 ppt	164 ppt	261 ppt	129 ppt	
BULK-4	102 ppt	43.0 ppt	528 ppt	216 ppt	344 ppt	169 ppt	113 ppb

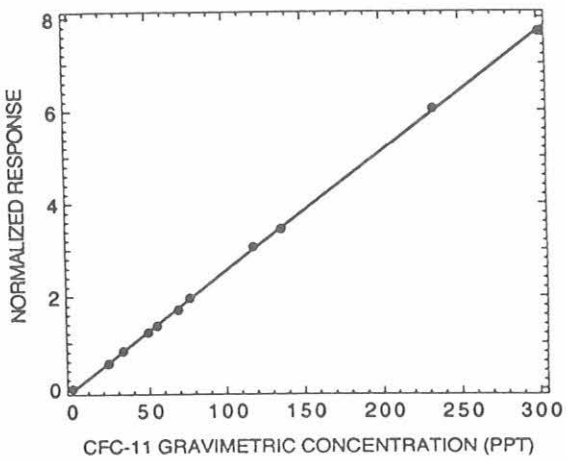

Fig. 5.19 CFC-11 gravimetric mixing ratios versus normalized instrument response of the ACATS GC using during AASE-II. Note the near-zero intercept and linear calibration of the GC over the range of the measurements.

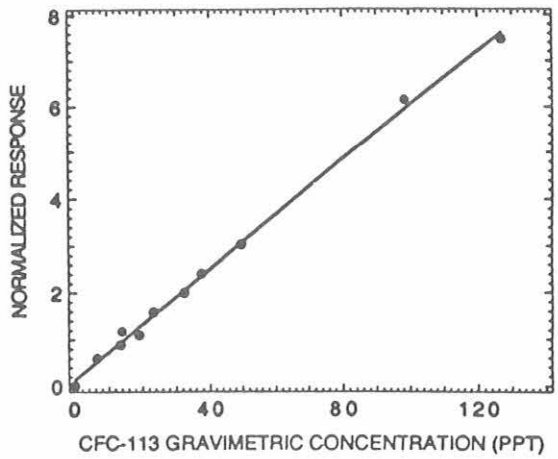

Fig. 5.20. CFC-113 gravimetric mixing ratios versus normalized instrument response of the ACATS GC using during AASE-II.

include measurements of CFC vertical profiles has become a major element of the RITS program at NOAA and a key responsibility of NOAA to the National Global Climate Change Program [*GCRP*, 1990]. Vertical profiles of CFCs are useful for comparing observed tropospheric mixing ratios to those calculated using industry estimates of emissions and simple box models. Specifically, knowledge of vertical profiles permits calculation of the fraction (*f*) of total CFC mass in the troposphere (see LEAPS section).

In 1991 our principal effort was the development of a new GC for measuring CFC-11 and CFC-113 every 2 minutes on the NASA ER-2 aircraft. This GC was built as a joint project between CMDL and AL. The schematic layout of the ACATS GC is shown in Fig. 5.21. Improvement in the sampling frequency over commercially available GCs was made possible by the addition of a two-position, 12-port gas sampling valve (GSV). The GSV injects a 5 cm^3 sample onto two separation columns coupled in series (SP 2100, Supelco), a main column and a pre-column. The use of two columns prevents air from entering the ECD and allows for backflushing of the pre-column after CFCs of interest enter the main column. The

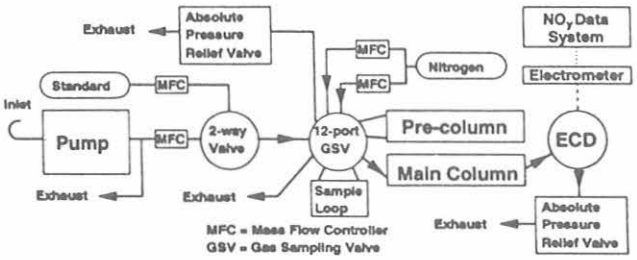

Fig. 5.21. Schematic layout of the ACATS GC.

net result is a chromatogram that contains two CFC peaks but no signal associated with air or other heavier halocarbons. The GC was mounted inside the NO_y instrument [*Fahey et al.*, 1989] in the main aft instrument compartment of the plane behind the cockpit (Q-bay). Because of limited space and weight considerations, both instruments shared a number of key components, including the onboard IBM PC, pump motor, and power lines.

The technological requirements for the airborne GC were demanding. In less than 6 months, a two-channel GC was built to fit within a 50 L volume (note that the equivalent station GC takes up a standard 2 m lab bench and weighs over 150 kg). The airborne GC's electrical and mechanical systems were required to meet or exceed military specifications for safety, and its design included several automatic shutdown features rarely found on commerical GCs. Special engineering was required so that the instrument response was independent of the wide pressure (250-1000 mb) and temperature (3-33°C) variations experienced in the Q-bay during a single flight.

The first application of ACATS on the ER-2 aircraft was to measure CFC-11 and CFC-113 for the NASA Arctic Airborne Stratospheric Expedition-II (AASE-II) that ran from August 1991 through March 1992. The goal of AASE-II was to investigate the formation, maintenance, and breakup of the arctic vortex and to quantify the amount of ozone depletion in the northern hemisphere resulting from the presence of CFCs. The expedition began in August with a series of test flights at the NASA Ames Research Center, Moffett Field, California. The initial flights occurred in September. During both test flight periods, flights were made south and east to measure the stratospheric extent of the volcanic plume from the Mt. Pinatubo eruption that had occurred in June. In order to measure the background levels of tracers and other reservoir species in the stratosphere prior to the formation of the arctic vortex, a series of flights were based out of Fairbanks, Alaska, in October and out of Bangor, Maine, in November and December. The formation, maintenance, and breakup of the vortex were monitored between December 1991 and March 1992. Several flights were directed south (as far south as 23°N) to examine the extent of ozone depletion and the influence of aerosols from Mt. Pinatubo into the mid-latitudes.

The scientific motivations for measuring CFC-11 and CFC-113 on the AASE-II were: (1) to define the CFC tracer field during the mission from 23° to 90°N; (2) to estimate the chemical ozone loss within the arctic vortex; (3) to record the evolution of organic chlorine (CCl_y, e.g. CFCs) and to support calculation of inorganic chlorine (Cl_y, e.g. ClO, $ClONO_2$, HCl) in the arctic vortex; and (4) to calculate local ODPs expected for HCFCs given the in situ measurements of CFCs by ACATS and CH_4 by ALIAS [*Webster et al.*, 1990], and the chemical model of *Solomon et al.* [1992]. Typical vertical profiles of CFC-11 and CFC-113 as measured by ACATS are shown in Figure 5.22 from a flight between Fairbanks and Moffett Field on October 14. Approximately 90% of the total atmospheric CFC-11 and CFC-113 reside in the troposphere. While the mixing ratio of CFC-113 is linearly correlated with N_2O measured by ATLAS [*Loewenstein et al.*, 1989], CFC-11 shows considerable curvature (Figure 5.23). The degree of curvature observed in these plots gives an indication of the local photochemical lifetime of the CFC relative to mixing times. A linear relationship indicates that local mixing times are shorter than the time for local photochemical loss. Non-linearity denotes more rapid local chemical loss of the tracer than can be resupplied by mixing. The relationship between N_2O, a long lived tracer with an atmospheric lifetime of ~130 years, and molecules with shorter lifetimes will be non-linear at low N_2O values, and this is consistent with the results shown in Figure 5.23 given that the accepted lifetime for CFC-11 is ~55 years and for CFC-113 is ~110 years.

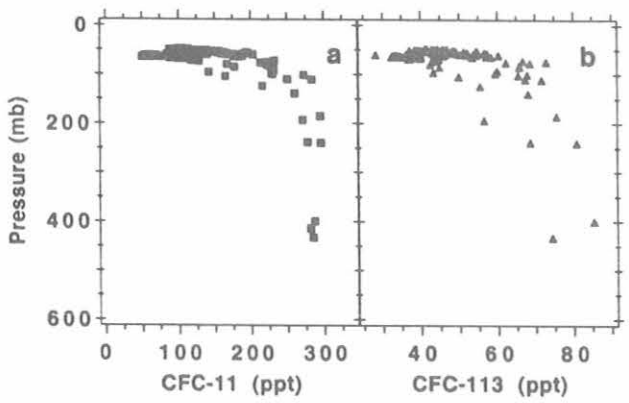

Fig. 5.22. Vertical profiles of (*a*) CFC-11 in squares and (*b*) CFC-113 in triangles measured using the ACATS GC on board the NASA ER-2 aircraft on October 14, 1991, during a ferry flight from Fairbanks, Alaska, to Moffett Field (NASA Ames Research Center), California. Note that the high values (>80 ppt) of CFC-113 were observed on the approach to Moffet Field over San Jose, California, an area where large amounts of CFC-113 are used by the electronics industry.

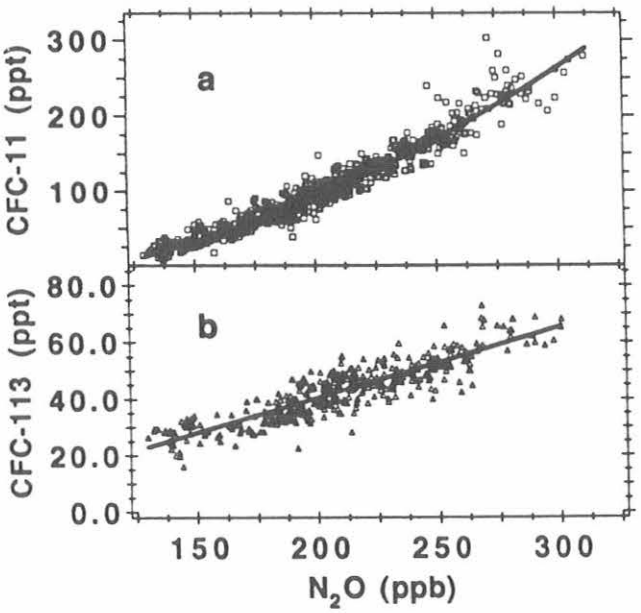

Fig. 5.23. Tracer plots from the AASE-II in 1991 for (*a*) CFC-11 versus N_2O and (*b*) CFC-113 versus N_2O. Both sets of data are preliminary. Data for N_2O were obtained from the ATLAS instrument (private communication, Max Loewenstein, NASA, Ames).

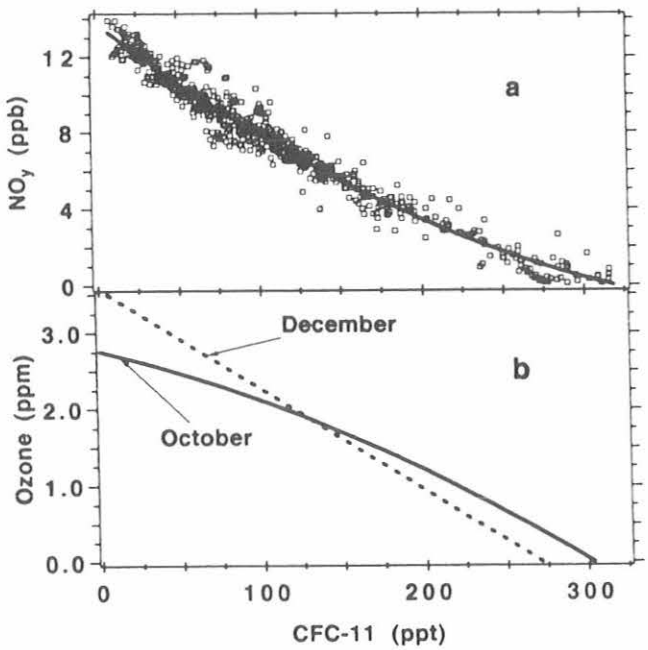

Fig. 5.24. Relationships of (*a*) reactive nitrogen (NO_y) versus CFC-11 and (*b*) ozone versus CFC-11 fitted curves for October and December. All sets of data are preliminary (NO_y [private communication David Fahey, NOAA/AL] and O_3 [private communication Michael Proffitt, CIRES].)

Mixing ratios of CFC-11 are inversely correlated with ozone [*Proffitt et al.*, 1992] and NO_y [*Fahey et al.*, 1989] (Figure 5.24). The low ozone (O_3) values observed in October when CFC-11 was also low are associated with summertime loss of O_3 in the higher latitude regions (Figure 5.24*b*.). Plots of O_3 versus tracers (for example, CFC-11 and N_2O) and their relationships establish a relative climatology for predicting O_3 mixing ratios, thereby permitting estimates of loss and production of this important trace gas over the period of the mission.

5.3. References

AFEAS (Alternative Fluorocarbons Environmental Acceptability Study), *Chlorofluorocarbons (CFC's) 11 and 12*, Report prepared for AFEAS by Grant Thornton, Washington, DC, 1991.

Anderson, J.G., W. H. Brune, S. A. Lloyd, D. W. Toohey, and S. P. Sander, Kinetics of O_3 destruction by ClO and BrO within the antarctic vortex: An analysis based on in situ ER-2 data, *J. Geophys. Res., 94*, 11480-11520, 1989.

Burkholder, J.B., R.R. Wilson, T. Gierczak, R. Talukdar, S.A. McKeen, J.J. Orlando, J.J., Vaghjiani, G.L., and A.R. Ravishankara, Atmospheric fate of CF_3Br, CF_2Br_2, CF_2ClBr, and CF_2BrCF_2Br, *J. Geophys. Res., 96*, 5025-5043, 1991.

Bullister, J.L. and R.F. Weiss, Determination of CCl_3F and CCl_2F_2 in seawater and air, *Deep Sea Res., 35(5)*, 839-853, 1988.

Butler, J.H., J.W. Elkins, T.M. Thompson, B.D. Hall, and C.M. Brunson, N_2O and Halocarbons Group, in *Geophysical Monitoring for Climatic Change No. 17, Summary Report, 1988*, edited by J.W. Elkins, and R.M Rosson, pp. 64-70, NOAA Environmental Research Laboratories, Boulder, CO, 1989.

Butler, J., J.W. Elkins, B.D. Hall, S.O. Cummings, and S.A. Montzka, A decrease in the growth rates of atmospheric halon concentrations, *Nature, 359*, 403-405, 1992.

Cunnold, D.M., R.G. Prinn, R.A. Rasmussen, P.G. Simmonds, F.N. Alyea, C.A. Cardelino, A.J. Crawford, P.J. Fraser, and R.D. Rosen, Atmospheric lifetime and annual release estimates for $CFCl_3$ and CF_2Cl_2 from 5 years of ALE data, *J. Geophys. Res.*, 91, 10,797-10,817, 1986.

Elkins, J.W., T.M. Thompson,, B.D. Hall, K.B. Egan and J.H. Butler, NOAA/GMCC halocarbons and nitrous oxide measurements at the South Pole, *Ant. J. U. S.*, 23, 76-77, 1988.

Elkins, J.W., T. M. Thompson, T. H. Swanson, J. H. Butler, S. O. Cummings, B. D. Hall, D. A. Fisher, and A.G. Raffo, Slowdown in the atmospheric growth rates of chlorofluorocarbon-11 and -12, submitted, *Nature*, 1992.

Fahey, D.W., D.M. Murphy, K.K. Kelly, M.K. W. Ko, M.H. Proffitt, C.S. Eubank, G.V. Ferry, M. Loewenstein, and K. R. Chan, Measurements of nitric oxide and total reactive nitrogen in the antarctic stratosphere: Observations and chemical implications, *J. Geophys. Res., 94*, 16,655-16,681, 1989.

Ferguson, E.E. and R.M. Rosson (Eds.), Climate Monitoring for Climate Monitoring and Diagnostics Laboratory, No. 19: Summary Report 1990, pp 19, NOAA Environmental Laboratories, Boulder, CO, 1991.

GCRP (Global Change Research Program), *Our Changing Planet: The FY 1991 Research Plan, The U.S. Global Change Research Program*, Report by the Committee on Earth Sciences, 120 pp., U.S. Geological Survey, Reston, VA, 1990.

Khalil, M.A.K., and R.A. Rasmussen, The trend of bromo-chlorodifluoromethane and the concentrations of other bromine-containing gases at the South Pole., *Ant. J. U. S., 20*, 206-207, 1985.

Loewenstein, M., J.R. Podolske, K.R. Chan, and S.E. Strahan, Nitrous oxide as a dynamical tracer in the 1987 Airborne Antarctic Ozone Experiment, *J. Geophys. Res., 94*, 11,589-11,598, 1989.

Lal, S., R. Borchers, P. Fabian, and B.C. Krüger, Increasing abundance of $CBrClF_2$ in the atmosphere, *Nature, 316*, 135-136 1985.

McFarland, M., and J. Kaye, Annual reviews, Chlorofluorocarbons and ozone, *J. Photochem. Photobiol,. 55*, 911-929, 1992.

Midgley, P.M., and D.A. Fisher, The production and release to the atmosphere of chloro-difluromethane (HCFC-22), submitted, *Atmos. Environ.*, 1992.

McCulloch, A. Global production and emissions of bromochlorodifluoromethane and bromotrifluoromethane (Halons 1211 and 1301), *Atmos. Environ., 26A*, 1325-1329, 1992.

Proffitt, M.H., S. Solomon, and M. Loewenstein, Comparison of 2-D model simulations of ozone and nitrous oxide at high latitudes with stratospheric measurements, *J. Geophys. Res., 97(D1)*, 939-944, 1992.

Rasmussen, R.A. and M.A.K. Khalil, Trends and distributions over the last decade, *Science, 232*, 1623-1624, 1986.

Rinsland, C.P., A. Goldan, F.J. Murcray, R.D. Blatherwick, J.J. Kosters, D.G. Murcray, N.D. Sze, and S.T. Massie, Long-term trends in the concentrations of SF_6, $CHClF_2$, and COF_2 in the lower stratosphere from analysis of high-resolution infrared solar occultation spectra, *J. Geophys. Res., 95*, 16,477-16,490, 1990.

Singh, O.N., R. Borchers, P. Fabian, S. Lal, and B. H. Subbaraya, Measurements of atmospheric BrO_x radicals in the tropical and mid-latitude atmosphere, *Nature, 334*, 593-595, 1988.

Singh, H.B., L.J. Salas, and R.E. Stiles, Selected man-made halogenated chemicals in the air and oceanic environment, *J. Geophys. Res., 88*, 3675-3683, 1983.

Solomon, S., M. Mills, L.E. Heidt, W.H. Pollock, and A.F. Tuck, On the evaluation of ozone depletion potentials, *J. Geophys. Res., 97*, 825-842, 1992.

Swanson, T.H., J.W. Elkins, T.M. Thompson, S.O. Cummings, J.H. Butler, and B.D. Hall, Decline in the accumulation rates of atmospheric chlorofluorocarbons 11 and 12 at the South Pole, submitted, *Ant. J. U. S.*, 1992.

UNEP (United Nations Environmental Program), *Montreal Protocol to Reduce Substances that Deplete the Ozone Layer Report, Final Report*, New York, 1987.

Webster, C.R., R.D. May, R. Toumi, and J.A. Pyle, Active nitrogen partitioning and the nighttime formation of N_2O_5 in the stratosphere: Simultaneous in situ measurements of NO, NO_2, HNO_3, O_3, and N_2O using the BLISS Diode Laser Spectrometer, *J. Geophys. Res., 95*, 13,851-13,866, 1990.

WMO (World Meteorological Organization), *Report of the International Ozone Trends Panel, 1988*, Vol. 2, Global Ozone Research and Monitoring Project Report No. 18, Geneva, Chapter 8, 1988.

6. Director's Office

6.1. Characterization of Mt. Pinatubo Aerosols Collected Over Laramie, Wyoming, Using Electron Microscopy

Patrick J. Sheridan (CIRES), Russell C. Schnell and David J. Hofmann

6.1.1. Introduction

The major eruptions of Mt. Pinatubo in the Philippines on June 15-16, 1991, were reported to have reached the 30-40 km level in the stratosphere [*Smithsonian*, 1991]. The volcanic cloud was observed to circle the globe in about 3 weeks, and was tracked by ground-, aircraft-, and satellite-based sensors, so that its location and extent were reasonably well known at all times. Initial observations of this violent eruption indicated that the aerosol cloud injected into the stratosphere was more extensive by a factor of 2-3 than that from the eruption of El Chichon in 1982 [*Smithsonian*, 1991].

Although the major portion of the Mt. Pinatubo aerosol cloud remained over the tropics, a fragment broke away and was first observed over Laramie on July 16, 1991. The cloud was originally present as a relatively thin layer at ~16-17 km altitude. Over the next 2 weeks, this volcanic layer thickened, and a higher layer centered at ~23 km was detected [*Deshler et al.*, 1992].

On several of the balloon flights during late July and early August, cascade impactors were used to sample these volcanic aerosols. In this paper, we report on electron microscope (EM) analyses of the aerosol particles that permitted us to characterize the physical and chemical nature of the volcanic debris. Size distribution information was obtained from the microanalyses, as were discrete particle and bulk aerosol composition, and are compared with OPC measurements.

6.1.2. Experimental Methods

On all flights, aerosol sampling commenced on the ascent just above the tropopause and continued for approximately 65 minutes up to the 37.5 km level. This permitted collection of particles from the enhanced aerosol layers at 17 and 23 km altitude. Aerosol particles were size segregated in single-orifice cascade impactors and deposited onto thin (~10-20 nm thick) formvar films supported by Ni transmission electron microscope (TEM) grids. The three impactor stages used for size fractionation had aerodynamic cutoff diameters (ACD's) of 4 μm, 1 μm, and 0.25 μm.

Particles on the three thin film substrates in each sample were analyzed using a 200-kV analytical electron microscope (AEM). The central aerosol deposit area on each grid was analyzed under low magnifications (200-600X) and the extent and approximate particle loading of the deposit over the film was documented. This provided a rough estimate of total particulate loading for each stage. Next, a suitable area of the grid was chosen for a particle identification and classification study. This area was often displaced slightly from the central high-loading area because some samples showed very heavy particulate loadings, and observation of discrete particles in the central aerosol deposit was difficult. All particles falling within a small rectangular analysis area at 20,000X magnification were counted and classified on each 1 μm and 0.25 μm ACD stage until 500 particles per stage were encountered. At this magnification, particles as small as 0.01 μm were easily observed and counted. Since the 4 μm stage substrates always collected few particles, formal 500-point counts of these films were not attempted.

The ultra-thin window (UTW) x-ray detector used for x-ray spectrometry was sensitive to x-rays from elements of $Z > 4$, which permitted direct detection of the light element x-rays C and O in individual particles. Details of the particle counting, x-ray analysis and particle classification procedures were presented in *Sheridan et al.*, 1992.

6.1.3. Results and Discussion

Three stratospheric aerosol samples were collected on July 26, July 30, and on August 14, 1991 (hereafter referred to in this paper as samples no. 1, no. 2 and no. 3, respectively), between the altitudes of ~15.5 and 37.5 km. This was during a period when the volcanic aerosols were consistently observed in relatively high concentrations over Laramie. The OPC's produced aerosol soundings of $r > 0.15$ μm particles during this mid-July to late-August time period that showed the aerosol layer centered at 17 km was spreading vertically [*Deshler et al.*, 1992]. In late July to early August, another major volcanic layer was detected at 23 km altitude. Figure 1 shows the vertical aerosol profile from the balloon sounding on July, 30, 1991. The volcanic layers centered at ~17 and 23 km showed significantly enhanced concentrations of particles of all sizes, including supermicrometer particles. The 23 km aerosol layer was sampled in addition to the lower layer on this balloon flight, whereas the overwhelming majority of aerosols on the July 26 and August 14 flights were collected below the 20 km level.

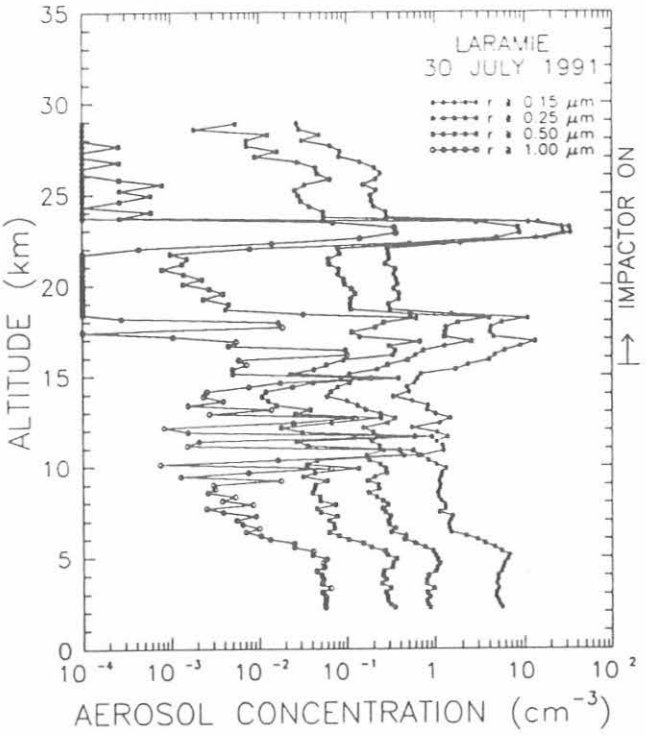

Fig. 1. Vertical aerosol profiles measured by optical particle counter from the July 30, 1991, balloon flight. Collection of cascade impactor sample no. 2 was initiated during the ascent at ~ 15.5 km altitude.

The samples were largely composed of neutralized sulfate particles, most of which were observed on the 0.25 μm ACD impactor stages. While it is difficult to determine absolute atmospheric aerosol concentrations with this sampling method [*Sheridan*, 1989], relative loadings (and relative aerosol concentrations) between samples are straightforward to ascertain. Based on the extent of the heavy central aerosol deposit on all 0.25 μm ACD grids and on point counts of particle numbers over limited grid areas, the three sample substrates showed similar loadings of fine particles. Figure 2 shows the central aerosol deposits of all three samples. Large numbers of supermicrometer H_2SO_4-coated crustal particles were observed on the sample no. 2 film (presumably from particle bounce from upstream stages), whereas the other 0.25 μm ACD substrates collected fewer large particles. The heaviest loading sample (sample no. 1) showed only ~30% more fine particles than did the lightest loading sample (sample no. 3). Since similar volumes of air were sampled, this is interpreted to mean that the average fine particle concentration during the sampling period was ~30% higher for sample no. 1 than for sample no. 3. This is consistent with OPC data that show the peak aerosol concentrations (r >0.15 μm particles) during collection of samples no. 1 and

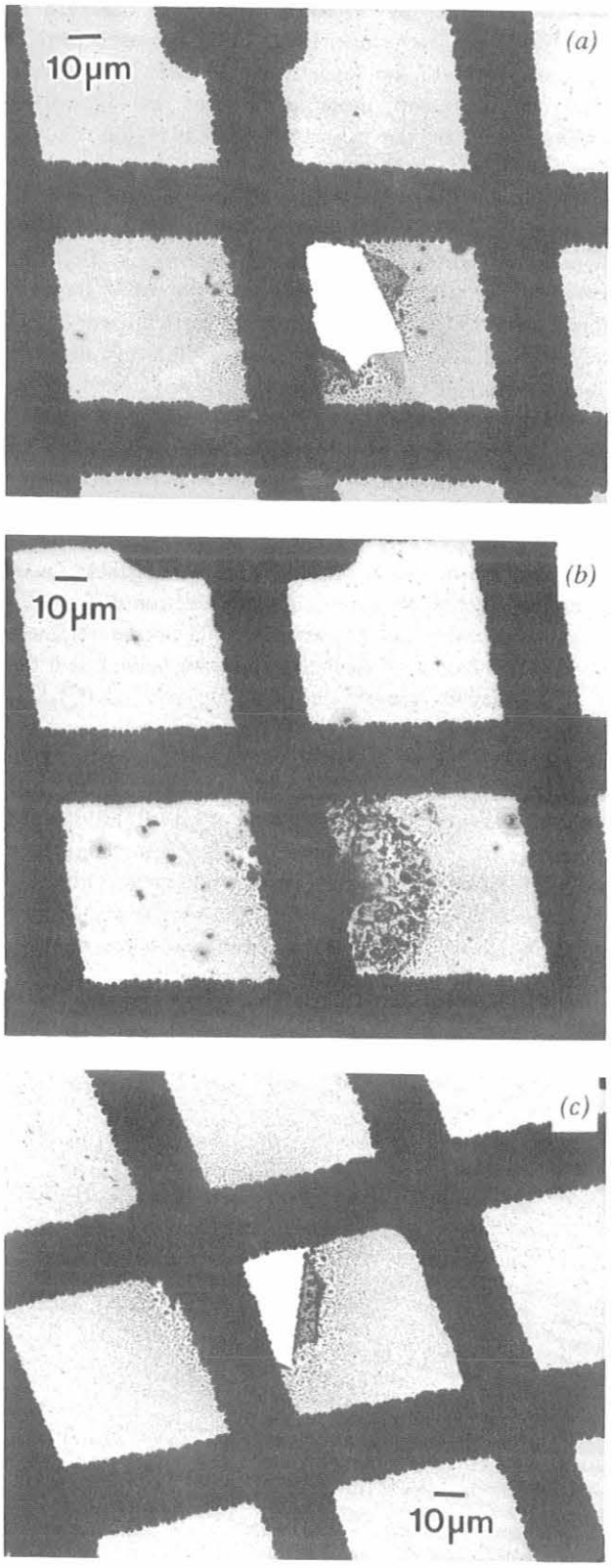

Fig. 2. Central aerosol deposits from all 0.25 μm ACD stage samples. (*a*) Sample no. 1. (*b*) Sample no. 2. (*c*) Sample no. 3.

no. 2 were higher by 50-100% over those observed in sample no. 3 [*Deshler et al.*, 1992]. The increased vertical thickness of the 17 km layer in sample no. 3 may have effectively decreased these differences by increasing sampling time in the aerosol-enhanced region on the August 14 flight.

Closer inspection of these fine sulfate particles revealed that most were surrounded by one or more rings of smaller S-containing particles. Figure 3 shows a field of submicrometer particles from the 0.25 μm ACD stage of sample no. 1. The "satellite" rings of particles were most likely formed upon or after impaction of liquid droplets onto the film, and acidic sulfate particles have been shown in previous works to be largely liquid [*Charlson et al.*, 1974; *Ferek et al.*, 1983]. These particles were probably collected as aqueous H_2SO_4 and were subsequently neutralized by ambient NH_3 during handling. The rectangular particles at the center of the rings are most likely products of this reaction. They are unstable under the intense electron beam required for electron diffraction, so direct mineralogical information could not be obtained. Since H_2O is driven off in the vacuum, we believe that the analyzed particles are small, relatively pure $(NH_4)_2SO_4$ crystals.

The 1 μm and 4 μm ACD stages were analyzed to determine the relative fractions of coarse particles in these samples. The 4 μm ACD stages were always lightly loaded and most particles on these stages were composite sulfate/crustal particles in the 2-5 μm size range. Figure 4 shows one of these large particles from sample no. 2 along with its x-ray spectrum. The solid crustal cores of these

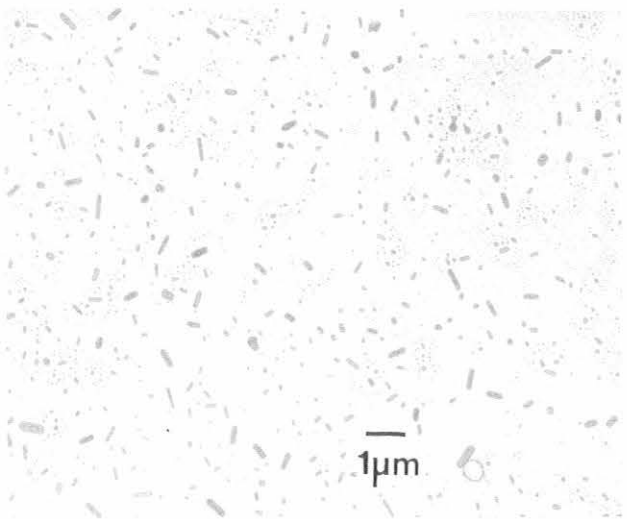

Fig. 3. Submicrometer sulfate particles from the 0.25 μm ACD stage of sample no. 1. Impaction satellite morphology and S-rich composition indicate that the particles impacted as liquid H_2SO_4 droplets.

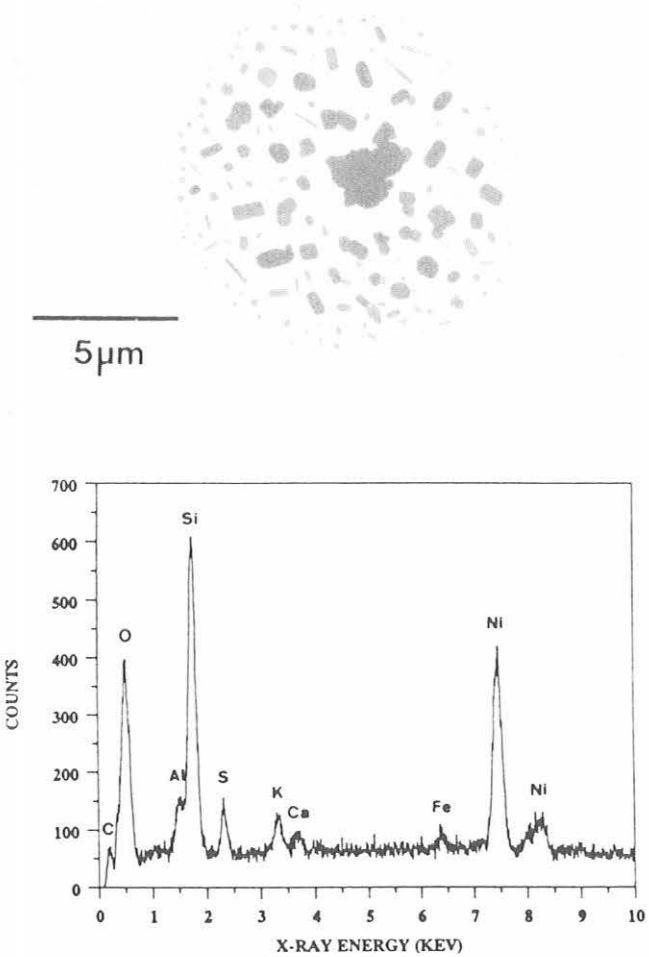

Fig. 4. Composite sulfate/crustal particle from 4 μm ACD stage of sample no. 2. Satellite sulfate particles were probably formed during impaction of the H_2SO_4-encased crustal particle. Nickel peaks in this spectrum are from the TEM grid.

particles were observed to range up to ~10 μm in size. The composite particles, including the H_2SO_4 surface coatings, would likely have been somewhat larger.

The 1 μm ACD impactor stages in all three samples resembled the corresponding 0.25 μm stage from the same sample in distribution of particle types, but aerosol loadings were usually lower by several orders of magnitude. The exception to this was sample no. 2, where a similar number of particles to that collected on the 0.25 μm stage was observed, and particulate mass appeared to be substantially greater. Figure 5 shows the central aerosol deposit area on the 1 μm stage from sample no. 2. Numerous solid, supermicrometer particles were observed, along with a considerable amount of large sulfate particles.

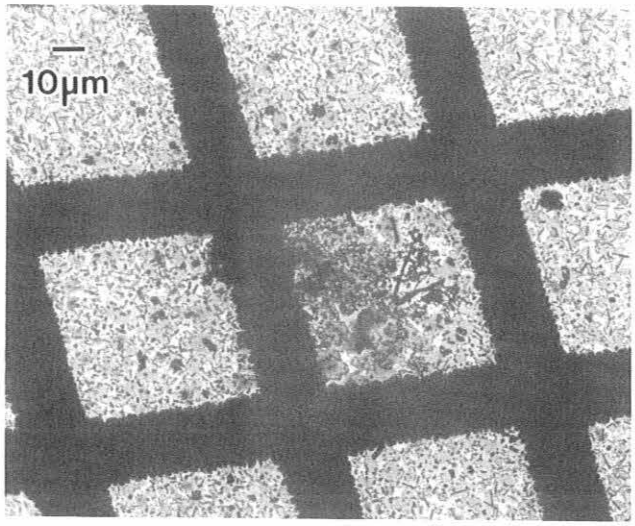

Fig. 5. Central aerosol deposit region from 1 μm stage of sample no. 2. This coarse-stage particulate deposit was far more extensive than any of the 0.25 μm stage aerosol deposits.

Many of the larger particles probably came from the well-defined aerosol layer at 23 km, where the concentrations of $r > 0.5$ μm and $r > 1$ μm particles reached ~9 cm^{-3} and ~0.5 cm^{-3}, respectively. These numbers are both several orders of magnitude higher than corresponding concentrations outside of this layer. Samples no. 1 and no. 3 showed smaller fractions of large particles, and the major layers were below 20 km altitude.

The three stratospheric impactor samples were all very similar in composition. Approximately 98 to > 99% of all analyzed particles in all three samples were collected as aqueous H_2SO_4. The absolute accuracy of this figure is questionable, due to uncertainties in the counting method caused by the presence of small impaction satellite particles. We do not believe this to be a major problem in this study, however, because of the predominance of the sulfate particles on the thin films, and a slightly different number for the fraction of sulfate particles in these samples would not change our assessment of a mostly H_2SO_4 aerosol. In other samples that contained several major particle types, this could cause significant counting errors.

Crustal particles coated with H_2SO_4 accounted for <1% of the particles on all of the 0.25 μm ACD stages. The 1 μm ACD stage films showed larger crustal particle number fractions, estimated to be in the 3-10% range. Of the relatively few particles collected on the 4 μm ACD stages, roughly 40-70% were composite crustal particles with sulfate coatings. The remaining coarse particles on 4 μm ACD substrates were large sulfate droplets.

One of the major questions we wanted to investigate was whether the H_2SO_4 was formed primarily through homogeneous or heterogeneous nucleation. This was accomplished by inspecting many sulfate particles at high magnification and then increasing the power density of the electron beam until the sulfate began to volatilize. Small, solid nucleus particles, if present, would have remained after the sulfate boiled away. Figure 6 shows two photomicrographs taken of the same grid area from the 0.25 μm ACD stage of sample no. 2, both before and after electron beam damage to the particles has occurred. At this magnification, solid particles down to ~0.01 μm in size can be observed. For a subset of the particles, the magnification was increased by a factor of two so particles

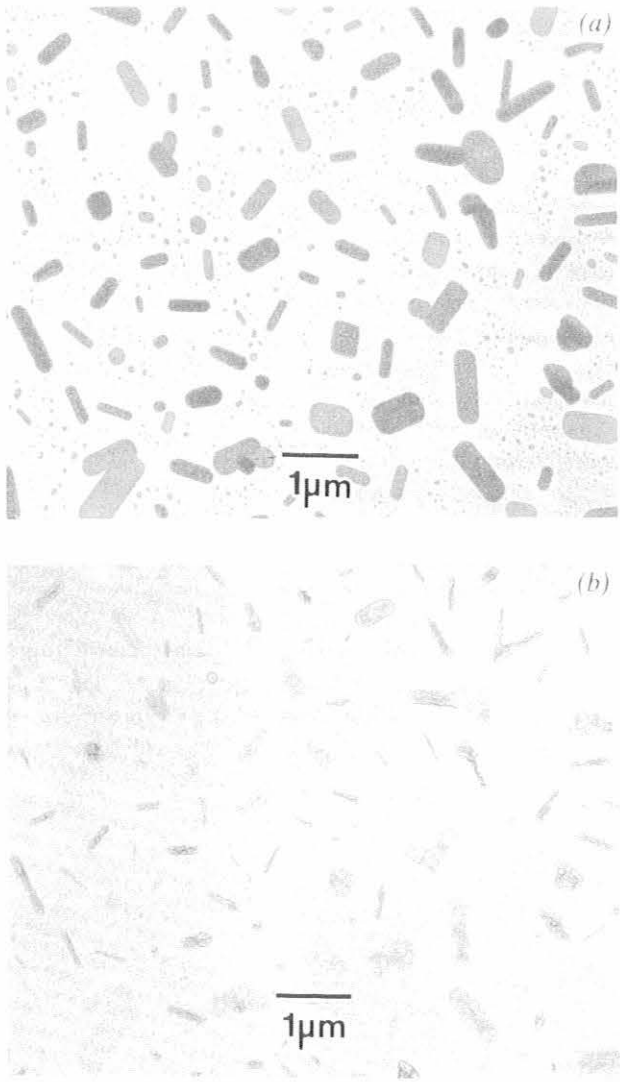

Fig. 6. Sulfate particles from the 0.25 μm ACD stage of sample no. 2. (*a*) before electron beam damage; (*b*) after electron beam has vaporized most of the sulfate. No solid particles that may have acted as condensation nuclei are evident.

as small as ~0.005 μm could be examined. After the sulfate had largely disappeared (Figure 6*b*), it is evident small solid particles were not left behind. This indicates that solid particles > ~0.01 μm were not present and acting as condensation nuclei for the H_2SO_4 droplets, unless they were dissolved by the acid. Since the particles usually showed only S and O as major detectable elemental constituents with no trace elements, the dissolution of solid particles of other compositions is unlikely and is discounted. Our microanalytical observations agree well with the OPC heated inlet data, which indicate that ~95-98% of particles of size r >0.15 μm disappeared after passage through an inlet heated to 150°C, which is hot enough to vaporize aqueous H_2SO_4 [*Deshler et al.*, 1992]. These data suggest that the vast majority of the H_2SO_4 aerosol was formed through homogeneous nucleation processes.

6.1.4. Conclusions

The use of cascade impactors on several balloon flights over Laramie, Wyoming, has permitted us to characterize particles in stratospheric aerosol layers that have been tracked from the eruption of Mt. Pinatubo. In all samples, the volcanic aerosol was composed predominantly (>~98%) of submicrometer H_2SO_4 droplets, which had subsequently changed to $(NH_4)_2SO_4$ during handling. Other types of particles observed in these aerosol samples were supermicrometer sulfate particles and composite sulfate/crustal particles.

The relative particle concentrations determined by microanalysis of the samples were consistent with OPC aerosol concentration data. The samples collected on July 26 and 30 showed 20-30% more fine particles on the 0.25 μm ACD stages than did the August 14 sample. Peak aerosol concentrations for r > 0.15 μm particles during the July flights were 50-100% higher than on the August profile. The increased thickness of the 17 km aerosol layer in August probably lengthened the volcanic aerosol sampling period for sample no. 3 and may have caused the impactor samples to show similar particle loadings.

Detailed inspection of many hundreds of the fine sulfate particles was performed to address the question of whether the H_2SO_4 was formed through homogeneous or heterogeneous nucleation processes. The electron flux to chosen fields of particles was increased to the point where the sulfate vaporized. Over 99% of the fine sulfate particles showed no small, solid particles could have acted as condensation nuclei associated with them. This supports OPC heated inlet data from the flights that indicates 95-98% of the particles of size r > 0.15 μm disappeared after passage through a 150°C inlet. We present these corroborating data as evidence for predominantly homogeneous nucleation of the H_2SO_4 aerosol in the Mt. Pinatubo volcanic cloud.

Acknowledgments. The balloon flights were supported by the National Science Foundation, Atmospheric Chemistry Program. Assistance in balloon operations by T. Deshler, B. Johnson, G. Olson, J. Hereford and L. Womack is gratefully appreciated.

6.2. References

Charlson, R.J., A.H. Vanderpol, D.S. Covert, A.P. Waggoner, and N.C. Ahlquist, $H_2SO_4/(NH_4)_2SO_4$ background aerosol: Optical detection in St. Louis region, *Atmos. Environ. 8*, 1257-1267, 1974.

Deshler, T., D.J. Hofmann, B.J. Johnson, and W.R. Rozier, Balloonborne measurements of the Pinatubo aerosol size distribution and volatility at Laramie, Wyoming, during summer of 1991, *Geophys. Res. Lett. 19*, 199-202, 1992.

Ferek, R.J., A.L. Lazrus, and J.W. Winchester, Electron microscopy of acidic aerosols collected over the northeastern United States, *Atmos. Environ. 17*, 1545-1561, 1983.

Sheridan, P.J., Analytical electron microscope studies of size segregated particles collected during AGASP-II, flights 201-203, *J. Atmos. Chem. 9*, 267-282, 1989.

Sheridan, P.J., R.C. Schnell, J.D. Kahl, J.F. Boatman, and D.M. Garvey, Microanalysis of the aerosol collected over south-central New Mexico during the ALIVE field experiment, May-December 1989, *Atmos. Environ.*, in press, 1992.

Smithsonian Institution, *Bull. Global Volcanism Net., 16(6)*, 2-5, 1991.

7. Cooperative Programs

Antarctic UV Spectroradiometer Monitoring Program: South Pole and Barrow Contrasts in UV Irradiance

C. R. BOOTH, T. LUCAS, J. MORROW, AND T. MASTECHKINA
Biospherical Instruments, San Diego, California 92117

1. INTRODUCTION

The Antarctic Ultraviolet Spectroradiometer Monitoring Network was established by NSF in 1988 in response to predictions of increased UV radiation in the polar regions. The network consists of a number of automated, high resolution spectroradiometers placed in strategic locations in Antarctica and the Arctic (Table 1), and a new operational site in San Diego for training and testing. The network makes essential measurements of UV spectral irradiance and provides a variety of biological dosage calculations of UV exposure. Biospherical Instruments Inc., under contract to Antarctica Support Associates (ASA), directed by NSF is responsible for operating and improving the network and distributing data to the scientific community.

The spectroradiometer system contains an irradiance diffuser, double holographic grating monochromator, photomultiplier tube (PMT), and calibration lamps. Tungsten-halogen and mercury vapor lamps are used for internal calibration of the optical pathway. The monochromator and PMT are located in individual temperature controlled subassemblies. Typically, this assembly is located on a building rooftop, away from obstructions. Only the irradiance collector and auxiliary sensors are located outdoors. The entire instrument is operated under computer control, including regular calibration cycles several times each day.

2. EXAMPLES OF DATA FROM THE AMUNDSEN-SCOTT SOUTH POLE STATION AND FROM BARROW, ALASKA

Most of the concern over ozone depletion has arisen due to the prediction that the resulting high levels of UV would have significant biological impact. The spectral expression of this impact is commonly called the dose weighting or action spectra weighting. Figure 1 shows the DNA damage action spectra as determined by *Setlow* [1974]. The total UV dosage that an organism with a similar spectral susceptibility would receive can be expressed as the integral of the product of the irradiance and dose weighting (Figure 2).

During the austral spring of 1991 at the South Pole, significant ozone depletion existed until mid-November when the ozone levels reported by TOMS (TOMS Update CD-ROM, available from NSSDC, Goddard Space Flight Center, 1992) jumped from 194 DU on day 315 to 392 DU on day 321. UV spectral irradiance measurements selected from these 2 days are shown in Figure 3. For comparison with higher total ozone values (487 DU), data from day 99 (1991) at BRW are also shown. Compared with day 315, the integrated dose at SPO on day 321 had declined from 0.095 to 0.031 mw·cm^2 (assuming the dose weighting is unitless). At the time shown for BRW the dose was roughly half at 0.015 mw·cm^2. The daily dosage at SPO would even be higher relative to BRW if the 24-hour day length was considered.

3. SUMMARY

The establishment of a monitoring network for (UV) radiation has been a crucial part of the United States Antarctic Program. Its purpose is to evaluate the consequences of stratospheric ozone depletion on the health and productivity of Antarctic organisms and personnel. Data products resulting from this network include analyses of various measures of UV, including UV-B, unweighted spectral integrals, and a variety of biologically weighted dosages. This monitoring network supports scientific researchers in polar regions and has provided

TABLE 1. Installation Sites

Site	Latitude	Longitude	Established	Location
McMurdo	77°51'S	166°40E	March 1988	Arrival heights
Palmer	64°46'S	64°03W	May 1988	Clean Air Facility
South Pole	90°00'S	0°	Feb. 1988	Clear Air Facility
Ushuaia, Argentina	54°59'S	68°W	Nov. 1988	CADIC*
Barrow, Alaska	71°18'N	156° 47W	Dec. 1990	UIC-NARL†
San Diego, California	32°47'N	117°14'W	Oct. 1992	Biospherical Instruments Inc.

*Centro Austral de Investigaciones Cientificas, Argentina.
†Ukpeagvik Inupiat Corporation-National Arctic Research Laboratory.

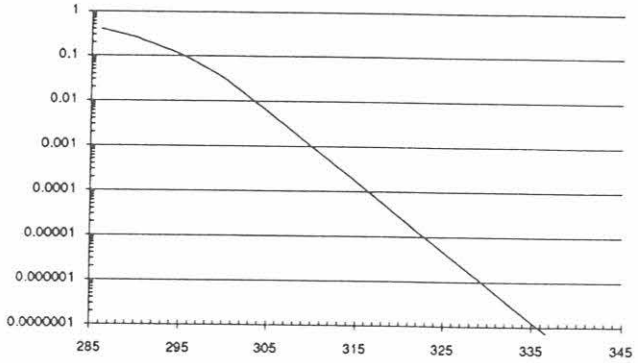

Fig. 1. *Setlow* [1974] DNA dose weighting factor as a function of wavelength in namometers.

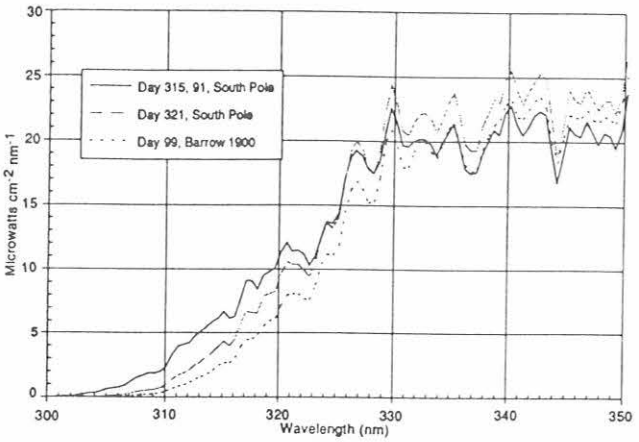

Fig. 2. SPO spectral irradiance for days 315 and 321 of 1991. Day 99 of 1991 from BRW is shown for comparison. All data scans were taken with the sun at a 71° solar zenith angle.

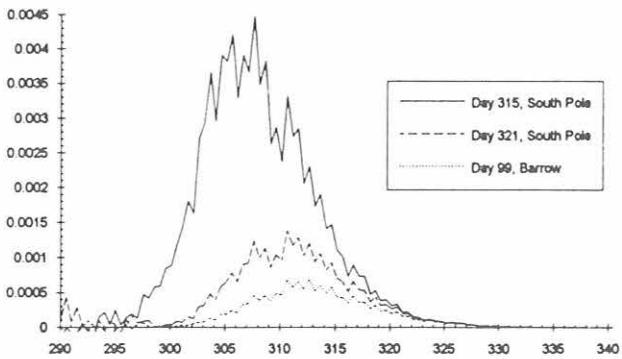

Fig. 3. Product of DNA dose weighting factor [*Setlow*, 1974] and iradiances for BRW and SPO all at a solar-zenith angle of 71°.

independent confirmation of the role of the ozone layer in moderating UV solar irradiance. Over the past 5 years, this network of instruments has provided data for the support of several research programs—the details of which may be found in the following references: *Lubin and Frederick* [1990, 1991, 1992*a,b*], *Lubin et al.* [1989, 1992], *Smith et al.* [1990, 1991, 1992], and *Stamnes et al.* [1990, 1991, 1992].

Data from the NSF UV Spectroradiometer Network is available to all qualified researchers. Data shown in this report are available on CD-ROM, ISO 9660 format. NSF grantees have priority access to these data. For more information, please contact: Dr. Polly Penhale, Division of Polar Programs, National Science Foundation, 1800 G St. N.W., Washington, D.C. 20550, or Biospherical Instruments, 5340 Riley St., San Diego, CA 92110.

Acknowledgments. This research and monitoring activity was funded by contract A1T-M1743 from Antarctic Support Associates under direction of NSF, Division of Polar Programs. B. Mendonca of NOAA/CMDL assisted in providing operators and support for the installations at SPO and BRW. A. Kruger of NASA/GSFC provided TOMS Total Ozone data for comparison purposes. Barrow operators include D. Norton, D. Roghair, L. Suvlu, and NOAA/CMDL personnel D. Endres and C. Churylo. The Ukpeagvik Inupiat Corporation of Barrow provided assistance in the installation. Operators at Palmer and McMurdo have been provided by ASA. Special thanks goes to John Gress of ASA who has been especially instrumental in the operation of the network.

5. References

Lubin, D. and J.E. Frederick, Column ozone measurements at Palmer Station, Antarctica: variations during the austral springs of 1988 and 1989, *J. Geoph. Res., 95*, 13,883-13,889, 1990.

Lubin. D. and J.E. Frederick, The ultraviolet radiation environment of the Antarctic Peninsula: the roles of ozone and cloud cover. *J. Appl. Meteorol., 30*, 478-493, 1991.

Lubin. D., Mitchell, B.G., J.E. Frederick, A.D. Alberts, C.R. Booth, T. Lucas, D. Neuschuler, A contribution toward understanding the biospherical significance of Antarctic ozone depletion, *J. Geophys. Res.*, in press, 1992.

Setlow, R.B., The wavelengths in sunlight effective in producing skin cancer: A theoretical analysis, *Proceedings, Nat.Acad. Sci., 71(9)*, 3363-3366, 1974.

Smith, R.C., Z. Wan, and K.S. Baker, Ozone depletion in Antarctica: Satellite and ground measurements, and modeling under clear-sky conditions, *J. Geophys. Res., 97*, 7383-7397, 1992*a*.

Smith, R.C., B.B. Prezelin, K.S. Baker, R.R. Bidigare, N.P. Boucher, T. Coley, D. Karentz, S. MacIntyre, H. A. Matlick, D. Menzies, M. Ondrusek, Z. Wan, K.J. Waters, Ozone depletion: Ultraviolet radiation and phytoplankton biology in antarctic waters, *Science, 256*, 952-959, 1992*b*.

Stamnes, K., J. Slusser, and M. Boden, Derivation of total ozone abundance and cloud effects from spectral irradiance measurements, *Appl. Optics, 30*, 4418-4426, 1991.

Stamnes, K., J.Z. Jin, J. Slusser, C. Booth, and T. Lucas, Several-fold enhancement of biologically effective ultraviolet radiation levels at McMurdo Station Antarctica during the 1990 ozone hole, *Geophys. Res. Lett.*, in press. 1992.

Stamnes, K., J. Slusser, M. Bowen, C. Booth, and T. Lucas, Biologically effective ultraviolet radiation, total ozone abundance, and cloud optical depth at McMurdo Station, Antarctica, September 15, 1988, through April 15, 1989, *Geophys. Res. Letters, 17*, 2181-2184, 1990.

Observation of Oil Smoke in the Upper Troposphere at Mauna Loa Observatory - a Middle Eastern Source?

THOMAS A. CAHILL, KENT WILKINSON, PAUL WAKABAYASHI, AND ROBERT ELDRED
Air Quality Group, Crocker Nuclear Laboratory University of California, Davis California 95616-8569

WILLIAM MALM
National Park Service, Colorado State University, Fort. Collins, Colorado 80523 USA

Fine particulate measurements of particles 2.5 μm diameter and below have been made at the NOAA Mauna Loa Observatory (MLO) on the island of Hawaii by one module of the Interagency Monitoring of Protected Visual Environments (IMPROVE) fine particulate network since 1988. These data extend other work by UC Davis at MLO begun in 1980 and are extended by a full IMPROVE system at Hawaii Volcanoes National Park, near the Kiluaea Visitor's Center southeast of MLO and at a lower elevation. Measurements at MLO are made both for only at night and for average conditions. The former, keyed to the cleanest winds and representing the upper troposphere at MLO.

The IMPROVE system samples twice per week: Friday 2000 to 0600, Saturday, Sunday, and Monday, and a second sample starting at 2000 Monday to typically 0600 Tuesday, Wednesday, and Thursday, again for nights only.

Samples are collected on 25 mm stretched Teflon filters with a size range below 2.5 micrometers in diameter set by a cyclone. The two filters per week are sent to UC Davis for analysis of mass, optical absorption, particulate hydrogen, and elements sodium and heavier. These protocols are subject to strict quality assurance protocols as required for the IMPROVE network and its equivalent cooperating programs, totaling up to 90 stations at certain periods. Typically, about 85% to 90% of the mass of particles collected on the filter can be ascribed to chemical species by these analyses, and detection limits for many species fall below 0.1 ng m^{-3}.

During the period between January 1 and April 1, 1991, elevated levels of fine particulate matter were observed at MLO. These particles were seen in the clean sector, in the downslope night winds that have been shown to reject local pollution sources from the Hawaiian Islands. Samples from this protocol are used for CO_2 and other species. The composition of the particles indicates a source dominated by fossil fuel combustion, as shown by elevated levels of soot and sulfur, with nickel and other trace species occasionally seen.

Figure 1 shows results from MLO for the period January 1 through March 31, 1991, for sulfur (by PIXE) and soot (by optical absorption). The episodes represent much higher levels of fine particles than evident in prior years. Figure 2 shows the data for fine soils in the same period of January 12, February 20, and March 24.

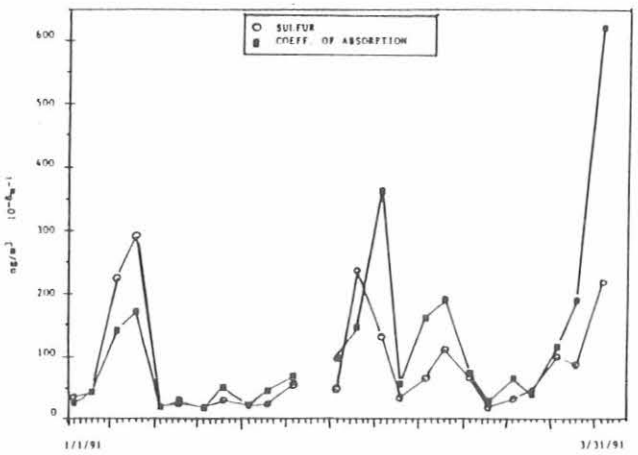

Fig. 1. Sulfur and soot aerosols at MLO, January-March 1991. Each sample integrates 3 or 4 nights, each 8 hours in duration, taken between 2200 and 0600 starting at the day on the graph. The three largest episodes were encountered on January 12, February 20, and March 24 in the winter quarters of 1989-1991.

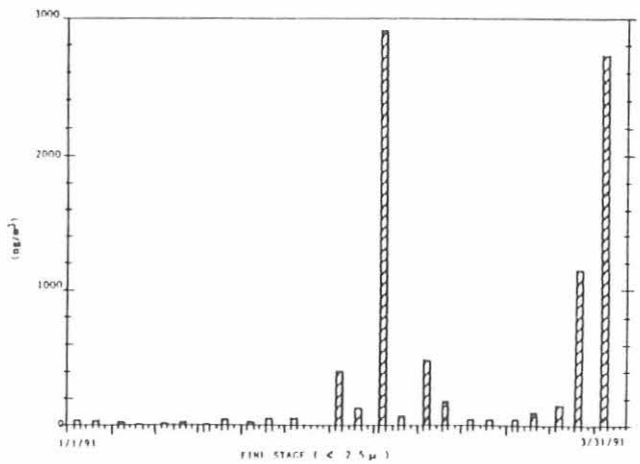

Fig. 2. Fine soils at MLO in the same period as Figure 1. The two episodes of February 20 and March 24 were the highest soil episodes seen in the winter quarters of 1989-1991.

The presence of fine soil-like particles was unexpected until airborne measurements over Kuwait in June showed massive amounts of fine soil in the combustion plume [*Cahill et al.*, 1992]. Two hypotheses can be supported: (1) the particles arise at or near the source area through entrainment of soil into the combustion plume, or (2) that the fine soil was added to the combustion products between the source and MLO. These hypotheses can be resolved through trajectory analyses.

However, the typical Chinese dust incursions that occur each spring also include sulfur, soil, and soot, so that careful analysis is needed to confirm or refute a Kuwaiti origin for some of the episodes seen at MLO. The levels seen each spring in April and May, can be as high as the levels seen in 1991. Again, trajectory analysis is required to help clarify the source of these plumes.

References

Cahill, T.A., K. Wilkinson, and R.C. Schnell, Compositional analyses of size-resolved aerosol samples taken from aircraft downwind of Kuwait, Spring, 1991, *J. Geophys. Res.*, in press, 1992.

Spectral UVB Fluxes: Comparison of MLO and Edgewater, Maryland

DAVID L. CORRELL, CARL O. CLARK, VERNON R. GOODRICH, and DOUGLASS R. HAYES, JR.
Smithsonian Environmental Research Center, P.O. Box 28, Edgewater, Maryland 21037

Our laboratory has been continuously monitoring surface spectral UVB radiation at MLO in a series of eight 5-nm band passes since the fall of 1984. Comparable measurements have been made continuously at Edgewater, Maryland (39°N, 77°W) since the fall of 1975. Measurements are made with precision, accurately calibrated, spectral radiometers [*Goldberg*, 1982; *Correll, et al.*, in press]. Data from the Edgewater site have been analyzed and published through 1990 [*Correll, et al.*, in press]. At present we are conducting a similar analysis of MLO data for future publication. Here we present a direct comparison of UVB fluxes at MLO and Edgewater on clear sky days at two sun angles; secant 1.5 (sun ~48.2° from vertical) and secant 2.5 (sun ~66.4° from vertical). The data were taken in 1989 at both sites and are summarized here as monthly means for various wavelengths. This comparison highlights the effects on UVB fluxes of the lower latitude (19.5°N), higher elevation (3400 m), and lower total column ozone at MLO.

Dobson total column ozone data for MLO and Wallop's Island (Figure 1) were obtained from NOAA ERL, Boulder, Colorado. Mean monthly ozone concentrations peaked for both locations in May and reached a minimum in November at Wallop's Island and in December at MLO. We chose to compare UVB global irradiance data for May and November, except for secant 1.5 data at Edgewater. In that case, we were forced to use October data. Monthly means of clear sky secant 1.5 and secant 2.5 ultraviolet flux data for 300 nm and 320 nm (Figures 2-5) illustrate the patterns. UVB fluxes were much higher at MLO, as expected. MLO fluxes were lowest in April or May and highest January or February, as expected from the ozone concentration patterns. Edgewater fluxes were lowest in the spring, but 300 nm flux was relatively constant with season and 320 nm flux paterns had little correlation to the ozone concentration pattern. The ratio of 300 nm to 320 nm flux for secant 1.5 and 2.5 (Figures 6-7) illustrates how much more biologically effective short wavelength

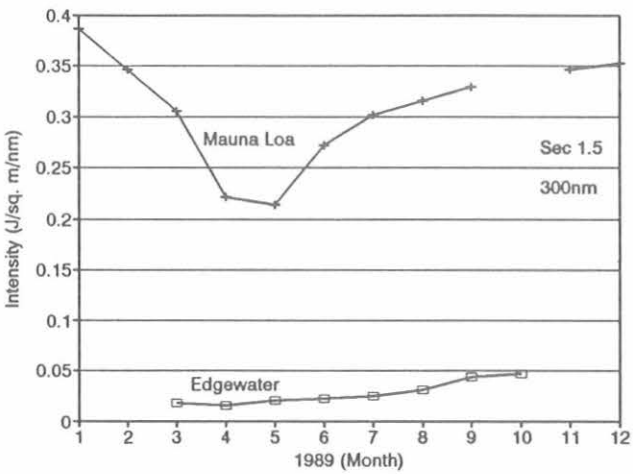

Fig. 2. Mean monthly 300 nm irradiance for clear sky days at secant 1.5.

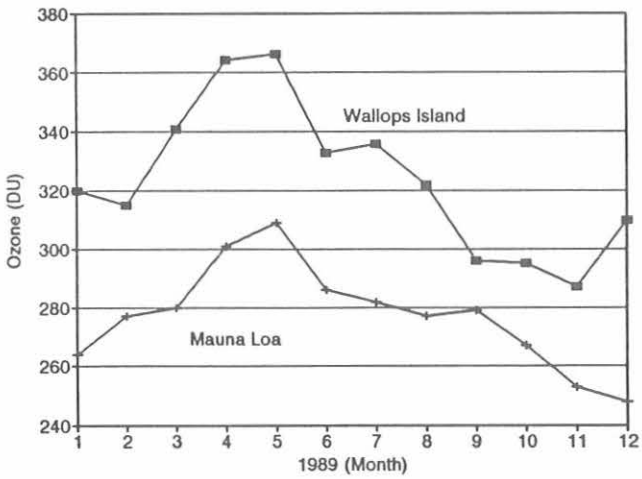

Fig. 1. Mean monthly total column ozone in Dobson units from NOAA network.

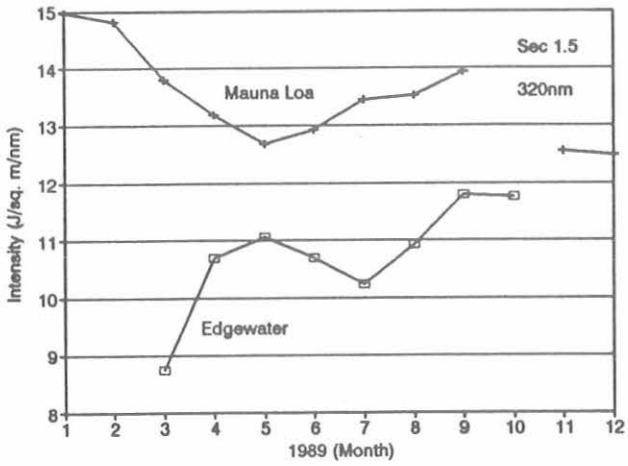

Fig. 3. Mean monthly 320 nm irradiance for clear sky days at secant 1.5.

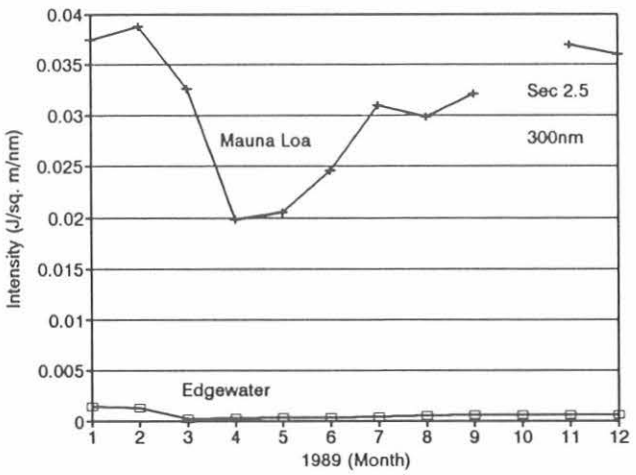

Fig. 4. Mean monthly 300 nm irradiance for clear sky days at secant 2.5.

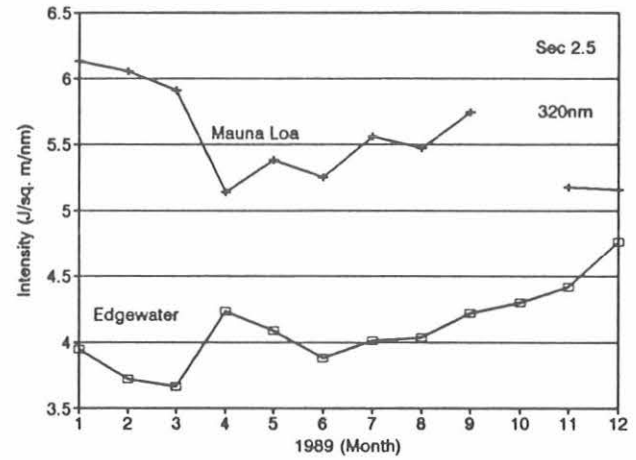

Fig. 5. Mean monthly 320 nm irradiance for clear sky days at secant 2.5.

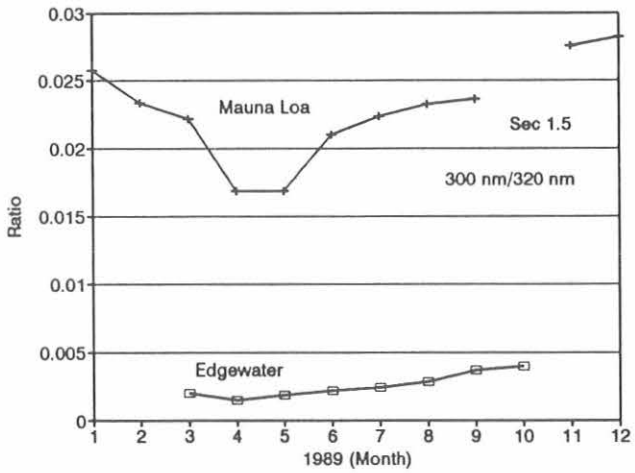

Fig. 6. Ratio of 300 nm to 320 nm irradiance for clear sky days at secant 1.5.

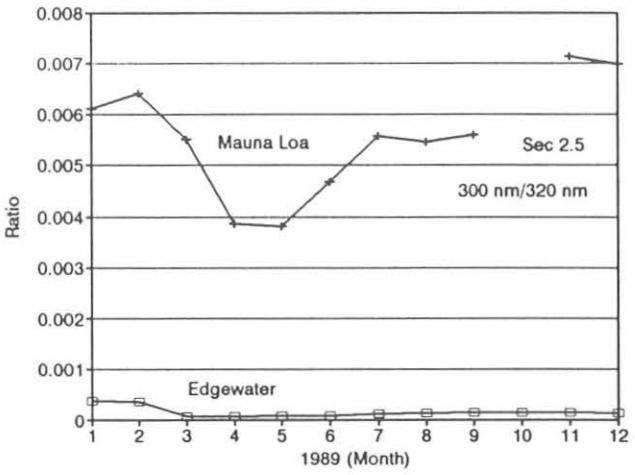

Fig. 7. Ratio of 300 nm to 320 nm irradiance for clear sky days at secant 2.5.

TABLE 1. Ratios of Clear-Sky Ultraviolet Flux (MLO/Edgewater)

	Nominal Spectral Band				
	300 nm	305 nm	310 nm	315 nm	320 nm
			Z = 1.5		
May	10.3	1.48	1.23	0.94	1.15
Fall	7.38	1.35	1.14	0.88	1.07
			Z = 2.5		
May	57.9	5.19	1.62	1.06	1.32
Fall	59.4	4.10	1.57	1.03	1.17

TABLE 2. Ratios of Clear Sky Ultraviolet Flux (Fall/May)

	Nominal Spectral Band				
	300 nm	305 nm	310 nm	315 nm	320 nm
			MLO		
Z = 1.5	1.62	1.36	1.16	1.06	0.99
Z = 2.5	1.80	1.48	1.20	1.06	0.96
			Edgewater		
Z = 1.5	2.72	1.50	1.25	1.12	1.06
Z = 2.5	1.76	1.87	1.24	1.09	1.08

radiation at all times of year was observed at MLO than at Edgwater. The ratios of UVB radiation at MLO to those at Edgewater (Table 1) were higher for secant 2.5 data and increased from longer to shorter wavelengths. Thus, the secant 1.5 300 nm flux was 10 times higher at MLO in the

spring, and the secant 2.5 300 nm flux was 58 times higher at MLO. Ratios of UVB radiation in the fall to those in May increased from near one at the longer wavelengths to about two at 300 nm (Table 2). Thus, the flux of the biologically most effective wavelengths was more variable both seasonally and between sites.

REFERENCES

Correll, D.L., C.O. Clark, B. Goldberg, V.R. Goodrich, D.R. Hayes, Jr., W.H. Klein, and W.D. Schecher, Spectral ultraviolet-B radiation fluxes at the Earth's surface: Long-term variations at 39°N, 77°W, *J. Geophys. Res.*, in press, 1992.

Goldberg, B., Radiometric measurements in the UV-B region of daylight, in *The Role of Solar Ultraviolet Radiation in Marine Ecosystems*, edited by J. Calkins, pp. 121-129, Plenum, New York, 1982.

Ground-Based Measurement of DMS in the Arctic Atmosphere at Barrow During Summer 1991

RONALD J. FEREK AND JOHN HERRING
University of Washington, Department of Atmospheric Sciences, Seattle, Washington 98195

During June 1990 the University of Washington conducted a series of airborne research flights over the Arctic Ocean north of Barrow. One goal of the project was to measure DMS and SO_2 in the summertime arctic atmosphere. While DMS concentrations were generally found to be in the range 20-50 pptv in the marine boundary layer, on several occasions they exceeded 200 pptv, some of the highest concentrations we have ever measured. At that time we questioned whether such high concentrations were the result of transport from more biologically productive regions or if they were due to blooms of phytoplankton in local arctic waters.

In order to address the question of the magnitude of local emissions, we asked the staff of the CMDL Monitoring Station at Barrow (BRW) to collect periodic DMS and SO_2 samples during the summer of 1991. Under conditions favoring airflow from the clean sector (NE of the station) we hoped to collect approximately two samples per week between June and September, bracketing the period of open water along the north coast of Alaska.

DMS was collected via preconcentration on gold wool [*Andreae et al.*, 1985] with subsequent analysis by GC/FPD in our laboratory at the University of Washington. SO_2 was collected on carbonate-impregnated filters with analysis by ion -chromatography [*Ferek et al.*, 1991]. Typically, SO_2 filters were exposed for 2 hours at a flow rate of about 150 Lpm, and two gold tubes were exposed to 2 Lpm for 10 minutes each at the beginning and end of each sampling period. A total of 16 filters and 32 gold tubes were collected between May 31 and October 22, 1991. Because of the relatively infrequent occurrence of flow from the clean sector, sampling frequency was somewhat less than the two per week originally planned. In addition, the occasional long delays involved with shipping fresh filters to BRW, waiting for good sampling conditions, and return shipment to the lab for analysis caused a number of the SO_2 filters to exceed their useful shelf life of approximately 2 weeks. As a result, blank values became excessive and, since the concentrations of SO_2 were generally very low, a number of filter samples produced no useful data (primarily those exposed later in the program). The DMS samples were not affected by long storage time and produced useful results.

Table 1 lists the measured DMS concentrations and SO_2 concentrations from those filters that provided reliable measurements. In general, the few SO_2 measurements indicated very low concentrations in air flowing off the Arctic Ocean. DMS concentrations generally showed low values early in the summer (with the exception of the May 31 samples), peak values in August, and low values again in the fall. While more data points would have been desirable, these data do indicate a seasonal trend in DMS emissions that are probably due to phytoplankton activity in local arctic waters. We note also that the peak concentrations were observed in August, the same month in which an annual peak in CN concentrations were observed at Barrow [*Bodhaine*, 1989]. This may indicate a natural source for much of the summertime CN in the arctic atmosphere.

TABLE 1. DMS and SO_2 Concentrations Measured at Barrow, Alaska, During Summer 1991

Date	Start Times	DMS, pptv	SO_2, pptv
May 31	1139, 1316	32, 44	
June 7	1700, 1849	3, 3	2.8
June 13	2130, 2323	5, 9	10.
June 14	1945, 2155	<1, <1	29.
July 5	1125, 1430	22, 17	11.
July 29	1511, 1717	15, 19	6.0
August 2	1445, 1702	24, 27	13.
August 12	0906, 1048	40, 41	
August 15	0913, 1113	98, 83	
August 22	1439, 1625	44, 35	
August 24	1100, 1350	33, 17	
September 10			
September 23			
October 9	1038, 1230	6, 7	
October 16	1011, 1211	10, 6	
October 25	1052, 1257	13, 3	

REFERENCES

Andreae, M.O., R.J. Ferek, F. Bermond, K.P. Byrd, R.T. Engstrom, S. Hardin, P.D. Houmere, F. LeMarrec, H. Raemdonck and R.B. Chatfield, Dimethylsulfide in the marine atmosphere. *J. Geophys. Res., 90* 12,891-12,900, 1985.

Bodhaine, B.A., Barrow surface aerosol: 1976-1986, *Atmos. Environ., 23*, 2357-2369, 1989.

Ferek, R.J., D.A. Hegg, J.A. Herring, and P.V. Hobbs, An improved filter pack technique for airborne measurement at low concentrations of SO_2, *J. Geophys. Res., 96*, 22,373-22,378, 1991.

South Pole Lidar

G. Fiocco, M. Cacciani, P. Di Girolamo, A. di Sarra, and D. Fuà
Universita "La Sapienza" 00185 Roma, Italy

The lidar built by the group of the University of Rome "La Sapienza" was installed in the Clean Air Facility at Amundsen-Scott South Pole Station in the austral summer of 1987. During following winter seasons the system was operated by CMDL winterovers, with the support of personnel from the University of Chicago (1990) and ASA (1991 and 1992). A relatively high quantity of data was obtained during the 1988, 1990, and 1991 campaigns. At this time the lidar is running satisfactorily. The observations have been directed mainly to studying Polar Stratospheric Clouds (PSCs), their evolution, and characteristics.

The experimental setup and the results obtained by the analyses of the 1988 data were described in the *CMDL Summary Report 1990* [*Ferguson and Rosson*, 1991] and in *Fiocco et al.* [1989, 1991, 1992], and *Fuà* [1992]. The system operation during 1990 and 1991 was sufficiently continuous to observe the seasonal evolution of the PSCs.

The first presence of cloud layers in the stratosphere is usually noticed at the end of May at about 20 km altitude where the temperature reaches the threshold for the condensation of the Nitric Acid Trihydrate (NAT). The Type I PSCs formed by the NAT are present until the end of October. When the stratospheric temperature drops below the threshold for the condensation of the water vapor (around the middle of June), sharp stratifications identified as Type II clouds (ice) appear in the lidar echoes, superimposed on the Type I PSCs. In June, July, and August the Type II PSCs have been observed from 9 km up to 25 km altitude. Type II clouds disappear at the beginning of September when everywhere in the stratosphere the temperature is above 190 °K.

In 1991 the aerosol content of the stratosphere was enhanced following the eruptions of Mt. Pinatubo in June and of Mt. Hudson in September. The Mt. Pinatubo eruption was much stronger than the Mt. Hudson eruption, causing a global perturbation of the stratosphere; but Mt. Hudson is closer to the Antarctic continent and could have influenced this region also.

Aerosol layers observed at SPO since the middle of October at altitudes where the relatively high temperatures would not allow for the formation of the PSCs, can be attributed to the arrival of the volcanic aerosol in the antarctic stratosphere after the breakdown of the polar vortex. Figure 1 is an example of a typical vertical profile of the backscattering ratio obtained by lidar measurements

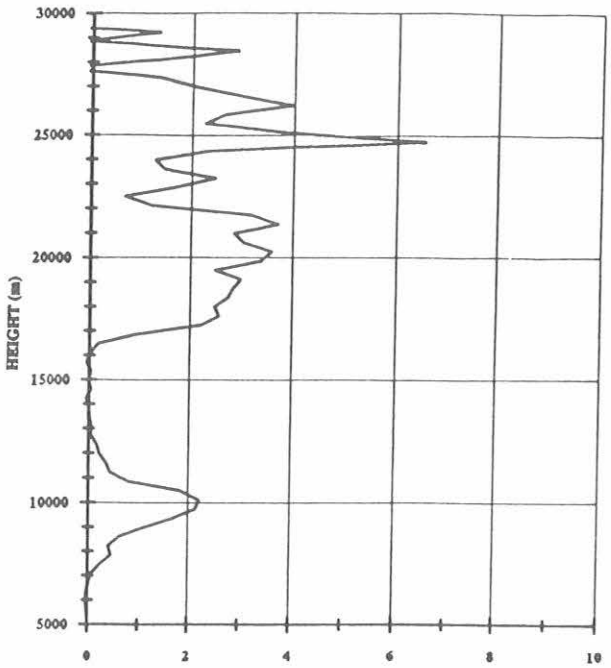

Fig. 1 Lidar backscattering ratio obtained on December 8, 1991.

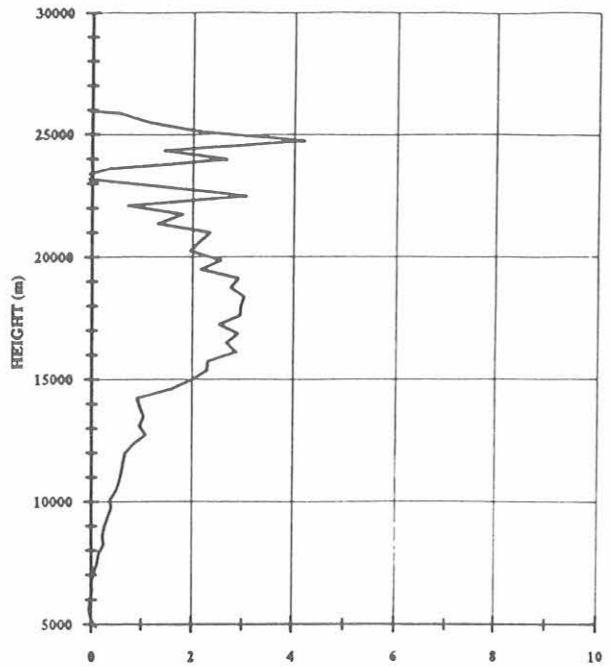

Fig. 2 Lidar backscattering ratio obtained on March 22, 1992.

at the beginning of December. Two distinct layers are present: a lower one centered around 10 km altitude and a higher and thicker one, with a bifurcated structure extending between 14 and 28 km.

The evolution of the aerosol layers was observed throughout the summer of 1991; the lower layer slowly disappeared and the peak of the upper layer shifted down to approximately 17 km. A typical profile at the beginning of autumn is shown in Figure 2.

REFERENCES

Ferguson, E.E., and R.M Rosson (Eds.) *Climate Monitoring and Diagnosics Laboratory No. 19: Summary Report 1990*, 133 pp., NOAA Climate Monitoring and Diagnostics Laboratory, Boulder, CO, 1991.

Fiocco, G., W. Komhyr, and D. Fuà, Is ozone destroyed during the Antarctic polar night in the presence of polar stratospheric clouds? *Nature, 341*, 426427, 1989.

Fiocco, G., D. Fuà, M. Cacciani, and P. DiGirolamo, On the temperature dependence of polar stratospheric clouds, *Geophys. Res. Lett., 18*, 424-427, 1991.

Fiocco, G., D. Fuà, M. Cacciani, P. Di Girolamo,and J. DeLuisi, Stratospheric clouds at South Pole during winter 1988: 1. Results of the lidar observations and their relatioship to temperature, *J. Geopys. Res.*, submitted, 1992.

Fuà, D., M. Cacciani, P. DiGirolamo, G. Fiocco, and A. deSarra, Stratospheric clouds at South Pole during winter 1988: 2. Their evolution in relation to atmospheric structure and composition, *J. Geophys. Res.*, submitted, 1992.

Multiple Scattering Effects on Multiple Field of View Sunphotometry

PAUL F. HEIN, JOHN M. DAVIS, AND STEPHEN K. COX
Department of Atmospheric Science, Colorado State University, Fort Collins, Colorado 80523

1. INTRODUCTION

The MFOV (Multiple Field Of View) sunphotometer has been deployed at MLO for several years. The instrument consists of five silicon photodiodes mounted in coaxially aligned collimating tubes that limit the respective full angle fields of view to 2, 5, 10, 20 and 28°; see *Raschke and Cox* [1983]. The MFOV was designed to estimate the optical thickness of thin clouds ($1 < \tau < 5$) by comparing the measured increase in the signal at the larger fields of view with modeled results of the same as a function of optical thickness. Since the instrument was designed for determination of cloud optical thickness, it is somewhat limited in application to aerosol studies such as the Pinatubo cloud whose optical thickness is much less than one. These constraints result primarily from a broad spectral bandpass (0.4 to 1.1 μm) which does not exclude the effects of water vapor absorption on derived optical thicknesses. A monochromatic theoretical analysis, however, lends itself quite naturally to application in the regime of smaller optical thicknesses. In particular, the contribution of multiple scattering at various fields of view and for different zenith angles is of interest since rather large errors in derived optical thicknesses will result if scattering effects are ignored.

2. BACKGROUND

The determination of aerosol optical thickness is at first glance an elegantly simple procedure in which monochromatic measurements of the transmittance of direct solar radiation are used to make the estimate. For a detector that produces an output voltage V, that is linear in its response to the transmitted monochromatic solar intensity, the simple Beer's law relation gives;

$$V = V_0 e^{-m\tau}$$

where m is the airmass (for all the results here m is $sec\ \theta$, where θ is the solar zenith angle), and V_0 is the detector voltage extrapolated to a condition of zero optical depth. Taking the natural log of this relation produces the simple result used in the Langley plots in which the optical thickness is the slope of a straight line relating $ln(V)$ and m. The assumptions here are that the optical thickness does not change during the period of observation and that the only contribution to the signal is the transmitted or unscattered radiation. The following paragraphs use modeling results to address possible errors that may be incurred in making the latter assumption.

3. MODELING DESCRIPTION AND RESULTS

The values presented here were produced using a Monte Carlo radiative transfer model *Davis et al.* [1979], which is a forward walk simulation accounting for the effects of multiple Rayleigh, Mie (by aerosol and/or water clouds) and surface scattering events and water vapor and aerosol absorptions. Measurements are simulated for each of the fields of view of the MFOV. In order to replicate the manner in which aerosol studies are conducted, monochromatic measurements at 0.55 m were simulated thus excluding water vapor absorption. The single particle scattering albedo of 0.85532 and a single scattering phase function thought to typify a fresh volcanic cloud adopted from the LOWTRAN7 code, *Kneizys et al.* [1988].

Simulations were carried out for several optical thicknesses, starting with a clear Rayleigh sky (τ = 0.0694) and in increments of 0.03 up to τ = 0.3694. For each optical thickness, the solar zenith angle was varied from 0° to 75° in increments of 15°, although the 75° results are not included here due to concerns about the effects of spherical geometry which are not included in this model. A Lambertian surface reflectance of 0.10 was used in all cases.

The initial results for a Rayleigh atmosphere are presented in tabular form since the Langley plot is less than revealing.

Table 1 shows the transmittances calculated for each field of view and from the direct component for each zenith angle. In the bottom row the derived optical depth for the simulated transmittances are displayed. The optical depth

TABLE 1. Modeled Transmittances as a Function of Field of View and Solar Zenith Angle

θ	28°	20°	10°	5°	2°	Direct
	Transmittances					
0°	0.934	0.933	0.933	0.933	0.932.	0.932
15°	0.934	0.933	0.932	0.932	0.932	0.930
30°	0.929	0.928	0.928	0.927	0.927	0.922
45°	0.918	0.917	0.916	0.916	0.916	0.906
60°	0.893	0.892	0.891	0.890	0.890	0.870
τ	0.0479	0.0487	0.0493	0.0496	0.0496	0.0696

*Shown in the last row is the optical depth determined from a Langley plot of these data.

as determined by the input parameters to the model was 0.0694.

As can be seen even for the thin Rayleigh atmosphere, there is an influence, due to scattering, which reduces the derived optical depth even for the 2° fov. These effects become evident at solar zenith angles of 30° or greater. It is noted that there is some bias toward higher transmittances at small zenith angles (the 0° direct result is too high by about 0.1%) and, based on an partial error analysis, the transmittance results are judged to have a precision of less than a few tenths of a percent.

An interesting aspect of the results is that it can be argued that the changes in transmittance between the direct beam only and the 2° fov are all at or below typical instrumentation errors. It should be noted that these results were derived from results at only a few zenith angles and that no results are shown for the larger zenith angles at which data for Langley plots are normally taken. Either of these alternatives may well alter the results in Table 1. For example, the results do not show the effects of scattering on optical depths derived from hundreds of transmittance measurements at airmasses between 2.0 and 6.0 as in commonly done in practice.

Results for the fresh volcanic aerosol show a similar pattern and are summarized in Figure 1. Plotted is the absolute error in the optical depth as derived from a Langley plot as a function of optical depth and for the various fields of view. Although the 28° line is an exaggeration of any operational procedure, the 10° fov is typical of the NIPs commonly in use. Note that there is a significant error, even in the 2° fov. The variation in the direct component is an indication of the precision of the model's calculation. As can be seen by these results, the contribution by scattering must be accounted for when using the Langley method, especially in this zenith angle regime.

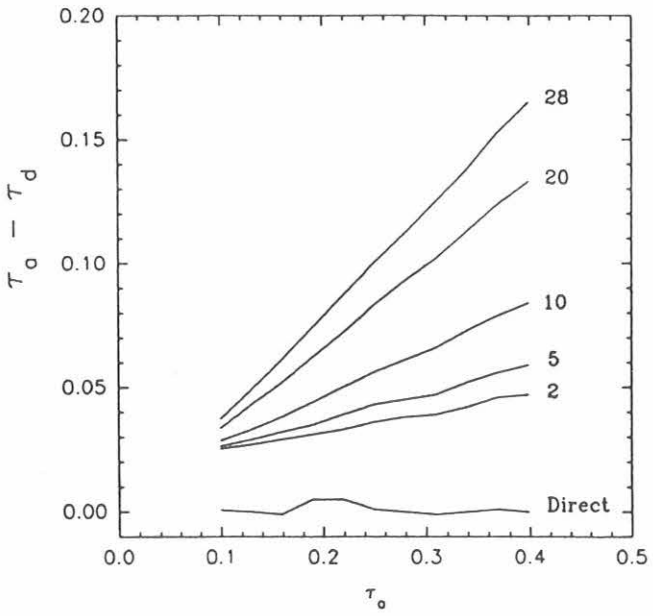

Fig. 1. Magnitude of the error in optical thickness derived from standard Langley plots due to scattering.

4. Further Discussion

The modeling results in Section 3 were limited to solar zenith angles smaller than 60° in order to avoid the effects of the curvature of the earth's atmosphere. In addition to the results above, errors in optical depth derived from individual transmittances also show increases at larger zenith angles. For the sake of brevity, it is simply noted that at 60° solar zenith, the error in optical thickness derived from individual transmittance measurements approaches 15% for a 10° fov for almost all cases studied. On an encouraging note, Table 2 displays transmittances for = 0.3394. In the bottom portion of the table the values of

$$\ln\frac{T_2}{T_1}/\left[\sec(\theta_1)-\sec(\theta_2)\right]$$

are shown, where T is transmittance and the subscripts increment on values of solar zenith angle. These numbers represent a simple two-point approximation to the Langley process.

Although the results are "noisy" and the errors in derived optical depth are still evident, the values improve slightly when simulations at larger solar zenith are used. It may be that the effects of scattering become more constant at the larger solar zenith angles and the effects cancel when

TABLE 2. Transmittances for τ = 0.3394 and Two-Point Langley Calculations of the Simulated Optical Thickness, as a Function of Field of View and Solar Zenith Angle θ

θ	28°	20°	10°	5°	2°	Direct
			Transmittances			
0°	.7842	.7637	.7345	.7203	.7137	.7121
15°	.7792	.7582	.7280	.7134	.7066	.7028
30°	.7616	.7389	.7061	.6904	.6830	.6749
45°	.7221	.6961	.6580	.6399	.6315	.6176
60°	.6420	.6097	.5630	.5408	.5306	.5070
			Two-Point Optical Depths			
0-15°	0.1812	0.2048	0.2518	0.2727	0.2832	0.3724
15-30°	0.1913	0.2160	0.2558	0.2745	0.2845	0.3393
30-45°	0.2052	0.2299	0.2719	0.2927	0.3021	0.3419
45-60°	0.2007	0.2262	0.2662	0.2872	0.2972	0.3369

calculating the slope of the curve. This effect is even more pronounced at smaller optical thicknesses. Thus it may be that by utilizing data for $\theta > 60°$, more accurate results would be obtained. Confirmation of this behavior must be made using a multiple scattering, spherical geometry model.

5. Summary

Simulations of measurements for the MFOV were made using a forward walk Monte Carlo model for conditions of pristine atmosphere and fresh volcanic aerosol. For the range and limited number of zenith angles examined, it was found that the Langley plot method resulted in significant errors in derived optical thickness. Errors increased with increasing field of view and optical thickness. A preliminary check on the trend of the slopes indicated that there is some improvement at larger zenith angles; however, a modeling effort that accounts for the atmosphere spherical geometry is needed for more conclusive results.

6. References

Kneizys, F. X., E. P. Shettle, L. W. Abreu, J. H. Chetwynd, G. P. Anderson, W. O. Gallery, J. E. A. Selby, and S. A. Clough, *Users Guide to LOWTRAN7*, Environmental Research Papers, No. 1010, U.S. Air Force Geophysics Laboratory, Hanscom AFB, MA, 1988.

Raschke, R. A., and S.K. Cox, Instrumentation and technique for deducing cloud optical depth, *J. Climate and Appl. Meteorology*, *22*, 1887-1893, 1983.

Tropospheric Temperature Trends in the Arctic: 1958-1986

JONATHAN D. KAHL
Department of Geosciences, University of Wisconsin-Milwaukee, Milwaukee, Wisconsin 53201

ROBERT S. STONE, MARK C. SERREZE, SPENCER SHIOTANI
CIRES, University of Colorado, Boulder, Colorado 80309

RUSSELL C. SCHNELL
Mauna Loa Observatory, NOAA/CMDL, Hilo, Hawaii 96721

INTRODUCTION

Theoretical studies have shown that the climatic impacts of increasing CO_2 concentrations may be greatest at high latitudes (e.g. *Schlesinger*, 1988). Efforts at detecting climate change in the Arctic, and hence verifying model predictions, have focused on terrestrial surface temperature trends. As predicted by theory, observed surface warming trends in the Arctic have been found to be more rapid and of greater magnitude than those at lower latitudes [*Kelly et al.*, 1982].

Analysis of temperature trends above the surface has been limited to sounding data at eight or ten Arctic stations [*Karoly*, 1989; *Angell*, 1986; *Angell and Korshover*, 1983]. In this paper we summarize an analysis of tropospheric temperature trends in the Arctic during the period 1958-1986. This study differs from previous studies in that (1) we utilize upper-air measurements at all routinely-reporting Arctic stations, and (2) we examine temperature trends in several tropospheric layers. Our results are intended both to describe the trends in Arctic tropospheric temperatures, and to provide verification data for model simulations of Arctic and global climate.

DATA AND PROCEDURES

The data base used is the Historical Arctic Rawinsonde Archive, described by *Kahl et al.* (1992*a*). The archive contains over 1.2 million rawinsonde ascents from fixed-position stations north of 65°N. The record begins in 1958 for most stations, and extends to 1986. A similar archive of rawinsonde observations made from Russian drifting ice platforms in the Arctic Ocean is currently being assembled by the authors.

Mean virtual temperatures were computed for four layers in each sounding: 850-700 hPa, 700-500 hPa, 500-400 hPa and 400-300 hPa. Temperatures in each layer were analyzed by season, resulting in 16 time series for approximately 50 stations. Trends were determined by linear regression. Further details regarding analysis procedures are provided by *Kahl et al.* (1992*b*).

RESULTS AND DISCUSSION

Figure 1 shows temperature trends for the 850-700 hPa layer during winter. The numbers give the trends in units of °C 30 yr^{-1}, plotted at the corresponding station location. Positive trends are enclosed by circles to indicate warming; negative trends are enclosed by squares to indicate cooling. Circles or squares drawn with bold outlines indicate statistical significance at the 90% confidence level as determined by the t-statistic. Trend results for all layers

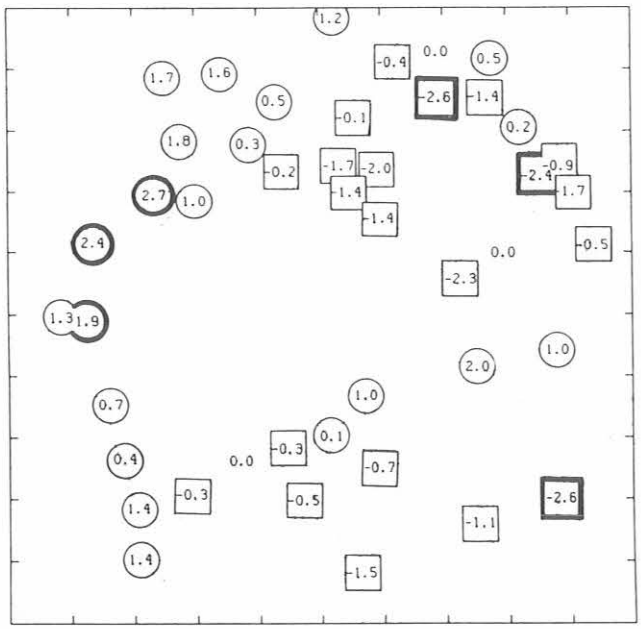

Fig. 1. Winter temperature trends for the 850-700 hPa layer, in units of °C 30 yr^{-1}, plotted at the corresponding station location. Trend values enclosed by circles indicate warming; values enclosed by squares indicate cooling. Circles or squares drawn with bold outlines indicate statistical significance at the 90% confidence level.

Table 1. Summary of Temperature Trend Results by Layer, Season and Quadrant

Layer (hPa)	E. Eurasia (90°E — 180°E)	W. Eurasia (0°E — 90°E)	W. North America (90°W — 180°W)	E. North America/Greenland (0°W — 90°W)
		Winter		
850 - 700	Warming	Cooling	Warming	?
700 - 500	Warming	Cooling	Cooling	?
500 - 400	?	Cooling	Cooling	Cooling
400 - 300	?	Cooling	Cooling	Cooling
		Spring		
850 - 700	Cooling	Warming	Warming	?
700 - 500	Cooling	Warming	Cooling	?
500 - 400	Cooling	Warming	Cooling	?
400 - 300	Cooling	Warming	Cooling	Warming
		Summer		
850 - 700	?	Warming	Cooling	Cooling
700 - 500	?	?	Cooling	?
500 - 400	?	?	Cooling	Cooling
400 - 300	Cooling	?	?	Cooling
		Autumn		
850 - 700	Warming*	Warming	Warming	?
700 - 500	Warming*	Warming	Warming	?
500 - 400	?*	Warming	Warming	Cooling
400 - 300	Cooling*	?	Cooling	Cooling

"Warming" and "cooling" indicate predominantly positive and negative trends, respectively. Question marks indicate the presence of both warming and cooling trends.

*Few trend values available.

and seasons are summarized in Table 1. Principal results are as follows:

(1) Absolute trends were as large as 7°C 30 yr^{-1}, with both cooling and warming tendencies observed in all layers.

(2) The majority of the temperature trends are not statistically significant at the 90% confidence level. Because many modeling studies agree that the possible climatic impacts of increasing CO_2 concentrations may be greatest at high latitudes, we thus conclude that the greenhouse-induced global warming "signal" in the Arctic, if present, is not yet detectable above the "noise" of natural variability, at least for the 1958-1986 period.

(3) There is considerable regional variability in the sign and magnitude of the temperature trends. Winter trends in the 850-700 hPa layer, which according to theory should be positive and large, are negative over western Eurasia and eastern North America and Greenland; and positive over eastern Eurasia and western North America.

(4) The trends vary strongly by season.

(5) Temperature trends at many stations in Eurasia and parts of Greenland are strongly sensitive to positive anomalies contained in the portion of the data archive covering the period 1958-1963 [see *Kahl et al.*, 1992*b*). Warming trends computed without these data become cooling trends when these early data are included. The present analysis is unable to conclusively determine whether the period 1958-1963 was in fact anomalously warm in Eurasia and Greenland.

Acknowledgements. This research was sponsored by the NOAA Climate and Global Change Program (contract NA90AA-D-AC794), the National Science Foundation (contract DPP-8822472), and the Electric Power Research Institute (contract

RP2333-07). It was conducted as part of the US-USSR Joint Committee on Cooperation in Environmental Protection, the Influence of Environmental Change on Climate (Working Group VIII). We thank Dr. Jim Angell, NOAA/ARL, for his helpful suggestions.

REFERENCES

Angell, J.K., Annual and seasonal global temperature changes in the troposphere and low stratosphere, 1960-1985, *Mon. Wea. Rev., 114*, 1922-1930, 1986.

Angell, J.K., and J. Korshover, Global temperature variations in the troposphere and stratosphere, 1958-1982, *Mon. Wea. Rev., 111*, 901-921, 1983.

Kahl, J.D., M.C. Serreze, S. Shiotani, S.M. Skony, and R.C. Schnell, In-situ meteorological sounding archives for Arctic studies, *Bull. Amer. Meteorol. Soc.*, in press, 1992*a*.

Kahl, J.D., M.C. Serreze, R.S. Stone, S. Shiotani, and R.C. Schnell, Tropospheric temperature trends in the Arctic: 1958-1986, *J. Geophys. Res.*, submitted, 1992*b*.

Karoly, D.J., Northern hemisphere temperature trends: A possible greenhouse gas effect? *Geophys. Res. Lett., 16*, 465-468, 1989.

Kelly, P.M., P.D. Jones, C.B. Sear, B.S.G. Cherry, and R.K. Tavakol, Variations in surface air temperatures: Part 2. Arctic regions, 1881-1980. *Mon. Wea. Rev., 110*, 71-83, 1982.

Schlesinger, M.E. (Ed.), Physically-Based Modelling and Simulation of Climate and Climatic Change, NATO ASI Series C, Vol. 243, Kluwer Academic, 1084 pp. 1988.

Variations in Atmospheric Molecular Oxygen at Mauna Loa

RALPH F. KEELING AND STEPHEN R. SHERTZ
National Center for Atmospheric Research, Boulder Colorado 80307

1. INTRODUCTION

In 1991 we began making measurements of atmospheric O_2 from air samples collected at the Mauna Loa Observatory (MLO). These samples augment our program that now includes regular sampling at several additional sites including Alert, Canada (82.5°N, 62.3°W), La Jolla, California (32.9°N, 117.3°W), and Cape Grim, Tasmania (40.7°S, 114.7°E).

Measurements of variations in atmospheric O_2 at the parts-per-million level can address several important issues pertaining to the global carbon cycle: (1) the magnitude of new production of organic matter in surface waters over expanses of the ocean where direct, in situ, observations are lacking, (2) the magnitude of any terrestrial carbon sink at northern latitudes, and (3) the relative importance of terrestrial ecosystems versus the oceans as a sink for anthropogenic CO_2 [*Keeling et al.*, 1992]. An improved understanding of these issues will be valuable for making more accurate forecasts of global climatic and biogeochemical changes in the decades ahead.

2. METHODS

We measure oxygen concentrations using a new interferometric technique [*Keeling*, 1988*a*, *b*). We choose to express changes in the O_2 in terms of relative changes in the O_2/N_2 ratio

$$\delta(O_2/N_2) = \frac{(O_2/N_2)_{sample}}{(O_2/N_2)_{reference}} - 1$$

We propose the convention of multiplying $\delta(O_2/N_2)$ by 10^6 and expressing the result in units of "per meg." In these units 1/0.2095 = 4.8 per meg is equivalent to 1 ppmV because O_2 comprises 20.95% of air by volume.

Our procedures for collecting and analyzing air samples were designed to minimize the effects of both heterogenous (surfaces) and homogenous (gas phase) fractionation of O_2 and N_2: air samples are only exposed to surfaces that have been well conditioned to dry air at the same pressure; we avoid exposing air samples to pressure changes except under conditions of steady flow.

Air samples are collected in 5-L glass flasks that are equipped with a pair of stopcocks so that they can be flushed through with sample air. The stopcocks have glass bores and Viton O-ring seats. The flasks are flushed at above ambient pressure using a pumping module that contains a small diaphragm compressor. Pressure control in the flasks is achieved by venting the air leaving the flasks through a backpressure regulator that is adjusted to achieve one atmosphere absolute pressure in the flasks. A bypass line is provided that allows the air to bypass the flasks and pass directly to the back-pressure regulator. The bypass line is opened just prior to closing off the flasks in order to eliminate pressure surges. Flasks are purged indoors in order to reduce any possible thermal gradients around the flasks that might corrupt the O_2/N_2 ratio as a result of thermal diffusive fractionation. The air is drawn from the 125-ft tower through a polyethylene-aluminum composite tubing and passes through a cold trap at below -60°C before entering the flasks. Samples are collected in triplicate at approximately 2 week intervals.

3. RESULTS

Results for O_2/N_2 spanning approximately 1 year are shown in Figure 1. Also shown for comparison are CO_2 concentrations measured (at NCAR) on the same samples and CO_2 concentrations measured on CMDL flasks (T. Conway, personal communication). Although data from August and September is lacking, a seasonal cycle is nevertheless evident in the O_2/N_2 data that is opposite in phase to the CO_2 cycle. Like the data collected at other sites in the northern hemisphere [Keeling and Shertz, "Seasonal cycles and depletion rate of atmospheric molecular oxygen" in preparation], the amplitude of the O_2/N_2 variation appears to be larger on a molecule for molecule basis than the CO_2 cycle. This amplitude difference can be explained by O_2 that is degassed and ingassed seasonally from the oceans and that augments the O_2 cycle caused by exchanges with terrestrial ecosystems. This amplitude difference can be used to constrain rates of biological organic carbon production in the ocean [*Keeling et al.*, 1992].

The O_2/N_2 record from MLO appears to exhibit greater short-term variability than we have observed at other sites (e.g. Alert and Cape Grim [Keeling and Shertz, in preparation]). At the present time we are not sure what causes this scatter in the MLO data. We note that the sampling procedures in use at MLO are, in fact, different from those at other sites owing primarily to the need to

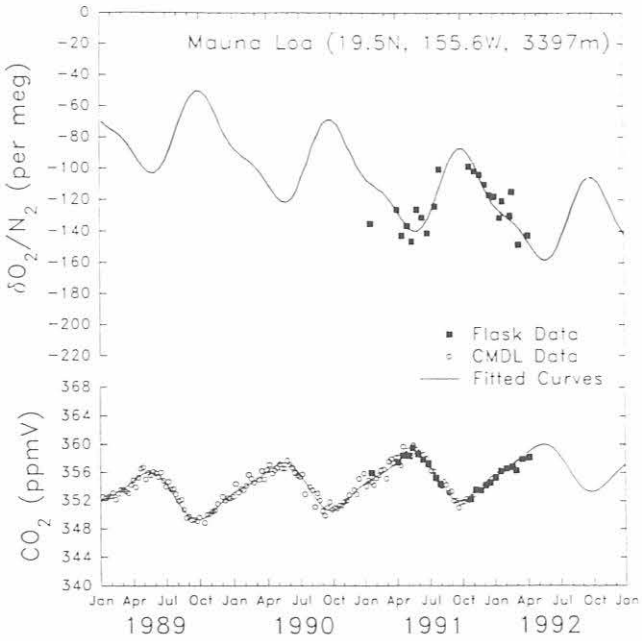

Fig. 1. Measurements of $\delta(O_2/N_2)$ and CO_2 mole from air samples collected at MLO. The axes are scaled (5 per meg ∝ 1 ppm) so that changes in $\delta(O_2/N_2)$ and CO_2 are directly comparable on a mole O_2 to mole CO_2 basis. Solid squares are averages of flasks taken on a given day. The curves are least-squares fits to the function $X = a + bt + c\sin(2\pi t) + d\cos(2\pi t) + e\sin(4\pi t) + f\cos(4\pi t)$ where t is in years. For the $\delta(O_2/N_2)$ data, the interannual trend is assumed to be the same as the trend observed at La Jolla [Keeling and Shertz, in preparation]. Thus the fit fixes the value of b at -18 per meg yr^{-1}. Supplemental CO_2 data from laboratories at NOAA/CMDL are also shown.

pressurize the flasks to above ambient pressure. It is conceivable that some unknown sampling difficulties are associated with this procedure.

It is interesting, however, that the scatter in the O_2/N_2 data appears to follow a seasonal pattern, with a lower degree of scatter in fall than at other times of year. A similar pattern is seen in the CO_2 data, although to a lesser degree. This suggests that the scatter may be the result of real atmospheric variability. More measurements are needed to test whether this pattern of variability persists from year to year.

Acknowledgements. We are grateful for the assistance of the staff at MLO for obtaining air samples. This work was supported by the National Science Foundation.

4. References

Keeling, R.F., Development of an interferometric oxygen analyzer for precise measurement of the atmospheric O_2 mole fraction, Ph. D. thesis, 178 pp, Harvard University, Cambridge, MA, 1988*a*.

Keeling, R.F., Measuring correlations in atmospheric O_2 and CO_2 mole fractions: a preliminary study in urban air, *J. Atmos. Chem.*, *7*, 153-176, 1988*b*.

Keeling, R.F., M. Bender, R. Najjar, P.P. Tans, What measurements of atmospheric oxygen can tell us about the global carbon cycle, *Global Biogeochem. Cycles*, submitted, 1992.

Decline in the Trend of Atmospheric Methane

M.A.K. KHALIL AND R.A. RASMUSSEN

Global Change Research Center, Department of Environmental Science and Engineering,, Oregon Graduate Institute, Beaverton, Oregon 97006 U.S.A.

1. INTRODUCTION

It is well known that the concentration of CH_4 is increasing in the earth's atmosphere. It has now become apparent that the rate of increase is slowing down in recent years [*Khalil and Rasmussen*, 1989, 1990]. In this paper we document the magnitude of the slowdown in trend as observed at sites distributed from the Arctic to the South Pole.

2. THE DATA

Two data sets were used for our analyses. The first is from flask samples obtained at BRW (71.5°N); Cape Meares, Oregon (45.5°N); Cape Kumukahi and MLO (19.3°N); SMO (14.1°S), Cape Grim, Tasmania (42°S); and SPO (90°S). The latitudinally weighted and globally averaged monthly CH_4 concentrations were calculated from measurements taken at these sites between September 1980 and September 1988. The results are discussed and tabulated by *Khalil and Rasmussen* [1990].

At Cape Meares we have also taken some 123,000 measurements between 1979 and 1992 using automated GC/FID instruments that sample air day and night. Monthly average concentrations of CH_4 were calculated from these data.

3. ANALYSES AND RESULTS

There are many ways to look at the changes in the trends during the times when data are available. First we calculated "moving trends." These are linear trend calculations for overlapping periods of time. The basic period over which the trend is calculated is specified as T. Then the moving trends are calculated for C(0) to C(T); $C(1)$ to $C(T+1)$; ...; $C(N-T)$ to $C(N)$ where $C(i)$ are concentrations at time i and i = 0, ..., N. The uncertainties are also calculated during these periods (all uncertainties quoted in this paper are 90% confidence limits). These calculations are performed by standard methods [*Snedecor and Cochran*, 1980]. The calculations are performed on de-seasonalized time series as discussed by *Khalil and Rasmussen* [1990]. The de-seasonalization has a large effect on the Cape Meares time series since the seasonal cycles are large but the effect of de-seasonalization is small on the global average time series.

Results of calculations for the global average data set and for the Cape Meares data are shown in Figures 1 and 2. The period of calculation is 5 years (T = 5 yrs). The differences in these two results are due, for the most part, to the different times spanned by the two data sets.

The second procedure is to divide the global data set C(t) into two time series - C_a (t) for the first half of the data spanning 4 years from October 1980 to September 1984 and C_b (t) for the second half spanning the 4 years from October 1984 to September 1988 (Eqs. 1 and 2).

$$C_a(t) = C(t) \qquad 0 < t < \delta T \tag{1}$$

$$C_b(t) = C(t) \qquad \delta T < t < N \tag{2}$$

These time series may be described by linear of exponential models as in Eqs. 3-6.

$$C_a = a_1 + b_1 t \tag{3}$$

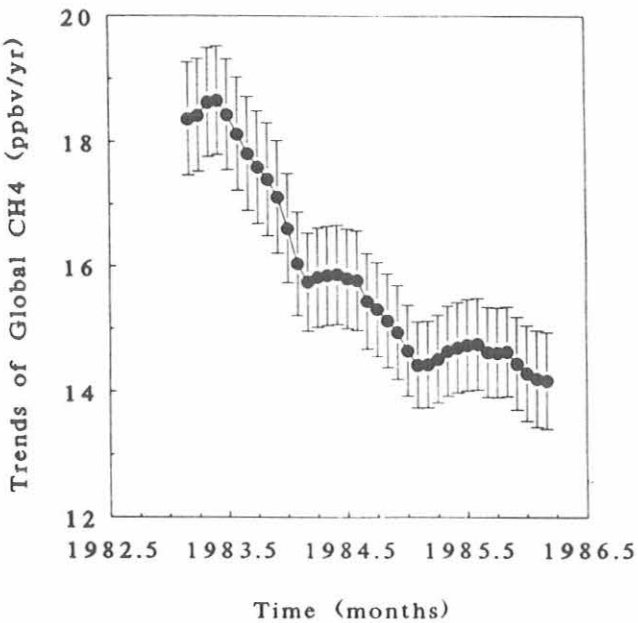

Figure 1: Moving trends of methane concentrations during 5-year overlapping periods. The trends are calculated using monthly and globally-averaged data from measurements taken at BRW; Cape Meares, Oregon; Cape Kumukahi and MLO; SMO; Cape Grim, Tasmania; and SPO.

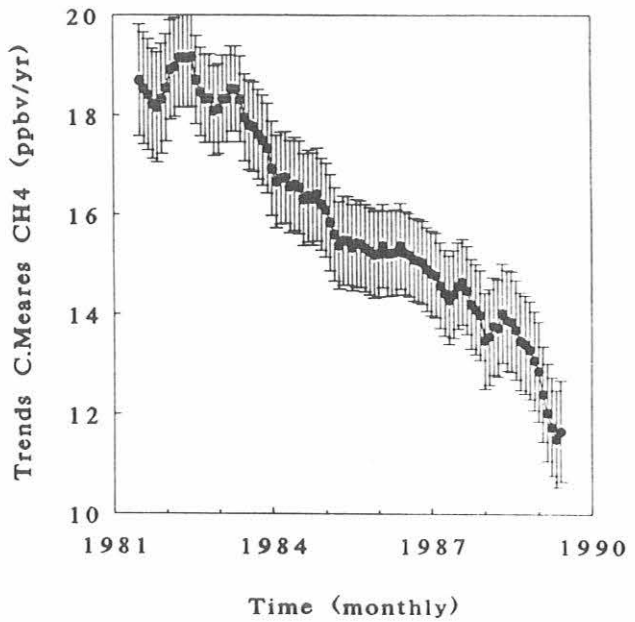

Figure 2: Moving trends of methane concentrations during 5-year overlapping periods. The trends are calculated using monthly averaged data from Cape Meares, Oregon. The original data base consists of about 123,000 individual measurements.

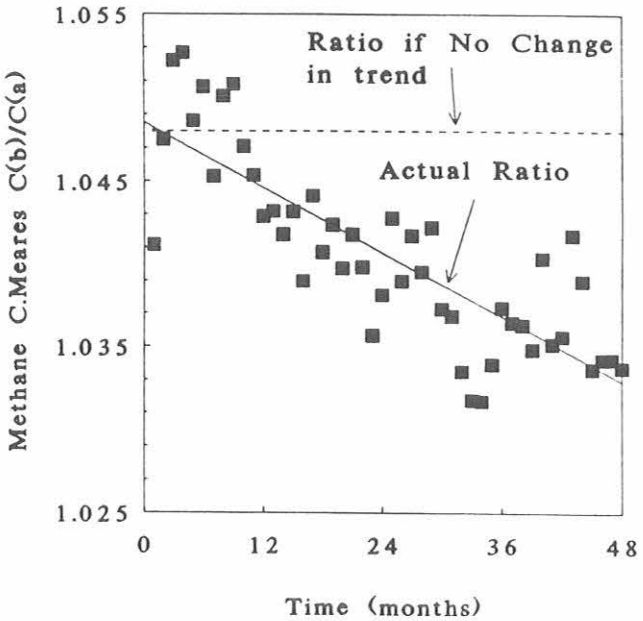

Figure 3: The ratio of concentrations between the first half and the second half of the globally and monthly averaged time series of methane concentrations. The data were divided into two series: October 1980—September 1984 and October 1984—September 1988. The first point is the average for October 1980 divided by the average concentration for October 1984; the second point is average concentration at November 1980 divided by the average concentration at November 1984; and so on. The ratio would be constant if there were no change of trend.

$$C_b = a_2 + b_2 t \tag{4}$$

$$C_a = \alpha_1 e^{\beta_1 t} \tag{5}$$

$$C_b = \alpha_2 e^{\beta_2 t} \tag{6}$$

In Eqs. 3-6, a_1, a_2, b_1, b_2, α_1, α_2, β_1, and β_2 are constants and $\delta T = 48$ months.

We now define the difference between the time series according to the two models as:

$$\Delta C = C_b - C_a = (a_2 - a_1) + (b_2 - b_1) \tag{7}$$

$$\delta C = C_b / C_a = (\alpha_2 / \alpha_1)\exp(\beta_2 - \beta_1)t \tag{8}$$

If the rate of increase was constant throughout the time of measurements, then $b_1 = b_2 = b$ and $\beta_1 = \beta_2 = \beta$, and thus ΔC and δC would be constants in time. The actual time series for δC is shown in Figure 3; the time series for ΔC is very similar. Clearly ΔC and δC are not constant but are decreasing functions of time, which implies that the trends in the latter half of the time series are smaller than in the first half.

The annual decline in the trend is estimated from these models as:

$$\Delta b = (b_2 - b_1)/\delta T \tag{9}$$

$$\Delta b\% = (\beta_2 - \beta_1)100\%/\delta T \tag{10}$$

We evaluated the trends in ΔC and δC by standard statistical analysis. We find that the differences between b_1 and b_2 and between β_1 and β_2 are indeed statistically significant, as shown in Table 1. The result is that the trend of CH_4 decreased at -1.3 $\pm$ 0.3 ppbv/yr^2 (Δ_b) or 0.4 $\pm$ 0.1%/yr^2 (Δ_b%) for data between October 1980 and September 1988 (the centered times over which trends are calculated are 5 years (= T) shorter; April 1983-March 1986; see Figure 1).

4. Conclusions and Speculations

While there have been considerable gains in understanding the global cycle of CH_4, including the reasons for increasing trends and seasonal or latitudinal variations, the causes for the decline in trends are still mostly unknown. There are three possibilities that may in some combination, be causing the slowdown in the

TABLE 1. Trends and Changes of Trends

Period	Site	d^2C/dt^2
	Changes of Trends	
Jan. 1979-Jan. 1992	Cape Meares	-0.9 ppbv/yr^2
Sept. 1980-Sept. 1988	Cape Meares	-1.2 ppbv/yr^2
Sept. 1980-Sept. 1988	Global Average	-1.3 ± 0.3 ppbv/yr^2
	Average Trends	
Jan. 1979-Jan. 1992	Cape Meares	15.7 ± 0.3 ppbv/yr
Sept. 1980-Sept. 1988	Cape Meares	16.7 ± 0.5 ppbv/yr
Sept. 1980-Sept. 1988	Global Average	16.4 ± 0.5 ppbv/yr

accumulation of CH_4: (1) the anthropogenic sources may not be increasing as fast as before, (2) the natural sources may be decreasing, or (3) tropospheric OH concentrations may be increasing, thus removing a greater amount of CH_4 from the atmosphere each year.

Of these possibilities, the first is likely to be the most significant contributor to the declining trends of CH_4. Qualitatively it is known that the large anthropogenic sources, namely cattle and rice agriculture, are not increasing as fast as in past decades. Over the last decade, both the hectares of rice harvested annually and the number of cattle in the world appear to be decreasing [see *Shearer & Khalil*, 1989]. An explanation for the changing trends is likely to reduce uncertainties in our present knowledge of the sources and sinks of methane.

Acknowledgments: We thank NOAA/CMDL for collecting flask samples at BRW, MLO, SMO. and SPO. We thank D. Stearns and R. Dalluge for laboratory measurements, and M. Shearer and F. Moraes for analysis of emissions and data. This project was supported in part by grants from ORAL, NSF, and DOE (#DE-FG06-85ER60313). Support for recent analyses of Cape Meares data was provided by a contract from the U.S. EPA to Andarz Co. Additional support was provided by the Biospherics Research Corp. The sponsors are not responsible for the contents of this paper.

REFERENCES

Khalil, M.A.K., and R.A. Rasmussen, The Global Methane Cycle, *Proceedings of the International Conference on Global and Regional Environmental Atmospheric Chemistry (IGREAC)*, L. Newman, W.-X. Wang, and C.S. Kiang, (Editors), Brookhaven National Laboratory, Upton, NY, 11973, 213-222, 1990.

Khalil, M.A.K., and R.A. Rasmussen, Atmospheric methane: Recent global trends, *Environ. Sci. Technol. 24*, 549-553, 1990.

Snedecor, G.W., and W.G. Cochran, *Statistical Methods*, Iowa State University Press, Ames, 1980.

Shearer, M.J., and M.A.K. Khalil, The global emissions of methane over the last century, *EOS 70(43)*, 1017, 1989.

Radioactivity in the Surface Air at BRW, MLO, SMO, and SPO during 1991

RICHARD J. LARSEN AND COLIN G. SANDERSON
U.S. Department of Energy, Environmental Measurements Laboratory, New York, New York 10014-3621

1. INTRODUCTION

Hi-volume air filter samples are routinely collected by CMDL personnel at BRW, MLO, SMO, and SPO for EML's Surface Air Sampling Program (SASP). The primary objective of this program is to study the temporal and spatial distribution of specific natural and anthropogenic radionuclides in the surface air. Of the radionuclides that are analyzed by gamma-ray spectrometry, only the naturally occurring radioisotopes ^{7}Be and ^{210}Pb are still readily measured in most of the filter samples. ^{7}Be (half-life 53.2 days) is produced by cosmic-ray interactions in the upper troposphere and the stratosphere. ^{210}Pb (half-life 22.3 years) is a decay product of ^{222}Rn, a noble gas that diffuses from soils. Because of their distinctly different source regions, these radioisotopes may serve as tracers for upper and lower tropospheric source and transport processes. Recently, global climate models have been tested by simulating ^{7}Be and ^{210}Pb concentrations [*Feichter et al.*, 1991; *Brost et al.*, 1991].

2. MATERIAL AND METHODS

Weekly air filter samples are continuously collected using Microdon or Dynaweb filter material. The air samplers move ~1700 m^3 of air per day through a 20.3-cm diameter filter. The weekly filter samples collected at BRWand MLO are analyzed by gamma-ray spectrometry using a high-purity germanium(HPGe) detector with a 1.5 cm diameter well. The individual weekly samples from SMO and SPO are not routinely analyzed. A monthly composite sample for each site was formed by adding

TABLE 1. Monthly Surface Air Concentrations of Radionuclides at BRW, MLO, SMO, and SPO During 1991

Site	Nuclide	Jan.	Feb.	March	April	May	June	July	Aug.	Sept.	Oct.	Nov.	Dec.
BRW	Gamma (cpm m^{-3})	<0.01	<0.01	<0.01	<0.01	<0101	<0.01	<0.01	<0.01	*	*	<0.01	<0.01
MLO	Gamma (cpm m^{-3})	<0.01	<0.01	<0.01	<0.01	<0.01	<0.01	<0.01	<0.01	<0.01	<0.01	<0.01	*
SMO	Gamma (cpm m^{-3})	<0.01	<0.01	<0.01	<0.01	<0.01	<0.01	<0.01	<0.01	<0.01	<0.01	<0.01	*
SPO	Gamma (cpm m^{-3})	<0.01	<0.01	<0.01	<0.01	<0.01	<0.01	<0.01	<0.01	<0.01	*	*	*
BRW	^{7}Be (mBq m^{-3})	1.6	1.7	2.1	1.7	0.9	0.5	0.2	0.6	*	*	1.0	1.3
MLO	^{7}Be (mBq m^{-3})	6.6	6.4	5.4	5.9	7.1	4.0	5.3	4.1	5.0	4.3	4.2	*
SMO	^{7}Be (mBq m^{-3})	1.3	1.1	1.7	1.1	2.3	1.6	2.2	2.2	2.2	2.0	1.2	*
SPO	^{7}Be (mBq m^{-3})	4.6*	4.2*	2.5*	2.7	2.3	2.0	1.9	2.7	2.1	*	*	*
BRW	^{95}Zr (μBq m^{-3})	<17.0	<12.0	<13.0	<12.0	<6.8	<8.7	<5.5	<2.5	*	*		
MLO	^{95}Zr (μBq m^{-3})	<33.0	<25.0	<21.0	<15.0	<15.0	<13.0	<5.2	<13.0	<34.0	<35.0	<17.0	*
SMO	^{95}Zr (μBq m^{-3})	<11.0	<9.0	<32.0	<11.0	<4.3	<6.9	<5.7	<14.0	<12.0	<14.0	<8.6	*
SPO	^{95}Zr (μBq m^{-3})	<330.0	<150.0	<99.0	<53.0	<33.0	<14.0	<39.0	<27.0	<16.0	*	*	*
BRW	^{137}Cs (μBq m^{-3})	<2.6	<2.5	<1.1	<1.4	<1.1	<1.1	<1.7	<0.9	*	*	<0.6	<2.1
MLO	^{137}Cs (μBq m^{-3})	<4.0	<3.4	<1.5	<1.7	<2.4	<3.1	<1.3	<2.4	<3.3	<3.0	<2.8	*
SMO	^{137}Cs (μBq m^{-3})	<1.5	<1.7	<2.6	<1.3	<0.8	<1.0	<1.5	<1.2	<1.3	<2.2	<1.4	*
SPO	^{137}Cs (μBq m^{-3})	<1.7	<1.9	<1.7	<1.6	<1.4	<0.9	<2.5	<2.7	<2.3	*	*	*
BRW	^{144}Ce (μBq m^{-3})	<12.0	<11.0	<5.4	<6.9	<3.6	<5.1	<5.9	<2.7	*	*	<2.1	<9.9
MLO	^{144}Ce (μBq m^{-3})	<19.0	<13.0	<6.6	<7.1	<12.0	<11.0	<4.8	<11.0	<12.0	<12.0	<11.0	*
SMO	^{144}Ce (μBq m^{-3})	<6.4	<6.8	<13.0	<4.9	<3.2	<4.2	<6.1	<6.4	<6.6	<7.8	<6.9	*
SPO	^{144}Ce (μBq m^{-3})	<18.0	<16.0	<14.0	<12.0	<9.3	<4.9	<15.0	<14.0	<12.0	*	*	*
BRW	^{210}Pb (mBq m^{-3})	1.10	1.10	0.59	0.48	0.17	0.07	0.05*	0.09	*	*	0.55	0.86
MLO	^{210}Pb (mBq m^{-3})	0.29	0.27	0.35	0.51	0.50	0.23	0.31	0.20	0.25	0.21	0.14	*
SMO	^{210}Pb (mBq m^{-3})	0.04*	0.04*	0.05*	0.03*	0.06	0.06	0.08	0.07*	0.10	0.09	0.05*	*
SPO	^{210}Pb (mBq m^{-3})	0.04*	0.03*	0.01§	0.02*	0.02‡	0.01‡	0.01‡	0.04	0.03‡	*	*	*

*No data, samples are being analyzed.
†Uncertainty is between 20% and 50%
‡Uncertainty is between 50% and 100%
§Uncertainty is greater than 100%

together one half of each of the weekly filter samples. These monthly composite samples are compressed into 45-cm^3 plastic or several gamma-ray emitting radionuclides using either n-type low-energy coaxial, high-purity germanium (HPGe) detectors or p-type coaxial high-resolution, germanium lithium or HPGe detectors. Detailed information on SASP is periodically published [*Larsen and Sanderson*, 1991].

3. Results

The results of the analyses of several radionuclides and the total gamma-ray activities for the monthly composite samples from filters collected at BRW, MLO, SMO, and SPO during 1991 are reported in Table 1. The total gamma-ray activities are reported in units of counts per minute (cpm) per standard cubic meter (15°C, 1 Atm) of sampled air. The surface air concentrations of ^{7}Be and ^{210}Pb are reported in millibecquerels (mBq) per standard cubic meter of air, and ^{95}Zr, ^{137}Cs, and ^{144}Ce are reported in microbecquerels (μBq) per standard cubic meter of air. The concentrations are reported as corrected for radioactive decay to the midpoint of the month of collection. The results of the analyses on the weekly samples from BRW and MLO are presently being prepared for publication as an EML report.

4. Discussion

There were no reported significant releases of radioactive materials into the atmosphere during 1991, and the concentrations of fission products such as ^{95}Zr, ^{137}Cs, and ^{144}Ce were at or below the lower limits of detection for the analytical and sampling techniques that we currently use to measure them.

The monthly mean concentrations of ^{7}Be and ^{210}Pb appear to continue to show seasonal cycles at all of the CMDL sites. *Feely et al.* [1989] described the factors that cause seasonal variations in the ^{7}Be concentrations in the surface air.

Acknowledgment. We wish to thank the CMDL staff at BRW, MLO, SMO, and SPO for the collection of air filter samples for the SASP.

5. References

Feely, H.F., R.J. Larsen, and C.G. Sanderson, Factors that cause seasonal variations in beryllium-7 concentrations in surface air, *J. Environ. Radioactivity*, *9*, 223-249, 1989

Brost, R. A., J. Feichter, and M. Heimann, Three-dimensional simulation of ^{7}Be in a global climate model, *J. Geophys. Res.*, *96*, 22,423-22,445, 1991.

Feichter, J., R.A. Brost, and M. Heimann, Three-dimensional modeling of the concentration and deposition of ^{210}Pb aerosols, *J. Geophys. Res.*, *96*, 22,447-22,460, 1991.

Larsen, R.J., and C.G. Sanderson, EML surface air sampling program, 1989 data, EML Rep. EML-541, Environmental Measurements Laboratory, U.S. Dept. of Energy, New York, 1991.

Long-Range Transport of Kuwaiti Oil-Fire Smoke

D.H. LOWENTHAL, R.D. BORYS, J.C. CHOW, AND F. ROGERS
Desert Research Institute, University of Nevada, Reno, Nevada 89506-0220

G.E. SHAW
Geophysical Institute, University of Alaska, Fairbanks, Alaska 9975-0800

1. INTRODUCTION

The Kuwaiti oil fires set during the Persian Gulf War raised concerns over their potential impact on regional and global climate. Far-reaching effects depend on the ability of significant amounts of these emissions to be transported long distances away from the Middle East. Long-range transport on the order of 10,000 km in the northern hemisphere has been observed for Asian dust over the Pacific and Sahara dust over the Atlantic, arctic haze, and radioactive debris from the Chernobyl reactor fire.

The principal light-active species in the oil-fire emissions is light-absorbing carbon soot. Identifying the Kuwaiti oil fires as a source of soot measured downwind of the Middle East is difficult because there are numerous other fossil and contemporary fuel combustion sources along the transport path. Furthermore, simply detecting soot from the oil fires does not imply a significant environmental effect. To study the potential effects of Kuwaiti oil-fire smoke after long-range transport, aerosols were collected in Hawaii during the late spring and summer of 1991 and analyzed for carbon and trace elements.

2. EXPERIMENTAL

Aerosol samples were collected on a weekly basis at the NOAA/CMDL Mauna Loa Observatory (MLO), located at an altitude of 3400 m (in the free troposphere) on the main island of Hawaii, some 15,000 km from Kuwait. For comparison, samples were also collected at a sea-level site in the marine boundary layer (MBL) on the island of Oahu. Daily averaged aerosol optical depths were determined at three wavelengths at MLO from May 9 to May 15. Orographic cloud and rain water samples were collected on the northeast coast of Hawaii from May 15 to May 17.

2.1. AEROSOL SAMPLING

Sampling at MLO and Oahu was wind-sector controlled to avoid local contamination. MLO and Oahu samples were collected under "downslope" and on-shore flow, respectively. Aerosol samples were collected on 47 mm Gelman (Ann Arbor, Michigan) 2.0 μm pore size PTFE Teflon membrane filters (#R2PJ047) and 47 mm Pallflex (Puttman, Connecticut) quartz fiber filters (#2500 QAT-UP). A Bendix 240 cyclone separator was used to collect aerosols of aerodynamic diameter less than 2.5 μm. Teflon and quartz filter samples were also collected during the National Center for Atmospheric Research (NCAR) aircraft experiment in the Middle East from May and June, 1991.

2.2. SUNPHOTOMETRY

A series of hand-held sunphotometer measurements were made at MLO during the first few hours after sunrise between May 9 and May 15. The instrument was developed by the Geophysical Institute at the University of Alaska using a silicon PIN-high impedance amplifier module and well-blocked Barr interference filters. Blue (425 nm), green (500 nm), and red (790 nm) wavelengths were measured. Half bandwidths were 10 nm.

2.3. CLOUD AND RAIN SAMPLING

Cloud and rain water samples were collected from an exposed grassy area within 3 m of the edge of a 450-m deep canyon formed by the Honokane Nui stream about 8 km from the northeast coast of Hawaii. Cloud water was collected with a passive Teflon screen collector. Rain water was collected with a plastic funnel and bottle.

2.4. CHEMICAL ANALYSIS

Elemental concentrations on Teflon filters were measured by x-ray fluorescence at the Desert Research Institute and by instrumental neutron activation analysis (INAA) at the University of Rhode Island's Graduate School of Oceanography. The quartz filters were analyzed for organic (OC) and elemental (EC) carbon by thermal/optical reflectance. Elemental concentrations in cloud and rain water were determined by drying the samples and collecting the residues on acid-washed, 47 mm Whatman 41 paper filters and subjecting the latter to INAA.

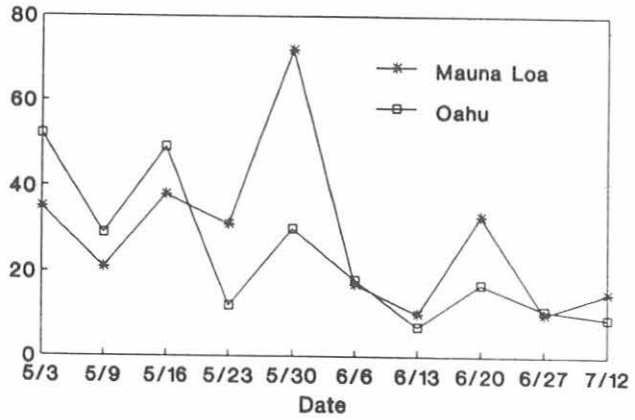

Fig. 1. Concentrations of elemental carbon at MLO and Oahu.

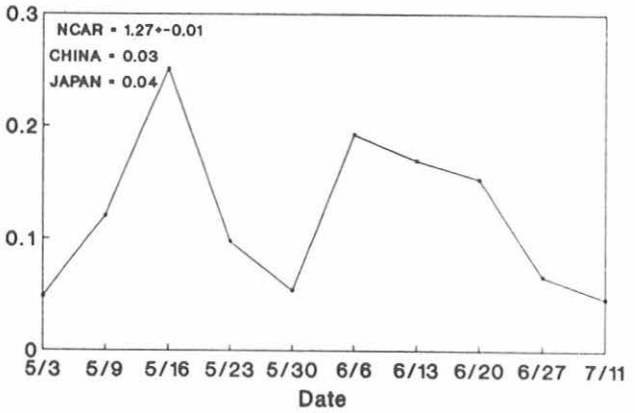

Fig. 3. Noncrustal V/Zn ratio at MLO. Ratios measured for samples collected during the NCAR flights in the Kuwaiti oil-fire plume and in regional aerosol from China and Japan, are also shown.

2.5. Air Mass Trajectories

Ten-day back trajectories calculated at 1000, 850, 700, and 500 mb for selected sample dates at MLO were for provided by NOAA/CMDL in Boulder, Colorado.

3. Results and Discussion

Elemental carbon (EC) concentrations at MLO and Oahu, shown in Figure 1, covaried and reached a maximum of 71 ng/m^3 at MLO in the sample beginning on May 30. The next highest EC concentration at MLO was 38 ng/m^3 for the sample beginning on May 16. Because more-efficient removal is expected in the MBL, the similarity between EC concentrations at MLO and Oahu was surprising.

Concentrations of EC and S, which are both produced by fossil-fuel combustion, covaried over the period at MLO, with peaks on May 16 and May 30. Organic carbon (OC) concentrations varied much less than EC at MLO and did not covary with those of EC or S. Elemental to organic carbon ratios at MLO averaged 0.17 ± 0.08. Concentrations of pollution-derived Pb, Zn, As, Sb, and noncrustal V (xV) and crustal Si, plotted in Figure 2, generally followed those of EC and S at MLO. However, during the May 16 sample when EC, S, and xV concentrations were high, concentrations of Pb, Zn, As, Sb, and Si were low. EC reached its highest weekly concentration during the May 30 sample. Although concentrations of other species also peaked during this sample, the xV concentration did not. These patterns suggest two different aerosol types: (1) May 16, with high EC, S, and xV but low Pb, Zn, As, Sb, and Si; and (2) May 30, with high EC, S, Pb, Zn, As, Sb, and Si but low xV concentration.

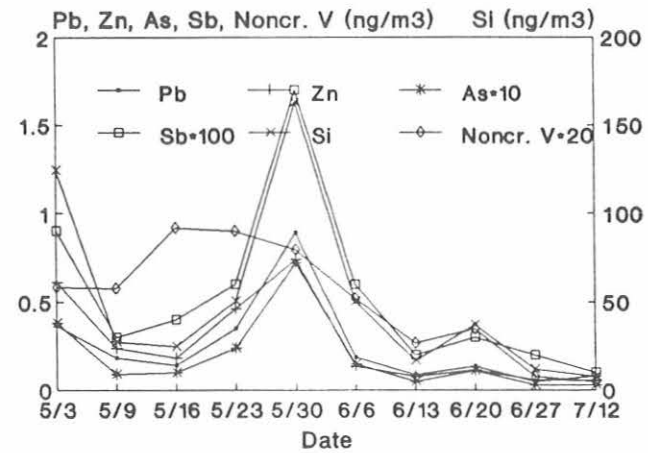

Fig. 2. Concentrations of Pb, Zn, As, Sb, noncrustal V, and Si at MLO.

We attempted to identify sources of aerosol at MLO based on elemental composition. Aerosol noncrustal vanadium is typically enriched in areas with high levels of oil-combustion emissions. Zinc is a more general urban/industrial pollutant. Maxima in the xV/Zn ratio at MLO may indicate greater aerosol contributions from oil-combustion sources, such as the Kuwaiti oil fires, relative to those from other anthropogenic activities. Figure 3 indicates that the xV/Zn ratio peaked at 0.25 during the May 16 sample, when EC also peaked, peaked again during the June 6, 13, and 20 samples, when EC concentrations were low, but decreased to a minimum of 0.05 on May 30, which had the highest EC of the period.

By comparison, xV/Zn ratios observed previously in aerosol samples collected in China and Japan averaged 0.03 and 0.04, respectively, while the xV/Zn ratio measured during the NCAR aircraft experiment over Kuwait was 1.27. The May 16 xV/Zn ratio was closer to the Kuwait

ratio than to the Asian ratios, suggesting that Kuwaiti oil-fire smoke contributed significantly to this sample. The 500 and 700 mb trajectories for the May 16 MLO sample indicated flow from the west. However, trajectories for the May 30 sample, which had the highest EC concentration of the period, came from the direction of the west coast of the United States.

Optical depths measured between May 9 and May 15 were lower than those measured previously during spring (0.02 at 500 nm). Although our results indicate that Kuwaiti oil smoke was present over MLO, the radiative effects of this material were not significant.

Chemical measurements showed that xV was more enriched in the cloud water than rain water. This suggests preferential fractionation of xV in the smaller cloud droplets, which are not efficiently removed in the warm-rain formation process. If this is true, it would help explain the unexpectedly high concentrations of pollutants such as EC and xV found in the MBL in Hawaii.

History of Strontium-90 Deposition at SMO and MLO

M. MONETTI
U.S. Department of Energy, Environmental Measurements Laboratory,New York, New York 10014-3621

1. INTRODUCTION

As part of the Global Fallout Program of the Environmental Measurements Laboratory (EML), deposition samples have been collected at American Samoa (SMO) and Mauna Loa, Hawaii (MLO) since the early 1960s. Sampling at both locations has been supported by CMDL for the majority of these years through a cooperative agreement. These samples, along with others collected in our global network, are regularly analyzed for ^{90}Sr. Strontium-90 is a radioactive fission product, and most of the ^{90}Sr measured in deposition samples has been produced as a result of atmospheric nuclear weapons testing. Strontium-90 is an important radionuclide from a health perspective because it has a long half-life (28 years), is produced in relatively large quantities during nuclear fission reactions, and has a high bioaccumulation potential. The data generated by this program are used to determine the distribution and inventories of ^{90}Sr deposited on the earth's surface. Many factors controlling the transport and fate of atmospherically released radionuclides have been revealed by this program. The results are published in annual reports [*Monetti and Larsen*, 1992].

2. MATERIAL AND METHODS

Deposition samples have been collected at MLO and SMO using two different collectors. An ion-exchange column was used at MLO and at SMO until 1976. The column is packed with Dowex-50W ion-exchange resin, glass wool and paper pulp. The resin material efficiently removes ^{90}Sr and other constituents from the aqueous phase of the sample, while the particulates are trapped in the paper pulp. The column is placed in a wooden housing unit, and a polyethylene funnel with a diameter of 30 cm is attached to the top of the column. Presently, an open 23-L polyethylene bucket, that has a diameter of 29 cm, is being used as a deposition sampler at both locations. Using either method, the collectors are exposed to bulk (wet and dry) atmospheric deposition, and a new sample is collected each month. The samples are shipped to EML where the precipitation samples collected in buckets are passed though an ion-exchange column. All Analyses are performed on the contents of the columns using established radiochemical procedures [*Chieco et al.*, 1990]. Strontium-90 is routinely measured in the samples, however, measurements of other radionuclides have also been made in the past. Another short-lived strontium isotope, ^{89}Sr ($t_{1/2}$ = 50 days), is among these radionuclides and is particularly relevant to the work presented here.

3. RESULTS

The yearly ^{90}Sr deposition data for MLO and SMO are summarized in Figure 1. The deposition is reported in units of activity per unit area (Bq^{90}Sr m^{-2}). Samples were not collected at SMO prior to 1965, therefore, no data are shown in the corresponding positions on the graph. In all other instances, a lack of data indicate that the samples contained ^{90}Sr activities that were below the detection limit. Figure 2 shows the natural logarithm of the ratio of ^{89}Sr activity to ^{90}Sr activity in a number of samples collected at MLO and SMO between 1959 and 1971. the data are presented in this form to attempt to elucidate the approximate age of the nuclear materials collected. This procedure is described in more detail in the discussion. Since ^{89}Sr was not measured in all of the samples collected, there are gaps in the data shown here (for example, from 1960 to 1962 and from 1965 to 1967). Strontium-89 was not measured in any samples collected at these two locations after 1971. The arrows at the bottom of the graph indicate months when atmospheric testing of nuclear weapons occurred.

4. DISCUSSION

The trend of ^{90}Sr deposition at MLO, shown in Figure 1, is characteristic of the depositional history throughout most of the world [*Larsen*, 1984]. There is generally a 1963 maximum value as a result of the large number and high fission yield of 1962 weapons tests. Reduced ^{90}Sr deposition is observed at both locations for the years 1965

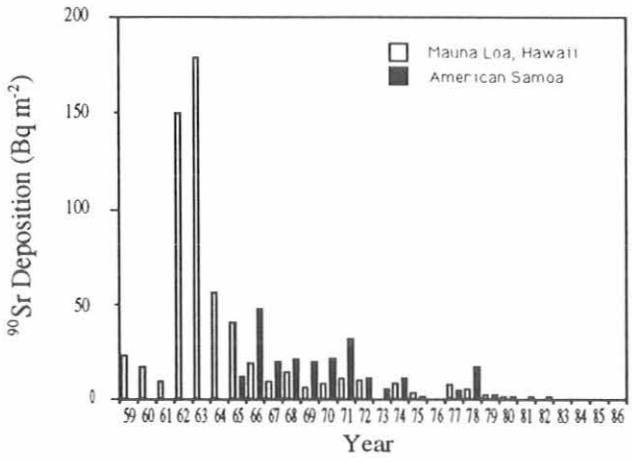

Fig. 1. Annual ^{90}Sr deposition at MLO and SMO for 1959 to 1986.

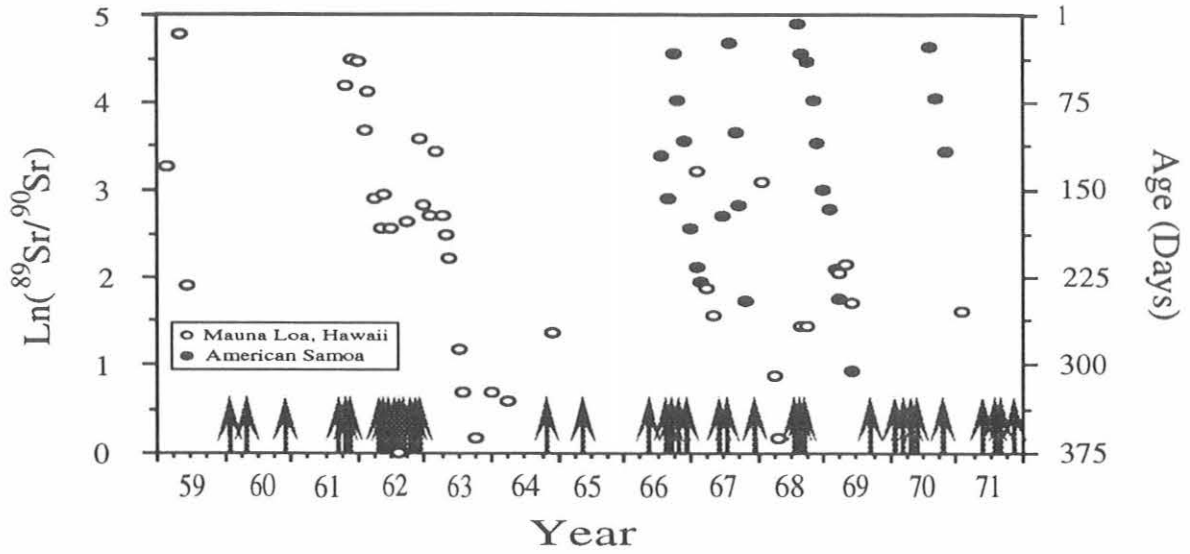

Fig. 2. Approximate age of radioactive material collected at MLO and SMO from 1959 to 1971. The ages were calculated using the ^{89}Sr to ^{90}Sr activity ratio as described in the text.

to 1986. The depositional trends during these years at the two locations were similar, however, deposition seems to be higher at SMO. No ^{90}Sr has been measured in samples collected at either sampling site after 1982. This is consistent with the fact that the last atmospheric test was conducted for EML's Global Fallout Program. Using data from all the sampling stations enables us to determine the global deposition and magnitude of ^{90}Sr deposition.

Nuclear weapons testing results in the production of ^{89}Sr and ^{90}Sr with a fairly consistent ratio (^{89}Sr to ^{90}Sr) of 150. Since the half-lives of these two strontium isotopes are very different, their ratio can be used to determine the age of the radioactive material collected. The right vertical axis in Figure 2 presents an aging scale based on the measured ^{89}Sr to ^{90}Sr ratio. The age scale is for the simple case in which only one release occurred. Since radioactive decay is an exponential process, the age is linearly related to the natural logarithm of the isotopic ratio. Numerous releases have been made over the past half-century. In this case, the actual date or dates of release of the material collected cannot be determined precisely using the ^{89}Sr to ^{90}Sr ratio, but the age of the nuclear debris can be estimated. The data in Figure 2 show that the approximate age of material deposited at MLO and SMO varied from a few days to over 1 year between 1959 and 1971. The "younger" material was collected at times when weapons testing was active. During periods when tests were not performed, the age of the material collected increased in time. This is particularly obvious between the last test of 1962 and the first test of 1964, as well as between the last one of 1968 and the first of 1969. This type of dating procedure can be useful for studies on the transport and fate of radioactive materials released, since the residence time of material in the atmosphere can be estimated.

Acknowledgment. I wish to thank the CMDL staff at MLO and SMO who have continued to provide EML with deposition samples for all of the years our program has been in operation.

5. REFERENCES

Chieco, N. A., D. C. Bogen, and E. O. Knutson (Eds.), *EML Procedures Manual, 27th Edition, HASL-300*, U.S. Department of Energy, Environmental Measurements Laboratory, New York, 1990.

Larson, R. J., *Graphic Presentation of Quarterly ^{90}Sr Fallout Data 1954-1982, EML-424*, 186 pp., U.S. Department of Energy, Environmental Measurements laboratory, New York, 1984.

Monetti, M. A. and R. J. Larsen, *Worldwide Deposition of Strontium-90 through 1986*, 31 pp., U.S. Department of Energy, Environmental Measurements Laboratory, New York, 1991.

Ultrahigh Resolution Infrared Solar Spectra from Mauna Loa Observatory

FRANK J. MURCRAY, SHELLE J. DAVID, AARON GOLDMAN, RONALD D. BLATHERWICK, DAVID G. MURCRAY
University of Denver, Department of Physics, Denver, Colorado 80208

INTRODUCTION

An ultrahigh resolution (0.0035 cm^{-1}) FTIR system was installed at Mauna Loa Observatory (MLO) in May 1991. This instrument is a prototype for the solar absorption FTIR instruments that will be used in the Network for Detection of Stratospheric Change (NDSC). Operation of this system is intended to provide some experience that may improve the final NDSC instrument design, as well as generating some valuable atmospheric data.

After the initial installation, University of Denver personnel returned to MLO to operate the equipment for 1-week periods in July and September. During the September run, the PC host computer was totally zapped (CPU, memory, disk controller and video card were all destroyed). We therefore returned with a new computer in November. When everything was running again, the system was left for the MLO staff to operate on a once-per-week basis. Data is returned to Denver once per month for processing. So far, the data has been of high quality.

The NDSC instrument will routinely monitor the total column amounts of several atmospheric gases including HCl, HNO_3, CH_4, N_2O, $ClONO_2$, F-12, and HF. In addition, stratospheric columns will be derived for some gases. We have so far only retrieved HCl and HNO_3.

INSTRUMENTATION

The interferometer system currently installed at MLO was manufactured by Bomem, Inc., Quebec, Canada. The actual NDSC interferometer will be one made by Bruker Instruments, Karlsruhe, Germany. The Bomem mechanically fits the dome better than the Bruker. Both systems have maximum path differences of more than 250 cm, corresponding to spectral resolution of about 0.0035 cm^{-1} (with weak apodization). The system has two liquid nitrogen cooled detectors: mercury-cadmium-telluride (MCT) for 5-15 microns (600-2000 cm^{-1}) and InSb for 2-5 microns (2000-5000 cm^{-1}). At the moment, each detector has only one filter installed, so that data are collected in only two intervals: 700-1250 cm^{-1} and 2800-3200 cm^{-1}. The interferometer is hosted by a 386 based PC, but has its own vector processor built in to provide fast fourier transforms of the data. The spectra are transferred to the host, and stored on the hard disk. A small section of two MLO spectra around the HCl line at 2925 cm^{-1} is shown in Figure 1. At the end of each run, the data are copied onto a digital audio tape (DAT). The DAT is shipped to Denver for analysis at the end of each month.

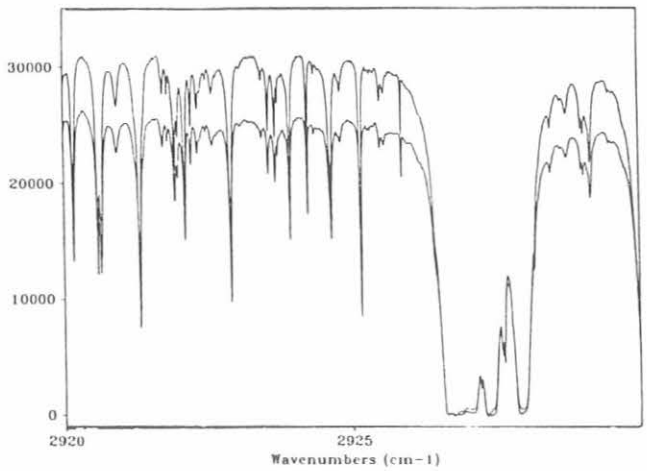

Fig. 1. Two spectra from MLO at two different solar elevation angles (the lower sun angle is on the top). The single sharp line at 2925.6 cm^{-1} is due to HCl. Intensity is in arbitrary units.

Solar radiation is brought into the interferometer through the fixed wall of the dome by an automatic 2-axis pointer that is mounted outside. The procedure followed by the operator is straightforward: the instrument is turned on about 1 hour before the start of the run, the tracker is uncovered and turned on, data collection is initiated by the operator running a batch file once the sun is high enough. The entire data collection procedure takes about 2 hours.

ANALYSIS

Analysis of the data proceeds by comparing a calculated spectrum and the observed spectrum. Input parameters to the calculation are changed iteratively until the differences are minimized (in a least squares sense). The input parameters include column or layer amounts of chemical species, the temperature-pressure profile, instrument functions, etc. Atmospheric line parameters are taken from the HITRAN92 data base. Radiosonde data from Hilo are used for the temperature profile. We have a program capable of fitting a few chemical species over a few wavenumbers that runs on a 386 based PC. We also have more extensive routines that run on larger machines. The data included here were analyzed using the PC version. A result of one of the fits is shown in Figure 2.

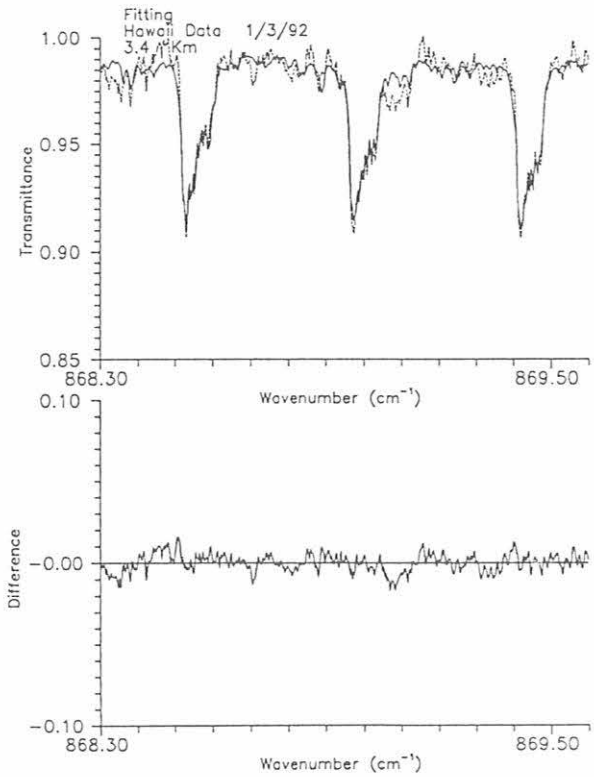

Fig. 2. An example of the fit achieved by the non-linear least squares fitting program for HNO_3. The upper panel shows both observed (dotted) and best fit calculated (solid) spectra on an expanded scale. The lower panel show the difference between calculated and observed.

DISCUSSION

Results from the first 4 months of operation are shown in Figure 3. The first important result is that there is data for almost every week (exceptions were cloudy sunrises). The variability in total column appears to be real, as retrievals

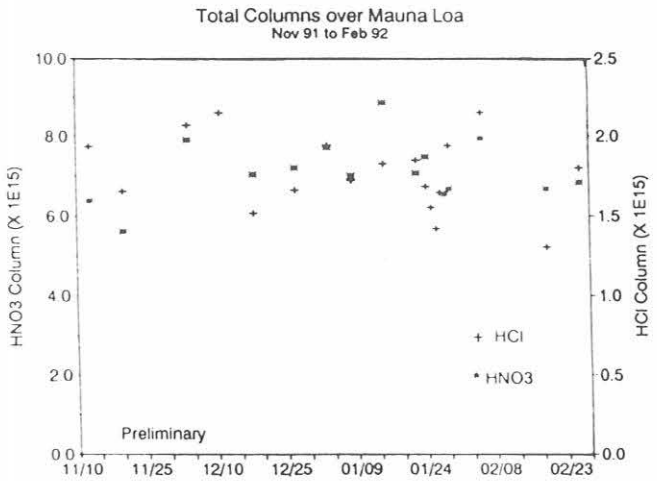

Fig. 3. Total column amounts for the first 4 months of operation of the MLO FTIR system.

from two spectra on the same day are usually consistent to within 2-3%. We await a longer run to be able to reach any conclusions about seasonal or secular variability.

The total column of HCl may still be subject to a systematic error. The vertical distribution profile that we have used here contains essentially no tropospheric HCl. This seems to give a better fit, and is consistent with our understanding that HCl should rain out at long distances from sources. However, the standard HCl profile contains significant amounts in the troposphere, and results in an increase in the total column of about 20%. We hope to have this uncertainty resolved soon.

Acknowledgments. We wish to thank the staff of MLO for their kind support. Elmer Robinson was very helpful in providing encouragement, space, and interest. Tom DeFoor helped on many occasions. We are particularly indebted to Bob Uchida for collecting most of this data very early each Wednesday morning.

Nitrate and Non-Sea-Salt Sulfate Aerosols at American Samoa: 1983-1990

J.M. PROSPERO AND D.L. SAVOIE
University of Miami, Rosenstiel School of Marine and Atmospheric Science
Division of Marine and Atmospheric Chemistry, Miami, Florida 33149-1098

1. INTRODUCTION

We have carried out an atmospheric aerosol sampling program at American Samoa since early 1983. The objective of this program is to develop a chemical climatology of the major aerosol species with a major emphasis on the sulfur and nitrogen cycles. The Samoa studies are carried out in parallel with similar measurements made at a number of other stations that we operate in the Pacific and also in other ocean regions. We have previously reported on our SMO measurements in Summary Report 1988, No. 17, [*Elkins and Rosson*, 1989] where we summarized the data from 1983 to 1987; at that time we commented on the seasonal variability of the concentrations of aerosol nitrate, non-sea-salt (nss) sulfate and methanesulfonate (MSA). In this current report, we summarize the entire data record which now extends from 1983 to 1990.

Samples are collected with a high-volume aerosol sampler using 20 × 25 cm Whatman 41 filters at a nominal flow rate of 1.1 m^3 min^{-1}. Samples are collected over 1-week periods except for special experiments such as those held in conjunction with the NASA GLOBE flights (November 1989 and May 1990) when daily samples were taken [see Summary Report 1990, No. 19, *Ferguson and Rosson*, 1991]. The sampler is activated only when winds blow from the sea at a speed greater than 1 m sec^{-1}. Samples are returned to Miami for analysis. Nitrate, sulfate and MSA were measured in aqueous extracts of the filters by means of ion chromatography. Nonseasalt (nss) sulfate is estimated as total sulfate minus sodium times 0.2517, the sulfate-to-sodium mass ratio in sea water.

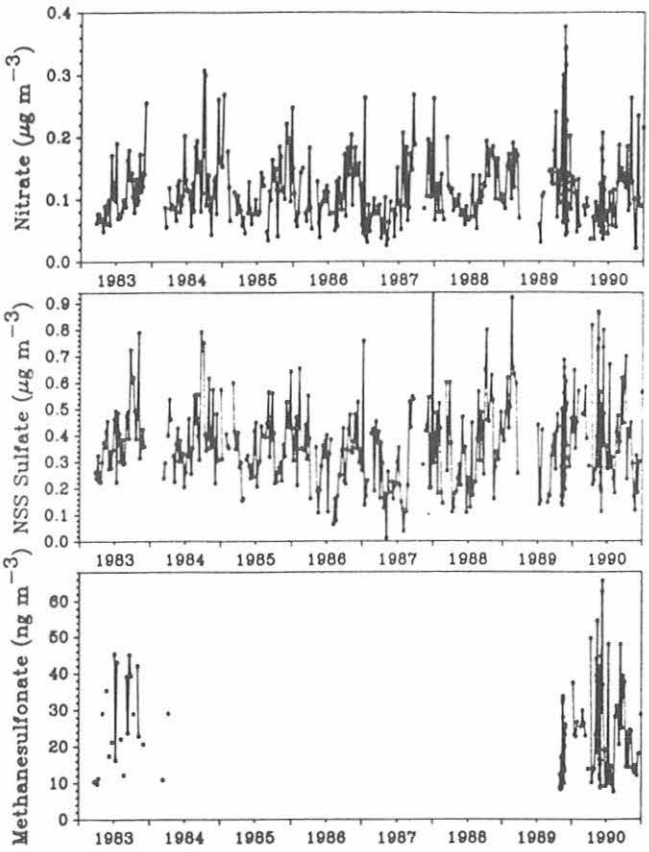

Figure 1. Time series plots of the nitrate, non-sea-salt (nss) sulfate, and methanesulfate (MSA) concentrations at American Samoa from 1983 through 1990.

2. RESULTS

The entire 8-year record is shown in Figure 1. Each dot represents the value for a specific sample; lines connect consecutive samples. The GLOBE program period is reflected in the high density of samples in late 1989 and early 1990. Annual mean values are presented in Table 1. Means for each of the individual months are plotted in Figure 2*a* (nitrate) and Figure 2*b* (nss-sulfate).

It is clear from Figure 1 that there is considerable variability from sample to sample. This variability is also apparent in the monthly means (Figures 2*a,b*). Nonetheless, seasonal cycles are apparent in the concentrations of both nitrate and nss-sulfate. The annual cycle is most clearly defined for nitrate, especially for the minimum which occurs in April-May. The maximum is much broader, spreading over the months September through December; in some years, high monthly means persisted into the early months of the year.

The nss-sulfate annual cycle is much more irregular than that for nitrate. A broad minimum occurs during the austral winter months and a broad and somewhat ragged maximum occurs during the Austral summer. The MSA data is much more limited than that for other species. We have analyzed every sample for 1990 and about half of the samples for 1983. This limited data set does not reveal any clear evidence of an annual cycle.

The annual means (Table 1) do not show any strong or coherent year-to-year trends in the nitrate concentrations. The MSA means are essentially identical for the 2 years of record, 1983 and 1990. In contrast, there is evidence that the nss-sulfate concentrations have varied slowly and

TABLE 1. Annual Means of Monthly Means ($\mu gm/m^3$)

Year	Number. Months	NO_3	Standard Deviation	xSO_4	Standard Deviation	Na	Standard Deviation	MSA	Standard Deviation
1983	9	0.107	0.029	0.388	0.098	5.95	0.750	0.025	0.010
1984	10	0.123	0.031	0.402	0.088	5.83	1.041		
1985	12	0.117	0.044	0.352	0.078	4.37	0.874		
1986	12	0.105	0.032	0.320	0.111	4.69	1.893		
1987	11	0.113	0.042	0.318	0.112	4.82	0.764		
1988	12	0.112	0.028	0.350	0.106	5.10	0.978		
1989	9	0.139	0.027	0.389	0.136	5.53	1.008		
1990	12	0.102	0.033	0.411	0.073	4.77	0.967	0.024	0.004

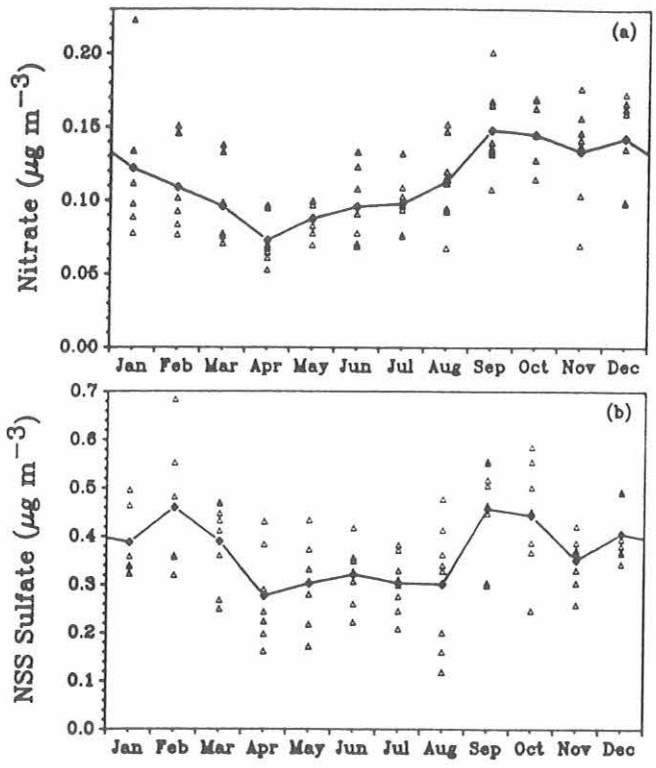

Fig. 2. Monthly mean concentrations of (*a*) nitrate and (*b*) non-sea-salt (nss) sulfate concentrations at American Samoa. Each point represents the mean for the given month in a specific year.

systematically over the years: annual means had maxima of about 0.4 $\mu g/m^3$ in 1983 and 1984; they decreased to minima of about 0.32 $\mu g/m^3$ in 1986 and 1987 and then increased to maxima of about 0.4 $\mu g/m^3$ in 1989 and 1990. It is interesting that the nss-sulfate means for 1983 and 1990 are comparable, as are the means for MSA for those years.

Previously we reported on the data obtained at American Samoa over the period 1983-1987 [*Savoie et al.*, 1989*a,b*]. The seasonal trends that we observe in the current data set are consistent with those observed in our earlier papers; hence, we assume that the conclusions reported at that time are still valid. In particular, we presented evidence that suggested that the period of high nitrate concentrations might be associated with transport from South America; this evidence included seasonal trends in isentropic trajectories and the fact that nitrate was highly correlated with 210Pb. In the case of nss-sulfate, the strong correlation with MSA suggests that oceanic sources are dominant.

3. References

Elkins, J.W., and R.M. Roson (Eds.), *Geophysical Monitoring for Climatic Change, No. 17: Summary Report 1988*, 142 pp., NOAA Climate Monitoring and Diagnostics Laboratory, Boulder, CO, 1990.

Ferguson, E.E., and R. M. Rosson (Eds.), *Climate Monitoring and Diagnostics Laboratory, No. 19: Summary Report 1990*, 133 pp., NOAA Climate Monitoring and Diagnostics Laboratory, Boulder, CO, 1991.

Savoie, D.L., J.M. Prospero, and E.S. Saltzman, Nitrate, non-seasalt sulfate and methanesulfonate over the Pacific Ocean, in *Chemical Oceanography, 10*, edited by J.P. Riley, R. Chester and R.A. Duce, pp. 219-250, Academic Press, London, 1989.

Savoie, D.L., J.M. Prospero, J.T. Merrill and M. Uematsu, Nitrate in the atmospheric boundary layer of the tropical South Pacific: Implications regarding sources and transport, *J. Atmos. Chem. 8*, 391-415, 1989.

USGS Barrow Observatory

JACK TOWNSHEND
U.S. Geological Survey, College Observatory, Fairbanks, Alaska 99775-5160

The USGS Barrow Observatory is the northernmost of this agency's 13 continuously recording, digital magnetic observatories. As such, it serves as a singularly important site in a global network of observing stations, whose combined data define the planetary magnetic field and track its secular change. Ground stations such as at the Barrow Observatory are controls for field modeling by harmonic analysis, essential reference stations for airborne and satellite surveys, and absolute calibration locations for field survey instrumentation. The observatory is operated from the USGS College Observatory at the University of Alaska in Fairbanks as a satellite station. Staff scientists from the College Observatory visit the site bimonthly to make absolute observations, perform routine equipment maintenance, and retrieve data on magnetic tape. Staff personnel from NOAA CMDL make weekly visits to the site to check equipment operation and occasionally perform emergency service when there is a problem and a College Observatory staff person is not available to make repairs.

The primary equipment used to acquire the magnetic data is an EDA FM-100-BR Triaxial fluxgate magnetometer, an EDA PPM-105 proton free-precession magnetometer, an observatory magnetometer interface system, and several pier-mounted instruments for absolute control observations. Data are retrieved by telephone periodically through a computer modem by the USGS office in Golden, Colorado. A seismograph is operated on site in a vault located 6.1 m beneath the ground surface. The present seismic program is operated in cooperation with the Geophysical Institute at the University of Alaska, Fairbanks.

The USGS Barrow Observatory has been in continuous operation since 1949.

Radon Daughter Measurements at MLO for Fast Radon Determination and Evaluation of Dry Deposition

S. WHITTLESTONE
Australian Nuclear Sciences & Technology Organisation, Menai, N.S.W. 2234, Australia

S.D. SCHERY AND RONG WANG
New Mexico Tech, Socorro, New Mexico 87801

1. INTRODUCTION

Radon has been established as a means of evaluating the degree of recent continental contact of air parcels sampled at baseline observatories [*Gras et al.*, 1992, *Whittlestone et al.*, 1992]. One problem with detectors of radon gas is that they are inherently slow, with a response time of the order of an hour. This is too slow for real-time control of samplers. At Cape Grim this problem has been circumvented by measuring the decay products of radon (radon daughters), which can be determined much more quickly than radon itself [*Whittlestone*, 1992]. In order to derive an estimate of the radon concentration, it is necessary to multiply the radon daughter concentration by an empirically determined equilibrium factor, F(CN), of the condensation nucleus concentration (CN). F is scaled to be unity when the daughters are in equilibrium with radon. This function depends on the rate of loss of radon daughters to surfaces such as the sea or land within the previous 2 hours. The absence of sea close to MLO and the possibility of air reaching the station with very little contact with land, means that the loss rate should be less at MLO than at Cape Grim. One motivation for the present study was, therefore, to measure the relationship between radon, radon daughters and CN at MLO.

A great deal more can be learned about the atmosphere from radon daughter measurements than the equilibrium factor, F(CN), referred to above. The loss of radon daughters is one facet of the phenomenon of dry deposition, and depends on air motions on scales from a kilometer to a fraction of a millimeter. One valuable feature of radon daughters is that they are present in the atmosphere in two forms with very different diffusion coefficients: reactive atoms, immediately after being formed from their parent nuclei; and attached to CN, in which case their transport and loss represents that of the CN superimposed on the radioactive decay. The first, "unattached" form lasts until the daughter either becomes attached to a condensation nucleus, is lost to the ground or decays.

Another convenient feature of the radon daughters is that their half lives are about 20 minutes. Thus land or sea more than 2 hours upwind of the sample has virtually no effect on the radon daughter concentration.

The study of radon daughter concentrations is best pursued by modeling the atmosphere in terms of measurable quantities [*Schery*, 1991] and comparing experimental results with the theory. Application of Schery's computer code shows that the concentration gradients of attached and unattached daughters, between a few mm and a few meters of the surface, can provide severe constraints on parameters of the dry deposition model. Measurement of these gradients was, therefore, a key part of the experiment. In this report only the results of measurements at MLO will be presented.

2. EQUIPMENT

The technique for the radon daughter measurement was to first draw air at about 400 L min^{-1} through a wire screen, to which the unattached daughters diffused, then through a Gelman type AE filter where the remaining attached daughters were caught. After sampling for 18 minutes, the filter and screen were transferred to computer controlled counters that recorded the gross alpha particle count in each 5-minute interval for the next hour. Two systems were operated, recording data from the top of the 40 m tower and 0.05 m above the ground. The flow rates were monitored by reading the pressure drop across an orifice, previously calibrated at the altitude of MLO. Calibration of the alpha counters was by means of a standard source, inserted before the start of measurements each day.

Other data recorded were from the MLO existing equipment, including temperatures at three heights, wind speed and direction at two heights, CN and radon. Some care has to be taken in interpretation of comparison of the daughter and radon results because the former represented an average over 20 minutes, while the latter were hourly averages smoothed by the instrument response time of 90 minutes.

3. RESULTS

The radon, radon daughter and CN measurements are given in Table 1 together with a subset of the meteorological data. As can be expected in such a short study, some of the common types of weather were not represented: upslope conditions never occurred with CN close to 1000 cm^{-3}; there were no periods of high radon from the free troposphere. Even so, some of the trends apparent in this data set are considered to be generally applicable.

The average equilibrium factor, F, on the tower was 0.57, markedly higher than the value of 0.45 found in the marine boundary layer at Cape Grim [*Whittlestone*, 1990] for similar CN concentrations. From this we infer that the loss of daughters to land or sea is less at MLO than at a coastal site.

A consequence of the lower daughter losses as air parcels approach MLO, is the marked difference between the daughter measurements on the tower and the ground, particularly in the unattached fractions. At MLO, high proportions of the unattached daughters at 40 m often remain in the air for tens of minutes and are not lost to the local land. It is only very close to the ground that the effect of loss to the surface is apparent. By contrast, at Cape Grim the unattached fractions at both ground level and 165 m were very low, which indicated turbulence taking the daughters from 165 m to contact the sea on time scales of a few minutes.

More insight to the processes governing the radon daughter concentrations can be gained by considering the dependence of the equilibrium factor, F, and the unattached fraction on CN concentration, as shown in Figure 1. The error bars indicate one standard deviation

TABLE 1. Radon Daughter, Radon and CN Concentrations, and Meteorological Data

TIME hour of day	DATE Apr. 1992	CN cm^{-3}	40 m WIND		DEW Pt. C	DIF. TEMP C	Daughters nJ m^{-3}		Rn mBq m^{-3}	Clas	Unattached Fraction		F
			DIR. deg	VEL. m/s			T	G			T	G	T
15	13	147	284	5.7	1.7	-1.4	.66	.35	146	DB	.41	.06	.80
16		120	266	6.0	0.9	-1.2	.23	.20	108	DB	.26	.10	.38
17		121	248	6.3	1.3	-1.2	.20	.21		DB	.15	.10	
18		98	254	8.1	1.0	-0.8	.34	.28	106	DB	.18	.11	.57
19		230	270	5.3	0.8	-0.6	.32	.19	105	DB	.34	.05	.54
20		138	265	5.0	1.2	-1.0	.21	.06	95	DB	.67	.17	.39
18	14	379	284	4.2	0.2	-0.8	.67	.70	160	DB	.39	.11	.75
19		243	287	3.6	0.6	-0.5	.71	.70	151	DB	.24	.17	.83
13	15	371	308	6.1	3.8	0.2	1.08	.97	334	UB	.12	.06	.58
14		295	296	5.1	5.3	-3.1	.78	.74	226	UB	.13	.04	.61
15		218	284	4.1	5.8	-3.0	.76	.53	210	DB	.17	.09	.64
16		240	322	4.1	2.9	-3.0	.96	.65	182	UB	.07	.03	.94
17		214	328	2.1	2.4	-1.6	.96	.76	200	UB	.06	.08	.85
18		196	339	2.6	1.2	-1.4	.35	.84	256	UB	.23	.10	.24
19		173	150	0.7	0.8	-0.6	.96	.70	271	DB	.06	.04	.63
20		157	232	0.4	7.7	0.9		.45	272	DB		.11	
21		154	297	1.0	10.8	1.2	.45	.27	232	UB	.29	.11	.35
22		145	225	1.0	9.2	1.6	.38	.23	208	DB	.24	.09	.32
23		140	133	1.0	5.7	2.2	.56	.32	202	DB	.25	.13	.49
17	16	161	326	2.0	2.2	-1.6	.64	.58	206	UB	.16	.05	.55
18		146	360	0.8	2.5	-1.3	1.0	.76	247	UB	.11	.07	.72
19		189	152	0.2	2.8	-0.1	.95	.54	264	DB	.26	.15	.64
20		177	165	0.7	-2.1	0.9	.96	.45	256	DB	.34	.11	.66
21		174	121	2.3	-5.1	1.4	.5	.35	221	DF	.36	.14	.40
22		142	133	4.8	-12	1.7	.36	.18	214	DF	.56	.11	.30
23		140	182	3.6	-12	2.7	.58	.29	182	DF	.31	.07	.57

"T" = Tower, "G" = Ground

"Clas" = wind and dewpoint classification:

"U" = upslope wind sector (292.5 through north to 67.5);

"D" = downslope (non-upslope) wind sector;

"B" = significant boundary layer influence indicated by dewpoint >-5°C;

"F" = free tropospheric air indicated by dewpoint < -5°C.

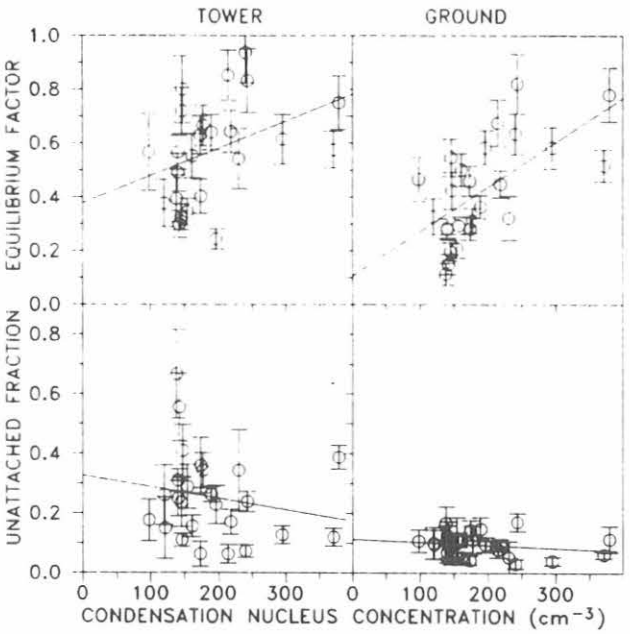

Fig. 1. Equilibrium factor and fraction of radon daughters not attached to CN, versus CN concentration (cm^{-3}) at 40 m on the tower and at ground level.

of the counting errors. Additional errors not shown are the systematic absolute calibration errors, which have been estimated to be 15%, and the effect of the different time response of the radon and radon daughter detectors.

It is evident from Figure 1 that F is positively correlated with CN. In other words, when there are more CN, fewer radon daughters are lost. This proves that the air parcels at MLO, even at the 40 m tower, are brought close enough to the land or sea for the daughters to be lost on a time scale of the order of half an hour.

The unattached fractions shown in Figure 1 are of interest not only because they illustrate the strong difference between the tower and ground on loss of unattached daughters, but also because it is apparent that only a small part of the variability of the unattached fraction is related to CN concentration. There are three processes governing the loss of unattached daughters: decay, which is constant; attachment to CN; and loss by dry deposition. Figure 1 indicates that CN has only a small effect, implying that dry deposition is the predominant cause of variability. The slight decrease of the unattached fraction with increasing CN is expected because, in the absence of other causes of variation, the unattached fraction will decrease monotonically from unity at zero CN to zero for infinite CN.

As noted above, there is a marked difference between the unattached daughter concentrations on the tower and on the ground. A quantitative measure of this is the ratio of the average of the unattached daughter concentrations at 40 m to that at ground level: 3.3 ± 0.6. For the attached daughters with their much lower diffusion coefficient, the ratio was 1.07 ± 0.18, which was not statistically different from unity.

4. Conclusions

Measurements of the relationship between radon, radon daughters and CN on the 40 m tower have demonstrated that it would be feasible to obtain moderately accurate estimates of radon concentration from radon daughter measurements. The estimate could be considerably improved by estimating the equilibrium factor from concurrent measurements of CN. An instrument similar to one deployed at Cape Grim would provide a radon estimate with a standard deviation of about 30% each 20 minutes.

Concentration gradient measurements between ground and 40 m have provided data suitable for verification of dry deposition models. Elementary analysis has shown that species as large as CN experience very little effect from the proximity of the ground. An appreciable fraction of smaller species such as the ion clusters that constitute radon daughters, do reach the 40 m tower. However, most of these are lost by dry deposition before they reach a sampling point at ground level.

By comparing the present results with measurements at Cape Grim, we conclude that loss of small ion clusters by dry deposition at the 40 m site at MLO is much less than at a coastal sampling point at 165 m.

Acknowledgments. The authors are grateful to NOAA/CMDL for providing the laboratory space and technical support for this work. The work would not have been possible without the support of the technical staff of the radon group at ANSTO. The help of Ken Eak at MNIMT in equipment preparation was much appreciated.

5. References

Gras, J.L., and S. Whittlestone, Radon and CN: complementary tracers of polluted air masses at coastal and island sites, *J. Radioanal. Nucl. Chem.*, Vols. 160 and 161, in press, 1992.

Schery, S.D., and R. Pout, A computer code for calculating the steady-state vertical distribution of radon progeny outdoors, ANSTO/E702, ISSN 1030-7745, ISBN 0 642 599173, 1991.

Whittlestone S., Baseline selection in real time using Radon, Baseline 89, available from Cape Grim Baseline Air Pollution Station, P.O. Box 346, Smithton, TAS 7300, Australia, 1992.

Whittlestone, S., E. Robinson, and S. Ryan, Radon at the Mauna Loa Observatory: Transport from distant continents, *Atmos. Environ., 26A(2)*, 251-260, 1992.

Whittlestone, S., Radon daughter disequilibria in the lower marine boundary layer, *J. Atmos. Chem., 11*, 27-42, 1990.

8. International Activities, 1991

The first meeting of the Atmospheric Chemistry Project under the U.S.-Brazil Science and Technology Bilateral Agreement in Sao Jose dos Campos, Brazil, was attended by E. Ferguson in May 1991. The CMDL program was outlined with a point of interest in obtaining CO_2 and other trace gas measurements from Amazonia. He expressed a willingness to cooperate in various ways in order to enable Brazilian scientists to tie into internationally recognized concentration standards maintained by CMDL.

In October, E. Ferguson and D. Endres attended the Annual Meeting of the Cape Grim Baseline Air Pollution Station in Smithton, Tasmania. E. Ferguson also visited and presented a paper at CSIRO in Melbourne, Australia.

J. Peterson was invited by the Mexican government to participate in a workshop on "Climate Change in the Mexican Tropics," held at Cancun, Mexico, in April. The focus of the workshop was on the development of environmental monitoring strategies for the region. In May, he traveled to Toronto, Canada, to serve as an invited member of the peer review panel of the Canadian Baseline Monitoring Program. The panel prepared a comprehensive report of the Program along with a list of recommendations. In August, he traveled to Helsinki, Finland, where he participated in a WMO-sponsored working group reviewing the global climate system for 1989-1991. He contributed two sections on trace gas and aerosol trends to the final document summarizing the global climate and its variability during the period.

In June, R.C. Schnell and P.J. Sheridan were members of the NCAR Electra science crew for the Kuwait oil-fire study operating out of Bahrain, Arabian Gulf. They oprated the NOAA 3-λ nephelometer, the airborne smoke aethalometer, and collected aerosol filter and gas flask samples of the oil fire smoke.

In July 1991, L. Waterman traveled to Singapore to join the Chevron refined products carrier, *M/V Carla A. Hills* to initiate the regular collection of air samples in the South China Sea. Samples are collected in evacuated 2.5-L flasks at every 3° of latitude on runs between Singapore and Hong Kong and return.

Fourteen pairs of samples were collected between July 5-8 (northbound) and July 10-14 (southbound) on the inaugural voyage of this program. A total of 358 samples were collected through the first 6 months of the program (December 31) by the vessel's deck officers.

Following the completion of the round-trip voyage, L. Waterman visited six shipping companies in Singapore as part of a feasibility study of sampling from commercial vessels in the Bay of Bengal on runs between Singapore and Calcutta and/or Chittagong. There were as many different shipping operations as companies contacted. It appears any cooperative sampling program would be very complicated or impossible to sustain.

In some cases the Bay of Bengal run is only a small portion of a much more extensive voyage, so few samples could be collected in the area of interest.

The idea of having a scientist making all or part of a voyage to train the sample-takers was met with resistance or outright rejection in every case.

The absence of a "core crew" and the complexity of crew rotation would make it very difficult to pass on the principles and technique of sampling without unwanted changes. It is likely there would also be language difficulties in some cases.

The Indian High Commission was also visited seeking information on the Andaman Islands in the eastern side of the Bay of Bengal as a possible air sample site. Very little information is available. Administered by India, the islands are accessible by air and ship from the Indian mainland. Logistics would be a major problem and the best exposures, on the west side are mainly populated by primitive tribal groups. It is most unlikely a sampling program could be initiated there without sponsorship of a college, university, or government agency such as the meteorological service and a visit by NOAA personnel.

On July 24-26, L. Waterman traveled to Cheongwon, South Korea, to visit Prof. Yong S. Chung at the Korea National University of Education (KNUE) and to inspect the new NOAA sampling network site at Tae-ahn Peninsula on the west coast, about 140 km from the university. Air samples were collected under typical conditions. A meeting was held with local teachers in a primary school adjacent to the sampling site. Prof. Chung arranged for one of the teachers to collect samples on some weeks so as to reduce the time needed for KNUE students to travel to and from the site. It was agreed the Carbon Cycle Division would provide a second MAKS unit and would look into ways to cut the cost of shipping the samples from Korea to the United States.

In July, E. Dlugokencky traveled to the Mongolian Peoples Republic as a member of an American delegation organized by the U.S. Department of State, Office of Cooperative Science and Technology. He first met with personnel from the Mongolian Hydrometeorological Research Institute in Ulaanbaatar and discussed a proposal for setting up a cooperative flask sampling program in the Gobi Desert. Later the delegation traveled to the proposed sampling site near the village of Ulaan Uul. The principal contact for the air sampling discussions was D. Dagvadorj. Accomplishments of this trip include agreements to

translate sampling instructions into Mongolian, begin work on a logistics plan for getting flasks in and out of the country, and a pledge to work out a training visit to Boulder for one of the Mongolian staff members.

The program to bring flask sampling network personnel to Boulder for training and consultation was continued. A. Glasspool, AEROCE, Bermuda Biological Station, visited the Carbon Cycle Division April 4-8. B. Sargeant, AES, Environment Canada, visited April 24-28 while on a furlough from the Mould Bay, N.W.T., Canada Weather Station. The visits continued with G. Spain, AEROCE, University College Atmospheric Research Station (Mace Head), Ireland, May 16-21; and R. Juega, Izaña Observatory, Tenerife, Canary Islands, Spain, August 25-29.

D. Dagvadorj, Mongolian Hydrometeorological Research Institute came to Boulder October 8-19 for training and wide-ranging talks about the Ulaan Uul sampling.

With cooperation from C. Burkle, Physical Science Laboratory, New Mexico State University, D. Patnode came to Boulder on December 16-17 prior to departing for Mahé, Seychelles.

In most instances, sampling site personnel hand carried MAKS back to their respective sampling sites. In some cases this deployment was in connection with adding new sites to the network; in others, it was the opportunity to upgrade sampling procedure.

B. Bodhaine visited Sable Island, Canada, and Bermuda in June to perform site surveys in preparation for the installation of aerosol monitoring instrumentation. In October he visited Florence, Italy, to present a paper entitled "Aerosol measurements at four baseline stations" for the Organization for New Technologies, Energy, and Environment, and then in Orvieto, Italy, presented a paper entitled "The U.S. aerosol monitoring program in Antarctica" at the Italian Workshop on Antarctic Atmosphere. Both B. Bodhaine and J. Ogren visited Atmospheric Environment Service in Toronto, Canada, in December to plan the construction of an atmospheric measurement station on Sable Island.

J. DeLuisi participated in a Global Baseline Surface Radiation Network (GBSRN) IR instrumentation workshop at Toronto, Canada, in April. In June, he continued collaboration work on analysis of Lidar measurements of the El Chichon dust cloud and SAGE II measurements in Rome/Frascati, Italy, and prepared a report on Umkehr results for the United Nations Environment Program in Geneva, Switzerland. During August, J. DeLuisi and E. Dutton visited Davos, Switzerland, to participate in the Baseline Surface Radiation Network (BSRN) Network Implementation Progress Review. They then traveled to Vienna, Austria, to participate in the International Association of Meteorology and Atmospheric Physics (IAMAP) Symposium.

D. Hofmann traveled to Stockholm and Kiruna, Sweden, in January as part of an experiment/cooperative research program with the University of Wyoming and the Max Planck Institute for Nuclear Physics, to study the relationship of stratospheric water vapor, nitric acid vapor, and polar stratospheric clouds in Arctic ozone depletion. In August, he continued his research collaboration with Dr. H. Jager on Lidar for the Network for the Detection of Stratospheric Change (NDSC) in Garmisch, Germany. He also presented three papers at the International Union of Geodesy and Geophysics (IUGG) Symposium in Vienna, Austria.

CMDL was represented at the annual meeting of AEROCE (Atmosphere-Ocean Chemistry Experiment) in Bermuda by D. Hofmann and S. Oltmans. S. Oltmans took advantage of his time in Bermuda by maintaining and calibrating the surface ozone equipment at the AEROCE field site there.

J. Ogren traveled to Bologna, Italy, in October, where he attended a workshop of EUROTRAC sub project GCE, chaired two sessions, and presented two papers.

S. Oltmans participated in an International Ozonesonde Intercomparison in Saskatoon, Canada, in May. In September, he visited Reykjavik, Iceland, to install surface ozone monitoring instrumentation and train personnel in station operation. In November, he presented a report on surface ozone data, their analysis, and related issues to a meeting of experts sponsored by the World Meteorological Organization (WMO).

J. Wendell traveled to the South Pole for the last 3 months of the year to assist in winterover 1990-1991 crew changeover, help set up ozone experiments, make ozonesonde flights, and maintain CMDL instruments during the Clean Air Facility roof replacement.

J. Elkins, T. Gilpin, G. Holcomb, T. Baring, J. Lobert, and J. Butler participated in international study that included scientists from Iceland, Great Britian, Australia, France, and Canada during NASA's Airborne Arctic Stratosphere Expedition-2 (AASE-2) from August through December 1991 by measuring atmospheric CFC-11 and CFC-113 aboard the ER-2 aircraft from Moffett Field, CA, Fairbanks, AK, and Bangor, Maine.

W. Sturges traveled to Resolute Bay, Canada, to make measurements of biogenic halocarbon emissions from Arctic sea ice algae, hosted by the Canadian Government's Polar Continental Shelf Project.

9. Publications and Presentations by CMDL Staff, 1991

Barrie, L.A., B.A. Bodhaine, R.C. Schnell, and G.A. Shaw, *Antarctic Tropospheric Chemistry Research*, Report of the International Symposium on the Tropospheric Chemistry of the Antarctic Region, June 3-6, 1991, Boulder, Colorado, NOAA Meetings Report, 20 pp., Boulder, Colorado, November 1991,

Bodhaine, B.A., Long-term aerosol measurements at the South Pole, paper P2.1 presented at the Symposium on the Tropospheric Chemistry of the Antarctic Region, June 3-6, 1991, Boulder, Colorado, 1991.

Bodhaine, B.A., The U.S. aerosol monitoring program in Antarctica, paper presented at the Fourth Workshop on Italian Research on Antarctic Atmosphere, October 21-23, 1991, Porano, Italy, 1991.

Bodhaine, B.A., and A.D.A. Hansen, Aerosol scattering and absorption measurements during DUNE in the Southern Soviet Union, Paper A51B-02 presented at the Fall American Geophysical Union Meeting, San Francisco, California, December 9-13, 1991.

Bodhaine, B.A., N.C. Alquist, and R.C. Schnell, Three-wavelength nephelomter suitable for aircraft measurement of background aerosol scattering coefficient, *Atmos. Environ. 25A(10)*, 2267-2276, 1991.

Bodhaine, B.A., L.A. Barrie, and R.C. Schnell, Antarctic tropospheric chemistry research, Report of the International Symposium on the Tropospheric Chemistry of the Antarctic Region, June 3-6, 1991, 20 pp., Boulder, Colorado, November 1991.

Bodhaine, B.A., J.J. DeLuisi, J.F. Boatman, Y. Kim, D.L. Wellman, R.L. Gunter, M.J. Post, R.E. Cupp, T. McNice, J.M Rosen, P.J. Sheridan, R.C. Schnell, D.M. Garvey, A.E. Wade, and R.G. Steinhoff, The second front-range lidar, aircraft, and balloon experiment, NOAA DR ERL CMDL-8, 142 pp., 1991.

Butler, J.H., The role of the ocean in regulating trace gases in the atmosphere, paper presented at Max Planck Institut für Chemie, Mainz, Germany, June 4, 1991.

Butler, J.H., and J.W. Elkins, An automated technique for the measurement of dissolved N_2O in natural waters, *Mar. Chem., 34*, 47-61, 1991.

Butler, J.H., and J.W. Elkins, Advances in measurement techniques for trace atmospheric gases, paper presented at the Gordon Research Conference on Atmospheric Chemistry, New Hampton, New Hampshire, June 16-21, 1991.

Butler, J.H, J.W. Elkins, and T.M. Thompson, Results of N_2O and halocarbon measurements on SAGA-2 and SAGA-3 and their significance, paper presented at Working Group VIII meeting joint US/USSR research for SAGA and DUNE programs, Leningrad, USSR. May 27-31, 1991.

Butler, J.H., J.W. Elkins, T.M. Thompson, B.D. Hall, T.H. Swanson, and V. Koropalov, Negative saturation anomalies of CH_3CCl_3 in the open ocean: Implications for tropospheric OH, paper presented at the Tenth International Symposium on Environmental Biogeochemistry, San Francisco, California, August 19-23, 1991.

Butler, J.H., J.W. Elkins, T.M. Thompson, B.D. Hall, T.H. Swanson, and V. Koropalov, Oceanic consumption of CH_3CCl_3: Implications for tropospheric OH, *J. Geophys. Res., 96, 22*,347-22,355, 1991.

Cahill, T., J. Schweitzer, K. Wilkinson, R.C. Schnell, J. Reid, R. Eldred, and R. Flocchini, Comparison of the physical and chemical characteristics of Kuwaiti smoke and smoke from Kuwaiti oils, *EOS, 72*, 81, 1991.

Cess, R.D., E.G. Dutton, J.J. DeLuisi, and F. Jiang, Determining surface solar absorption from broadband satellite measurements for clear skies: Comparison with surface measurements, *J. Climate, 4(2)*, 236-247, 1991.

Cook, E., T. Bird, M. Peterson, M. Barbetti, B. Buckley, R.D'Arrigo, R. Francey, and P. Tans, Climatic change in Tasmania inferred from a 1089-year tree-ring chronology of huon pine, *Science, 253*, 1266-1268 1991.

Cummings, S.O., T.M. Thompson, B.D. Hall, J.W. Elkins, J.H. Butler, T. Swanson, and M. Losleben, Atmospheric halocarbon and N_2O concentrations at Niwot Ridge, Colorado, paper presented at American Geophysical Union Front Range Meeting, Boulder, Colorado, February 11-12, 1991.

DeLuisi, J., R. Haas, E. Dutton, D. Nelson, R.C. Schnell, P. Reddy, D. Longenecker, and T. McNice, Aerosol and radiation characteristics of smoke from the Yellowstone fire of 1988, paper presented at the XX General Assembly, IUGG, Vienna, Austria, August 11-24, 1991.

Deshler, T., and D.J. Hofmann, Ozone profiles at McMurdo Station, Antarctica, the austral spring of 1990, *Geophys. Res. Lett., 18(4)*, 657-660, 1991.

Dutton, E.G., A coherence between the QBO and the amplitude of the Mauna Loa atmospheric transmission annual cycle, paper presented at the IUGG/IAMAP Bi-Annual Meeting, Vienna, Austria, August 11-14, 1991.

Dutton, E.G., Radiation measurements at U.S. global background sites, paper presented at the Second WMO Workshop on the Implementation of the Baseline Surface Radiation Network, Davos, Switzerland, August 1991.

Dutton, E.G., and D.J. Endres, Date of snowmelt at Barrow, Alaska, U.S.A., *Arctic Alpine Res., 23(1)*, 115-119, 1991.

Dutton, E.G., R.S. Stone, D.W. Nelson, and B.G. Mendonca, Recent interannual variations in solar radiation, cloudiness, and surface temperature at the South Pole, *J. Climate, 4*, 848-858, 1991.

Elliott, W.P., J.K. Angell, and K.W. Thoning, Relation of atmospheric CO_2 to tropical sea and air temperatures and precipitation, *Tellus, 43B*, 144-155, 1991.

Elkins, J.W., Current update on atmospheric nitrous oxide (N_2O), CFC's, and the replacement CFC's or HCFC's, invited talk at the NCAR Atmospheric Chemistry Summer Course, Boulder, Colorado, June 10, 1991.

Elkins, J.W., Recent ocean and aircraft measurement of atmospheric CFCs, invited talk for the Center for Earth and Planetary Physics, Harvard University, Cambridge, Massachusetts, November 17, 1991.

Elkins, J.W., J.H. Butler, and T.M. Thompson, Uncertainties in the global atmospheric nitrous oxide budget, paper presented at the Tenth International Symposium on Environmental Biogeochemistry, San Francisco, California, August 19-23, 1991.

Elkins, J.W., T.M. Thompson, and T. H. Swanson, Nitrous oxide and halocarbon measurements from NOAA/CMDL observatories, invited talk at the Fourth Meeting of AGAGE, MIT Endicott House, Boston, Massachusetts, November 17-20, 1991.

Elkins, J.W., J.H. Butler, T.M. Thompson, B.D. Hall, and T.H. Swanson, Measurements of nitrous oxide and chlorofluorocarbons by in-situ gas chromatography and from flask samples collected at South Pole, invited talk at the Symposium on the Chemistry of the Antarctic Region, Boulder, Colorado, June 3-5, 1991.

Ferguson, E.E., Ion chemistry of the middle atmosphere, in *The Middle Atmosphere and Space Observations*, Cépaduès-Editions, Toulouse, France, 355-371, 1991.

Ferguson, E.E., Laboratory measurements of relevant middle atmosphere reaction rate constants, in *The Middle Atmosphere and Space Observations*, Cépaduès-Editions, Toulouse, France, 355-371, 1991.

Ferguson, E.E., and R.M. Rosson (Eds.), *Climate Monitoring and Diagnostics Laboratory No. 19: Summary Report 1990*, 133 pp., NOAA Environmental Laboratories, Boulder, CO, 1991.

Fiocco, G., D. Fuà, M. Cacciani, P. DiGirolamo, and J. DeLuisi, On the temperature dependence of polar stratospheric clouds, *Geophys. Res. Lett., 18(3)*, 424-427, 1991.

Gobbi, G.P., T. Deshler, A. Adriani, and D.J. Hofmann, Evidence for denitrification in the 1990 Antarctic spring stratosphere: I, lidar and temperature measurements, *Geophys. Res. Lett., 18(11)*, 1995-1998, 1991.

Gunter, R.L., J. Boatman, R.C. Schnell, A.D.A. Hansen, High-resolution measurements of aerosol black carbon from an instrumented light aircraft, Proceedings, 4th International Soot Carbon Conference, Vienna, Austria, April 3-5, 1991.

Hall, B.D., J.W. Elkins, J.H. Butler, T.M. Thompson, and C.M. Brunson, Improvements in nitrous oxide and halocarbon measurements at the South Pole, *Ant. J. U. S., 25(5)*, 252-253, 1991.

Hansen, A.D.A., and B.A. Bodhaine, Aerosol black carbon measurements at South Pole Observatory: Identification of long-range aerosol transport events, paper 2.7 presented at the Symposium on the Tropospheric Chemistry of the Antarctic Region, June 3-6, 1991, Boulder, Colorado, 1991.

Harris, J.M., P. Tans, E. Dlugokencky, K. Masarie, P. Lang, S. Whittlestone, and L.P. Steele, Variations in atmospheric methane at Mauna Loa Observatory related to long-range transport, paper presented at 1991 American Geophysical Union Fall Meeting, San Francisco, December 9-13, 1991.

Herbert, G.A., Interannual changes in northern hemispheric tropospheric temperature 1960-1989, in *International Conference on the Role of the Polar Regions in Global Change: Proceedings of a Conference Held June 11-15, 1990, at the University of Alaska, Fairbanks*, G. Well, C.L. Wilson, and B.A.B. Severin (eds.), Geophysical Institute, University of Alaska Fairbanks and Center for Global Change and Arctic System Research, 159-163, 1991.

Hofmann, D.J., Atmospheric aerosols in climate and global change, paper presented at the National Science Foundation Workshop on Clouds, Radiation, Aerosols, and Hydrology, Silver Spring, Maryland, January 25, 1991.

Hofmann, D.J., Global stratospheric changes, paper presented at the University of Wyoming Seminar-Workshop on Global Change, Laramie, February 27, 1991.

Hofmann, D.J., Measurement of sulfuric acid aerosol in the wake of stratospheric aircraft, paper presented at XX General Assembly of the International Union of Geodesy and Geophysics, Vienna, Austria, August 19, 1991.

Hofmann, D.J., Monitoring the vertical distribution of atmospheric aerosols at Laramie, Wyoming, 1971-1991, presented at XX General Assembly of the International Union of Geodesy and Geophysics, Vienna, Austria, August 20, 1991.

Hofmann, D.J., Aerosol, ozone, and water vapor measurements in the Pinatubo plume, presented at the Interagency Technical/Programmatic Review of Research on the Pinatubo Eruptions, September 11, 1991, Washington, D.C., 1991.

Hofmann, D.J., Depletion of ozone over Antarctica, paper presented at the American Geophysical Union Chapman Conference on Auroral Plasma Dynamics, Minneapolis, Minnesota, October 21-25, 1991.

Hofmann, D.J. and T. Deshler, Stratosphere ozone profile measurements in the Arctic winter: evidence for chemical depletion, presented at XX General Assembly of the International Union of Geodesy and Geophysics, Vienna, Austria, August 17, 1991.

Hofmann, D.J., S.J. Oltmans, and T. Deshler, Simultaneous balloonborne measurements of stratospheric water vapor and ozone in the polar regions, *Geophys. Res. Lett., 18(6)*, 1011-1014, 1991.

Hofmann, D.J., T. Deshler, B. Johnson, and W.R. Rozier, Balloonborne measurements of the Pinatubo aerosol, paper presented at the 1991 American Geophysical Union Fall Meeting, San Francisco, California, December 9-13, 1991.

Hogan, A.W., B.A. Bodhaine, T. Conway, and A.D.A. Hansen, Covariation of some components of the Antarctic troposphere, paper P5A.9 presented at the Symposium on the Tropospheric Chemistry of the Antarctic Region, June 3-6, 1991, Boulder, Colorado, 1991.

Hopper, J.F., H.B. Ross, W.T. Sturges, and L.A. Barrie, Regional source discrimination of atmospheric aerosols in Europe using the isotopic composition of lead, *Tellus, 43B*, 45-60, 1991.

Kahl, J., P. Sheridan, and R.C. Schnell, Real-time forecasting of atmospheric debris transport, paper presented at the NATO/CCMS, International Technical Meeting. on Air Pollution Modeling and Applications, Athens, Greece, September 1991.

Kahl, J., R.C. Schnell, P.J. Sheridan, B.D. Zak, H.W. Church, A.S. Mason, J.L. Heffter, and J.M. Harris, Predicting atmospheric debris transport in real-time using a trajectory forecast model, *Atmos. Environ., 25(8)*, 1705-1713, 1991.

Komhyr, W.D., The adequacy of ozone measurements for monitoring regional and global ozone concentrations, paper presented at a Meeting of the Climate Research Committee, Board of Atmospheric Science, National Academy of Sciences, Irvine, California, April 29, 1991.

Komhyr, W.D., Possible influence of long-term sea-surface temperature anomalies in the tropical Pacific on global ozone, paper presented at the Spring American Geophysical Union Meeting, Baltimore, Maryland, May 29, 1991.

Komhyr, W.D., Dobson spectrophotometer observations: Corrections to existing records, paper presented at the International Dobson Instrument Data Workshop, Lanham, Maryland, September 11-13, 1991.

Komhyr, W.D., J. Wendell, and J.A. Lathrop, ECC ozonesonde observations at Pt. Barrow, Alaska, during January 16-April 19, 1989, NOAA DR ERL-CMDL-7, 155 pp., 1991.

Komhyr, W.D., S.J. Oltmans, R.D. Grass, and R.K. Leonard, Possible influence of long-term sea surface temperature anomalies in the tropical Pacific on global ozone, *Can. J. Phys., 69*, 1093-1102, 1991.

Kopcewicz, B., C. Nagamoto, F. Parungo, J. Harris, J. Miller, H. Sievering, and J. Rosinski, Morphological studies of sulfate and nitrate particles on the East Coast of North America and over the North Atlantic Ocean, *Atmos. Res., 26*, 245-271, 1991.

Lipschultz, F., S.C. Wofsy, B.B. Ward, L.A. Codispoti, G. Friedrich, and J.W. Elkins, Bacterial transformations of inorganic nitrogen in the oxygen-deficient waters of the Eastern Tropical South Pacific Ocean, *Deep-Sea Res., 37(10)*, 1513-1541, 1990.

Lobert, J.M., Biomass burning in Cote d'Ivoire, Africa: Airborne measurements of CO, CO_2, NO_2, CH_4, an O_3 during

DECAFE 91, paper A22C-2 presented at the American Geophysical Union Fall Meeting, San Francisco, California, December 9-13, 1991.

Lobert, J.M., Biomass burning as a source of sulfur to the atmosphere, paper A22C-10 presented at the American Geophysical Union Fall Meeting, San Francisco, California, December 9-13, 1991.

Masarie, K.A., L.P. Steele, and P.M. Lang, A rule-based expert system for evaluating the quality of long-term, in situ, gas chromatographic measurements of atmospheric methane, NOAA TM ERL CMDL-3, 37 pp., 1991.

McPeters, R.D., and W.D. Komhyr, Long-term changes in the total ozone mapping spectrometer relative to world primary standard Dobson spectrophotometer 83, *J. Geophys. Res., 96(D2)*, 2987-2993, 1991.

Montzka, S.A., B.M. Hybertson, R.M. Barkley, and R.E. Sievers, Low temperature oxidation of $YBa_2Cu_3O_{6.0}$ with nitrogen dioxide, *J. Mater. Res., 6*, 891, 1991.

Montzka, S.A., M. Trainer, P.D. Goldan, W.C. Kuster, and F.C. Fehsenfeld, Methyl vinyl ketone and methacrolein during ROSE 1, paper presented at the American Geophysical Union 1991 Fall Meeting, , San Francisco, California, December 9-13, 1991.

Murphy, P.P., R.A. Feely, R.H. Gammon, K.C. Kelly, and L.S. Waterman, Autumn air-sea disequilibrium of CO_2 in the South Pacific Ocean, *Mar. Chem, 35*, 77-84, 1991.

Murphy, P.P., R.A. Feely, R.H. Gammon, D.E. Harrison, K.C. Kelly, and L.S. Waterman, Assessment of the air-sea exchange of CO_2 in the South Pacific during austral autumn, *J. Geophys. Res., 96(C11)*, 20,455-20,465, 1991.

Nelson, D., and J. Hickey, The evolution/modification of NOAA SOLRAD network tracker 1986-1991, *Solar World Congress*, Proceedings of the Biennial Congress of the International Solar Energy Society, Vol. 1, Pt. 2, Denver, Colorado, August 19-23, 1991, edited by M.E. Arden, S.M.A. Burley, and M. Coleman, Pergamon Press, New York, 1089-1092, 1991.

Novelli, P.C., J.W. Elkins, and L.P. Steele, The development and evaluation of a gravimetric reference scale for measurements of atmospheric carbon monoxide, *J. Geophys. Res., 96(D7)*, 13,109-13,121, 1991.

Novelli, P.C., J.W. Elkins, and L.P. Steele, The development of a gravimetric reference scale for measurements of atmospheric carbon monoxide and implications for tropospheric CO concentrations, *J. Geophys. Res., 96 (D7)*, 13,109-13,121, 1991.

Ogren, J.A., B.A. Bodhaine, J.M. Harris, and D.J. Hofmann, Detection of Kuwait smoke particles at Mauna Loa Observatory, paper A21A-11 presented at the Fall American Geophysical Union Meeting, San Francisco, California, December 9-13, 1991.

Ogren, J.A., Measurements of the size-dependence of the scavenging efficiency of aerosol particles in fog, presentation to the NOAA Aeronomy Laboratory, Boulder, Colorado, December 1991.

Oltmans, S.A., Arctic ozone chemistry, in *Pollution of the Arctic Atmosphere*, W.T. Sturges (Ed.), Elsevier, Essex, England, 185-215, 1991.

Oltmans, S.J., D.J. Hofmann, T. DeFoor, M. Post, and T. Deshler, Balloonborne measurements of ozone and water vapor following the eruption of Pinatubo, paper presented at the 1991 American Geophysical Union Fall Meeting, San Francisco, California, December 9-13, 1991.

Parungo, F., C. Nagamoto, R.C. Schnell, and P. Sheridan, Analyses of aerosol samples collected during AGASP, IUGG Assembly, Vienna, Austria, August 11-24, 1991.

Parungo, F., C. Nagamoto, R.C. Schnell, P. Sheridan, and C. Zhou, Aerosol particles in Kuwait oil-fire plumes: their morphology, size distribution, and chemical composition, paper presented at the American Geophysical Union Fall Meeting, San Francisco, California, December 9-13, 1991.

Parungo, F., C. Nagamoto, B. Kopacwicz, J. Harris, Z. Mingyu, L. Naiping, and S. Hoyt, Geographic and temporal variations of sulfate aerosols over the Pacific Ocean, *Ocean Sci., 10(1)*, 47-72 1991.

Polissar, A.V., V.N. Kapustin, B.A. Bodhaine, and A.D.A. Hansen, Measurements of aerosol black carbon at Wrangel Island, USSR, and Barrow, Alaska: Estimates of the gradient and deposition to the ice surface, paper presented at the Fourth International Conference on Carbonaceous Particles in the Atmosphere, Vienna, Austria, April 3-5, 1991.

Schnell, R.C., Arctic Gas and Aerosol Sampling Program: Highlights, *Arctic Res., 5*, 14-16, 1991.

Schnell, R.C., Airborne black carbon measurements, paper presented at the GIV Aerosol Conference, Frankfurt, Germany, March 11-14, 1991.

Schnell, R.C., Bulk aerosol and individual particle black carbon measurements over the Southwestern United States, paper presented at the 4th International Soot Carbon Conference, Vienna, Austria, April 3-5, 1991.

Schnell, R.C., Seasonal and secular variations of tropospheric ozone in Antarctica, paper presented at the Antarctic Tropospheric Chemistry Meeting, Boulder, Colorado, June 1991.

Schnell, R.C., and S. Shiotoni, Soot emission from commercial aviation in a heavily traveled air corridor, paper presented at the 4th International Soot Carbon Conference, Vienna, Austria, April 3-5, 1991.

Schnell, R.C., J.F. Boatman, and A.D.A. Hansen, Building ventilation measured with a passive continuous soot carbon (aethalometer) technique, Proceedings, 10th Annual Meeting, AAAR, Traverse City, Michigan, October 1991.

Schnell, R.C., A.D.A. Hansen, and B.A. Bodhaine, Continuous aerosol black carbon measurements inside and outside a large office building, paper presented at the Fourth International Conference on Carbonaceous Particles in the Atmosphere, Vienna, Austria, April 3-5, 1991.

Schnell, R.C., R. Fall, M. Nemecek-Marshall, K. Sweeting, and R. La Duca, A new INA bacterium from high altitude equatorial vegetation, paper presented at the 5th International Conference on Biological Ice Nuclei, Madison, Wisconsin, August 4-7, 1991.

Schnell, R.C., S.C. Liu, S.J. Oltmans, R.S. Stone, D.J. Hofmann, E.G. Dutton, T. Deshler, W.T. Sturges, J.W. Harder, S.D. Sewell, M. Trainer, and J.M. Harris, Decrease of summer tropospheric ozone concentrations in Antarctica, *Nature, 351*, 726-729, 1991.

Sheridan, P., D. Hofmann, R.C. Schnell, T. Deshler, and B. Johnson, Individual particle electron microscope analyses of Mt. Pinatubo stratospheric aerosols collected by balloon-borne impactors, paper presented at the American Geophysical Union Fall Meeting, San Francisco, California, December 9-13, 1991.

Sheridan, P., D. Hofmann, R.C. Schnell, T. Deshler, and B. Johnson, Electron microscope studies of Kuwait oil smoke aerosols collected by aircraft-based and balloon-borne impactors, May-July 1991, paper presented at the American

Geophysical Union Fall Meeting, San Francisco, California, December 9-13, 1991.

Stone, R.S., and J.D. Kahl, Variations in boundary layer properties associated with clouds and transient weather disturbances at the South Pole during winter, *J. Geophys. Res., 96(D3)*, 5137-5144, 1991.

Sturges, W.T. (Ed.), *Pollution of the Arctic Atmosphere*, Elsevier, Essex, England, 334 pp., 1991.

Sturges, W.T., and G.F. Cota, Ice algal production of volatile organic bromine compounds: Release to seawater, the atmosphere, and potential influence on surface ozone, American Geophysical Union 1991 Fall Meeting, San Francisco, December 9-13, 1991.

Sturges, W.T., R.C. Schnell, C.W. Sullivan, L.E. Heidt, and W.H. Pollack, Biogenic bromine gases at McMurdo: Ice algal production, atmospheric concentrations and potential influence on surface ozone, paper presented at the Symposium on the Tropospheric Chemistry of the Antarctic Region, University of Colorado, Boulder, Colorado, June 3-6, 1991.

Thompson, T.M., Nitrous oxide and halocarbon measurements at Alert, paper presented at the Canadian Baseline Program Review, Alliston, Ontario, Canada, May 28-31, 1991.

Winchester, J.W., and B.A. Bodhaine, Resolution of physical and chemical components of the 1982 winter aerosol at South Pole station by factor analysis, paper P2.9 presented at the Symposium on the Tropospheric Chemistry of the Antarctic Region, June 3-6, 1991, Boulder, Colorado, 1991.

Yamato, M., Y. Iwasaki, R.C. Schnell, P. Sheridan, M. Nishikawa, and T. Mizoguchi, Aerosols emitted into the atmosphere from Kuwait fires, paper presented at the Japan Meteorological Society, October 23-25, 1991, Tokyo, 1991.

10. Acronyms and Abbreviations

AEROCE	Atmosphere/Ocean Chemistry Experiment
AES	Atmospheric Environment Service, Canada
AGASP	Arctic Gas and Aerosol Sampling Program
AGL	above ground level
AL	Aeronomy Laboratory, Boulder, Colorado (ERL)
ALE/GAGE	Atmospheric Lifetime Experiment/Global Atmospheric Gases Experiment
ALT	Alert Observatory, Canada
ANL	Argonne National Laboratory
ANSTO	Australian Nuclear Science and Technology Organization
AOML	Atlantic Oceanographic and Meteorological Laboratory, Miami, Florida (ERL)
ARL	Air Resources Laboratory, Silver Spring, Maryland (ERL)
ASC	Ascension Island, South Atlantic Ocean
ASA	Antarctic Support Associates, Inc.
ASASP	Active Scattering Aerosol Spectrometer Probe
ASCII	American Standard Code For Information Interchange
ASL	above sea level
BAO	Boulder Atmospheric Observatory
BC	black carbon
BSRN	Baseline Surface Radition Network
BRW	Barrow Observatory, Barrow, Alaska (CMDL)
CAF	Clean Air Facility
CAMS	Control and Monitoring System
CD-ROM	compact disk/random only memory
CEAREX	Coordinated Eastern Arctic Experiment
CFC	chlorofluorcarbon
CFC-11	trichlorofluoromethane
CFC-12	dichlorodifluoromethane
CGO	Cape Grim, Tasmania, baseline station
CIRES	Cooperative Institute for Research in Environmental Sciences, University of Colorado, Boulder
CMDL	Climate Monitoring and Diagnostics Laboratory, Boulder, Colorado (ERL)
CN	condensation nuclei
CNC	condensation nucleus counter
COR	correlation coefficient
CSIRO/DAR	Commonwealth Scientific and Industrial Research Organization/Division of Atmospheric Research, Australia
CSU	Colorado State University, Fort Collins, Colorado
DB	direct-beam [irradiance]
DMS	dimethyl sulfide
DOE	Department of Energy
DSIR	Department of Scientific and Industrial Research, New Zealand
DU	Dobson units
ECC	electrochemical concentration cell
ECD	electron capture detector
EC-GC	electron capture-gas chromatograph
ECMWF	European Centre for Medium Range Weather Forecasts
EML	Environmental Measurements Laboratory
ENSO	El Niño/Southern Oscillation
EPA	Environmental Protection Agency
ERL	Environmental Research Laboratories, Boulder, Colorado (NOAA)
FIRE	First ISCP (International Satellite Cloud Climatology Project) Regional Experiment
FPD	flame photometric detector
FRLAB	Front Range Lidar, Aircraft, and Balloon experiment

FSSP	Forward Scattering Spectrometer Probe
FTIR	Fourier transform infrared (spectroscopy)
GC	gas chromatograph
G.E.	General Electric
GMT	Grennwich Mean Time
GLOBE	Global Backscatter Experiment
GRIB	"Gridded in Binary" format for ECMWF-TOGA analyses
HP	Hewlett-Packard
HST	Hawaii standard time
IC	ion chromatography
IEEE	International Electrical and Electronic Engineers
INSTAAR	Institute for Arctic and Alpine Research, University of Colorado, Boulder
IR	infrared
ISWS	Illinois State Water Survey
ITCZ	Intertropical Convergence Zone
JPL	Jet Propulsion Laboratory
LEAPS	Low Electron Attachment Potential Species
LORAN	LOng Range Aid to Navigation
LST	local standard time
LW	longwave
LWD	longwave downward irradiance
LWRF	longwave radiative forcing
MAKS	Martin and Kitzis Sampler (portable air sampler)
MASC	Mountain Administration Support Center (NOAA)
MLO	Mauna Loa Observatory, Hawaii (CMDL)
MLOPEX	MLO Photochemical Experiment
MSL	mean sea level
NADP	National Atmospheric Deposition Program
NARL	National Arctic Research Laboratory, Barrow, Alaska
NASA	National Aeronautics and Space Administration
NAVSWC	Naval Surface Warefare Center, Department of Defense
NCAR	National Center for Atmospheric Research
NDIR	non-dispersive infrared analyzer
NESDIS	National Environmental Satelite, Data and Information Service (NOAA)
NIP	normal incidence pyrheliometer
NIST	National Institute for Standards and Technology (formerly NBS)
NMC	National Meteorological Center
NOAA	National Oceanic and Atmospheric Administration
NOAH	Nitrous Oxide And Halocarbons Division, Boulder, Colorado (CMDL)
NRBS	non-Rayleigh backscatter
NSF	National Science Foundation
NSSDC	National Space Science Data Center
NSO	National Solar Observatory
NWR	Niwot Ridge, Colorado
NWS	National Weather Service
ODP	ozone depletion potential
OGIST	Oregon Graduate Institute of Science and Technlogy
PBL	planetary boundary layer
PC	personal computer
PDB	pee dee belemnite
PE	Perkin Elmer Corporation
PESA	proton elastic scattering analysis
PIXE	Proton-Induced X-ray Emission
PMEL	Pacific Marine Environmental Laboratory, Seattle, Washington (ERL)

PMOD	Physikalisch-Meteorologisches Observatorium Davos (World Radiation Center)
PMT	photomultipier tube
PSC	Polar stratospheric cloud
PSP	precision sunphotometer
P^3	Portable Pressurizer Pack (air sampler)
QBO	quasi-biennial oscillation
RITS	Radiatively Important Trace Species
RSD	residual standard deviation
SAGA	Soviet-American Gas and Aerosol Experiment
SAGE	Stratospheric Aerosol and Gas Experiment
SASP	Surface Air Sampling Program
SBUV	solar backscattered ultraviolet (satellite ozone instrument)
SCS	Soil Conservation Service, Anchorage, Alaska
SEAREX	Sea-Air Exchange Experiment
SEASPAN	SEAREX South Pacific Aerosol Network
SERI	Solar Energy Research Institute
SEY	Mahé Island, Seychelles
SIO	Scripps Institution of Oceanography
SMO	Samoa Observatory, American Samoa (CMDL)
SOI	Southern Oscillation Index
SOLRAD	Solar Radiation
SPO	South Pole Observatory, Antarctica (CMDL)
SRF	spectral response function
SRM	standard reference material
SSL	slightly stable layer
SST	sea-surface temperature
TECO	Thermal Electron Company
TEM	transmission electron microscope
TOGA	Tropical Ocean Global Atmosphere
TOMS	Total Ozone Mapping Spectrometer
TSI	Thermo Systems Incorporated
TSL	Technical Services Laboratory
TSP	total suspended particulate
UCI	University of California, Irvine
UPS	uninteruptable power supply
URAS	[a commercial CO_2 analyzer]
URI	University of Rhode Island
USDA	United States Department of Agriculture
USGS	United States Geological Survey
UT	universal time
UV	ultraviolet
UVB	ultraviolet B spectral band
WHOI	Woods Hole Oceanographic Institute
WOCE	World Ocean Circulation Experiment
WMO	World Meteorological Organization
WPL	Wave Propagation Laboratory, Boulder, Colorado (ERL)

*U.S. GOVERNMENT PRINTING OFFICE: 1993-774-025/69048